ARS JOURNAL

RUSSIAN SUPPLEMENT

Igor Jurkevich, Editor

Published Under National Science Foundation Grant-in-Aid

Stability of Motion of a Gyroscope With a Cardan Suspension

L. M. MARKHASHOV

THE STABILITY of a gyroscope with a Cardan suspension and an outer gimbal with vertical axis, operating in regular precession and constant rotation, was investigated in detail by Magnus (1)[1] and Rumyantsev (2). If the motion of the gyroscope is stable, then the method developed by Chetaev (3,4) makes it possible to estimate the maximum value of the angle of nutation θ during the course of motion as a function of the values of the disturbed constants of motion. This estimate is obtained by solving a certain system of inequalities.

We develop here a method of obtaining this estimate with any desired accuracy.

1. The problem reduces to a study of the distribution and an estimate of the roots of the polynomial

$$\frac{1}{ae} f(u) \equiv \frac{1}{ae} [(\alpha - au)(\epsilon - eu^2) - (\beta - br_0 u)^2]$$

$$\equiv u^3 - a_1 u^2 + a_2 u - a_3$$

$$|u_1| \leq |u_2| \leq |u_3| \qquad [1.1]$$

which are always real in a mechanical problem. The coefficients of the polynomial are constants that depend on the initial data and on the structural parameters of the gyroscope. Here a is always positive.

We shall distinguish two cases. The first is where

$$e = (B_1 + A - C_1)/(A + A_1) > 0$$

Here

A = moment of inertia of the gyroscope rotor
A_1, B_1, C_1 = moments of inertia of the internal gimbal of the suspension

Then

$$|u_3| > 1 \qquad u_1 \leq u_0 = \cos\theta_0 \leq u_2$$

The interval Δ of the variation of the quantity u during the course of motion is a function of the values of u_i

$$\Delta = \begin{cases} 2 & \text{for} \quad |u_1| \quad |u_2| \geq 1 \\ |1 + u_2| & \text{for} \quad -1 \leq u_2 \leq 0 \quad u_1 \leq -1 \\ |u_1 - u_2| & \text{for} \quad |u_1| \quad |u_2| \leq 1 \\ |1 - u_1| & \text{for} \quad 0 \leq u_1 \leq 1 \quad u_2 \geq 1 \end{cases} \qquad [1.2]$$

Let us write the conditions under which

$$\Delta < \epsilon' \qquad [1.3]$$

where ϵ' is a small arbitrary positive quantity.

We denote by u_p the value of u corresponding to undisturbed motion. In this case the following conditions are satisfied: For regular precession

$$f(u_p) = f'(u_p) = 0 \qquad u_p \neq \pm 1$$

for permanent rotation about the vertical

$$f(u_p) = 0 \qquad u_p = \pm 1 \qquad [1.4]$$

By virtue of the unavoidable disturbance of the initial conditions

$$|u_0 - u_p| < \delta \qquad [1.5]$$

where δ is a certain positive quantity which depends on the accuracy of the means used to start up the gyroscope.

Since the gyroscope's motion is possible only when $f(u_0) \geq 0$, the fulfillment of inequality 1.5 signifies that $f(u)$ assumes non-negative values in the δ vicinity of u_p. This will be assumed from now on.

Without loss of generality, we can assume $0 < u_p \leq 1$. For inequality 1.3 to be satisfied it is necessary that for $u_p < 1$

$$f(u_p - \delta - \epsilon') < 0 \qquad f(u_p + \delta + \epsilon') < 0 \qquad [1.6]$$

for $u_p = 1$

$$f(1 - \delta - \epsilon') < 0 \qquad [1.7]$$

These conditions together with inequality 1.5 are equivalent to the requirement

$$u_p - \delta - \epsilon' \leq u_1 \leq u_2 \leq u_p + \delta + \epsilon' \quad \text{for} \quad u_p < 1$$

$$1 - \delta - \epsilon' \leq u_1 \leq u_2 \quad \text{for} \quad u_p = 1$$

On the other hand, to satisfy inequality 1.3, it is sufficient to have

$$f(u_p - \tfrac{1}{2}\epsilon') < 0 \qquad f(u_p + \tfrac{1}{2}\epsilon') < 0 \quad \text{for } u_p < 1 \qquad [1.8]$$

$$f(1 - \epsilon') < 0 \quad \text{for} \quad u_p = 1 \qquad [1.9]$$

These conditions imply that

$$|u_0 - u_p| < \tfrac{1}{2}\epsilon' \quad \text{for} \quad u_p < 1$$

$$|1 - u_p| < \epsilon' \quad \text{for } u_p = 1$$

and together with the latter are equivalent to the requirement

$$u_p - \tfrac{1}{2}\epsilon' \leq u_1 \leq u_2 \leq u_p + \tfrac{1}{2}\epsilon' \quad \text{for} \quad u_p < 1$$

$$1 - \epsilon' \leq u_1 \leq u_2 \quad \text{for} \quad u_p = 1$$

The problem consists of finding those maximum values of ϵ', at which the inequalities 1.6 and 1.7 are not violated, or else those minimum values of ϵ', at which inequalities 1.8 and 1.9 are not violated. The violation of these inequalities is accompanied by a conversion of some of these inequalities into equalities, which leads to the problem of estimating the roots of the polynomial in Eq. 1.1.

Translated from *Izvestiia Akademii Nauk SSSR, Otdel. Tekh. Nauk, Mekhanika i Mashinostroenie* (*Bulletin of the Academy of Sciences USSR, Div. Tech. Sci., Mechanics and Machine Building*), 1959, no. 5, pp. 79–83. Translated by J. George Adashko.

[1] Numbers in parentheses indicate References at end of paper.

The second case is where $e < 0$. Unlike the case $e > 0$, the segment $[-1, 1]$ can contain all three roots of the polynomial in Eq. 1.1, which makes the analysis more cumbersome.

2. Assume that it is required to find the approximate value of the root z_k of the polynomial

$$\varphi(z) = z^n - b_1 z^{n-1} + \ldots + (-1)^n b_n \qquad (b_n \neq 0) \quad [2.1]$$

specified in the complex plane (z). Furthermore, let the root z_k be separated. That is, there is given a complex number z_0 and the real number ρ, such that

$$|z_\nu - z_0| < \rho \quad \text{for} \quad \nu = k, \qquad |z_\nu - z_0| > \rho \quad \text{for} \quad \nu \neq k$$

The linear transformation

$$z = z_0 + \rho/w \qquad [2.2]$$

maps the region outside the circle ρ in the plane (z) on the region inside a unit circle with the center at the origin in the plane (w); the roots of polynomial 2.1 are transformed here into the roots of the polynomial

$$f(w) = \frac{w^n}{(-1)^n b_n} \varphi\left(z_0 + \frac{\rho}{w}\right) =$$

$$w^n - a_1 w^{n-1} + \ldots + (-1)^n a_n$$

$$w_\nu = \rho/(z_\nu - z_0) \qquad (\nu = 1, \ldots, n)$$

$$\ldots\ldots\ldots\ldots\ldots\ldots\ldots\ldots\ldots\ldots\ldots\ldots\ldots\ldots\ldots\ldots\ldots\ldots [2.3]$$

The points $w_1, \ldots, w_{k-1}, w_{k+1}, \ldots, w_n$ are found to be included within a unit radius circle with its center at the point $w = 0$. Consequently

$$|w_\nu| < 1 \quad (\nu \neq k) \qquad |w_k| > 1 \qquad [2.4]$$

From Vieta's formulas we have

$$\sum_{\nu=1}^{m} w_\nu{}^n = F_n{}^{(m)}(a_1, \ldots, a_n) \qquad [2.5]$$

where Newton's sum in the left half is made up of components of the form

$$w_\nu{}^n = r_\nu{}^n (\cos n\varphi\nu + i \sin n\varphi_\nu)$$

By induction in m and n it is possible to show that the sequence $F_n{}^{(1)}, \ldots, F_n{}^{(m)}$ is a sequence of the principal diagonals of the minors of the matrix

$$\begin{Vmatrix} a_1 & 1 & 0 & 0 & \ldots \\ 2a_2 & a_1 & 1 & 0 & \ldots \\ 3a_3 & a_2 & a_1 & 1 & \ldots \\ \ldots & \ldots & \ldots & \ldots & \ldots \\ na_n & a_{n-1} & a_{n-2} & a_{n-3} & \ldots \\ 0 & a_n & a_{n-1} & a_{n-2} & \ldots \\ \ldots & \ldots & \ldots & \ldots & \end{Vmatrix}$$

Choosing m sufficiently large, we can obtain from Eq. 2.5, by virtue of 2.4, the following approximations, which can be made as accurate as desired

$$r_k{}^m = |w_k|^m \approx |F_n{}^{(m)}|$$

$$\varphi_k = \arg w_k \approx \frac{1}{m} \tan^{-1} \frac{\operatorname{Im}[F_n{}^{(m)}]}{\operatorname{Re}[F_n{}^{(m)}]}$$

$$\ldots\ldots\ldots\ldots\ldots\ldots\ldots\ldots\ldots\ldots\ldots\ldots\ldots\ldots\ldots\ldots\ldots\ldots [2.6]$$

and which converge rapidly to the true values, if w is sufficiently removed from unity. Consequently, taking Eq. 2.2 into account we obtain approximate values of $|z_k|$ and of $\arg z_k$.

3. Here, the first case is where $e > 0$. At first, let $u_p < 1$. We estimate the value of the difference $u_2 - u_1$. From Vieta's formulas we have

$$(u_2 - u_1)^2 = -3u_3{}^2 + 2a_1 u_3 + a_1{}^2 - 4a_2 =$$

$$-f'(u_3) + a_1{}^2 - 3a_2 \quad [3.1]$$

We also have

$$u_1 \leq u_2 < u^* = \sqrt{\epsilon/e} < u_3 \qquad u^* > 1$$

To estimate the root u_3, it is best to transform the polynomial 1.1 by using the substitution $u = (u^* - u_0)z + u_0$. We obtain

$$\frac{1}{(u^* - u_0)^3} \varphi(z) = f[(u^* - u_0)z + u_0] = z^3 +$$

$$\frac{1}{2} \frac{f''(u_0)}{u^* - u_0} z^2 + \frac{f'(u_0)}{(u^* - u_0)^2} z + \frac{f(u_0)}{(u^* - u_0)^3}$$

The roots of the equation $\varphi(z) = 0$ are such that

$$-1 < z_1 \leq 0 \leq z_2 < 1 < z_3$$

The approximate value of the quantity $(u^* - u_0)^m z_k{}^m$, according to section 2, is determined by the principal diagonal minor D_m of order m of the matrix

$$\begin{Vmatrix} -\frac{1}{2}f''(u_0) & 1 & 0 & 0 \\ 2f'(u_0) & -\frac{1}{2}f''(u_0) & 1 & 0 \ldots \\ -3f(u_0) & f'(u_0) & -\frac{1}{2}f''(u_0) & 1 \ldots \\ 0 & -f(u_0) & f'(u_0) & -\frac{1}{2}f''(u_0) \ldots \\ \ldots & \ldots & \ldots & \ldots \end{Vmatrix}$$

The approximate value of the root u_3 is

$$U_3 = u_0 + D_m{}^{1/m} \qquad [3.2]$$

For odd m we have

$$Z_3{}^m = z_1{}^m + z_2{}^m + z_3{}^m < z_2{}^m + z_3{}^m < (z_2 - z_1)^m + z_3{}^m =$$

$$z_3{}^m + \Delta^m/(u^* - u_0)^m$$

$$Z_3{}^m = z_1{}^m + z_2{}^m + z_3{}^m > z_1{}^m + z_3{}^m > (z_1 - z_2)^m + z_3{}^m =$$

$$z_3{}^m - \Delta^m/(u^* - u_0)^m$$

Hence

$$(U_3 - u_0)^m - \Delta^m < (u_3 - u_0)^m < (U_3 - u_0)^m + \Delta^m$$

Let $[\psi]$ denote the order of the small quantity ψ. By virtue of the assumed smallness of Δ we obtained from the last inequality

$$U_3 - \frac{\Delta^m}{m(U_3 - u_0)^{m-1}} < u_3 < U_3 + \frac{\Delta^m}{m(U_3 - u_0)^{m-1}}$$

In this case the meaning of the inequality does not change, since the order of the discarded terms is equal to $2m[\Delta]$. Considering that $f^*(u_3) > 0$, we find

$$-f'\left(U_3 + \frac{\Delta^m}{m(U_3 - u_0)^{m-1}}\right) < -f'(U_3) + O_1(\Delta^m)$$

$$-f'\left(U_3 - \frac{\Delta^m}{m(U_3 - u_0)^{m-1}}\right) > -f'(U_3) + O_2(\Delta^m)$$

where $O_1(\Delta^m)$ and $O_2(\Delta^m)$ are quantities of order $m[\Delta]$. Expressing the coefficients a_1 and a_2 in terms of the function $f(u)$ and its derivatives at the point $u = u_0$, we obtain from Eqs. 3.1 and 3.2

$$\Delta^2 \equiv (u_2 - u_1)^2 \approx -3D_m{}^{2/m} - f''(u_0)D_m{}^{1/m} +$$

$$(1/4)\{f''(u_0)\}^2 - 4f'(u_0) \equiv \Delta_*{}^2 \quad [3.3]$$

for $0 < u_p < 1$ with accuracy to the kth significant figure

$$k = -(m - 2)[\Delta] \qquad m = 2m_1 + 1 \qquad m_1 \geq 1$$

With the same accuracy we have

$$u_1 = \tfrac{1}{2}(a_1 - u_3 - \Delta) \approx u_0 + \tfrac{1}{4}f''(u_0) - \tfrac{1}{2}D_m{}^{1/m} - \tfrac{1}{2}\Delta_*$$

$$u_2 = \tfrac{1}{2}(a_1 - u_3 + \Delta) \approx u_0 + \tfrac{1}{4}f''(u_0) - \tfrac{1}{2}D_m{}^{1/m} + \tfrac{1}{2}\Delta_*$$

From this we obtain finally for $t \geq t_0$

$$\tfrac{1}{4}f''(u_0) - \tfrac{1}{2}D_m{}^{1/m} - \tfrac{1}{2}\Delta_* \leq |u(t) - u(t_0)| \leq \tfrac{1}{4}f''(u_0) - \tfrac{1}{2}D_m{}^{1/m} + \tfrac{1}{2}\Delta_* \quad [3.4]$$

When $u_p = 1$ the necessary lower estimate of the root u_1 is reached by converting the polynomial 1.1 by means of a suitable substitution with subsequent application of Eq. 2.6.

It is possible, however, to simplify substantially the final result by taking into account the smallness of the quantity $1 - u_1$. Accurate to a quantity of order $3[\Delta] = 3[1 - u_1]$ we have

$$u_1 - u_0 \approx \frac{-f'(u_0) - \sqrt{f'^2(u_0) - 2f(u_0)f''(u_0)}}{f''(u_0)}$$

$$(f''(u_0) \neq 0)$$

so that for all $t \geq t_0$

$$u_0 - \frac{f'(u_0) + \sqrt{f'^2(u_0) - 2f(u_0)f''(u_0)}}{f''(u_0)} \lesssim u(t) \leq 1 \quad [3.5]$$

and the lower limit of the variation of $u(t)$ is accurate to the kth significant figure; $k = -2[\Delta]$. Consequently, in this latter case the accuracy depends only on the order of the quantity Δ and is not arbitrary.

The second case is where $e < 0$. Let u° be the smallest root of the quadratic equation $f'(u) = 0$. Then

$$u_1 < u^\circ < u_2 < u_0 < u_3$$

The roots are separated, and it is easy to find linear transformation for the polynomial 1.1, which then permits the use of estimates of the type 2.6.

Let us return to the mechanical meaning of the coefficients of the polynomial

$$f(-1) = (\alpha + a)(\epsilon - e) - (\beta + br_0)^2 = \frac{1}{(A + A_1)^2}[(h + 2P\xi - Cr_0^2)(I + C_1) - (K + Cr_0)^2] = -\frac{C}{(A + A_1)^2}(C + C_1 + I)r_0^2 + \ldots$$

$$f(1) = (\alpha - a)(\epsilon - e) - (\beta - br_0)^2 = -\frac{C}{(A + A_1)^2}(C + C_1 + I)r_0^2 + \ldots$$

Here

I = moment of inertia of the gyroscope casing about its axis of rotation
ξ = applicate of the center of gravity of the system
r_0, K = cyclic constants
h = the kinetic energy constant

The dots stand for a group of components, which are linear in r_0. At sufficiently large r_0 we have $f(-1) < 0$ and $f(1) < 0$, from which we see that for such r_0 a stable permanent rotation of the gyroscope about the vertical is impossible, and the regular precession, if it does take place at all, is stable. The limits of the variation of $u(t)$ in time are determined from 3.4, if the function $f(u)$, which is contained in this formula, is replaced by $f(-u)$. When $u_p = 1$ [when of necessity $f(1) > 0$] formula 3.5 can be employed directly.

4. Inequalities 1.7 and 1.9 can be considered as conditions for a special type of conditional stability, which is defined in the following manner.

No matter how small the number $\epsilon' > 0$, there is a $\delta > 0$, such that the inequality $|u(t) - u_0| < \delta$ is not violated for all $t \geq t_0$, provided u_0 is such that $|u_0 - u_p| < \delta$, and the remaining initial conditions satisfy inequalities 1.7 and 1.9. Then inequalities 1.7 and 1.9 solve a problem that is the inverse of that considered in sections 1–3: They yield the conditions that must be imposed on the constants of disturbed motion in order to realize inequality 4.1. In such a problem, δ and ϵ' should be specified beforehand.

If the motion is unconditionally stable when $u_p = 1$, then inequality 1.7 is of necessity satisfied for vanishing values of δ and ϵ'. Taking Eqs. 1.4 into account, this yields

$$-f'[1 + l(\delta + \epsilon')](\delta + \epsilon') < 0 \qquad (|l| < 1) \quad [4.1]$$

Hence, by virtue of the continuity of $f'(u)$

$$f'(1) > 0 \quad [4.2]$$

On the other hand, the expansion of the left part of inequality 1.9 in a Taylor series shows that condition 4.2 is also sufficient for unconditional stability. Putting $\psi_0' = \Omega$, $r_0 = \omega$, and expanding condition 4.2

$$f'(1) \equiv -(\epsilon - e)(2e\Omega - 2b\omega\Omega + a) \equiv -2(\epsilon - e)[(B_1 + A - C_1)\Omega^2 - C\omega\Omega + P\xi] > 0$$

we get the condition previously found in (2) by the method of the tie-in integral.

I would like to thank V. V. Rumyantsev for his attention to my work and for many important comments.

References

1 Magnus, K., "On the Stability of Motion of a Heavy Symmetrical Gyroscope in a Cardan Suspension," *Prikladnaia Matematika i Mekhanika* (*Appl. Math. and Mech.*), vol. 22, no. 2, 1958.

2 Rumyantsev, V. V., "On the Stability of Motion of a Symmetrical Gyroscope in a Cardan Suspension," *Prikladnaia Matematika i Mekhanika* (*Appl. Math. and Mech.*), vol. 22, no. 3, 1958.

3 Chetaev, N. G., "On a Gyroscope in a Cardan Suspension," *Prikladnaia Matematika i Mekhanika* (*Appl. Math. and Mech.*), vol. 22, no. 3, 1958.

4 Chetaev, N. G., *Ustoichivost' dvizheniya* (*Stability of Motion*), Gostekhizdat, 1955.

—*Received May 8, 1959*

Reviewer's Comment

This paper deals with the mathematical determination of nutation limits of a gyroscope freely suspended in a gimbal system whose outermost axis is vertical. The similarity of Eq. 1.1 with the equation describing nutation of a spinning top [Eq. (5), p. 78, *Mechanics of the Gyroscope*, by Richard F. Deimel, Dover Publications, Inc., 1950, originally published 1929] indicates that the analysis is based on a pendulous gyroscope.

The polynomial in Eq. 1.1 is proportional to the square of the rate of change of u with respect to time. u is the cosine of the angle between the gyroscope spin axis and the vertical. Thus finding the roots of the polynomial provides maximum and minimum values of u for whatever nutation pattern may exist.

In Eq. 1.1 the symbol a appears to contain the gyro pendulosity. Setting a equal to zero results in a quadratic expression for limits of deviation of the spin axis from its average position. (This special case would be more easily determined by solving the complete equations of motion of a nonpendulous gyroscope.)

The contribution made by this paper is a method for finding the roots of Eq. 1.1. The method is one which allows approximations to be made to any accuracy desired using techniques of establishing bounding inequalities and finding solutions which satisfy these inequalities.

—D. P. CHANDLER
Autonetics Division
North American Aviation, Inc.

Investigation of the Iron-Chromium-Titanium Phase Diagram in a Region of Iron- and Chromium-Rich Alloys

N. G. BORISKINA and
I. I. KORNILOV

THE PURPOSE of this investigation was to explain the nature of the reaction of iron with chromium and titanium and to establish an equilibrium diagram for the Fe-Cr-Ti system in a region of iron- and chromium-rich alloys.

Binary systems Fe-Cr, Fe-Ti and Cr-Ti, on the sides of the ternary structural diagram Fe-Cr-Ti, are now being studied in detail.

A great amount of work has been devoted to the reaction of iron with chromium; a critical review of which is given in monograph (1).[1]

The slight difference in the atomic radii of iron and chromium (1.26 and 1.27), the identical type of crystal lattice and the closeness in the parameters lead to the formation of a continuous solid solution of these elements. At temperatures below 900–850 C, within a concentration range of 40–63% Cr, iron and chromium base solid solutions undergo decomposition with the formation of σ-phase compounds of FeCr stoichiometric composition. It was shown in (2 and 3) that the decomposition of the solid solution in this system, at low temperatures, proceeds with the formation of a series of chemical compounds of the σ-phase type. The authors of (4) indicate the existence of a high temperature β-phase in the Ni-Cr system, linking its appearance with the polymorphic transformation of chromium. Although this work is not the only one dealing with the high temperature modification in chromium, the literature still contains no Fe-Cr structural diagrams which include the β-modification of chromium. It has been established that chromium strongly narrows the γ-iron region. At 900 C, the maximum amount of chromium dissolved in γ-Fe is $\sim$12.37%.

Lamort (5) was the first to study the Fe-Ti structural diagram from the iron side. He established the presence of the Fe_3Ti compound with a tetragonal lattice which formed eutectic mixtures with an α-solid solution of iron at 1298 C. Later, using purer materials, the authors of a series of works (6–9) showed that in an Fe-Ti system, in a region of iron-rich alloys, only one metallic compound with a $TiFe_2$ composition forms which has the $MgZn_2$-type structure. In (8), the solubility of titanium in α-iron was given a detailed study. Research data (10) showed that titanium strongly narrows the γ-iron region.

Employing a basically metallographic method, McQuillan (11) plotted the first structural diagram for the Ti-Cr system with the purest materials. He established a continuous series of solid solutions between β-titanium and chromium. At 1360 C, the solid solution decomposes, forming a metallic compound. Duwez and Taylor (12), employing metallographic and x-ray analyses, established that this is the only compound in the Ti-Cr system and corresponds to the $TiCr_2$ composition with a $MgCu_2$-type structure. It was shown in (13) that this compound has a polymorphic transformation, and that at temperatures above 1000 C it has the $MgZn_2$-type lattice. In (14), a detailed study was made of the solubility of titanium in chromium.

In Fig. 1 are binary structural diagrams, narrowing the examined part of the ternary system.

There are little data in the literature covering the Fe-Cr-Ti ternary system in the region of iron- and chromium-rich alloys. The joint influence of Ti and Cr on γ-iron regions was studied in (10). The authors established that, just as in binary systems Fe-Cr and Fe-Ti, chromium and titanium strongly narrow the region of the γ-iron base ternary solid solution. At 1070 C, the maximum solubility of titanium in γ-iron is $\sim$1.3%, and of chromium 7%. Vogel and Wendrott (15), employing microstructural, thermal and x-ray analyses,

Translated from *Izvestiia Akademii Nauk SSSR, Otdel. Tekh. Nauk, Metallurgiia i Toplivo* (*Bulletin of the Academy of Sciences USSR, Div. Tech. Sci., Metallurgy and Fuel Series*), 1960, no. 1, pp. 50–58. Translated by Primary Sources, New York.

[1] Numbers in parentheses indicate References at end of paper.

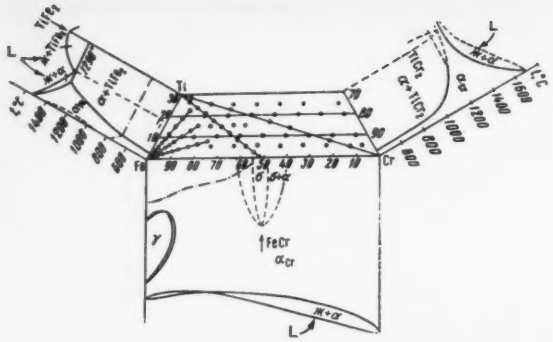

Fig. 1 Compositions of examined alloys

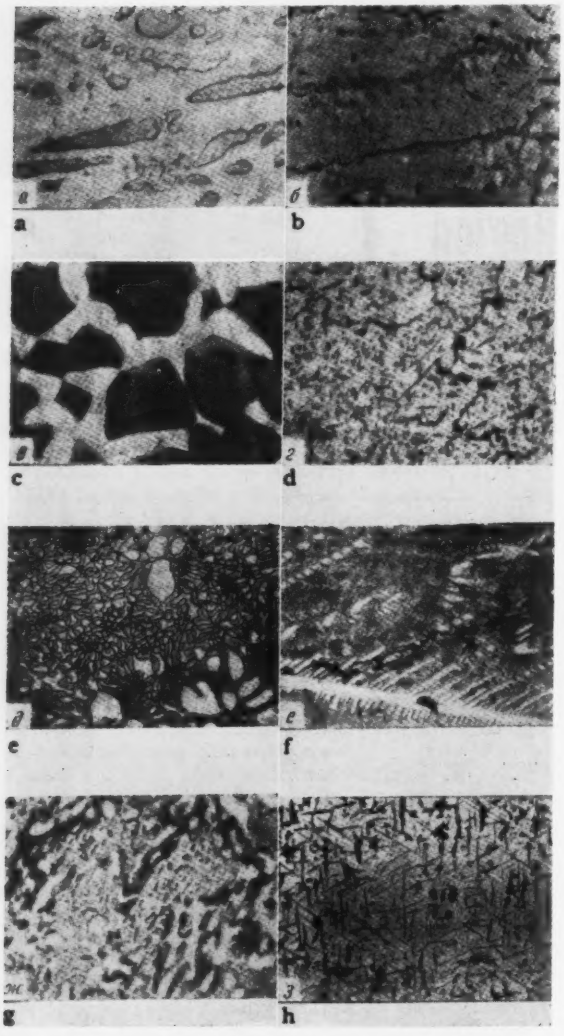

Fig. 2 Microstructures of examined alloys. a: Cast alloy No. 3 of section $TiFe_2$-FeCr ($\gamma + \chi$); b: Cast alloy No. 5 of section $TiFe_2$-FeCr (χ); c: Alloy No. 7 of section $TiFe_2$-FeCr, following quenching ($\alpha + \chi$); d: Alloy No. 5 of section $TiFe_2$-FeCr, following extended annealing ($\chi + \gamma$); e: Cast alloy No. 4 of section $TiFe_2$-Cr ($\alpha + \gamma$); f: Cast alloy No. 7 of radial section I ($\gamma + \alpha$); g: Alloy No. 6 of radial section II, following quenching from 1000 C ($\chi + \alpha + \gamma$); h: Alloy No. 9 of radial section II, following quenching from 1000 C ($\chi + \gamma + \alpha$)

studied the part of the Fe-Cr-Ti structural diagram adjoining the Fe-Cr side and bound by the Fe_2Ti-Ti_3Cr_2 section.

They established two phase components, found in equilibrium, in the iron corner of the structural diagram: An iron and chromium base ternary solid solution, and an Fe_2Ti compound base solid solution. The Ti_3Cr_2 compound is found in the region of chromium-rich alloys in equilibrium with these solid solutions. According to their data, all three phase components form a ternary eutectic, coinciding with the binary eutectic, established by extrapolation, and corresponding to 42% Ti at 1400 C. The authors of this work had at their disposal for preparing the alloys titanium which was strongly contaminated with impurities (95% Ti); open melting in a Tamman furnace further contaminated the resultant alloys with nitrides and carbides, making the phase analysis of the resultant alloys difficult.

Experimental Part

Alloys from the $TiFe_2$-FeCr section were selected for the investigation in order to explain the nature of the reaction between the Laves phase and the σ-phase; alloys from the $TiFe_2$-Cr section for the possible triangulation of the Fe-Cr-Ti system; alloys from the three radial sections with fixed ratios for Ti:Cr = 3:1, 1:1 and 1:3; and some alloys from sections with parallel Fe-Cr sides, having 5, 10, 15, 20 and 25% Ti. The compositions of all the studied alloys are given in the table and are plotted on the composition triangle (Fig. 1).

Materials and Methods of Preparing Alloys

Electrolytic iron, with a composition of 99.94% Fe, 0.028% C, 0.01% Mn and 0.009% Si, was used as the starting material. Also used was electrolytic chromium, containing 99.95% Cr and 0.02% O_2; and titanium iodide, 99.85% Ti pure, in which the main impurities were 0.01% Fe, 0.02% Mg, 0.03% Al and 0.03% O_2.

The alloys were prepared by arc melting under argon with a nonconsumable electrode. The specimens were remelted three to four times in order to achieve a complete mixture of the components. There was a random chemical analysis. Alloy composition control was maintained by precise weighing, following melting. Alloys whose weight did not deviate by more than 0.5% of the charge were considered satisfactory.

Cast alloys, enclosed in quartz ampoules, were homogenized at 1100 C for 100 hr. Following quenching from 1000 C (100-hr soaking) and after annealing at 550 C for 500 hr, the alloys were examined.

The alloys were studied mainly by microstructural and x-ray analyses. Measurements were also taken of the hardnesses and the microhardnesses of the individual phase components of the alloys.

X-ray analysis was conducted by using unfiltered vanadium radiation in an RKU86 chamber. A Vickers unit employing a diamond pyramid with a load of 10 kg was used to measure hardness.

The $TiFe_2$-FeCr Section

A microstructural investigation of alloys Nos. 2, 3 and 4 in this section, in a cast state, showed that they are basically two-phase. The initially crystallized dendrites were surrounded by a less etched phase which had a microstructure of the same type as the initially crystallized dendrites (845 kg per mm²) (Fig. 2a). Accordingly, alloy No. 5, containing 15.7% Ti, 25.8% Cr and 58.5% Fe in atomic percentages, is single-phase in a cast state (Fig. 2b). The initially crystallized phase in alloys Nos. 6 and 7 has a microhardness which is considerably less (350 kg per mm²) than the phase formed with it in the peritectic reaction (825 kg per mm²).

The following distribution of phase components is observed in alloys of this section, quenched at 1000 C. Alloy No. 1 is a

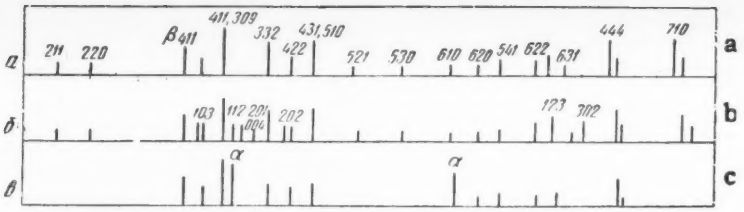

Fig. 3 Characteristic x-ray photographs of section $TiFe_2$-FeCr. a: X-ray photograph of cast alloy No. 5 (χ-phase); b: X-ray photograph of alloy No. 5, after annealing ($\chi + \gamma$) (γ-phase indexes are marked); c: X-ray photograph of alloy No. 7 ($\chi + \alpha$)

$TiFe_2$ base solid solution. The phase, formed in alloys Nos. 3 and 4 in the peritectic reaction, partially decomposes. Alloy No. 5 shows the greatest degree of decomposition. Alloy No. 7 (Fig. 2e) most clearly characterizes the peritectic nature of the formation of the new chemical compound which surrounded the more etched grains of the iron and chromium base solid solution. Alloys Nos. 9 and 10 are α-Fe and Cr base solid solutions.

Extended annealing at 550 C brought little change to the alloy microstructure. Alloy No. 5 underwent a more complete decomposition with the formation of a fine dispersed phase, frequently needle-shaped, and separating at the grain boundaries and in the grain field.

X-ray analysis of the alloys in this section showed that all the reflection sines of single-phase cast alloy No. 5 correspond to a body centered lattice of the α-Mn type, with an 8.904 kX parameter. In alloys Nos. 2, 3 and 4, this phase is found in equilibrium with the γ-solid solution having a $TiFe_2$ base, and in alloys 6 and 7 with an Fe and Cr base α-solid solution.

According to the x-ray analysis data, decomposition of this phase is accompanied by the separation of the Laves phase of $TiFe_2$. Fig. 3 shows the characteristic x-ray photographs of this section. Decomposition of the new phase is also accompanied by a reduction in the parameter of its crystal lattice. The presence of the FeCr compound (σ-phase) together with the α-solid solution is observed only on the x-ray photograph of the annealed alloy No. 9 with 2% Ti; this is because the new ternary metallic compound is present in practically all of the alloys in this section.

We ascribed formula $Ti_3Cr_7Fe_{17}$ to the new compound, in accordance with the composition of alloy No. 5, although it is possible that this alloy is only a solid solution based on the compound, whose composition is close to that found. As with phases in systems Fe-Cr-Mo, Co-Cr-Ti and Re-Ti, we treated this compound as a χ-type phase with a partially regulated atom distribution in the cell (16).

The table shows the hardness and phase composition of the alloys in this section, quenched from 1000 C and annealed at 550 C. The hardness of annealed alloys is considerably greater than the hardness of alloys quenched at 1000 C. This fact is connected with the more complete decomposition of the χ-phase.

The $TiFe_2$-Cr Section

From the microstructural analysis data, the crystallization of the cast alloys in this section, Nos. 3–8, is observed to have a eutectic character. Alloy No. 4 (Fig. 2e) is a pure binary eutectic, consisting of a $TiFe_2$ base solid solution and an Fe and Cr base α-solid solution. Alloy No. 1, containing 5% Cr and 28.5% Ti, is a $TiFe_2$ base solid solution. Quenching from 1000 C and extended annealing at 550 C did not change the phase composition of the alloys in this section. From x-ray analysis data the χ-phase was found in alloys Nos. 2 and 3, in equilibrium with the $TiFe_2$ base γ-solid solution. In this connection, this section $TiFe_2$-Cr is not quasi-binary, although in the Fe-Cr-Ti system there is such a section between the corresponding solid solutions (γ and α). The table shows the alloy hardness values in this section.

Radial Sections

The microstructures of cast alloys with a Ti:Cr ratio of 3:1 (section I) characterize the crystallization of the eutectic mixtures in them. Alloy No. 7 (Fig. 2f) lies close to the line of binary saturation in the ternary system and is an almost pure $\alpha + \gamma$ binary eutectic. The high microhardness of the initially crystallized phase in alloy No. 8 (830 kg per mm²) and the relatively low microhardness in alloy No. 6 confirms that in alloys having higher titanium contents than alloy No. 7, the γ-solid solution crystallizes first; in alloys with lower Ti contents, the α-solid solution crystallizes first.

Eutectic crystallization also takes place in cast alloys Nos. 6 and 7 having a Ti:Cr ratio of 1:1 (section II). All cast alloys with Ti:Cr ratios of 1:3 (section III) characterize the crystallization of α-solid solutions.

Investigation of microstructures of alloys in section I, following quenching from 1000 C, showed that titanium and chromium solubility in iron is ~7.8% at 1000 C. Alloy solid solutions with 10 and 12.5% (Ti + Cr) undergo decomposition. Further increases of the total Ti and Cr in alloys lead to the formation of binary eutectic mixtures around the initially crystallized grain of the α-solid solution. The amount of eutectic increases to alloy No. 7, following which it decreases to alloy No. 9.

At 1000 C, titanium and chromium solubility in iron is 10.5% in the alloys of section II. An alloy with 15% Ti + Cr is already composed of three phases $\alpha + \gamma + \chi$ (Fig. 2g). The amount of α-phase in these alloys is sharply reduced as the Ti and Cr in the alloys increase; in alloys Nos. 8 and 9, the main phase component is the χ-phase, which undergoes decomposition with the formation of $TiFe_2$ needles (Fig. 2h). The unspent α-solid solution, in the reaction $L + \alpha \rightarrow \chi$, is distributed along the microsection field in the form of separate dark points.

At 1000 C, the total solubility of chromium and titanium in the alloys of section III is ~15.0%. The solid solution decomposes in all the remaining alloys in this section. At 550 C, titanium and chromium solubility in iron is markedly reduced. In alloys of section I, it is 5% Ti + Cr; in section II, 5% Ti + Cr; in section III, ~10.5% Ti + Cr. From microstructural analysis we note that there are no changes in the remaining phase compositions of annealed alloys. X-ray analysis shows that the decomposition of solid solutions in alloys of section I and II proceeds with the formation of the $TiFe_2$ compound; for section III, the χ-phase.

"Composition hardness" curves were plotted, using the data in the table (Fig. 4). Hardness of alloys in section I, quenched from 1000 C, differed little from those with up to 20% Ti + Cr, annealed at 550 C; it increased rapidly as total Ti + Cr contents in them increased, in connection with increases of γ-phases in the alloys. The hardness of alloys in section II,

quenched and annealed, was almost the same with up to 15% Ti + Cr. Its sharp increase with 15% Ti + Cr is explained by the joint appearance of the χ-phase and the γ-solid solution in the alloys. The higher hardness values for annealed alloys, containing more than 15% Ti + Cr, is explained by the more complete decomposition of the χ-phase. There is an almost identical hardness to the quenched and annealed alloys in section III. There still is no explanation for the sharp hardness jump of the annealed alloy with 30% Ti + Cr inasmuch as its microstructure differs but little from that quenched from 1000 C.

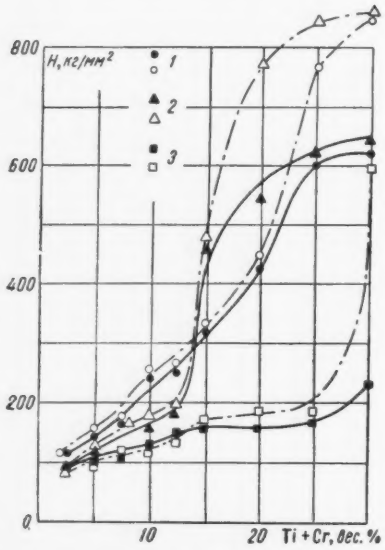

Fig. 4 Hardness of alloys in radial sections after quenching (solid lines) and annealing (dashed lines). 1: Section I; 2: Section II; 3: Section III

Parallel Sections

A study was made of the alloys in sections with parallel Fe-Cr sides and having a fixed titanium content of 25, 20, 15, 10 and 5%. The aim was to plot more accurate boundaries for the phase regions on the structural diagram of the investigated system. Alloys in the section having 25 and 20% Ti characterize the crystallization of the eutectic mixtures.

X-ray analysis showed the examined alloys of these sections to be two-phase and to consist of solid solutions with a base of Fe and Cr α-solid solution and a γ-solid solution of compounds $TiFe_2$ and $TiCr_2$.

In alloys of the section containing 25% Ti, the γ-phase is dominant; in alloys with 20% Ti, the α-solid solution is dominant. Alloy No. 6 of the section with 20% Ti, consists of the γ-solid solution and the χ-phase, according to x-ray data. Alloys Nos. 11 and 12 of the section with 15% Ti in cast state, represent χ-phase solid solutions, which decompose at 1000 C and at 550 C with the formation of $TiFe_2$. In alloys Nos. 13 and 15, with 10% Ti, the α-solid solution crystallizes first and the χ-phase causes a peritectic reaction with it. In alloy No. 16 of the section with 10% Ti, the initially crystallized grain of the α-solid solution surrounded the α + γ eutectic. In alloys with 5% Ti, the α-solid Fe and Cr base solutions are crystallized with the exception of alloy No. 24, in which traces of eutectic crystallization remain. At 550 and 1000 C, solid solutions decompose with the formation of the χ-phase in alloys Nos. 19–22 and the γ-solid solution in No. 23.

Isothermal Sections

Using microstructural and x-ray analysis data, phase diagrams were plotted for Fe-Cr-Ti system, at 550 and 1000 C. Fig. 5 shows the phase diagram at 550 C. Three γ-, α- and χ-phase base solid solutions are found in this system in a two- and three-phase equilibrium with one another. We used the dashed line to mark the homogeneous χ-phase region, since no single-phase alloys were struck in the examined alloys when quenching from 1000 and 550 C. It is evident, however,

Chemical, Phase Composition and Hardness of Examined Alloys

No. of alloy	Chemical composition, weight % Fe	Cr	Ti	Phase composition: Quenching from 1000 C	Phase composition: Annealing at 550 C	Hardness, kg/mm²: Quenching from 1000 C	Hardness, kg/mm²: Annealing at 550 C
				$TiFe_2$-FeCr			
1	68.0	5.00	27.00	γ	γ + χ	694	695
2	66.0	10.00	24.00	γ + χ	γ + χ	620	757
3	64.5	15.00	20.50	γ + χ	γ + χ	673	810
4	63.0	20.00	17.00	γ + χ	γ + χ	665	824
5	61.0	25.00	14.00	γ + χ	γ + χ	681	835
6	59.0	30.00	11.00	χ + α + (γ)	χ + α + (γ)	882	882
7	57.0	35.00	8.00	α + χ	α + χ	585	812
8	55.0	40.00	5.00	α	α + χ	381	397
9	53.0	45.00	2.00	α	(α) + σ	227	772
				$TiFe_2$-Cr			
1	66.5	5.00	28.50	γ	γ	724	752
2	59.5	15.00	25.50	γ + χ	γ + χ	...	752
3	52.5	25.00	22.50	γ + χ	γ + χ	743	772
4	45.0	35.00	20.00	γ + α	γ + α	690	762
5	38.0	45.00	17.00	γ + α	γ + α	620	734
6	31.0	55.00	14.00	γ + α	γ + α	...	681
7	24.0	65.00	11.00	γ + α	γ + α	560	585
8	17.0	75.00	8.00	γ + α	γ + α	445	542
9	10.0	85.00	5.00	γ + α	γ + α	409	383

No. of alloy	Chemical composition, weight % Fe	Cr	Ti	Phase composition — Quenching from 1000 C	Phase composition — Annealing at 550 C	Hardness, kg/mm² — Quenching from 1000 C	Hardness, kg/mm² — Annealing at 550 C
				Section I (Ti:Cr = 3:1)			
1	97.5	0.63	1.87	α	α	115.3	116.5
2	95.0	1.25	3.75	α	α	143.1	150.5
3	92.5	1.87	5.63	α	$\alpha + \gamma$	159.0	177
4	90.0	2.5	7.50	$\alpha + \gamma$	$\alpha + \gamma$	242	262
5	87.5	3.13	9.37	$\alpha + \gamma$	$\alpha + \gamma$	251	260
6	85.0	3.75	11.25	$\alpha + \gamma$	$\alpha + \gamma$	322	327
7	80.0	5.00	15.00	$\alpha + \gamma$	$\alpha + \gamma$	429	455
8	75.0	6.25	18.75	$\alpha + \gamma$	$\alpha + \gamma$	602	772
9	70.0	7.50	22.50	$\alpha + \gamma$	$\alpha + \gamma$	720	858
				Section II (Ti:Cr = 1:1)			
1	97.5	1.25	1.25	α	α	93.6	96.7
2	95.0	2.50	2.50	α	α	115.9	118.3
3	92.5	3.75	3.75	α	$\alpha + \chi$	155.0	169
4	90.0	5.00	5.00	α	$\alpha + \chi$	160	176
5	87.5	6.25	6.25	$\alpha + \gamma$	$\alpha + \chi$	182	197
6	85.0	7.50	7.50	$\alpha + \gamma + \chi$	$\alpha + \gamma + \chi$	468	483
7	80.0	10.00	10.00	$\alpha + \gamma + \chi$	$\alpha + \gamma + \chi$	540	772
8	75.0	12.50	12.50	$\alpha + \gamma + \chi$	$\alpha + \gamma + \chi$	627	847
9	70.0	15.00	15.00	$\alpha + \gamma + \chi$	$\alpha + \gamma + \chi$	645	845
				Section III (Ti:Cr = 1:3)			
1	97.5	1.87	0.63	α	α	94.9	92.2
2	95.0	3.75	1.25	α	α	104.1	98.9
3	92.5	5.63	1.87	α	α	103.6	114.8
4	90.0	7.50	2.50	α	α	128.4	121.9
5	87.5	9.37	3.13	α	$\alpha + \chi$	138.4	137.7
6	85.0	11.25	3.75	α	$\alpha + \chi$	150.5	168
7	80.0	15.00	5.00	$\alpha + \chi$	$\alpha + \chi$	155	189
8	75.0	18.75	6.25	$\alpha + \chi$	$\alpha + \chi$	164	168
9	70.0	22.50	7.50	$\alpha + \chi$	$\alpha + \chi$	236	606
				Parallel sections			
1	50.0	25.00	25.00	$\gamma + \alpha$	$\gamma + \alpha$	711	813
2	40.0	35.00	25.00	$\gamma + \alpha$	$\gamma + \alpha$	787	782
3	30.0	45.00	25.00	$\gamma + \alpha$	$\gamma + \alpha$	694	787
4	20.0	55.00	25.00	$\gamma + \alpha$	$\gamma + \alpha$	539	724
5	5.0	70.00	25.00	$\gamma + \alpha$	$\gamma + \alpha$	...	...
6	55.0	25.00	20.00	$\gamma + \chi$	$\gamma + \chi$	711	907
7	35.0	45.00	20.00	$\gamma + \alpha$	$\gamma + \alpha$	792	734
8	25.0	55.00	20.00	$\gamma + \alpha$	$\gamma + \alpha$	707	690
9	15.0	65.00	20.00	$\gamma + \alpha$	$\gamma + \alpha$	665	673
10	5.0	75.00	20.00	$\gamma + \alpha$	$\gamma + \alpha$	627	673
11	65.0	20.00	15.00	$\chi + \gamma$	$\chi + \gamma$	882	870
12	55.0	30.00	15.00	$\chi + \gamma$	$\chi + \gamma$	835	894
13	50.0	35.00	15.00	$\chi + \alpha$	$\chi + \alpha$	882	858
14	65.0	25.00	10.00	$\chi + \alpha$	$\chi + \alpha$	342	772
15	45.0	45.00	10.00	$\chi + \alpha$	$\chi + \alpha$	690	705
16	35.0	55.00	10.00	$\alpha + \gamma$	$\alpha + \gamma$	508	592
17	15.0	75.00	10.00	$\alpha + \gamma$	$\alpha + \gamma$	405	464
18	5.0	85.00	10.00	$\alpha + \gamma$	$\alpha + \gamma$	455	575
19	70.0	25.00	5.00	$\alpha + \chi$	$\alpha + \chi$	314	542
20	60.0	35.00	5.00	α	$\alpha + \chi$	535	669
21	50.0	45.00	5.00	$\alpha + \chi$	$\alpha + \chi$	488	657
22	40.0	55.00	5.00	α	$\alpha + \chi$	489	545
23	30.0	65.00	5.00	α	$\alpha + \chi$	468	539
24	20.0	75.00	5.00	$\alpha + \gamma$	$\alpha + \gamma$	483	508
25	5.0	90.00	5.00	$\alpha + \gamma$	$\alpha + \gamma$	433	512

that such a very narrow region exists in the system Fe-Cr-Ti so that, by using our data, it is possible to mark off the regional boundaries for two- and three-phase equilibria of χ-phase with Fe and Cr base α-solid solutions and with $TiFe_2$ and $TiCr_2$ base γ-solid solutions. The boundary of the α-solid solution in the chromium-rich alloy region is also shown by a dashed line, since all alloys of the section with 5% Ti decompose at 550 C; alloys with still smaller Ti contents were not included in the program of investigation.

Titanium does not contribute to the formation of the σ-phase; at 550 C, the region of its existence was very slight. Alloys located to the right of section $TiFe_2$-Cr lie mainly in a wide region of $\alpha + \gamma$ two-phase equilibrium. At 1000 C, the isothermal section of the system Fe-Cr-Ti (Fig. 6) differs from

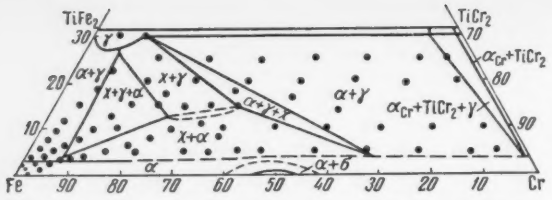

Fig. 5 Isothermal section of system Fe-Cr-Ti, at 550 C

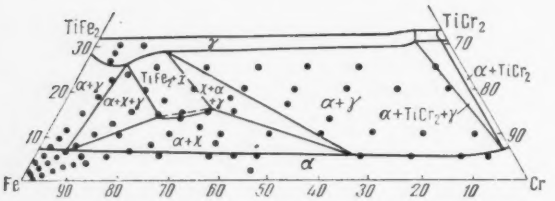

Fig. 6 Isothermal section of system Fe-Cr-Ti, at 1000 C

the section shown in Fig. 5 (at 550 C) by a wider region of α- and γ-solid solutions and by the absence of a σ-phase region.

Conclusions

1 Using microstructural and x-ray analyses, the part of the Fe-Cr-Ti structural diagram adjoining the Fe-Cr side was studied. Alloy hardness was investigated at 1000 and 550 C.

2 An α-Mn type ternary intermetallic compound with a $Ti_5Cr_7Fe_{17}$ composition was revealed in a peritectic reaction of $L + \alpha \rightarrow \chi$, $L + \gamma \rightarrow \chi$. At high temperatures, the $Ti_5Cr_7Fe_{17}$ compound forms a narrow region of solid solutions with α- and γ-phases, which decompose at 1000 and 550 C, with the formation of a Laves phase of $TiFe_2$.

3 The eutectic character was established for crystallization in the region of alloys adjoining the Ti-Fe side for alloys of the $TiFe_2$-Cr section, and the wide region of alloys lying to the right of this section and with higher chromium contents.

4 At 1000 and 550 C, the regions of Fe and Cr base ternary solid solutions are located along the Fe-Cr side. Ti solubility in α-solid solutions, at 1000 C, increases from the Ti-Fe side, on an average of about 5%; it decreases at 550 C.

5 The regions of phase distribution were established at temperatures of 1000 and 550 C.

6 The hardnesses of the examined alloys have maximum values in annealed alloys in the χ-phase region, decreasing with the formation of the $TiFe_2$ compound.

—*Submitted Oct. 5, 1959*

References

1 Kornilov, I. I., *Ferrous Alloys*, vol. 1, Isd-vo AN SSSR M (Publishing House of the Academy of Sciences, USSR, Moscow), 1945.

2 Kornilov, I. I. and Mikheyev, V. V., "A Study of the Transformation of α-Solid Solutions of Iron-Chrome Employing High-Speed Transformation," *Doklady Akad. Nauk SSSR (Proc. Acad. Sci., USSR)*, 1949, vol. 68, no. 3.

3 Masumoto, H., Saito, H. and Sugihara, M., "On the Anomaly of the Specific Heat at High Temperatures in α-Phase Alloys of Iron and Chromium," *Sci. Reps. Res. Insts.*, Tohoku Univ., 1953, vol. A5, no. 3.

4 Bloom, D. S. and Grant, N. I., *J. Metals*, 1951, no. 11.

5 Hansen, M., *Constitution of Binary Alloys*, N. Y.-Toronto-London, 1958.

6 Witte, H. and Wallbaum, N. I., "Thermal and X-Ray Diffraction Studies in the Iron-Titanium System," *Z. Metallkunde (Metallurgy J.)*, 1938, Bd. 30

7 Duwez, P. and Taylor, J. L., "The Structure of Intermediate Phases in Alloys of Titanium with Iron, Cobalt and Nickel," *J. Metals*, 1950, vol. 188, p. 1173.

8 Kornilov, I. I. and Boriskina, N. G., "Ti-Fe Structural Diagram," *Doklady Akad. Nauk SSSR (Proc. Acad. Sci., USSR)*, 1956, vol. 108, no. 6.

9 Golubtsova, P. B., "A Study of the Metallic Compound Formed in Fe-Ti Alloys," *Doklady Akad. Nauk SSSR (Proc. Acad. Sci., USSR)*, 1958, vol. 118, no. 1.

10 Roe, W. P. and Fishel, W. P., "Gamma Loop Studies in the Iron-Titanium, Iron-Chromium and Iron-Titanium-Chromium Systems," Trans. Amer. Soc. Metals, 1952, vol. 44, p. 1030.

11 McQuillan, M. K., "A Provisional Constitutional Diagram of the Chromium-Titanium Systems," *J. Inst. of Metals*, 1951, vol. 79, p. 379.

12 Duwez, P. and Taylor, J. K., "A Partial Titanium-Chromium Phase Diagram and the Crystal Structure of $TiCr_2$," Trans. Amer. Soc. Metals, 1952, vol. 44, p. 495.

13 Lewinger, B. W., "High Temperature Modification of $TiCr_2$," Trans. Amer. Inst. Min. Metall. Engrs., 1953, vol. 197, p. 196.

14 Kornilov, I. I., Mikheyev, V. S. and Chernova, T. S., "Ti-Cr Structural Diagram," *Tr. In-ta Metallurgii im. A. A. Baykova AN SSSR, vyp. II, Izd-vo AN SSSR, M (Trans. A. A. Baykov Inst. of Metallurgy, Acad. Sci., USSR)*, no. II, Pub. Acad. Sci., USSR, Moscow, 1957.

15 Vogel, R. and Wendrott, B., "The Fe-Fe_2Ti-Cr_2Ti-Cr Diagram," *Arch. Eisenhottenwesen*, 1940, Bd. 14, p. 279.

16 Boriskina, N. G. and Kornilov, I. I., "Ternary Metallic Compounds in the System Fe-Cr-Ti," *Zh. Neorganich. Khim. (J. Inorganic Chemistry)*, 1959, vol. IV, no. 2.

Reviewer's Comment

The authors have investigated a rather limited area of the titanium-iron-chromium ternary at temperatures of 1000 and 550 C. All alloys studied were in the region containing less than 30 atomic % titanium. A detailed study of the three binaries is now being made.

Materials used were of fair purity and random chemical analyses were used. The alloys were arc melted, encapsulation annealed, and examined by hardness, microstructure and x-ray diffraction. A newly reported compound (χ) corresponding to $Ti_5Cr_7Fe_{17}$ is said to have the α-Mn structure. This intermetallic compound is the result of a peritectic reaction at a high temperature (not reported) and decomposes at lower temperatures (not reported) with the formation of a $TiFe_2$ Laves phase.

Titanium solubility in the iron and chromium terminal solid solutions was determined at 550 and 1000 C. (These results are reported rather vaguely.)

Hardness data for some of the alloys are reported with the main point of interest being the high maximum value in the χ-phase (α-Mn structure).

—E. C. VAN REUTH
Department of Metallurgy
University of Illinois

Radiation Measurements During the Flight of the Second Cosmic Rocket

S. N. VERNOV,
A. E. CHUDAKOV,
P. V. VAKULOV,
YU. I. LOGACHEV
and A. G. NIKOLAEV

THE INSTRUMENTATION for measurement of radiation aboard the second Soviet cosmic rocket launched to the moon on Sept. 12, 1959 was installed with the objective of obtaining new data on the outer radiation belt of Earth, recording the radiation of cosmic rays along the path from Earth to the moon, and searching for a possible radiation belt of the moon.

The number of instruments and the measurement scope were increased in comparison to the first cosmic rocket (1).[1] In addition, some of the radiation recording instruments were mounted outside the hermetically sealed container (at a distance of 56 cm from its surface), which considerably reduced the shielding of these instruments by other apparatus.

The entire instrumentation consisted of six gas discharge counters and three scintillation detectors.

Mounted inside the container were the following instruments:

1 Scintillation counter *A* (a detector consisting of a cylindrical crystal of sodium iodide, having a diameter of 39.5 mm and a height of 40 mm). This instrument recorded the entire ionization produced by the ionizing radiation in the crystal and the counting rate corresponding to the different energy outputs in the crystal: Over 60 kev (threshold I); over 600 kev (threshold II) and over 3.5 mev (threshold III).

2 Gas discharge counter No. 4, having a diameter of 1 cm and a length of 5 cm, surrounded by a supplementary copper shield 1.5-mm thick.

3 Gas discharge counter No. 5, having a diameter of 1 cm and a length of 5 cm, surrounded by supplementary shields of lead 3-mm thick and of aluminum 1-mm thick.

These three instruments were covered by a 1-gm per cm² thick aluminum envelope. Also, approximately 20% of the entire solid angle was covered with material with a thickness of 10 gm per cm².

Mounted outside the container were the following instruments:

4 Scintillation counter *B* (a detector consisting of a cylindrical crystal of sodium iodide having a diameter of 39 mm and a height of 40 mm). This instrument recorded the entire ionization produced in the crystal; the rate of impulse counting corresponded to the different energy levels in the crystal: Over 45 kev (threshold I) and over 450 kev (threshold II). The crystal of this counter was shielded with a layer of aluminum 1-gm per cm² thick, and only 5% of the entire solid angle was covered with a larger amount of material (up to 10 gm per cm²).

5 Scintillation counter *V* (a detector consisting of a crystal of cesium iodide 3-mm thick, having a diameter of 30 mm, covered on the side of the open space with an aluminum coating 1.2-mg per cm² thick). This instrument recorded the total ionization produced in the crystal.

6 Gas discharge counter No. 1, encased in a lead shield 3-mm thick and an aluminum shield 1-mm thick, with a window having an area of 0.28 cm².

7 Gas discharge counter No. 2, encased in a similar shield and with a window having an area of 1.6 cm² covered by copper foil 0.2 mm-thick.

8 Gas discharge counter No. 3, encased in a similar shield with a window having an area of 1.6 cm² covered by aluminum foil 0.7-mm thick.

The wall thicknesses of all counter housings were 50 mg per cm² of stainless steel. Counters Nos. 2 and 3 operated only in the high intensity range. Outside the high intensity range, the corresponding telemetry channels were used to transmit information concerning the counting rate of scintillation counter *B* (thresholds I and II).

The indicated change in the measurement program was carried out at a certain radiation intensity. An additional counter (without supplementary shield) serving this purpose was installed inside the container. The switching took place when the rate of this counter reached about 500 pulses per second.

Electronic design of all instruments was based on the use of semiconductors. The resolving time of the scalar layouts and discriminators was 10^{-5} sec.

This article describes partial conclusions based on a preliminary evaluation of measurements in the flight intervals 8 to 120 km $\times 10^3$ from the center of Earth, and in the lunar area, beginning with 40 km $\times 10^3$ from the surface of the moon.

Data on the Spatial Distribution of the Outer Radiation Belt

Fig. 1 shows the trajectories of the first and second cosmic rocket with respect to Earth's magnetic field and results of ionization measurement.

The rocket trajectories differ only slightly from each other. The track of the second cosmic rocket passes the zone of high intensity 200 to 300 km closer to the plane of the geomagnetic equator than the track of the first rocket. The indicated shift of trajectory cannot be responsible for the change in form and the displacement of the maximum of the curve describing the dependence of the intensity upon the altitude of the flight; it only increases this difference.

The overall picture of the deformation of the high intensity zone on September 12 relative to its position on Jan. 2, 1959 is reduced to a displacement of the zone in the direction of the inner regions of the magnetic field.

The maximum intensity was observed on September 12 at a distance of 17,000 km from Earth's center on the 59 deg line of force[2]; on January 2 the maximum intensity was recorded at a distance of 27,000 km (on the 63 deg line of force).

What are the reasons for the observed deformation of the outer radiation belt? It should be noted that the flights of the first and second cosmic rockets followed trajectories quite close with respect to geographic coordinates, but basically

Translated from *Artificial Earth Satellites*, 1960, no. 5, pp. 24–29. Translated by Research Information Service, New York.

[1] Numbers in parentheses indicate References at end of paper.

[2] The line of force is denoted by the geomagnetic latitude at which it intersects Earth's surface.

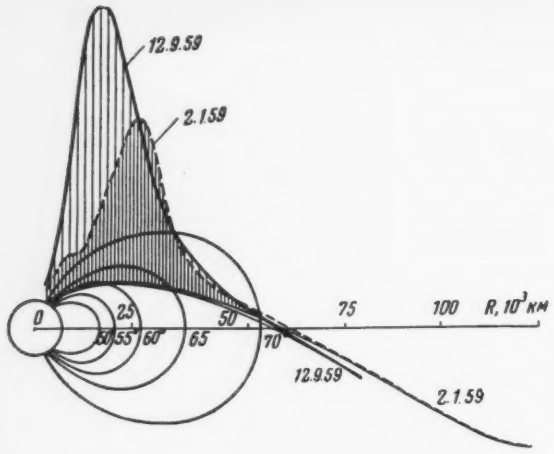

Fig. 1 Trajectories of the first and second cosmic rockets with respect to Earth's magnetic field

Lengths of vertical lines resting on the trajectories are proportional to the radiation intensity at a given point of the trajectory. Shown are the magnetic lines of force crossing Earth's surface at the geomagnetic latitudes of 50, 55, 60, 65 and 70 deg (the magnetic field has been approximated by a dipole field with the following coordinates in the geomagnetic pole: Latitude 78.5 deg and longitude 67 deg)

different with respect to their orientation toward the sun, which could have produced a systematic deformation of Earth's magnetic field. It is more likely, however, that the deformations of the outer radiation belt are connected with the varying character of solar corpuscular streams, and accordingly with the varying nature of particle injection into the high intensity zone. The variation in the energy spectrum of particles observed in the January 2 and September 12 experiments indicates this, as well as the comparison between the overall intensity rate and the data obtained during the flight of the American rocket "Pioneer III" (2).

In the latter case, the direction of the flight trajectory with respect to the sun was close to the trajectory of the first Soviet cosmic rocket. However, the maximum intensity was recorded at a distance of 22,000 km from Earth's center on a line of force of 57 deg, which is in better accord with the flight data of the second than the first rocket. In this connection, it may be assumed that the data from the second rocket give a more typical picture of the location of the outer radiation belt.

Composition of the Radiation in the Outer Radiation Belt of Earth

Readings of certain instruments of the second cosmic rocket, relating to the distance to Earth's center are given in Fig. 2.

The counting rate of the scintillation detector with a threshold of 3.5 mev (curve 1) confirms with much greater accuracy (than does the first rocket) that particles in the range of several gm per cm^2 do not exist in the outer belt. A small increase in the count (by 30%) in the region of the maximum may also possibly be explained in this case as the superposition of impulses of a smaller amplitude.

Thus, the flux of electrons with an energy greater than 5 mev (or of protons with an energy greater than 30 mev) constitute less than 1 particle$\cdot cm^{-2} \cdot sec^{-1}$ even in the zone maximum.

Essentially, the new results are from observations of gas discharge counters Nos. 4 and 5 located inside the container and shielded by additional filters made of copper and lead (curves 2 and 3). The data of the scintillation detector with a threshold of 3.5 mev show that an increase of the rates in counters Nos. 4 and 5 cannot be caused by charged particles penetrating the casing of the container. This means that both counters register photons. Inasmuch as the counting intensity in counters Nos. 4 and 5 differs only by a multiple of one and a half, a relatively high energy (over 400 kev) must be attributed to these photons.

In principle, the appearance of photons of the observable energy can be explained by two reasons:

1 X-ray radiation of electrons with an energy of 2 to 3 mev; it should be noted that the permissible energy interval for decelerating electrons is quite narrow.

2 Induced radioactivity originating in the casing of the container during proton bombardment with an energy of the order of 10 mev. In the same manner as with electrons, the spectrum of these protons is sharply interrupted on the high energy side (protons with an energy higher than 30 mev are practically absent).

The first reason seems to be more probable at this moment. However, in this case the energy spectrum of the particles (electrons) proves to be extremely surprising. The estimate of the flux of electrons with an energy of the order of 2 mev in the region of maximum intensity, based on the readings of counters Nos. 4 and 5, amounts to 5×10^8 particles$\cdot cm^{-2} \cdot sec^{-1}$; the flux of electrons in the energy range 0.1 to 1 mev is of the same order or less; the flux of electrons with an energy over 5 mev is less than 1 particle$\cdot cm^{-2} \cdot sec^{-1}$, as mentioned before. At the same time, tests on the first cosmic rocket disclosed quite a large flux of electrons with an energy of 20 to 50 kev (10^{10} particles $\times$ $cm^{-2} \cdot sec^{-1}$). This soft part of the spectrum has also been detected by scintillation counters on the periphery of the zone in the experiment with the second cosmic rocket. In the area of the maximum, it is less pronounced than it was on January 2, but still contributes noticeably to the output of counter No. 1 (curve 4).

Thus, data have been obtained concerning the existence of two separate particle groups: Electrons with an energy of about 20 kev and electrons with an energy of the order of 10 mev. It seems that the formation mechanism of both groups is basically different. The energy of the particles of the first group is close to the average energy for protons of solar corpuscular streams, and this leads us to assume that a thermodynamic equilibrium is reached between protons and electrons in the course of their penetration into Earth's magnetic field. On the other hand, the formation of the second group is apparently due to processes which are not in equilibrium. It appears that the electron impulses of the second group are, with respect to their magnitudes, close to the proton impulses of corpuscular streams.

Search for an Increased Radiation Belt Near the Moon

When approaching the moon, up to a distance of 1000 km from its surface, no increase in radiation exceeding the cosmic background by more than 10% was noted. It is difficult to obtain data in the range 0 to 1000 km from the surface of the moon because of the short duration of the flight in this region, but no substantial increase of intensity was discovered at these altitudes.

If the intensity of emission in a hypothetical lunar radiation belt is compared with the maximum intensity of the outer belt of Earth, based on readings of the most sensitive (for soft radiation) detectors—scintillation counters—then for distances above 1000 km the relation of intensities is 10^{-6} or less, and for distances of 0 to 1000 km the relation of intensities is 10^{-4} or less. Thus, it can be said that a lunar radiation belt is practically nonexistent.

If it is assumed that the existence of an outer radiation belt and the intensity of particles in it are determined by the in-

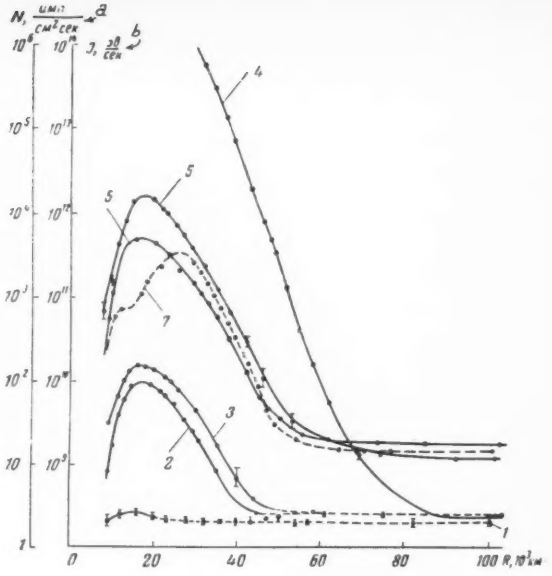

Fig. 2 Radiation intensity as a function of the distance to Earth's center. [a]N, pulses per cm²sec; [b]E, ev per sec

Values for the ionization in the crystal (ev·sec^{-1}) and counting rates of counters per unit area of the cross section are plotted on the vertical axis. For counter No. 1 during measurement inside the zone, only the window area was considered. 1: Counting rate of the scintillation detector A (threshold III); 2: Counting rate of counter No. 4 (shield 1.5-mm copper, inside the container); 3: Counting rate of counter No. 5 (shield 3-mm lead and 1-mm aluminum, inside the container); 4: Counting rate of counter No. 1 (window thickness 0.2 mm aluminum, outside the container); 5: Ionization in crystal A; 6: Ionization in crystal B; 7: Ionization in the crystal based on data of the first cosmic rocket

tensity of the magnetic field, then the intensity of the terrestrial magnetic field at the boundary of the upper belt determines the upper limit for the magnetic field on the surface of the moon. This limit is 10^{-3} of the field at Earth's surface.

Measurement of the Intensity of Cosmic Rays

After leaving the outer radiation belt of Earth, beginning with a distance of 70,000 km from Earth and on the lunar section, a steady intensity was recorded by all instruments. The mounting of certain instruments outside the container gave a perceptible result in the sense of a decrease in the input of the secondary radiation resulting from the action of cosmic rays on the material surrounding the instrument. Fig. 2 shows the results of ionization measurement inside the container (curve 5) and outside of the container (curve 6).

Inside the radiation belt curve 6 extends noticeably higher than curve 5, which can be explained by absorption of a comparatively soft radiation. The effect outside the zone of soft radiation as was expected is reversed.

An analogous result has been obtained with other parameters. The summary of the measurement data for various radiation components carried out on the first and second cosmic rockets is given in Table 1.

The data obtained are in good agreement. The most accurate data on the intensity of the primary cosmic rays are given on the bottom line of the table (instruments outside of the container).

References

1 Vernov, S. N., Chudakov, A. E., Vakulov, P. V. and Logachev, Yu. I., Proc. Acad. Sci. USSR, 1959, vol. 125, p. 304.
2 Van Allen, J. A. and Frank, L. A., *Nature*, 1959, vol. 183, p. 430.

Table 1[a]

Date	Location of instrument	Gas discharge intensity counters, particles·cm^{-2}·sec^{-1}	Scintillation counters — Threshold energy	Scintillation counters — Intensity[e]	Ionization in an NaI crystal weighing 180 gm, 10^9 ev·sec^{-1}
1/2/59	inside the container	2.3 ± 0.1	4.5 mev 450 kev 45 kev	1.9 ± 0.1 3.0 ± 0.15 6.75 ± 0.3	1.42 ± 0.05
9/12/59	inside the container	2.46 ± 0.1[b]	3.5 mev 600 kev	2.12 ± 0.1 2.77 ± 0.15	1.55 ± 0.05
		2.46 ± 0.1[c]	60 kev	6.7 ± 0.3	
9/12/59	outside the container	1.98 ± 0.1[d]	450 kev	2.02 ± 0.1	1.15 ± 0.05

[a] Errors indicate the maximum scattering in the detector area.
[b] Counter with a supplementary shield 1.5 Cu.
[c] Counter with a supplementary shield 3 mm Pb.
[d] Counter with a supplementary shield 3 mm Pb.
[e] Noted are the number of impulses per second related to a unit area of the crystal (19 cm²).

Reviewer's Comment

The results reported in this paper are of considerable interest for several reasons. Instrumentally, the large variety of detectors and shields permits a detailed examination of energy spectra. Also, the fact that three Geiger counters and two scintillators were located *outside* the vehicle so that only 10% of the solid angle was observed by the mass of the spacecraft, is a great improvement in evaluating fluxes in space.

The observation that there is no increase in counting rate in the neighborhood of the moon is, of course, of great importance. The authors are able to infer from this that the magnetic field around the moon cannot exceed 10 γ.

The authors also comment on the large fluctuations observed in the outer Van Allen belt. This is quite in accord with the results (1) of Explorer VII, although that vehicle was constrained to lower altitudes. The instruments on board that satellite were rather similar to those flown on the second cosmic rocket in that several differently shielded Geiger counters were incorporated. The instruments flown (2,3) on Pioneer V to an altitude of 15,000,000 miles had a somewhat higher cutoff energy than those on this rocket.

The most surprising result is the observation of a large flux (5×10^5 cm^{-2} sec^{-1}) of electrons in the outer belt with energies of the order of 2 mev. This conclusion is based by the authors on the measurement of energetic photons. It should perhaps be noted that this result is in disagreement with other measurements. For example, Walt et al. have found (4) no electrons with energies greater than 0.78 mev, at least at the lower edge of the outer belt. Although it is, of course, possible that this situation changes with altitude, it would seem difficult to reconcile so large a discrepancy. This measurement is of great importance in evaluating the various theories concerning the origin of the belts.

—Robert C. Hayme
Department of Physic
New York University

1 Van Allen, J. A. and Lin, W. C., *J. Geophys. Res.*, 1960, vol. 65, p 2998.
2 Fan, C. Y., Meyer, P. and Simpson, J. A., *J. Geophys. Res.*, 1960, vol 65, p. 1862.
3 Arnoldy, R. L., Hoffman, R. A. and Winckler, J. R., *J. Geophys. Res.*, 1960, vol. 65, p. 3004.
4 Walt, M., Chase, L., Cladis, J., Imhof, W. and Kneebt, D., *First International Space Science Symposium*, North Holland Publishing Co., Amsterdam, 1960.

Connection Between the Motion of Matter in the Corona and the Prominences

M. G. KARIMOV and
N. S. SHILOVA

1. Observational Data

THIS paper deals with the investigation of the motions of coronal matter as revealed by emission line 6374 Å and that of prominences (H_α line). In both cases the investigation was carried out from the same position angle and at the same distance from the surface of the sun.

Data was obtained daily in the form of spectrograms from a coronograph at the corona observation station of the Astrophysical Institute of the Academy of Sciences of Kazakh SSR. The layout of the diffraction spectrograph has been shown elsewhere (1).[1] The dispersion of the spectrograph is 10 Å per mm in the wave length band under consideration, and a grating of the third order was utilized. The film contained 10 frames of sentinel rounds of the sun. On each individual frame the 6374.5 Å line of the corona and the H_α line of the prominence emission were taken. This simultaneous photographing of the H_α and 6374.51 Å line insured uniform exposure and development. A microphotometer MF 2 with a magnification of 30 × and a slot width of 0.3 mm was used for the photometric work. Profiles of the H_α lines, the 6374 Å line and also of a series of Fraunhofer lines adjacent to the studied lines were plotted.

To determine the Doppler shift, three or four Fraunhofer lines with longer or shorter wave lengths than the lines under investigation were used. Dispersion equations were developed to determine the wave length of the line being observed. The dispersion equations were arrived at arithmetically without resorting to the method of least squares. Fig. 1 shows a photometric cross section of the region near the red line of the corona. The distances X_1 and X_2 were measured; with the wave length known, the number of Angstroms per mm $\Delta\lambda/\Delta X$ could be determined. In the case of Fig. 1, $\Delta\lambda/\Delta X$ was equal to 0.1 Å per mm for one set of Fraunhofer lines and 0.1 Å per mm for another. If the values did not coincide, an average would have been taken. The distance of the line being investigated from one of the reference lines, e.g., from line 6380.75 Å, is $X_2 = 66$ mm, which corresponds to a wave length interval of 6.6 Å. Thus the wave length being observed is 6380.75 Å − 6.6 Å = 6374.15 Å, and the Doppler shift in the violet direction is 0.36 Å.

Then, the shifts were converted into speeds in sight line direction in accordance with the known equation

$$V = c(\Delta\lambda/\lambda)$$

An analogous computation was made for H_α.

Considering the inadequate dispersion (10 Å per mm) for measurement of a displacement of the order of 0.1 Å, a statistical method was used. Sixty-three spectra were measured; on each of these both the outline of the H_α line and the 6374.51 Å line, as well as of the Fraunhofer lines, were measured. The latter were used to increase the accuracy of the determination of the center of the absorption lines, and, thus, also of the distances between them.

Translated from *Bulletin of the Astrophysical Institute, Academy of Sciences, Kazakh SSR*, 1959, vol. 9, pp. 10–20. Translated by Research Information Service, New York.

[1] Numbers in parentheses indicate References at end of paper.

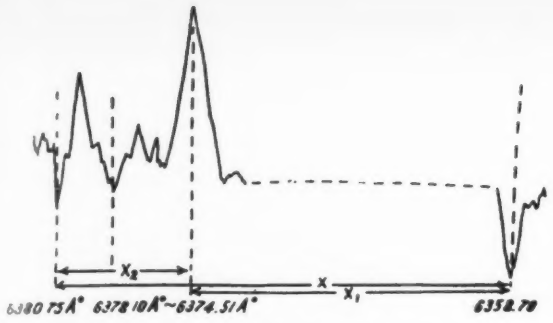

Fig. 1 **Determination of V_{radial} in the region of coronal line 6374.51 Å**

Speeds of the red corona line and of prominences in the H_α line are given in Tables 1 and 2.

The tables reveal numerical values as well as certain relationships of the speeds. For the 63 cases the following were obtained:

a Average speed of prominence matter in the line of sight is $V_{prom} = 31 \pm 5$ km per sec.

b Average speed of ions FeX of the corona in sight line is $V_{cor} = 12 \pm 3$ km per sec.

In this study in eight out of 63 cases, V_{cor} was larger than V_{prom}. Most frequently V_{cor} was smaller than V_{prom} by a considerable margin: $V_{cor} = 12 \pm 3$ km per sec, $V_{prom} = 31 \pm 5$ km per sec, $V_{cor}/V_{prom} = 0.39 \pm 0.11$ km per sec.

Table 1

Date	Position angle, deg	Prominence speed, km per sec	Corona speed, km per sec
8/28/56	277	49	11
10/18/56	92	4	13
2/3/57	255	25	2
2/28/57	220	−26	−4
2/28/57	85	34	9
3/3/57	82	71	19
9/11/57	47	13	−4
9/19/57	260	29	−9
10/20/57	87	115	−1
12/1/57	245	−5	−95
12/2/57	87	−64	8
2/8/58	25	16	4
	53	13	13
	252	−1	−5
2/11/58	2	20	12
2/11/58	235	−14	−8
2/21/58	37	14	0
2/24/58	242	24	3
2/28/58	248	−24	−10
6/2/58	62	91	9
6/2/58	244	46	1
6/5/58	247	46	21
6/6/58	250	−2	−11
6/8/58	13	20	0
6/23/58	65	204	6
6/23/58	217	−24	9
8/15/58	90	70	0
	265	70	−8
	287	35	15
9/4/58	50	15	22
9/7/58	297	17	32

Table 2

Date	Position angle, deg	Doppler speeds in the corona line 6374 Å km per sec		
		In position angle P	In position angle $>P$	In position angle $<P$
4/29/56	37	−14	107	−4
7/28/56	277	11	−16	12
10/18/56	92	13	−12	−37
2/3/57	255	1	−8	6
2/28/57	85	9	25	27
2/28/57	220	−4	−8	−12
3/3/57	82	19	24	7
9/19/57	260	9	−13	12
12/1/57	245	−95	0	−11
12/2/57	87	8	line missing	0
1/15/58	35	−3	4	−6
2/8/58	25	4	−4	−4
2/8/58	215	−5	−7	16
2/11/58	02	12	4	−6
2/11/58	235	8	line missing	−6
2/20/58	225	−1	1	line missing
2/21/58	37	0	6	−13
2/28/58	248	−10	9	−76
6/2/58	62	9	line missing	15
6/5/58	247	21	8	−13
6/6/58	250	−11	−11	−6
6/8/58	13	0	line missing	−4
6/23/58	217	9	14	−13
7/23/58	65	6	line missing	line missing
8/15/58	90	0	−81	0
8/15/58	287	15	−4	−6
9/4/58	50	22	2	3
9/7/58	297	32	−1	73

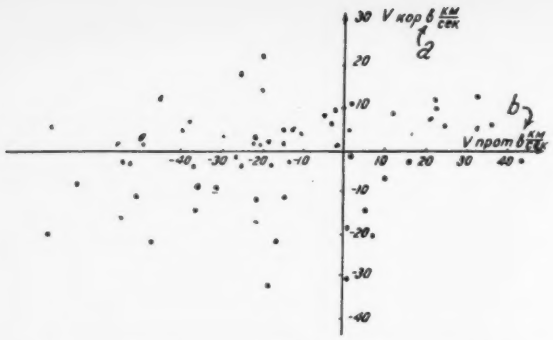

Fig. 2 Graph of the relationship of speed of corona and prominence. [a]V_{cor}, km per sec; [b]V_{prom}, km per sec

It is interesting to note that with

$$\frac{V_{cor}}{V_{prom}} \leq 0.5 \text{ then } \overline{\frac{V_{cor}}{V_{prom}}} = 0.17$$

with

$$\frac{V_{cor}}{V_{prom}} \geq 0.5 \text{ then } \overline{\frac{V_{cor}}{V_{prom}}} = 0.74$$

The directions of corona and prominence matter motion have a tendency to coincide. However, in 25 out of 63 cases they were found to be opposite. The numerical values are as follows:

For motions in the same direction

V_{prom} = 33 km per sec $\quad$ V_{cor} = 16 km per sec

For motions in the opposite directions

V_{prom} = 29 km per sec $\quad$ V_{cor} = 7 km per sec

Let us note that in the case of movement of prominences and of the corona in opposite directions, the speed of the corona is less than half of its speed when moving into the same direction as the prominences. A graph was plotted to show the dependence of the speed of the corona upon the speed of the prominence (Fig. 2). This graph can be represented by a straight line, parallel to the abscissa. The graph in our opinion indicates that the speeds of the prominence exceed approximately three times the coronal speeds, although Newkirk (2), for example, is of the opinion that in a similar graph [(2), Fig. 4] one can observe a definite relationship of the form

$$\sigma \leq V_{cor} \leq V_{prom} + \sigma \text{ when } V_{prom} \geq 0$$

$$-\sigma \geq V_{cor} \geq V_{prom} - \sigma \text{ when } V_{prom} \leq 0$$

where σ = 7 km per sec. In addition, the following quantitative data was obtained by the same author

$$V_{prom} = 34 \text{ km per sec}$$

$$V_{cor} = 14 \text{ km per sec}$$

$$V_{cor}/V_{prom} = 0.33$$

if

$$\frac{V_{cor}}{V_{prom}} \leq 0.5 \text{ then } \overline{\frac{V_{cor}}{V_{prom}}} = 0.1$$

if

$$\frac{V_{cor}}{V_{prom}} \geq 0.5 \text{ then } \overline{\frac{V_{cor}}{V_{prom}}} = 1$$

These relationships are close to values obtained by us in the 63 cases. Newkirk, however, asserts that the direction of motion of the corona and prominence, located on the same position angle, will invariably coincide. Our observational data do not confirm this viewpoint.

In order to clarify the problem of whether prominences have any effect on the direction of motion of the corona, classification of prominences was undertaken. The "prominence charts" published by the Pic du Midi Observatory, the bulletin *Solar Data* of the Academy of Sciences USSR, and prominence observations by the corona station of the Astrophysical Institute of the Academy of Sciences of Kazakh SSR were used for this purpose. The results are given in Tables 3 and 4. Table 3 contains data on prominences with corona and prominence matter moving in opposite directions; Table 4 contains data on corona and prominences with the same direction. It may be inferred from these tables that prominences moving in opposite directions have a low intensity (only four out of 16 reach intensity 3), are mostly calm (12 out of 18 are calm), and rise to smaller heights. If one disregards the obviously anomalous occurrences of Feb. 10, 1958 at the position angle of 2 deg and of June 23, 1958 at the position angle of 45 deg, then the average height of the prominences equals 2.71 × 10^4 km, and, taking the

Table 3

Date	Position angle, deg	Prominence intensity in three-point scale	Height of prominence 10^4km	Appearance of prominence
4/30/57	35	2	1.53	calm
10/20/57	87	1	2.00	eruption from calm
1/15/58	35	2	1.53	calm
1/23/58	260	1	3.82	interacting
1/23/58	40	2	4.52	calm-active
2/8/58	215	3	2.29	calm
2/10/58	2		6.05	eruptive
	55	1-2	1.99	calm
	235		3.82	eruptive
	297	2	1.53	eruption from calm
2/11/58	47	1	3.06	interacting close to calm
2/11/58	240	3	2.17	calm
2/20/58	255	2	3.82	active
6/2/58	37	1	2.90	calm
6/6/58	35	1-2	3.06	calm
6/23/58	47	3	2.29	calm
7/23/58	45	1	11.47	quasi-eruptive
8/15/58	265	3	2.75	calm

Table 4

Date	Position angle, deg	Prominence intensity in three-point scale	Height of prominence 10^4km	Appearance of prominence
3/3/57	82	3	4.59	calm $P = 20$
9/15/57	72	2	6.12	quasi-eruptive
			0.76	eruptive
9/16/57	260	3	2.29	interacting
9/19/57	260		3.63	actively interactive
12/1/57	245		1.53	interacting of spot type
12/2/57	87	1	4.59	active
1/23/58	215		3.63	quasi-eruptive
2/8/58	25	3	6.58	calm-active
	53	3	1.53	interacting
	252	3	3.82	calm
2/9/58	27	2–3	7.65	quasi-eruptive
2/9/58	60	1–2	ejection to 3.82 calm to 1.53	ejection from calm
2/10/58	200	2	3.06	quasi-eruptive
2/24/58	242	3	4.29	calm
6/2/58	62	3	3.06	calm
6/2/58	244	2	1.53	calm
6/5/58	247	2–3	5.35	active-calm
6/6/58	250	3	5.05	quasi-eruptive
6/8/58	13	1	3.82	calm $P = 20$
6/23/58	65	3	1.22	active
8/15/58	90	3	3.06	active
8/15/58	287	2	4.59	actively interactive
9/4/58	50	1	4.59	tornado
9/7/58	297	3	base to 1.53 eruption to 13.77	eruption from calm
9/27/58	295	2	6.12	corona type sun spots

anomalous prominences into consideration, their height reaches 3.3×10^4 km.

When the directions of motion of corona and prominences coincide, prominences of high intensity can be observed (only three out of 23 have an intensity of 1 in the three-point scale). They are of the most diverse appearance (only nine out of 25 are calm), and rise higher than prominences discussed in the preceding case (average height 4.29×10^4 km). The conclusions drawn from such observations are discussed in the following.

In order to investigate the variation of Doppler speeds of the corona and prominences in relation to the position angle, graphs were plotted as shown in Fig. 3.

Dashed lines on the graph indicate the location of the base line, and arrows, the observed shifts. Two arrows placed one under the other next to each of the dashed lines correspond to speeds of space regions separated by a distance of 70,000 km measured along the limb. A gradual two- to threefold increase in velocity (along the sight line) of the corona substance, a change from a positive to a negative velocity (Fig. 3a) and, though not as frequently observed, a double change in direction (Fig. 3b), are possible between two points 140,000 km apart, as indicated on the graphs. Thus, the scale of macroscopic eddies in the corona is larger than 70,000 km. The presence of a prominence does not cause an increase in the velocity of the corona located at the same position angle in the direction of prominence (e.g., the phenomenon observed on Oct. 16, 1958).

Since the position angle for each photographic section was known, it was possible to establish the section of the chromosphere and photosphere (by degree of activity) over which the emitting region of the corona was located. For this purpose synoptic charts of the Pic du Midi Solar Observatory and the bulletin *Solar Data* of the Academy of Sciences USSR for the years 1956, 1957 and 1958 were utilized. Investigation showed that in 65% of all cases, floccules, filaments and spots corresponded to corona radiation as well as prominences. Floccules are found more frequently. This confirms the belief that the flare marks the location of the disturbed regions in the sun (3), and, consequently, also of the floccules, as a formation most closely connected with the flare.

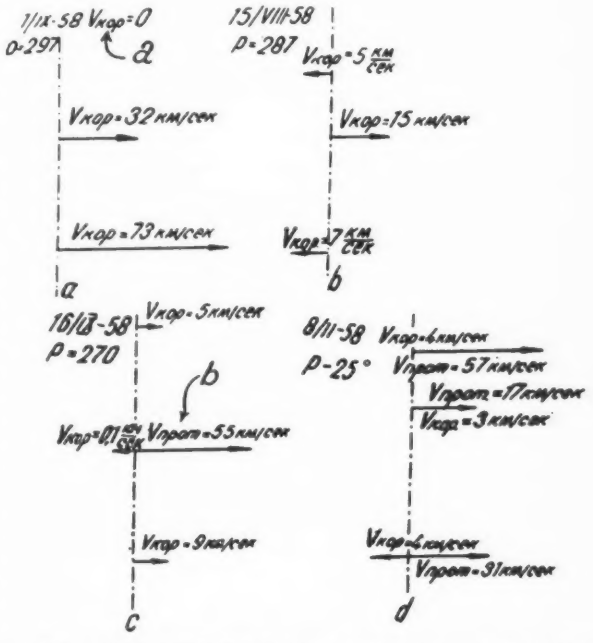

Fig. 3 Doppler velocities of corona and prominences at adjacent position angles. [a]cor; [b]prom

In Table 1 prominences with extremely high velocities are shown: 115 km per sec over a floccule of the second magnitude, and 204 km per sec over a complex formation which included floccules of the first magnitude, inside of which seven small flares occurred. This means that the activity of seats of disturbance located in the lower chromosphere and photosphere influences the speed of the prominences. However, statistical computations did not indicate a speed increase of the corona over active regions of the photosphere and lower chromosphere. When the corona and the prominences have velocities of opposite sign, a certain effect is observed: The speed of prominences changes from 42 to 25 km per sec above active formations or without them, respectively, the speed of the corona being from 5 to 9 km per sec.

There are different opinions regarding the intensification of weakening of the corona near prominences. For instance, Becker (4) thinks that the coronal matter must flow into the prominence, thus lowering the intensity of the coronal luminescence. Pikel'ner (5) is of a contrary opinion with regard to the behavior of the coronal matter in regard to the prominence.

In our investigation, the intensity of the luminescence of the "red" corona was measured by the half width of the 6374.5 Å line. Actually, as seen in approximately 200 plotted cross sections, the half width changes almost proportionally with the intensity of the line. Cross sections of lines are shown in Fig. 4. If half width of line 6374.51 Å is set to equal unity in a section located at the same position angle as the prominence, then in 66 out of 100 cases the half width at the adjacent position angle becomes less than unity. Thus, according to the statistical data, near the prominence an increase, rather than a decrease, in the coronal luminescence of line 6374.51 Å is more likely. As is known, this is confirmed by the existence of dome-shaped envelopes and high powered radiation over the prominences (6). The presence of prominences substantially changes the half width of the red line of luminescence of the neighboring coronal region. This, however, does not apply to the influence of active regions of the photosphere and lower chromosphere on the corona. As our computations showed, the half width of line 6374.51 Å is, on the average, the same over floccules, spots and filaments as it is outside of them.

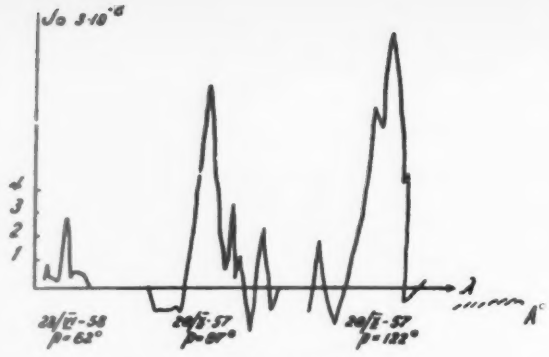

Fig. 4 Cross section of line 6374.51 Å

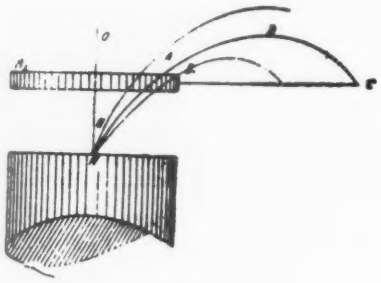

Fig. 5

2. Some Considerations Relating to Mechanisms of Interaction Between the Luminescence of the Corona and the Prominences

We have established the following:

1 The prominences and the corona most frequently move in the same direction.

2 $V_{cor}/V_{prom} = 0.39 \pm 0.11$.

3 The intensity of the luminescence of the corona increases near the prominence and does not increase noticeably over the active photosphere and lower chromosphere.

Let us look at certain theoretical hypotheses dealing with the motions in the corona and the chromosphere. One of them states that the change of the overall magnetic field of the sun in the disturbance seats of the chromosphere and photosphere brings about fluctuations of the field up to the coronal region; this hypothesis was advanced by several authors (2,7,8). Coronal matter, as well as chromosphere matter, move along the lines of force formed at the height of the corona. In this way a huge loop is formed, in the interior of which lies the chromosphere, and in the exterior, the corona. Consequently, their matter is most frequently found to move in the same direction. However, our observational data show that in 30 out of 100 cases there are no seats of photosphere activity under the coronal radiation and, at the same time, no decrease in either the shift of the line of the corona or in the half width. Consequently, the observed cases do not point to the existence of a very close relationship between the coronal luminescence and the action of the photosphere. Near the prominences, as already shown, the coronal luminescence has a tendency to increase. Furthermore, during weak, low and calm prominences, the corona does not move in their direction; during strong, active and high prominences, the prominences seem to pull the corona with them. Consequently, the hypothesis that the magnetic field is inherent in the prominence alone (9), as a result of the motion of its conductive matter in the overall field of the sun and spots, is more probable. The influence of the field of low activity prominences is insufficient to direct the turbulent motion of the corona along their lines of force; the field merely decreases the velocity with which the corona moves in the opposite direction. A field of strong and active prominences has the energy to regulate the turbulent motions of the corona, which by themselves reach a sufficient height (10).

Al'fven (9) observed the following model of formation of currents in the prominence: Disk B_1B_2 revolves in a magnetic field around the axis aa parallel to $\mathbf{H}$. A field is formed

$$\mathbf{E} = (1/c)[\mathbf{V} \times \mathbf{H}]$$

pointing in the direction of the radius of the disk. Between points A and B_1 there arises a difference of potential

$$V = \frac{1}{c}\int_A^B [\mathbf{V} \times \mathbf{H}]dS$$

The section of the photosphere B_1C completes the circuit over which the current flows (Fig. 5). The current, in turn, forms a magnetic field in the form of concentric rings which tend to contract. Thus, we can assume that a decrease in the radius of these rings leads to a contraction of coronal elements toward the axis of the current. The density of the corona increases. Apparently, the luminescence of line 6374.51 Å

coincides with the regions of increased density (14) as opposed to line 5302.86 Å, which is most frequently bright in the region of high temperature.

The increase in intensity of the coronal lines near the prominence can be caused by the outflow of matter from it, even if small and of low density (5). Such matter when encountering even a very weak field in the corona (of the order of 10^{-3} oersted) slows down, and after passing this spot again accelerates. Similarly, a region of increased density is formed.

The compression of matter during the contraction of the rings of the magnetic lines of force and the deceleration of the matter flying apart from the prominence can be jointly acting factors. The result of their action is an increase in luminescence of the corona near the prominence.

If we estimate the intensity of the field of the prominence with a known speed in accordance with the familiar equation (11)

$$\frac{H^2}{8\pi} = \frac{1}{2}\rho V^2$$

it turns out to be close to the value obtained, for example, from the motion of nodes in the plane of the plate.

With a density of the prominence $\rho \simeq 2 \cdot 10^{-14}$ gm per cm^3 and a speed of 31 ± 5 km per sec, H changes from 1.4 to 1.8 gauss. In accordance with the motion of the nodes (12), H_{prot} = 3–5 gauss. Consequently, this computation indirectly confirms the motion of matter of the prominence in accordance with the lines of force. A similar estimate of the H corona at maximum radiation density $3 \cdot 10^{-15}$ gm per cm^3 gives only 0.29 gauss.

Newkirk (2) does not offer any explanation as to what causes the speed of the prominences to exceed the speed of the corona, as found in our investigation. However, this fact can be theoretically explained by studying the equation

$$\mathbf{V} = \frac{c^2}{\sigma_0 H^2}\left(\mathbf{\Phi} - \frac{\omega\tau}{H}\,[\mathbf{\Phi} \times \mathbf{H}]\right) \qquad [*]$$

indicated by Pikel'ner (5) on the basis of calculations by Gurevich and Lebedinskiy (13). In the foregoing equation

σ_0 = conductivity along the magnetic field or in the absence of a field
τ = free path
ω = cyclic frequency of rotation of ions in the magnetic field

Eq. [*] is derived by taking into account the action of the ponderomotive force and the hydrodynamic force of the density on the aggregate of ionic particles. It should be noted that by estimating the speed of FeX ions in this manner, we assume at the same time that the effect on their acceleration by coronal protons is relatively small. A subsequent review does not qualitatively alter the relationship: $V_{cor}/V_{prom} < 1$ if the protons increase the speed of FeX ions by not more than four times.

Let us substitute for $\mathbf{\Phi} \times \mathbf{H}$ the simple product $\Phi \cdot H$. Such a substitution is justified, since, on one hand, in this case the motion of the matter takes place along magnetic lines of force coinciding with the line of sight, and, on the other hand, $\mathbf{\Phi}$ is a force composed of the action of the pressure gradient and gravity force, which are perpendicular to the solar surface. Consequently, $\mathbf{\Phi}$ is perpendicular to $\mathbf{H}$.

Let us evaluate the pressure gradient based on the equation of state of the gas

$$\frac{dP}{dz} = -\frac{g\mu}{R}\frac{p}{T}$$

where $R = 8.31 \times 10^7$ erg/mol·deg. At a distance of 40″ from the limb of the sun to which our observations apply

$$\left(\frac{dP}{dz}\right)_{cor} \simeq 10^{-17}\,\frac{\text{dyne}}{\text{cm}^3}$$

As long as the pressure gradient in the upper chromosphere is anomalously small, it can be neglected with respect to the gravity force because of the low accuracy of our estimate of V_{cor} and V_{prom}.

With a prominence density $n_e = 10^{10}\text{cm}^{-3}$, the force of gravity is

$$\Phi_{cor} = 4.55 \cdot 10^{-13}\ \text{gm·cm/sec}^2$$
$$\Phi_{prom} = 4.55 \cdot 10^{-10}\ \text{gm·cm/sec}^2$$

Let us consider the expression

$$\bar{\Phi} - \frac{\omega\tau}{H}\,[\bar{\Phi} \times \bar{H}] = \sqrt{\Phi^2 + \omega^2\tau^2\Phi^2} \qquad [**]$$

In determining $\omega = eH/mc$, let us assume $H \simeq 1$ oersted, which coincides with determinations made by others (12). Then, the second term in Eq. [**] is found to be much larger than the first one, for the corona as well as for the prominence. Then, $\omega_{cor}/\omega_{prom} = 0.2$ if protons are assumed as the ions of the prominence and the ions of the corona—nine times ionized iron.

Starting out from the obtained numerical values of Φ and ω, V_{cor}/V_{prom} can be estimated from Eq. [*]. We obtain finally

$$\frac{V_{cor}}{V_{prom}} = \frac{\omega_{cor} n_{prom} \Phi_{cor}}{n_{cor}\omega_{prom}\Phi_{prom}} = 0.2$$

Thus, the observational data for the speed of the corona and prominences can be explained theoretically on the assumption that the motion of matter of both types takes place along the lines of force of the same magnetic field. This confirms once more the electromagnetic nature of motions of all strata of the solar atmosphere and the closeness of their relationships.

References

1 Karimov, M. G. and Obashev, S. O., *Bulletin of the Astrophysical Institute*, 1957, vol. 5, issue 7.
2 Newkirk, G., *Annals d'astroph.*, 1957, vol. 20, no. 3.
3 Kiepenheuer, K. O., *Atti convegni, Accad. naz. Lincee*, 1953, no. 11.
4 Becker, U., *J. Astrophys.*, 1953, vol. 33, no. 3.
5 Pikel'ner, S. B., *Achievements of Astronomical Sciences*, 1954, vol. 6.
6 Boguslavskaya, E. Ya., *The Structure of the Solar Corona*, MGU, 1950.
7 Billings, D. E., Liebenberg, D. H., Roberts, W. O., *Astronomical J.*, 1953, vol. 58, no. 8.
8 Billings, D. E., *Sky and Telescope*, 1954, vol. XIII, no. 8.
9 Al'fven, G., *Cosmic Electrodynamics*, I.L., 1952.
10 Prokof'eva, I. A., *Bulletin GAO*, 1957, vol. 21, Issue 1, no. 160.
11 Fermi, E., *Phys. Rev.*, 1949, vol. 75, p. 1169.
12 Idlis, G. M., Karimov, M. G., Delone, A. B. and Obashev, C. O., *Izv. Astrophiz. IN-TA*, 1956, vol. II.
13 Gurevich, L. E. and Lebedinskiy, A. I., *Doklady Akad. Nauk SSSR*, 1945, vol. 49, p. 92; *also ZAETF*, 1946, vol. 16, pp. 832–840.
14 Trellis, M., *Supplements aux annals d'astrophisique*, no. 5, p. 81.

Reviewer's Comment

General Significance

Measurements of the velocities of coronal and prominence material can yield information on the mechanisms producing the motions of the solar plasma, since it is possible to observe the velocities of particles of considerably different charge-to-mass ratio. Moreover, measurement of radial velocities insures that real, macroscopic motions of the material are pres-

ent rather than merely the passage of waves of excitation through the medium.

Specific Comments

The authors discuss at some length the significance of several instances of coronal and prominence radial velocities of opposite sign. This observation is contrary to that reported by Newkirk, who found no significant cases of opposed velocities. It is well to remember in evaluating the discrepancy that the low dispersion of the authors' spectrograph (10 Å per mm) and the thermal width of the coronal line ($\backsim$1 Å) lead to an error in V_{cor} of about 10 km per sec.

The error of measurement of the velocity of the narrower Hα line of the prominence is, perhaps, 5 km per sec. An examination of Fig. 2 shows that the majority of the opposed motions cannot be considered as significant when the errors of measurement inherent in V_{cor} and V_{prom} are taken into account. The three or four remaining cases of opposed motion may well be due to the opposed motion of knots of coronal and prominence emission, which are along the same line of sight but which do not coincide in space and have unrelated velocities. With the exception of the significance ascribed to the opposed motions, the results of the authors' observations and of my work are in good agreement.

In their interpretation of the observations, Karimov and Shilova remark that the magnetic field associated with the prominence and not necessarily that of an active region influences the motions of the coronal material. My conclusion was that 92% of the coronal radial velocity regions examined were associated with the appearance of the 5694 Å coronal line. This line appears only over the most active solar regions. None of the coronal radial velocities which I examined occurred with prominences isolated from an active region.

In relation to their discussion of the fact that $V_{prom} > V_{cor}$ it should be pointed out that there may be two modes of motion occurring:

1 Expansions or contractions of the magnetic loop containing the prominence and the coronal material. In this case, both ions are dragged along with the field, and radial velocities measured perpendicularly to the field should show $V_{cor} = V_{prom}$.

2 Flow along the magnetic loop. My conclusion was that in this case $V_{prom} > V_{cor}$.

I do not fully understand the derivation of the basic relation between V_{cor} and V_{prom} made by Karimov and Shilova however, it is of interest to note that if an electromotive force is set up, as the authors show schematically in Fig. 5, the accelerations along the field will be in the ratio

$$\frac{\dot{V}_{cor}}{\dot{V}_{prom}} = \frac{Z_{FeX} m_H}{m_{Fe}} = 0.16$$

This value is close to the ratio of velocities observed and may be evidence for the operation of an electrostatic acceleration mechanism.

—Gordon Newkirk Jr.
High Altitude Observatory
University of Colorado

Numerical Solution of Equations of Finite Differences and Their Application to the Calculation of Orbits of Artificial Earth Satellites

G. P. TARATYNOVA

THIS paper discusses methods of numerical solution of equations of finite differences and their application to the calculation of the orbits of artificial Earth satellites. The development of such methods is required for solving certain problems of celestial mechanics which entail the solution of a system of nonlinear differential equations describing motions for large time periods. These are problems such as determining the lifetime of an artificial satellite, determining the evolution of the satellite's orbit during its lifetime, long range forecasts of the orbits of satellites, etc.

The developed methods are of a general nature and can be applied to calculating a large group of nonlinear oscillating systems.

Translated from *Artificial Earth Satellites*, 1960, no. 4, pp. 56–85. Translated by Astrid Werner, New York.

In the case of an artificial Earth satellite, equations in osculating orbital elements, which as a rule are employed in celestial mechanics, are used as equations of motion.

Earth's atmospheric resistance, deviations of Earth's gravity field as a result of the existence of compression of Earth, and, in certain instances, anomalies of the force of gravity must be taken into account as excitation forces influencing an artificial Earth satellite. The perturbing influence on account of attraction by the sun and the moon is small and, usually, negligible.

The equations of motion of the artificial Earth satellite are nonlinear differential equations, the right-hand sides of which contain small parameters. In the case of studying the motion of an artificial Earth satellite in the presence of basic perturbing forces (atmospheric resistance and deviation of Earth's gravity field), these parameters are the density of the at-

mosphere at a certain fixed altitude and compression of Earth. For zero values of small parameters, the equations of motion are integrated in finite form: The orbit is an ellipse. In the case of small parameters different from zero, the orbit of the artificial Earth satellite is an envelope of a family of osculating ellipses, and the system of equations does not have an analytical solution.

On solving the system of equations in osculating elements in a general case for relatively small time periods, different methods of numerical integration are employed. However, in the case of large time periods (for example, when the satellite completes hundreds and thousands of rotations around Earth), these methods entail rather time-consuming calculations using electronic computers. Actually, variations of the osculating elements for the duration of a period, equal to 2π, is of a fluctuational nature and the step of integration cannot be large.

In this connection, it was first proposed in (1 and 2)[1] to convert from the system of equations in osculating elements of the true anomaly ϑ, or the argument of latitude u, which are usually employed in celestial mechanics, to a system of equations derived by integrating the first system for a period equal to 2π.

The left-hand side of the derived equations are the perturbation values of osculating elements of the orbit for a revolution. Due to the smallness of these perturbations per revolution, the specified works assumed them approximately equal to derivatives of osculating elements for the number of revolutions N, where $N = (\vartheta - \vartheta_0)/2\pi$ or $N = (u - u_0)/2\pi$. Instead of the original system of equations in osculating elements with respect to the true anomaly or argument of latitude, the system of differential equations was integrated with respect to N the number of rotations. The right-hand portions of such equations represent a certain combined system of integrals. This system of integrals can be replaced by a corresponding system of differential equations. In such a case, the solution of the transformed system of equations is reduced to a dicyclic algorithm: External integration over argument N the number of revolutions, and internal integration over the true anomaly ϑ or argument of latitude u for period 2π, that is, over a revolution. The inner integration must be performed every time when computing the right-hand sides of the external system of equations.

The proposed method of dicyclic integration is very efficient when calculating the orbit of artificial Earth satellites. The calculation of typical orbits of artificial satellites was based on integration of the external system of equations over the number of revolutions, the latter being 100. This made it possible, without reducing the accuracy, to obtain values of osculating elements of the orbit for large time periods from relatively simple calculations.

However, the specific method of dicyclic integration is not quite as accurate, for example, as a well-known method of numerical integration of standard differential equations. Actually, replacing the increments of osculating elements for a revolution by derivatives of these elements for the number of revolutions, introduces a systematic error. Obviously, such a systematic error is greater, the smaller the step of integration of the external system of equations. For this reason, for relatively small altitudes when the step of integration of the external system ΔN decreases, the specified method of dicyclic integration is not applicable. Strictly speaking, instead of the specified external system of differential equations, it is necessary to seek a solution for the system of equations of finite differences for the osculating elements of the orbit, the right-hand sides of which represent a certain combined system of integrals.

Further development and application of the methods of numerical solution directly applicable to equations of finite differences completely eliminate the systematic error specified.

Recent literature does not concern itself with the problem of numerical solution of equations of infinite differences of the general form. Exact solutions of certain groups of difference equations of a particular form are known [for example, equations with constant coefficients, with sufficiently simple right-hand sides (3)].

Analogous to the methods of numerical integration of standard differential equations, two methods of numerical solution of the equations of finite differences have been developed: Runge-type methods and Adams-type interpolation methods.

In a limiting case when the small difference for which the difference equation is defined tends to zero and the difference equation itself transforms into a standard differential equation, the derived methods correspond to methods of numerical integration of standard differential equations of the specified type. In this sense, the developed methods of numerical calculation of difference equations can be considered as a generalization of the method of numerical integration of differential equations.

1. Generalization of the Runge Method

We have an equation of first-order finite differences

$$y_{n+1} - y_n = f(x_n, y_n) \qquad (n = 1, 2, \ldots) \qquad [1.1]$$

where

$x_{n+1} = x_n + h$
$f(x,y)$ = function which can be differentiated

Let us assume that Eq. 1.1 satisfies the initial condition for $x = x_0$, $y = y_0$. The problem of numerical solution of Eq. 1.1 is formulated in the following manner: Find the value of the desired function y which satisfies Eq. 1.1 from $x = x_n + H$ (where $H = Nh$ and N = positive integer) if the value of the desired function y for $x = x_n$ is known.

The function y is expressed in terms of an expansion with the aid of Newton's interpolation polynomial

$$y(x_n + H) = y_n + Nf_n + \frac{N(N-1)}{2!}\delta f_n + \frac{N(N-1)(N-2)}{3!}\delta^2 f_n + \frac{N(N-1)(N-2)(N-3)}{4!}\delta^3 f_n + \ldots \qquad [1.2]$$

$$f_n = f(x_n;\ y_n)$$

$$\delta f_n = f(x_n + h;\ y_{n+1}) - f(x_n;\ y_n)$$

$$\delta^2 f_n = f(x_n + 2h;\ y_{n+2}) - 2f(x_n + h;\ y_{n+1}) + f(x_n;\ y_n)$$

Analogous to the Runge methods of the fourth-order numerical integration of standard differential equations, the increment of function y is expressed in the form of four combined expressions

$$\begin{aligned} k_1 &= Nf(x_n;\ y_n) \\ k_2 &= Nf(x_n + \alpha_1 H;\ y_n + \beta_1 k_1) \\ k_3 &= Nf(x_n + \alpha_2 H;\ y_n + \beta_2 k_1 + \beta_3 k_2) \\ k_4 &= Nf(x_n + \alpha_3 H;\ y_n + \beta_4 k_1 + \beta_5 k_2 + \beta_6 k_3) \end{aligned} \qquad [1.3]$$

Let us now show that it is possible to select parameters α_1, α_2, α_3, β_1, β_2, β_3, β_4, β_5, β_6 and weight functions R_1, R_2, R_3, R_4, dependent on N, in such a manner that with an accuracy to fourth-order the following equality is satisfied

$$\Delta y = y(x_n + h) - y(x_n) = R_1 k_1 + R_2 k_2 + R_3 k_3 + R_4 k_4 \qquad [1.4]$$

(Items containing expressions of the type $f(\partial^3 f/\partial x^3)$, $f(\partial^3 f/\partial x^2 \partial y)$, . . ., etc., relate to fourth-order terms.)

It is known that in the case of numerical integration of

[1] Numbers in parentheses indicate References at end of paper.

standard differential equations, the specified parameters and the weight functions are essentially certain constant numbers.

Functions k_i ($i = 1, 2, 3, 4$) in Eqs. 1.3 are more general than usually assumed in the Runge method for integrating standard differential equations. Attempting to represent functions k_i, as in the case of differential equations, in a simpler form

$$\begin{aligned} k_1 &= Nf(x_n;\ y_n) \\ k_2 &= Nf(x_n + \tfrac{1}{2}H;\ y_n + \tfrac{1}{2}k_1) \\ k_3 &= Nf(x_n + \tfrac{1}{2}H;\ y_n + \tfrac{1}{2}k_2) \\ k_4 &= Nf(x_n + H;\ y_n + k_3) \end{aligned} \qquad \ldots\ldots\ldots\ldots\ldots\ldots\ldots\ldots\ldots\ldots [1.5]$$

it appears that it is impossible to select only the weight functions R_i ($i = 1, 2, 3, 4$) in such a manner that Eq. 1.4 is satisfied with an accuracy to the fourth order of magnitude. Mathematically this is evident in that the system of algebraic equations for determinating the weight functions is not completely satisfied. Therefore, certain additional parameters are introduced, namely, α_i ($i = 1, 2, 3$) and B_j ($j = 1, 2, \ldots, 6$) determining the points in which functions k_i are considered, and the latter are expressed in most general form, Eqs. 1.3.

Finite differences δf_n, $\delta^2 f_n$, . . ., can be expressed through well-known formulas in terms of functions $f(x_n, y_n)$, $f(x_n + h, y_n + f_n)$ . . . . Resolving the latter, as well as functions k_i ($i = 1, 2, 3, 4$) in a Taylor series over two variables in point (x_n, y_n), limiting ourselves to fourth-order terms and comparing coefficients for identical derivatives in Eq. 1.4, we have an algebraic system of fourth-order equations for determining parameters $\alpha_1, \alpha_2, \ldots, \beta_6$ and weight functions R_i ($i = 1, 2, 3, 4$). This system is not derived here because of its complex nature.

Analysis of the derived system of equations indicates that parameters α_i and β_i must be related to the relationships

$$\alpha_1 = \beta_1 \qquad \alpha_2 = \beta_2 + \beta_3 \qquad \alpha_3 = \beta_4 + \beta_5 + \beta_6$$

Furthermore, it appears that two of the desired parameters can be given in an arbitrary manner. The derived two-parameter family of solutions of the algebraic system of equations, dependent on any two parameters, corresponds to the two-parameter group of methods of numerical solution of equations of finite differences.

It is convenient to select α_1 and α_2 as free parameters. In this case, solution is as follows

$$\begin{aligned} \alpha_3 &= (N-1)/N \qquad \beta_1 = \alpha_1 \\ \beta_2 &= \frac{\alpha_2[\alpha_1(4\alpha_1 N - 3N + 5) + \alpha_2(N-3)]}{2\alpha_1(2\alpha_1 N - N + 1)} \\ \beta_3 &= \frac{\alpha_2(\alpha_1 - \alpha_2)(N-3)}{2\alpha_1(2\alpha_1 N - N + 1)} \\ R_3 &= \frac{(N-1)(N-2)(2\alpha_1 N - N + 1)}{12\alpha_2 N^2(\alpha_2 - \alpha_1)(\alpha_2 N - N + 1)} \\ R_4 &= \frac{3N(N-1) + \alpha_1 N(3\alpha_2 N - 4N + 2) + \alpha_2 N(3\alpha_1 N - 4N + 2)}{12(\alpha_1 N - N + 1)(\alpha_2 N - N + 1)} \\ R_2 &= \frac{(N-1) - 2(\alpha_2 R_3 + \alpha_3 R_4)}{2\alpha_1 N} \\ R_1 &= 1 - R_2 - R_3 - R_4 \\ \beta_6 &= \frac{(N-1)(N-2)(N-3)}{24\alpha_1\beta_3 N^3 R_4} \\ \beta_5 &= \frac{(N-1)(N-2) - 6N^2(\alpha_2\beta_6 R_4 + \alpha_1\beta_3 R_3)}{6\alpha_1 N^2 R_4} \\ \beta_4 &= (N-1)/N - \beta_5 - \beta_6 \end{aligned} \qquad \ldots\ldots\ldots\ldots\ldots\ldots\ldots\ldots\ldots\ldots [1.6]$$

Deriving the general solution of Eqs. 1.6, the cases which are termed particular cases are excluded

1) $\alpha_1 = 0$
2) $\alpha_2 = 0$
3) $\alpha_1 = \alpha_2$
4) $\alpha_2 = \alpha_3$
5) $\alpha_1 = (N-1)/N$
6) $\alpha_1 = (N-1)/2N$
7) $\alpha_2 = (N-1)/N$
8) $R_2 = 0$
9) $R_3 = 0$
10) $R_4 = 0$

It can be shown that if in the specified cases the system of equations for determining parameters $\alpha_1, \alpha_2, \ldots, \beta_6$ and $R_1, \ldots, R_4$ is soluble, then with the exception of the case $\alpha_2 = (N-1)/N$, there is always a family of solutions dependent on a parameter, and consequently it corresponds to a one-parameter family of methods of numerical solutions of equations of finite differences.

Let us now give solutions for the particular cases:

1) $\alpha_1 = 0$. The system of equations for determining $\alpha_1, \alpha_2, \ldots, R_4$ is not satisfied for any finite values of the desired parameters.

2) $\alpha_2 = 0$. We have a one-parameter family of solutions

$$\begin{aligned} \alpha_1 &= \frac{N-1}{2N} \qquad \alpha_3 = \frac{N-1}{N} \qquad \beta_1 = \alpha_1 \\ \beta_2 &= -\beta_3 \qquad \beta_4 = \alpha_3 - \beta_5 - \beta_6 \\ \beta_5 &= \frac{(N-2)(3N-1)}{2N(N+1)} \\ \beta_6 &= \frac{(N-1)(N-2)(N-3)}{2N^2\beta_3(N+1)} \\ R_1 &= 1 - R_2 - R_3 - R_4 \qquad R_2 = \frac{2(N-2)}{3(N-1)} \\ R_3 &= \frac{(N-2)(N-3)}{12\beta_3 N(N-1)} \qquad R_4 = \frac{N+1}{6(N-1)} \end{aligned} \qquad \ldots\ldots\ldots\ldots\ldots\ldots\ldots\ldots\ldots\ldots [1.7]$$

β_3—free parameter.

3) $\alpha_1 = \alpha_2$. The one-parameter family of solutions is as follows

$$\begin{aligned} \alpha_1 &= \alpha_2 = \frac{N-1}{2N} \qquad \alpha_3 = \frac{N-1}{N} \qquad \beta_1 = \alpha_1 \\ \beta_2 &= \alpha_2 - \beta_3 \qquad \beta_4 = 1/N \\ \beta_5 &= \frac{N-2}{N} - \beta_6 \qquad \beta_6 = \frac{(N-1)(N-2)(N-3)}{2\beta_3 N^2(N+1)} \\ R_1 &= \frac{N+1}{6(N-1)} \qquad R_2 = \frac{2(N-2)}{3(N-1)} - R_3 \\ R_3 &= \frac{(N-2)(N-3)}{6\beta_3 N(N-1)} \qquad R_4 = \frac{N+1}{6(N-1)} \end{aligned} \qquad \ldots\ldots\ldots\ldots\ldots\ldots\ldots\ldots\ldots\ldots [1.8]$$

β_3—free parameter.

The group of methods of numerical solution of difference equations which corresponds to this one-parameter family of solutions contains a method which is a direct generalization of a more applicable method of numerical integration of standard differential equations (see Eqs. 1.5). The formulas of this method are derived for $\beta_3 = (N-3)/2N$ and are

$$\Delta y_n = \frac{N+1}{6(N-1)}k_1 + \frac{N-2}{3(N-1)}k_2 + \frac{N-2}{3(N-1)}k_3 + \frac{N+1}{6(N-1)}k_4 \qquad [1.9]$$

where

$$k_1 = Nf(x_n;\ y_n)$$

$$k_2 = Nf\left(x_n + \frac{N-1}{2N}H;\ y_n + \frac{N-1}{2N}k_1\right)$$

$$k_3 = Nf\left(x_n + \frac{N-1}{2N}H;\ y_n + \frac{1}{N}k_1 + \frac{N-3}{2N}k_2\right)$$

$$k_4 = Nf\left(x_n + \frac{N-1}{N}H;\ y_n + \frac{1}{N}k_1 + \frac{2(N-2)}{N(N+1)}k_2 + \frac{(N-1)(N-2)}{N(N+1)}k_3\right)$$

4) $\alpha_2 = \alpha_3$. The corresponding family of solutions is as follows

$$\alpha_1 = \frac{1}{N} \qquad \alpha_2 = \frac{3N-1}{4N} \qquad \alpha_3 = \frac{3N-1}{4N}$$

$$\beta_1 = \alpha_1 \qquad \beta_2 = \frac{(3N-1)(-3N+13)}{32N}$$

$$\beta_3 = \frac{(3N-1)(3N-5)}{32N} \qquad \beta_4 = \frac{3N-1}{4N} - \beta_5 - \beta_6$$

$$\beta_5 = \frac{(-8\beta_6 N + 3N - 5)(3N-1)}{32N}$$

$$R_1 = 1 - R_2 - R_3 - R_4 \qquad R_2 = \frac{N^2-1}{6(3N-5)}$$

$$R_3 = \frac{4(N-1)(N-2)(4\beta_6 N - N + 3)}{3\beta_6 N(3N-1)(3N-5)}$$

$$R_4 = \frac{4(N-1)(N-2)(N-3)}{3\beta_6 N(3N-1)(3N-5)}$$

. . . . . [1.10]

β_6—free parameter.

5) $\alpha_1 = (N-1)/N$. The one-parameter family of solutions is as follows

$$\alpha_2 = \frac{N-1}{2N} \qquad \alpha_3 = \frac{N-1}{N} \qquad \beta_1 = \frac{N-1}{N}$$

$$\beta_2 = \frac{3N-1}{8N} \qquad \beta_3 = \frac{N-3}{8N}$$

$$\beta_4 = \frac{N-1}{N} - \beta_5 - \beta_6 \qquad \beta_5 = -\frac{\beta_6(N-3)}{4(N-1)}$$

$$R_1 = \frac{N+1}{6(N-1)} \qquad R_2 = \frac{N+1}{6(N-1)} - R_4$$

$$R_3 = \frac{2(N-2)}{3(N-1)} \qquad R_4 = \frac{N-2}{3\beta_6 N}$$

. . . . . [1.11]

β_6—free parameter.

6) $\alpha_1 = (N-1)/2N$. It can be shown readily that this case reduces to case 3.

7) $\alpha_2 = (N-1)/N$. For this value of parameter α_2 we do not have a one-parameter family of solutions, but a single solution corresponding to the case when $R_3 = 0$. This solution is as follows

$$\alpha_1 = \frac{1}{N} \qquad \alpha_3 = \frac{3N-1}{4N} \qquad \beta_1 = \frac{1}{N}$$

$$\beta_2 = -\frac{(N-1)(N-4)}{2N} \qquad \beta_3 = \frac{(N-1)(N-2)}{2N}$$

$$\beta_4 = -\frac{(3N-1)(3N^2-18N+11)}{64N(N-1)}$$

$$\beta_5 = \frac{(N-1)(3N-1)(3N-5)}{64N(N-2)}$$

$$\beta_6 = \frac{(N-3)(3N-1)(3N-5)}{64N(N-1)(N-2)}$$

$$R_1 = -\frac{(N-7)(N+1)}{6(3N-1)} \qquad R_2 = \frac{N^2-1}{6(3N-5)}$$

$$R_4 = \frac{16(N-1)(N-2)}{3(3N-1)(3N-5)} \qquad R_3 = 0$$

. . . . . [1.12]

8) $R_2 = 0$. We have the following one-parameter family of solutions

$$\alpha_2 = \frac{2\alpha_3(2N-1) - 3N + 3}{6\alpha_3 N - 4N + 2}$$

$$R_3 = \frac{(N-1)(3\alpha_3 N - 2N + 1)}{6\alpha_2 N^2(\alpha_3 - \alpha_2)}$$

$$R_4 = \frac{-2\alpha_2 N R_3 + N - 1}{2\alpha_3 N} \qquad R_1 = 1 - R_3 - R_4$$

$$\beta_6 = \frac{R_3(\alpha_3 - \alpha_2)(N-3)}{R_4(4\alpha_3 N - 3N + 1)}$$

$$\beta_3 = \frac{(N-1)(N-2)(N-3)}{24\alpha_1\beta_6 R_4 N^3}$$

$$\alpha_1 = \frac{12\alpha_2^2\beta_6 R_4 N^2 - (N-1)^2(N-2)}{12\alpha_2\beta_6 R_4 N^3 - 2N(N-1)(N-3)}$$

$$\beta_1 = \alpha_1 \qquad \beta_2 = \alpha_2 - \beta_3 \qquad \beta_4 = \alpha_3 - \beta_5 - \beta_6$$

$$\beta_5 = \frac{(N-1)(N-2)}{6\alpha_1 R_4 N^2} - \frac{\alpha_2}{\alpha_1}\beta_6 - \frac{R_3}{R_4}\beta_3$$

. . . . . [1.13]

α_3—free parameter.

9) $R_3 = 0$. The corresponding solution, which is expressed in terms of radicals and in practical cases is inconvenient, is not given here.

10) $R_4 = 0$. The system of equations for determining parameters α_i, β_j and weight functions R_k is not satisfied for any finite values of the desired parameters.

The set of the two-parameter family of methods dependent on parameters α_1 and α_2 and the given one-parameter group of methods contain all possible fourth-order methods of numerical solutions of the Runge-type equations of finite differences.

Third-order methods of numerical calculation of equations of finite differences are derived in an analogous manner.

The increment of the desired function is represented in terms of three combined equations

$$k_1 = Nf(x_n;\ y_n)$$
$$k_2 = Nf(x_n + \alpha_1 H;\ y_n + \beta_1 k_1)$$
$$k_3 = Nf(x_n + \alpha_2 H;\ y_n + \beta_2 k_1 + \beta_3 k_2)$$

. . . . . [1.14]

Let us select parameters α_1, α_2, β_1, β_2, β_3 and weight functions R_1, R_2, R_3 in such a manner that, with an accuracy to third-order terms, the following equation is satisfied

$$\Delta y_n = y_{n+1} - y_n = R_1 k_1 + R_2 k_2 + R_3 k_3 \qquad [1.15]$$

Proceeding in the same manner as in the case of fourth-order methods, we derive the algebraic system of third-order equations for determining parameters α_i, β_j and the weight functions R_k. From this system of equations, which is not

given here, it must follow that

$$\alpha_1 = \beta_1 \qquad \alpha_2 = \beta_2 + \beta_3$$

Furthermore, in this case, two of the desired parameters can also be given in an arbitrary manner.

It is convenient to select parameters α_1 and α_2 as such free parameters. In this case, we have the following two-parameter family of solutions

$$\beta_3 = \frac{\alpha_2(\alpha_1 - \alpha_2)(N-2)}{\alpha_1(3\alpha_1 N - 2N + 1)} \qquad R_1 = 1 - R_2 - R_3$$

$$R_2 = \frac{(N-1)(3\alpha_2 N - 2N + 1)}{6\alpha_1 N^2(\alpha_2 - \alpha_1)}$$

$$R_3 = \frac{(N-1)(3\alpha_1 N - 2N + 1)}{6\alpha_2 N^2(\alpha_1 - \alpha_2)} \qquad [1.16]$$

A group of third-order methods, dependent on two parameters, corresponds to the given two-parameter family of solutions.

The family of solutions 1.16 does not contain such solutions for which any of the parameters are not finite. These are as follows

1) $\alpha_1 = 0$
2) $\alpha_2 = 0$
3) $\alpha_1 = \alpha_2$
4) $\alpha_1 = (2N - 1)/3N$

Let us investigate these cases:

1) $\alpha_1 = 0$. The system of equations for determining parameters $\alpha_1, \alpha_2, \ldots, R_3$ is not satisfied.

2) $\alpha_2 = 0$. We have a one-parameter family of solutions

$$\alpha_1 = (2N-1)/3N \qquad R_1 = 1 - R_2 - R_3$$

$$R_2 = \frac{3(N-1)}{2(2N-1)} \qquad R_3 = \frac{(N-1)(N-2)}{2\beta_3 N(2N-1)} \qquad [1.17]$$

β_3—free parameter.

3) $\alpha_1 = \alpha_2$. The one-parameter family of solutions is as follows

$$\alpha_1 = \frac{2N-1}{3N} \qquad \alpha_2 = \frac{2N-1}{3N} \qquad R_1 = \frac{N+1}{2(2N-1)}$$

$$R_2 = \frac{(N-1)(3\beta_3 N - N + 2)}{2\beta_3 N(2N-1)} \qquad R_3 = \frac{(N-1)(N-2)}{2\beta_3 N(2N-1)} \qquad [1.18]$$

β_3—free parameter.

4) $\alpha_1 = (2N - 1)/3N$. This case can be reduced either to case 2 or case 3.

When Runge-type methods of numerical solution of equations of finite differences are employed, step $H = Nh$ must be selected correctly; however, this entails evaluation of the magnitude of error of the desired function. We are not concerned here with the problem of accurate evaluation of the error of solutions for the desired functions. We note that an accurate evaluation of the error in a general case and for standard differential equations has not been made as yet [see, for example, (4)]. An adequately simple method of determining certain terms of probably a higher order of magnitude in expansion 1.2 is given here.

Varying only the selection of weight functions, it is possible that

$$\Delta^{(k)} y_n = R_1^* k_1 + R_2^* k_2 + R_3^* k_3 + R_4^* k_4 \qquad [1.19]$$

contains only terms of the third order of smallness and also certain terms of a higher order of magnitude.

Formulas for determining such weight functions in this case are

$$R_1^* = \frac{D_1}{D} \qquad R_2^* = \frac{D_2}{D} \qquad R_3^* = \frac{D_3}{D} \qquad R_4^* = \frac{D_4}{D} \qquad [1.20]$$

where

$$D_1 = [(N-1)/6N^2][(2N-1)(\alpha_2 - \alpha_1)(\alpha_1\beta_5 + \alpha_2\beta_6) - \alpha_1\beta_3(2N-1)(\alpha_3 - \alpha_1) - (N-2)(\alpha_3 - \alpha_2) \times (\alpha_3 - \alpha_1)]$$

$$D_2 = [(N-1)/6N^2][\alpha_2\alpha_3(N-2)(\alpha_3 - \alpha_2) + \alpha_1\alpha_3\beta_3(2N-1) - \alpha_2(2N-1)(\beta_1\beta_5 + \alpha_2\beta_6)]$$

$$D_3 = [\alpha_1(N-1)/6N^2][(\alpha_1\beta_5 + \alpha_2\beta_6)(2N-1) + \alpha_3(N-2)(\alpha_1 - \alpha_3)$$

$$D_4 = [\alpha_1(N-1)/6N^2][\alpha_2(\alpha_2 - \alpha_1)(N-2) - \alpha_1\beta_3(2N-1)$$

$$D = \alpha_1\alpha_2(\alpha_2 - \alpha_1)(\alpha_1\beta_5 + \alpha_2\beta_6) + \alpha_1^2\alpha_3\beta_3(\alpha_1 - \alpha_3)$$

Let us assume that we have a certain concrete method of numerical solution of equations of finite differences. It corresponds to certain parameters $\alpha_1, \alpha_2, \ldots \beta_6$, and weight functions R_k ($k = 1, 2, 3, 4$) dependent on N. Determining the new weight functions R_k^* ($k = 1, 2, 3, 4$) in accordance with formulas 1.20 for former values of function k_i ($i = 1, 2, 3, 4$), the magnitude of the term of the third order of smallness in expansion 1.2 is determined in accordance with formula 1.19. The magnitude of the error of solution can be judged by the magnitude of the third-order term in the expansion.

Analogous formulas are derived in the case of third-order methods.

Two-parameter families of third- and fourth-order Runge-type methods of numerical solution of equations of finite differences are given in the foregoing. Selection of one or the other method from the given group of methods depends on conditions of simplicity, symmetry, the existence of the one or the other constant in the memory of the machine in the case of computer programming, etc. However, it is possible to manage with two free parameters in such a manner that the remainder term is reduced to a minimum and the difference between the principal terms of expansion 1.2, not taken into account, and the part of these terms taken into account in the formula for the increment of the desired function 1.4, would equal zero.

Let us now investigate a family of third-order methods; in this case, the corresponding formulas are rather simple. The increment Δy of the desired function determined in accordance with formula 1.15 contains a part of the fourth-order terms.

The equation for this part is

$$\Phi = (R_2\alpha_1^3 + R_3\alpha_2^3)A_1 + R_3\alpha_1^2\beta_3 A_2 + R_3\alpha_1\alpha_2\beta_3 A_3$$

where

$$A_1 = \frac{1}{6}NH\left(\frac{\partial}{\partial x} + \frac{f}{h}\frac{\partial}{\partial y}\right)^3 f$$

$$A_2 = \frac{1}{2}N^2H^2\frac{\partial f}{\partial y}\left(\frac{\partial}{\partial x} + \frac{f}{h}\frac{\partial}{\partial y}\right)^2 f$$

$$A_3 = N^2H^2\left(\frac{\partial}{\partial x} + \frac{f}{h}\frac{\partial}{\partial y}\right)f\left(\frac{\partial}{\partial x} + \frac{f}{h}\frac{\partial}{\partial y}\right)\frac{\partial f}{\partial y}$$

The given formulas employ the differential operator of the form

$$\left(\frac{\partial}{\partial x} + \frac{f}{h}\frac{\partial}{\partial y}\right)f = \frac{\partial f}{\partial x} + \frac{f}{h}\frac{\partial f}{\partial y}$$

On the other hand, the fourth-order term in the precise formula 1.2 equals

$$\Psi = \frac{3}{2}\frac{(N-1)^2}{N^2} A_1 + \frac{1}{12}\frac{(N-1)^2(N-2)}{N^3} A_2 + \frac{(N-1)(N-2)(3N-1)}{24N^3} A_3 + \frac{(N-1)(N-2)(N-3)}{24N^3} A_4$$

where

$$A_4 = N^3 H \left(\frac{\partial f}{\partial y}\right)^2 \left(\frac{\partial}{\partial x} + \frac{f}{h}\frac{\partial}{\partial y}\right) f$$

Let us express R_2, R_3 and β_3 in terms of free parameters α_1, α_2 in accordance with Eqs. 1.16. Hence we have

$$R_2\alpha_1^3 + R_3\alpha_2^3 = \frac{(N-1)[-3N\alpha_1\alpha_2 + (2N-1)(\alpha_1+\alpha_2)]}{6N^2}$$

$$R_3\beta_3\alpha_1^2 = \frac{(N-1)(N-2)\alpha_1}{6N^2}$$

$$R_3\alpha_1\alpha_2\beta_3 = \frac{(N-1)(N-2)\alpha_2}{6N^2}$$

Let us select free parameters α_1 and α_2 in such a manner that the following condition is satisfied

$$\Psi - \Phi = 0 \qquad [1.21]$$

This means that the accuracy of the method of numerical solution of equations of finite differences is raised from the third to the fourth order.

Condition 1.21 can be expressed in the following terms

$$\alpha_1\alpha_2 T_1 + \alpha_1 T_2 + \alpha_2 T_2 + T_3 = 0 \qquad [1.22]$$

where

$$T_1 = \frac{N(N-1)}{2N^2} A_1$$

$$T_2 = -\frac{(N-1)(2N-1)}{6N^2} A_1 - \frac{(N-1)(N-2)}{6N^2} A_2$$

$$T_3 = \frac{3(N-1)^2}{2N^2} A_1 + \frac{(N-1)^2(N-2)}{12N^3} A_2 + \frac{(N-1)(N-2)(3N-1)}{24N^3} A_3 + \frac{(N-1)(N-2)(N-3)}{24N^3} A_4$$

Eq. 1.22 gives

$$\alpha_2 = -(\alpha_1 T_2 + T_3)/(\alpha_1 T_3 + T_1) \qquad [1.23]$$

Thus for any value of the free parameter α_1, there exists a value of parameter α_2 which is optimum in the sense previously discussed, determined from formula 1.23. In this case, the optimum value of parameter α_2 varies along the solution of the initial equation of finite differences, since it is dependent on the derivatives of the first and higher orders from the right-hand side of Eq. 1.1. In principle, it is possible to select in every step an optimum value of α_2 in the process of numerical calculation of difference equation.

In the case of fourth-order methods of numerical calculation of equations of finite differences, the problem of optimum determination of free parameters α_1, α_2 is solved also; however, in this case the solution is much more complex and is, therefore, not given here.

2. Generalization of the Adams Method

This section discusses the interpolation methods of numerical solution of equations of finite differences which are a generalization of the Adams method. Two cases are investigated: The case of equidistant points and the case of non-equidistant points.

Let us study the case of equidistant points. Let us assume that the values of increments Δy of the desired function, satisfying the equation of finite differences 1.1, is known for four values of the argument

$$x_{n-3N} = x_n - 3H \qquad x_{n-2N} = x_n - 2H$$

$$x_{n-N} = x_n - H \text{ and } x_n$$

where $H = Nh$. It is necessary to determine the value of the desired function y_{n+N} for the value of the argument $x_{n+N} = x_n + H$. The same limitations as in the foregoing section are imposed on functions $f(x, y)$.

The known increments of the desired functions for the specified values of the argument are determined as follows

$$f_{n-3N} = y(x_n - 3H + h) - y(x_n - 3H)$$

$$f_{n-2N} = y(x_n - 2H + h) - y(x_n - 2H)$$

$$f_{n-N} = y(x_n - H + h) - y(x_n - H)$$

$$f_n = y(x_n + h) - y(x_n)$$

Let us select coefficients α, β and γ in such a way that, with an accuracy to first-order terms, the following equality is satisfied

$$\Delta y_n = y_{n+N} - y_n = Nf_n + \alpha N\Delta f_{n-N} + \beta N\Delta^2 f_{n-2N} + \gamma N\Delta^3 f_{n-3N} \qquad [2.1]$$

where Δy_n is the increment of the desired function y determined by Eqs. 1.2.

Resolving the corresponding functions in Taylor series at point x_n and comparing coefficients for identical derivatives y'', y''', . . ., we have equations for determining α, β and γ. Solving the derived equations in relation to α, β and γ, we finally have

$$\alpha = \frac{N-1}{2N} \qquad \beta = \frac{(N-1)(5N-1)}{12N^2}$$

$$\gamma = \frac{(N-1)(3N-1)}{8N^2}$$

Expressing the increment of the desired function Δy_n directly through the functions f_{n-3N}, f_{n-2N}, f_{n-N} and f_n we have

$$\Delta y_n = R_1 Nf_{n-3N} + R_2 Nf_{n-2N} + R_3 Nf_{n-N} + R_n Nf_n \qquad [2.2]$$

where

$$R_1 = -(N-1)(3N-1)/8N^2$$
$$R_2 = (N-1)(37N-11)/24N^2$$
$$R_3 = -(N-1)(59N-13)/24N^2$$
$$R_4 = (55N^2 - 36N + 5)/24N^2$$

The given Eqs. 2.1 and 2.2 are generalizations of the Adams interpolation method for a diagonal line. The corresponding formulas for a horizontal and a broken line are given in the following.

In the case of the horizontal line, we have

$$\Delta y_n = Nf_{n-3N} + \alpha' N\Delta f_{n-3N} + \beta' N\Delta^2 f_{n-3N} + \gamma' N\Delta^3 f_{n-3N} \qquad [2.3]$$

where

$$\alpha' = (N-1)/2N$$
$$\beta' = -(N^2-1)/12N^2$$
$$\gamma' = (N^2-1)/24N^2$$

or in another form

$$\Delta y_n = R_1' N f_{n-3N} + R_2' N f_{n-2N} + R_3' N f_{n-N} + R_4' N f_n \quad [2.4]$$

where

$$R_1' = -(N+1)(3N+1)/8N^2$$
$$R_2' = (N-1)(19N+7)/24N^2$$
$$R_3' = -5(N^2-1)/24N^2$$
$$R_4' = (N^2-1)/24N^2$$

In the case of a broken line, we have

$$\Delta y_n = N f_{n-N} + \alpha'' N \Delta f_{n-N} + \beta'' N \Delta^2 f_{n-2N} + \gamma'' N \Delta^3 f_{n-3N} \quad [2.5]$$

where

$$\alpha'' = (N-1)/2N$$
$$\beta'' = -(N^2-1)/12N^2$$
$$\gamma'' = -(N^2-1)/24N^2$$

and, correspondingly, in another form

$$\Delta y_n = R_1'' N f_{n-3N} + R_2'' N f_{n-2N} + R_3'' N f_{n-N} + R_4'' N f_n \quad [2.6]$$

where

$$R_1'' = (N^2-1)/24N^2$$
$$R_2'' = -5(N^2-1)/24N^2$$
$$R_3'' = (N+1)(19N-7)/24N^2$$
$$R_4'' = (N-1)(9N-1)/24N^2$$

Employing the specified methods of numerical solution of difference equations, it is necessary to have four starting values of the desired function for certain values of the argument. Such starting values are requisite at the start of the process of numerical solution as well as during variation (increase or decrease) of step H. Here the procedure is analogous to the one for the theory of standard differential equations (4). The initial values can be found in accordance with one of the Runge-type methods; the so-called "initial approximations" can be used also. In the case of equations of finite differences "initial approximations" are as follows.

First Approximation

Assuming that the value of the desired function y_{n-3N} for the value of the argument x_{n-3N} is known, increment Δy_{n-3N} is determined in accordance with the formula

$$\Delta y_{n-3N} = N f_{n-3N}$$

where

$$f_{n-3N} = f(x_{n-3N}, y_{n-3N})$$

and consequently

$$y_{n-2N} = y_{n-3N} + N f_{n-3N}$$

Furthermore we determine

$$f_{n-2N} = f(x_{n-2N}, y_{n-2N}) \qquad \Delta f_{n-3N} = f_{n-2N} - f_{n-3N}$$

Second Approximation

Increments Δy_{n-3N} and Δy_{n-2N} are determined in accordance with the formulas

$$\Delta y_{n-3N} = N f_{n-3N} + [(N-1)/2N] N \Delta f_{n-3N}$$
$$\Delta y_{n-2N} = N f_{n-2N} + [(N-1)/2N] N \Delta f_{n-3N}$$

and consequently

$$y_{n-2N} = y_{n-3N} + \Delta y_{n-3N}$$
$$y_{n-N} = y_{n-2N} + \Delta y_{n-2N}$$

Then we determine

$$f_{n-2N} = f(x_{n-2N}, y_{n-2N}) \qquad f_{n-N} = f(x_{n-N}, y_{n-N})$$
$$\Delta f_{n-3N} = f_{n-2N} - f_{n-3N} \qquad \Delta f_{n-2N} = f_{n-N} - f_{n-2N}$$
$$\Delta^2 f_{n-3N} = f_{n-N} - 2f_{n-2N} + f_{n-3N}$$

Third Approximation

Increments Δy_{n-3N}, Δy_{n-2N} and Δy_{n-N} are determined:

a) In accordance with formula 2.3 for the horizontal line

$$\Delta y_{n-3N} = N f_{n-3N} + \frac{N-1}{2N} N \Delta f_{n-3N} - \frac{N^2-1}{12N^2} N \Delta^2 f_{n-3N}$$

b) In accordance with formula 2.5 for the broken line

$$\Delta y_{n-2N} = N f_{n-2N} + \frac{N-1}{2N} N \Delta f_{n-2N} - \frac{N^2-1}{12N^2} N \Delta^2 f_{n-3N}$$

c) In accordance with formula 2.1 for the diagonal line

$$\Delta y_{n-N} = N f_{n-N} + \frac{N-1}{2N} N \Delta f_{n-2N} + \frac{(N-1)(5N-1)}{12N^2} N \Delta^2 f_{n-3N}$$

and consequently

$$y_{n-2N} = y_{n-3N} + \Delta y_{n-3N}$$
$$y_{n-N} = y_{n-2N} + \Delta y_{n-2N}$$
$$y_n = y_{n-N} + \Delta y_{n-N}$$

Functions $f_{n-2N} = f(x_{n-2N}, y_{n-2N})$, $f_{n-N} = f(x_{n-N}, y_{n-N})$ and $f_n = f(x_n, y_n)$ are then determined. This completes the approximations.

Let us study the case of nonequidistant points. Let us assume that the values of increments Δy of the desired function are known for four values of the argument

$$x_{n-3N} = x_n - \alpha_1 H \qquad x_{n-2N} = x_n - \alpha_2 H$$
$$x_{n-N} = x_n - \alpha_3 H \text{ and } x_n$$

where

$H = Nh$
$\alpha_1, \alpha_2, \alpha_3$ = arbitrary numbers
$\alpha_1 \neq \alpha_2 \neq \alpha_3 \neq 0$

It is necessary to determine the values of the desired function y_{n+N} for the value of argument $x_n + H$. Proceeding in a manner analogous to the case of equidistant points, the following formula for determining Δy_n (for the case of a diagonal line) is derived

$$\Delta y_n = R_1 N f_{n-3N} + R_2 N f_{n-2N} + R_3 N f_{n-N} + R_4 N f_n \quad [2.7]$$

where

$$R_1 = \frac{(N-1)\{[4(\alpha_2+\alpha_3)+3(1+2\alpha_2\alpha_3)]N - [2(\alpha_2+\alpha_3)+3]\}}{12N^2\alpha_1(\alpha_1-\alpha_2)(\alpha_3-\alpha_1)}$$

$$R_2 = \frac{(N-1)\{[4(\alpha_3+\alpha_1)+3(1+2\alpha_3\alpha_1)]N - [2(\alpha_3+\alpha_1)+3]\}}{12N^2\alpha_2(\alpha_2-\alpha_3)(\alpha_1-\alpha_2)}$$

$$R_3 = \frac{(N-1)\{[4(\alpha_1+\alpha_2)+3(1+2\alpha_1\alpha_2)]N-[2(\alpha_1+\alpha_2)+3]\}}{12N^2\alpha_3(\alpha_3-\alpha_1)(\alpha_2-\alpha_3)}$$

$$R_4 = 1 - R_1 - R_2 - R_3$$

It can be readily seen that the formulas for determining the weight functions R_1, R_2 and R_3 can be derived from one another as a result of cyclic permutation of elements α_1, α_2 and α_3. This circumstance can be used, for example, for programming the proposed method for an electronic computer.

* * *

The Runge and the Adams types of methods of numerical solution of equations of finite differences have been given. The question arises: In which cases is it expedient to employ one or the other concrete method? The problem is solved as in the case of numerical integration of standard differential equations.

On the one hand, the Adams-type interpolation methods have an advantage over the Runge-type methods in that they require less calculating for determining the increment of the desired function for every step (in the case of fourth-order methods the right-hand sides must be computed once, whereas the Runge-type method requires calculation four times). On the other hand, in the case of programming the specified algorithms for solving equations of finite differences on electronic computers, the Adams-type interpolation methods require a considerably larger memory than do the Runge-type methods.

These two circumstances must be taken into account in every concrete case.

3. Limiting Cases

As shown in the case of methods of numerical solution of equations of finite differences, in contrast to the methods of numerical integration of differential equations, parameters α_i, β_j and the weight functions R_k appear dependent on ratio N of the step of numerical solution H to elementary step h where the initial difference Eq. 1.1 is determined.

Let us investigate the limiting case: $h \to 0$ or $N \to \infty$. The equation of finite differences, Eq. 1.1, after division by magnitude h and transition to the limit converts to the standard differential equation of the form

$$dy/dx = F(x, y)$$

where

$$F(x, y) = \lim_{h \to 0} \frac{f(x, y)}{h}$$

(it is assumed that the limit exists on the right side).

In this limiting case, the families of Runge-type fourth- and third-order methods of numerical solution of equations of finite differences correspond to the family of methods of numerical integration of standard differential equations. Separate representations of these families are available in the literature.

The Runge-type methods of numerical solution of equations of finite differences are of the same structure. Limiting methods for the case of standard differential equations include methods of a different form than the ones usually employed.

Let us first investigate fourth-order Runge-type methods. From Eqs. 1.6 for $N \to \infty$, we have

$$\alpha_3 = 1 \qquad \beta_1 = \alpha_1 \qquad \beta_2 = \frac{\alpha_2[\alpha_1(3-4\alpha_1)-\alpha_2]}{2\alpha_1(1-2\alpha_1)}$$

$$\beta_3 = \frac{\alpha_2(\alpha_2-\alpha_1)}{2\alpha_1(1-2\alpha_1)} \qquad \beta_4 = 1 - \beta_5 - \beta_6$$

$$\beta_5 = \frac{(1-\alpha_1)[2(1-\alpha_2)(2\alpha_2-1)-(\alpha_2-\alpha_1)]}{2\alpha_1(\alpha_2-\alpha_1)(6\alpha_1\alpha_2-4\alpha_1-4\alpha_2+3)}$$

$$\beta_6 = \frac{(1-\alpha_1)(1-\alpha_2)(1-2\alpha_2)}{\alpha_2(\alpha_2-\alpha_1)(6\alpha_1\alpha_2-4\alpha_1-4\alpha_2+3)}$$

$$R_1 = 1 - R_2 - R_3 - R_4$$

$$R_2 = \frac{2\alpha_2 - 1}{12\alpha_1(1-\alpha_1)(\alpha_2-\alpha_1)}$$

$$R_3 = \frac{1-2\alpha_1}{12\alpha_2(1-\alpha_2)(\alpha_2-\alpha_1)}$$

$$R_4 = \frac{6\alpha_1\alpha_2 - 4\alpha_1 - 4\alpha_2 + 3}{12(1-\alpha_1)(1-\alpha_2)}$$

Parameters α_1 and α_2 can be given in an arbitrary manner (taking the limitations specified in Section 1 into account). Assuming, for example, that $\alpha_1 = \frac{1}{4}$, $\alpha_2 = \frac{1}{2}$, we have one of the fourth-order algorithms

$$\Delta y_n = \tfrac{1}{6}k_1 + \tfrac{2}{3}k_3 + \tfrac{1}{6}k_4$$

where

$$k_1 = HF(x_n, y_n)$$

$$k_2 = HF(x_n + \tfrac{1}{4}H;\ y_n + \tfrac{1}{4}k_1)$$

$$k_3 = HF(x_n + \tfrac{1}{2}H;\ y_n + \tfrac{1}{2}k_2)$$

$$k_4 = HF(x_n + H;\ y_n + k_1 - 2k_2 + 2k_3)$$

Let us also cite the limiting values for $N \to \infty$ for weight functions R_i^*, employed for evaluating the error of the desired function. Converting to the limit in Eq. 1.19, we have for the case of differential equations

$$\Delta^{(k)}y = R_1^*k_1 + R_2^*k_2 + R_3^*k_3 + R_4^*k_4$$

where

$$R_1^* = D_1/D$$

$$R_2^* = D_2/D$$

$$R_3^* = D_3/D$$

$$R_4^* = D_4/D$$

$$D_1 = \tfrac{1}{6}[2(\alpha_2-\alpha_1)(\alpha_1\beta_5+\alpha_2\beta_6) - 2\alpha_1\beta_3(\alpha_3-\alpha_1) - (\alpha_2-\alpha_1)(\alpha_3-\alpha_2)(\alpha_3-\alpha_1)]$$

$$D_2 = \tfrac{1}{6}[\alpha_2\alpha_3(\alpha_3-\alpha_2) + 2\alpha_1\alpha_3\beta_3 - 2\alpha_2(\alpha_1\beta_5+\alpha_3\beta_6)]$$

$$D_3 = (\alpha_1/6)[2(\alpha_1\beta_5+\alpha_2\beta_6) + \alpha_3(\alpha_1-\alpha_3)]$$

$$D_4 = (\alpha_1/6)[\alpha_2(\alpha_2-\alpha_1) - 2\alpha_1\beta_3]$$

$$D = \alpha_1\alpha_2(\alpha_2-\alpha_1)(\alpha_1\beta_5+\alpha_2\beta_6) + \alpha_1^2\alpha_3\beta_2(\alpha_1-\alpha_3)$$

It is expedient to assume that the values of the remaining parameters $\alpha_1, \alpha_2, \ldots, \beta_6$ are the same as for the determination of the increment of the desired function y. In this case, the reference term $\Delta^{(k)}y$ is expressed through the same functions k_i ($i = 1, 2, 3, 4$) as increment Δy_n.

The limiting methods of integrating standard differential equations which correspond to particular solutions for difference equations are not given here. They can be derived readily by limiting transformation in Eqs. 1.7 to 1.13. Limiting methods for the case $R_2 = 0$ are given only because this case corresponds to the limiting methods whose structure is different from those which are employed as a rule.

Direct conversion to the limits in Eq. 1.4, where $\alpha_1, \alpha_2, \ldots, R_4$ are expressed in terms of Eqs. 1.13, gives

$$\Delta y_n = R_1 k_1 + R_2 k_2 + R_3 k_3 + R_4 k_4$$

where

$$\begin{aligned}
k_1 &= HF(x_n;\ y_n)\\
k_2 &= HF(x_n;\ y_n)\\
k_3 &= HF(x_n + a_1 H;\ y_n + a_1 k_1 + a_2 H^2 (dF/dx)_n)\\
k_4 &= HF(x_n + a_3 H;\ y_n + a_4 k_1 + a_5 k_3 + a_6 H^2\,(dF/dx)_n)\\
a_1 &= \lim_{N\to\infty} \alpha_2\\
a_2 &= \lim_{N\to\infty} \alpha_1 \beta_3\\
a_3 &= \lim_{N\to\infty} \alpha_3\\
a_4 &= \lim_{N\to\infty} (\beta_4 + \beta_5)\\
a_5 &= \lim_{N\to\infty} \beta_6\\
a_6 &= \lim_{N\to\infty} \alpha_1 \beta_5
\end{aligned}$$

and weight functions R_k ($k = 1, 2, 3, 4$) assume the following limiting values

$$R_1 = \frac{6\alpha_3^2 - 6\alpha_3 + 1}{6\alpha_3(4\alpha_3 - 3)} \qquad R_2 = 0$$

$$R_3 = \frac{2(3\alpha_3 - 2)^3}{3(4\alpha_3 - 3)(6\alpha_3^2 - 8\alpha_3 + 3)}$$

$$R_4 = \frac{1}{6\alpha_3(6\alpha_3^2 - 8\alpha_3 + 3)}$$

Here, α_3 is a free parameter.

The given one-parameter family of fourth-order methods of integrating differential equations is characterized in that in it, the increment of the desired function is dependent not on four, but on three, functions k_i and, in addition, on the complete derivative of x from the right-hand side of the initial equation. It is expedient to use these methods in instances when dF/dx is a comparatively simple function (for example, when F is a polynomial, and so on).

For example, the concrete method of this family corresponding to the value $\alpha_3 = \frac{1}{2}$ is

$$\Delta y_n = \tfrac{1}{6} k_1 + \tfrac{1}{6} k_3 + \tfrac{2}{3} k_4$$

where

$$\begin{aligned}
k_1 &= HF(x_n;\ y_n),\\
k_3 &= HF(x_n + H;\ y_n + k_1 + \tfrac{1}{2}H^2(dF/dx)_n)\\
k_4 &= HF(x_n + \tfrac{1}{2}H;\ y_n + \tfrac{3}{8}k_1 + \tfrac{1}{8}k_3)
\end{aligned}$$

Limiting third-order methods are not given here.

Well-known methods of numerical integration of standard differential equations correspond to the interpolation method of numerical solution of equations of finite differences in the case $N \to \infty$.

In the case of equidistant points at the limit for $N \to \infty$, Eqs. 2.2, 2.4, and 2.6 give:

a) For a diagonal line

$$\Delta y_n = H\left(-\frac{3}{8} F_{n-3N} + \frac{37}{24} F_{n-2N} - \frac{59}{24} F_{n-N} + \frac{55}{24} F_n\right)$$

b) For a horizontal line

$$\Delta y_n = H\left(\frac{3}{8} F_{n-3N} + \frac{19}{24} F_{n-2N} - \frac{5}{24} F_{n-N} + \frac{1}{24} F_n\right)$$

c) For a broken line

$$\Delta y_n = H\left(\frac{1}{24} F_{n-3N} - \frac{5}{24} F_{n-2N} + \frac{19}{24} F_{n-N} + \frac{9}{24} F_n\right)$$

The formulas of "initial approximation" for determining three initial values of the desired function at the limit convert to the well-known formulas of "initial approximation" for the case of standard differential equations.

In the case of nonequidistant points for the increment of the desired function at the limit for $N \to \infty$, Eq. 2.7 gives

$$\Delta y_n = H(R_1 F_{n-3N} + R_2 F_{n-2N} + R_3 F_{n-N} + R_4 F_n)$$

where

$$R_1 = \frac{4(\alpha_2 + \alpha_3) + 3(1 + 2\alpha_2\alpha_3)}{12\alpha_1(\alpha_1 - \alpha_2)(\alpha_3 - \alpha_1)}$$

$$R_2 = \frac{4(\alpha_3 + \alpha_1) + 3(1 + 2\alpha_3\alpha_1)}{12\alpha_2(\alpha_2 - \alpha_3)(\alpha_1 - \alpha_2)}$$

$$R_3 = \frac{4(\alpha_1 + \alpha_2) + 3(1 + 2\alpha_1\alpha_2)}{12\alpha_3(\alpha_3 - \alpha_1)(\alpha_2 - \alpha_3)}$$

$$R_4 = 1 - R_1 - R_2 - R_3$$

4. Application of Dicyclic Methods of Integrating to the Calculation of Orbits of Artificial Earth Satellites

The perturbed motion of an artificial satellite is described in terms of differential equations in osculating elements in accordance with the independent variable u, the argument of latitude (1,2)

$$\frac{dp}{du} = F 2r\tilde{T}$$

$$\frac{de}{du} = F\left[\tilde{S}\sin\vartheta + \left(1 + \frac{r}{p}\right)\tilde{T}\cos\vartheta + e\,\frac{r}{p}\,\tilde{T}\right]$$

$$\frac{d\omega}{du} = F\left[-\frac{1}{e}\,\tilde{S}\cos\vartheta + \frac{1}{e}\left(1 + \frac{r}{p}\right)\tilde{T}\sin\vartheta - \frac{r}{p}\,\operatorname{cotan} i\,\tilde{W}\sin u\right]$$

$$\frac{d\Omega}{du} = F\,\frac{r}{p}\,\frac{\sin u}{\sin i}\,\tilde{W} \qquad \frac{di}{du} = F\,\frac{r}{p}\,\tilde{W}\cos u \qquad \frac{dt}{du} = F \qquad \ldots\ldots\ldots\ldots\ldots\ldots [4.1]$$

where

$$F = \frac{1}{\sqrt{pfM}/r^2 - (r/p)\operatorname{cotan} i\,\tilde{W}\sin u}$$

$\vartheta = u - \omega$
$r = 1/(1 + e\cos\vartheta)$
$\tilde{S} = (\sqrt{p}/\sqrt{fM})S$
$\tilde{T} = (\sqrt{p}/\sqrt{fM})T$
$\tilde{W} = (\sqrt{p}/\sqrt{fM})W$
f = factor of gravity
M = mass of Earth
ϑ = true anomaly
p = orbit parameter
e = eccentricity
ω = angular distance of perigee from ascending node
Ω = longitude of ascending node
i = inclination of orbit
S,T,W = components of perturbing acceleration along the radius vector, perpendicular to it in the orbital plane and normal to orbital plane, respectively

The components of the perturbing acceleration S,T,W are

represented in the following terms

$$S = S_1 + S_2 + S_3$$
$$T = T_1 + T_2 + T_3$$
$$W = W_1 + W_2 + W_3$$

where

S_1, T_1, W_1 = components of perturbing acceleration due to the compression of Earth
S_2, T_2, W_2 = components of perturbing acceleration produced by the force of atmospheric resistance
S_3, T_3, W_3 = components of perturbing acceleration produced by anomalies of the force of gravity

The potential of Earth's attraction with an accuracy to the order of the square of compression is as follows (5)

$$V = (fM/r)\{1 + (r_0/r)^2[c_{20}P_{20}(\sin\psi) + (c_{22}\cos 2\lambda + d_{22}\sin 2\lambda)P_{22}(\sin\psi)] + (r_0/r)^3[c_{30}P_{30}(\sin\psi) + (c_{31}\cos\lambda + d_{31}\sin\lambda)P_{31}(\sin\psi) + (c_{32}\cos 2\lambda + d_{32}\sin 2\lambda)P_{32}(\sin\psi) + (c_{33}\cos 3\lambda + d_{33}\sin 3\lambda)P_{33}(\sin\psi)] + (r_0/r)^4[c_{40}P_{40}(\sin\psi) + (c_{41}\cos\lambda + d_{41}\sin\lambda)P_{41}(\sin\psi) + (c_{42}\cos 2\lambda + d_{42}\sin 2\lambda)P_{42}(\sin\psi) + (c_{43}\cos 3\lambda + d_{43}\sin 3\lambda)P_{43}(\sin\psi) + (c_{44}\cos 4\lambda + d_{44}\sin 4\lambda)P_{44}(\sin\psi)]\} \quad [4.2]$$

where

ψ, λ = geocentric latitude and longitude of the satellite
$P_{ik}(\sin\psi)$ = spherical functions of the corresponding order of magnitude

constants r_0, f, M, c_{ik} and d_{ik} are given in (5).

Limiting ourselves in expansion 4.2 for the potential of Earth's attraction, to the principal terms with c_{20} and c_{40}, we have

$$V_1 = \frac{fM}{r}\left[1 + \left(\frac{r_0}{r}\right)^2 c_{20}P_{20}(\sin\psi) + \left(\frac{r_0}{r}\right)^4 c_{40}P_{40}(\sin\psi)\right]$$

For the principal spherical functions of Legendre's polynomials, we have (5)

$$P_{20}(\sin\psi) = \tfrac{1}{2}(3\sin^2\psi - 1)$$
$$P_{40}(\sin\psi) = \tfrac{1}{8}(35\sin^4\psi - 30\sin^2\psi + 3)$$

Differentiating the equations for V_1 over r and ψ, and projecting the acceleration projection on axes S,T,W, we derive formulas for determining the projection of the perturbing acceleration S_1, T_1, W_1

$$S_1 = -\frac{fM}{r^2}\frac{r_0^2}{r^2}\left[3c_{20}P_{20}(\sin\psi) + 5\frac{r_0^2}{r^2}c_{40}P_{40}(\sin\psi)\right]$$

$$T_1 = \frac{fM}{r^2}\frac{r_0^2}{r^2}\left[c_{20}P_{20}'(\sin\psi) + \frac{r_0^2}{r^2}c_{40}P_{40}'(\sin\psi)\right]\times \frac{\cos u}{\cos\psi}\sin i$$

$$W_1 = \frac{fM}{r^2}\frac{r_0^2}{r^2}\left[c_{20}P_{20}'(\sin\psi) + \frac{r_0^2}{r^2}c_{40}P_{40}'(\sin\psi)\right]\frac{\cos i}{\cos\psi}$$

where $P_{20}'(\sin\psi)$ and $P_{40}'(\sin\psi)$ denote derivatives of Legendre's polynomials $P_{20}(\sin\psi)$ and $P_{40}(\sin\psi)$ over ψ

$$P_{20}'(\sin\psi) = 3\sin\psi\cos\psi$$
$$P_{40}'(\sin\psi) = \frac{5}{2}\sin\psi\cos\psi(7\sin^2\psi - 3)$$
$$\cos\psi = \sqrt{1 - \sin^2\psi}$$

The projection of perturbing acceleration of the resistive force is expressed in terms of formulas given in (1 and 2)

$$S_2 = -(c_x s/2m)\rho v_{rel} v_r$$
$$T_2 = -(c_x s/2m)\rho v_{rel}(v_n - \Omega_3 r\cos i)$$
$$W_2 = (c_x s/2m)\rho v_{rel}\Omega_3 r\sin i\cos u$$

where

m = mass of the satellite
v_{rel} = velocity of the satellite relative to the atmosphere
Ω_3 = angular velocity of Earth's rotation
c_x = coefficient of aerodynamic resistance
s = cross section of the aerodynamic coefficient
ρ = atmospheric density
v_r = $(\sqrt{fM}/\sqrt{p})\,e\sin\vartheta$, radial component of absolute velocity
v_n = $(\sqrt{fM}/\sqrt{p})(1 + e\cos\vartheta)$, transversal component of absolute velocity

For the variation of the atmospheric density with altitude we have assumed a law based on the data concerning physical parameters of the atmosphere as given in (6). Trajectory measurements made on the first Soviet artificial Earth satellites indicate that the atmospheric density at the perigee of the orbit, i.e., at an altitude $h = 225$ km, is greater than given in (6) by approximately 1.3 times (7,8), so that the atmospheric density for all altitudes is increased 1.3 times correspondingly; however, the law of density variation with altitude was left unchanged in this case. For an approximation of the law of density variation with altitude, the same kind of functions were used as in (1 and 2).

The perturbation potential for the anomaly of the force of gravity (9) is

$$V_2 = \gamma_m \sum_{n=2}^{8}\left(\frac{R_m}{r}\right)^{n+1}\sum_{m=0}^{n}(\alpha_{nm}\cos m\lambda + \beta_{nm}\sin m\lambda)P_{nm}(\sin\varphi) \quad [4.3]$$

where

R_m, γ_m = mean values of the magnitude of the radius vector and the surface gravity of Earth's ellipsoid
φ, λ = geographical latitude and longitude
$P_{nm}(\sin\varphi)$ = spherical functions
α_{nm}, β_{nm} = constant coefficients

The values of these coefficients are given in (9).

The equations for S_3, T_3, W_3, the projections of acceleration on account of the anomaly of the force of gravity, can be derived readily on the basis of Eq. 4.3 for V_2

$$S_3 = \partial V_2/\partial r$$
$$T_3 = \frac{1}{r}\frac{\partial V_2}{\partial\varphi}\frac{\cos u}{\cos\psi}\sin i + \frac{1}{r\cos\varphi}\frac{\partial V_2}{\partial\lambda}\frac{\cos i}{\cos\varphi}$$
$$W_3 = \frac{1}{r}\frac{\partial V_2}{\partial\varphi}\frac{\cos i}{\cos\varphi} - \frac{1}{r\cos\varphi}\frac{\partial V_2}{\partial\lambda}\frac{\cos u}{\cos\varphi}\sin i$$

where

$$\frac{\partial V_2}{\partial r} = -\frac{\gamma_m}{R_m}\sum_{n=2}^{8}(n+1)\left(\frac{R_m}{r}\right)^{n+2}\times$$

$$\sum_{m=0}^{n}(\alpha_{nm}\cos m\lambda + \beta_{nm}\sin m\lambda)P_{nm}(\sin\varphi)$$

$$\frac{1}{r}\frac{\partial V_2}{\partial \varphi} = \frac{\gamma_m}{R_m}\sum_{n=2}^{8}\left(\frac{R_m}{r}\right)^{n+2}\sum_{m=0}^{n}(\alpha_{nm}\cos m\lambda +$$

$$\beta_{nm}\sin m\lambda)\,P_{nm}'(\sin\varphi)$$

$$\frac{1}{r\cos\varphi}\frac{\partial V_2}{\partial \lambda} = \frac{\gamma_m}{R_m\cos\varphi}\sum_{n=2}^{8}\left(\frac{R_m}{r}\right)^{n+2}\times$$

$$\sum_{m=0}^{n}(-\alpha_{nm}\sin m\lambda + \beta_{nm}\cos m\lambda)mP_{nm}(\sin\varphi)$$

Recurrent relationships can be used for determining the spherical functions:

For $n+1 \neq m$

$$P_{n+1,m} = \frac{(2n+1)\sin\varphi P_{nm} - (n+m)P_{n-1,m}}{n-m+1}$$

for $m = n+1$

$$P_{n,n} = (2n-1)\cos\varphi P_{n-1,n-1}$$

where

$$P_{00} = 1$$
$$P_{10} = \sin\varphi$$
$$P_{11} = \cos\varphi$$

Differentiating the given equations for P_{nm} over φ, we have corresponding formulas for polynomials P_{nm}':

For $n+1 \neq m$

$$P'_{n+1,m} =$$

$$\frac{(2n+1)\cos\varphi P_{nm} + (2n+1)\sin\varphi\, P_{nm}' - (n+m)P'_{n-1,m}}{n-m+1}$$

for $m = n+1$

$$P_{nn}' = (2n-1)\cos\varphi P'_{n-1,n-1} - (2n-1)\sin\varphi P_{n-1,n-1}$$

where

$$P_{00}' = 0$$
$$P_{10}' = \cos\varphi$$
$$P_{11}' = -\sin\varphi$$

Let us now derive the formula for the energy integral which can be used as a reference during the calculation.

In our case, the system of forces under investigation is not a conservative one. Therefore, the standard law of conservation of mechanical energy, which equals the sum of kinetic and potential energy, is not applicable. However, if the quantity of energy scattered at every moment of time as a result of deceleration of the satellite by the atmosphere is known, then we have

$$E = T + V + E_\rho = \text{const} \qquad [4.4]$$

where

T = kinetic energy
V = potential energy of the satellite
E_ρ = scattered energy

Hence, we have

$$E_\rho = \int_{u_0}^{u} ds\cdot\mathbf{R}$$

where the expression for the elementary work function completed by the force of resistance is under the sign of the integral.

Since $ds = vdt$, then

$$E_\rho = \int_{u_0}^{u}(v_r S_2 + v_n T_2)F\,du \qquad [4.5]$$

where $F = dt/du$.

Substituting expressions for the kinetic and potential energies in the right-hand side of Eq. 4.4, and applying Eq. 4.5, we finally have the following equation for the energy integral

$$E = \frac{v^2}{2} + V_1 - V_2 + \int_{u_0}^{u}(v_r S_2 + v_n T_2)F\,du$$

Solution of the system of differential equations, Eqs. 4.1, which describe the motion of the satellite for considerably small time intervals, permits the use of the method of numerical integration. In the case of large time intervals, such methods are not very suitable.

In this connection we convert from the initial system of equations, Eqs. 4.1, to a system of equations which is derived as a result of integrating over u for one revolution (that is, for the period 2π) of system 4.1. Such a system of equations may serve to describe variations of osculating elements of the satellite's orbit in time. As a result, we have a system of equations of finite differences for the osculating elements of the orbit and time t of the following form

$$\begin{aligned}
\delta p &= \chi_1(u, p, e, \ldots)\\
\delta e &= \chi_2(u, p, e, \ldots)\\
\delta\omega &= \chi_3(u, p, e, \ldots)\\
\delta\Omega &= \chi_4(u, p, e, \ldots)\\
\delta i &= \chi_5(u, p, e, \ldots)\\
\delta t &= \chi_6(u, p, e, \ldots)
\end{aligned} \qquad \ldots\ldots\ldots\ldots\ldots\ldots\ldots\ldots\ldots [4.6]$$

where $\delta p, \delta e, \ldots, \delta t$ denote the variations of osculating elements of the orbit $p, e, \ldots$ and time t for a revolution, i.e., on variation of u by 2π, and functions χ_j $(j = 1, 2, \ldots, 6)$ denote the integrals

$$\chi_1 = \int_u^{u+2\pi}\frac{dp}{du}du \qquad \chi_2 = \int_u^{u+2\pi}\frac{de}{du}du$$

$$\chi_3 = \int_u^{u+2\pi}\frac{d\omega}{du}du \qquad \chi_4 = \int_u^{u+2\pi}\frac{d\Omega}{du}du$$

$$\chi_5 = \int_u^{u+2\pi}\frac{di}{du}du \qquad \chi_6 = \int_u^{u+2\pi}\frac{dt}{du}du$$

and the derivatives under the integral signs are determined by Eqs. 4.1.

Let us assume that the system of equations 4.6 satisfy initial conditions $u = u_0$, $p = p_0$, $e = e_0$, $\omega = \omega_0$, $i = i_0$, $\Omega = \Omega_0$, $t = t_0$.

The system of equations of finite differences, Eqs. 4.6, the right-hand side of which is expressed through values of a set of integral systems, describes variations of the elements of the satellite's orbit in time. Solution of this system represents a discrete sequence of osculating elements of the orbit for integral values of N or for values of the argument of latitude $u = u_0 + 2\pi k$ $(k = 1, 2, \ldots)$.

Conversion from solution of the system of differential equations, Eqs. 4.1, to the solution of the system of equations of finite differences, Eqs. 4.6, is shown geometrically in Fig. 1.

Solid lines show the curves of variation of osculating elements p and e of a certain orbit, described by the system of equations 4.1 for the duration of the first four revolutions. The dashed lines represent curves of variation of the same osculating elements corresponding to the system of difference equations.

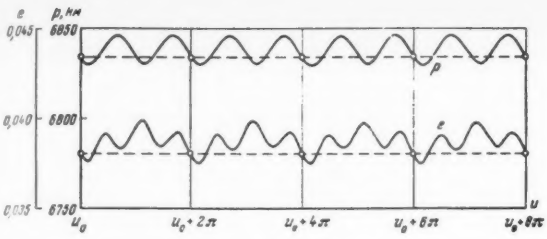

Fig. 1

The integrals in the right-hand sides of the equations must be replaced by corresponding differential equations. In such a case, solution of the system of equations of finite differences, Eqs. 4.6, is reduced to a dicyclic algorithm: The external, numerical solution of argument N (h must be equal to 1 in this case) and the internal, integration over argument u; the latter must be carried out in every point of the external algorithm on calculation of the right-hand side of the equations.

The step $H = Nh$ of the numerical solution of the system of difference equations 4.6 is selected in such a manner that the error of determining the desired functions would not exceed a pre-assigned value (on condition that the integration step for the internal system Δu is selected in a corresponding manner). Note that the step H can be variable.

In the next section the results of calculations of certain trajectories of artificial Earth satellites are given. In this case the step of numerical solution of the system of difference equations at high altitudes was considerable and was taken as large as 100 revolutions. In the course of time this step was gradually decreased.

Furthermore, it must be borne in mind that step H must be such that functions k_j ($j = 1, 2, 3, 4$), which serve for the determination of the increment of the desired functions in the case of difference equations 4.6, are calculated for points separated by $u + 2\pi k$, where k is an integer.

It is clear that if the internal system of differential equations is integrated from a certain value of the independent variable u, to a value $u + 2\pi$, h is assumed equal to 1. In such a case, N stands for the number of complete revolutions over u. The internal system of equations can be integrated from value u to $u + 4\pi$ and so on. Then, h must equal 2, and so on.

5. Some Results of the Calculation of Orbits

The method of dicyclic solution was employed for calculating the orbits of artificial Earth satellites.

This section gives some results of such calculations for the structural parameters of a satellite which are close to the parameters of the first Soviet artificial Earth satellite.

The initial values of osculating elements of the orbit were assumed equal to

$$p_0 = 6846.7 \text{ km} \qquad e_0 = 0.03881$$

$$\Omega = 0.5940 \qquad i_0 = 1.132$$

They correspond to the following values of the altitude of the apogee, altitude of the perigee and the velocity at the perigee

$$h_{a_0} = 752.0 \text{ km} \qquad h_{\pi_0} = 219.7 \text{ km} \qquad v_{\pi_0} = 7.922 \text{ km/sec}$$

The external system of equations of finite differences were solved numerically with the aid of the fourth-order Runge-type algorithm. The step of integrating the external system at first equaled 128 revolutions. The step decreased with decreasing altitude.

Calculations were made for the following cases:

1 All specified perturbation forces are active.
2 Atmospheric resistance is absent.
3 Compression of Earth absent.

Figs. 2–4 show the results of the calculations. Fig. 2 shows curves of variation of parameter p, eccentricity e, inclination of orbit i, and the longitude of ascending node Ω for a period of time equal to 94 days. Fig. 3 shows curves of the variation of altitudes of the apogee h_a, altitude of the perigee h_π and the velocity at the perigee v_π, for the same case. Fig. 4 shows curves of variation of parameter p and eccentricity e for a period equal to 1200 days, for case 2.

Curves of variation of the osculating elements of the orbit, representing case 3, are analogous to the curves shown in Figs. 2 and 3 and, therefore, are not given separately.

It should like to express my deep gratitude to D. E. Okhotsimskii for his invaluable advice and attention to this work and also to V. I. Shelykhin for his assistance in the mathematical work.

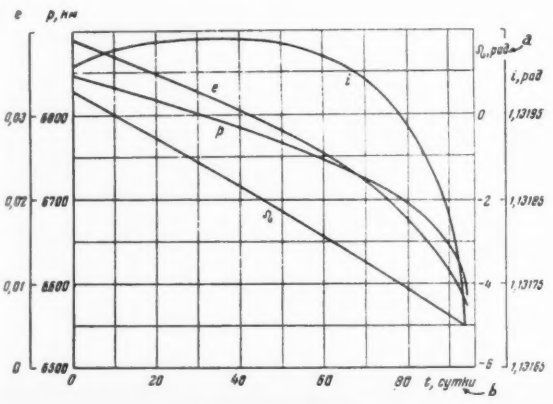

Fig. 2 [a]Rad; [b]days

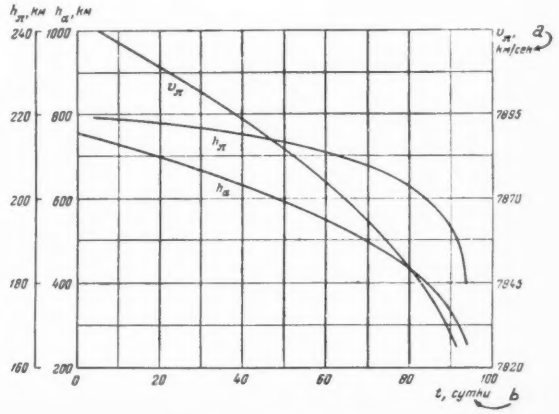

Fig. 3 [a]Km/sec; [b]days

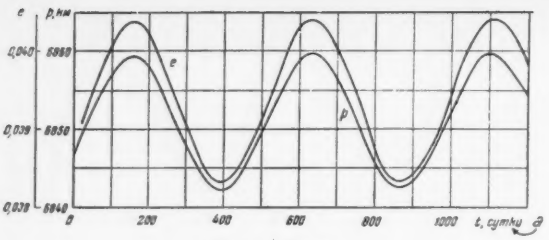

Fig. 4 [a]Days

References

1 Okhotsimskii, D. E., Eneev, T. M. and Taratynova, G. P., *Usp. Fiz. Nauk (Progress in Physical Sciences)*, vol. 63, 1957, p. 33.

2 Taratynova, G. P., *Usp. Fiz. Nauk (Progress in Physical Sciences)*, vol. 63, 1957, p. 51.

3 Gel'fond, A. O., *Ischislenie Konechnykh Raznostei (Computation of Finite Differences)*, 1952.

4 Kollatts, L., *Chislennye Metody Resheniia Differentsial'nykh Uravnenii (Numerical Methods for Solving Differential Equations)*, IL, 1953.

5 Zhongolovich, I. D., *Biulleten' ITA*, 1957, vol. 6, no. 8 (81).

6 Mitra, S. K., *Verkhniaia Atmosfera (Upper Atmosphere)*, IL, 1955.

7 Lidov, M. L., *Iskusstvennye Sputniki Zemli (Artificial Earth Satellites)*, no. 1, p. 9, IZD-VO AN SSSR (Publishing House of the Academy of Sciences USSR), 1958.

8 El'iasberg, P. E., *Iskusstvennye Sputniki Zemli (Artificial Earth Satellites)*, no. 1, p. 21, IZD-VO AN SSSR (Publishing House of the Academy of Sciences USSR), 1958.

9 Zhongolovich, I. D., *Trans. Inst. Theoret. Astronomy, Akad. Nauk SSSR*, no. 3, 1952.

Reviewer's Comment

The introductory part of this article is descriptive, but it furnishes an essential background for the detailed developments of the main body of the paper beginning with Section 1, "Generalization of the Runge Method."

Briefly this introduction may be stated as follows:

Let p_i be the six elements of a perturbed orbit. Then the equations of motion are

$$dp_i/du = f_i(p_1, \ldots, p_6, u)$$

The solution of these equations of motion would yield the elements as functions of the independent variable u. The author prefers to use as independent variable the argument of the latitude for an artificial satellite. Actually, the choice of independent variable is, to a large extent, immaterial.

If a sufficiently small interval is used, the increment of the elements

$$\delta p_i = \chi_i(p_1, p_2, \ldots, p_6) \qquad [A]$$

for a single revolution, from ascending node to ascending node, may be obtained by numerical integration. Again, another method may be used to obtain this information.

In some problems in celestial mechanics the changes of the elements δp_i over a revolution are essentially the same from one revolution to the next. Yet replacing the difference equation A by a differential equation

$$dp_i/dN = \chi_i(p_1, \ldots, p_6)$$

is an approximation. N stands for the number of revolutions that constitutes a step.

The major part of the article deals with the development of a numerical theory of difference equations, applicable to this type of problem.

The term dicyclic integration is introduced to characterize the procedure. For occasional revolutions (say 1, 6, 11, . . .; or 1, 101, 201, . . .) a precise integration is made over an entire period. This is the short (internal) cycle, whereas the cycle of five or 100 periods represents the long (external) cycle.

This is a new approach that is especially applicable to artificial satellite motion. A paper by David Mace and L. H. Thomas (*Astronomical J.*, vol. 65, 1960, p. 300) deals with essentially the same problem, but the theory of difference equations here developed appears to be a significant step forward and an important contribution to numerical analysis.

—Dirk Brouwer
Yale University Observatory

Propagation of Forced Plane Compression Waves of Small Amplitude in a Viscous Gas When Radiation Is Taken Into Account

V. A. PROKOF'EV

STOKES (1)[1] and Rayleigh (2) have considered the effects of radiative cooling in accordance with Newton's law on the attenuation of sound waves in an inviscid gas. Radiative transfer affects the propagation of small amplitude waves not only for hot gases (for which one would expect thermal radiation to be important) but also for some gases under ordinary conditions. Direct calculations for moist air under ordinary conditions show that radiation has an effect on the absorption of audible low frequency sound waves comparable to those of viscosity and heat conduction; moreover, the latter two effects become negligible relative to the first for sub-audible frequencies.

Translated from *Izvestiia Akademii Nauk SSSR, Mekhanika i Mashinostroenie (Bulletin of the Academy of Sciences USSR, Mechanics and Machine Building)*, 1960, no. 2, pp. 17–33. Translated by Research Information Service, New York.

[1] Numbers in parentheses indicate References at end of paper.

I have given (3) the characteristic (frequency) equation for plane harmonic waves of small amplitude in an unbounded compressible fluid having a finite viscosity and a finite thermal conductivity; in deriving it allowance was made for the effects caused by the radiation field created by small perturbations, for which purpose the equation for the transfer of radiant energy was used in a form averaged with respect to frequency and to direction, the velocity of propagation of the radiation being taken as infinitely great.

Here a more rigorous treatment of the propagation of waves in a radiation field is given, to which end are used linearized equations for the hydrodynamics of a radiating fluid and equations from the theory of radiation fields (4) in which allowance is made for the finite velocity of propagation (the speed of light) and for the distributions of the radiation in frequency and in direction. Absorption and emission are allowed for; so are the internal radiation energy and the mechanical effects of the radiation.

1. The Characteristic Equation

If the radiation obeys Kirchhoff's law, and if the equation of state is taken in the general form

$$f(p,\rho,T) = 0 \qquad \epsilon_T = \varphi(p,\rho,T)$$

we can use a method given elsewhere (5) to find the characteristic (frequency) in the dimensionless form

$$[\gamma + (1 + \gamma i X)m^2][(i + ZX^{(0)})m + 6i\beta\xi X^{(1)} - \Theta m^3] + im^2(\gamma - 1 + b_1)(m - 12\xi X^{(2)}/h_2) = 0 \quad [1.1]$$

This equation describes the motion of forced plane harmonic waves of infinitesimal amplitude in an unbounded viscous conducting medium, the waves being of the form $\rho^*(x, t) = \rho^* = (0,0)\exp(ax + i\sigma t)$ and being generated by a harmonic source maintained by external means and situated at the origin. Some symbols which shall be used are

$$\begin{aligned}
m &= c_0 a/\sigma & h_3 &= -(\partial\epsilon_T/\partial\rho)\rho \\
X &= (\lambda + 2\mu)_0\sigma/\gamma p_0 h_1 & h_4 &= c_{v0}T_0 \\
\Theta &= k_0 T_0\sigma/\gamma p_0 h_1 h_4 & \beta &= p_0/\rho_0 h_4 \\
Z &= 16\pi I_0/\rho c_0 h_4 & \gamma &= 1 + (h_2/h_1h_4)(h_3 + p_0/\rho_0) \\
\xi &= pR_0/p_0 & \pi I_0 &= \sigma_R T_0^4 \\
h_1 &= (\partial \ln p/\partial \ln \rho)_0 & p_{R0} &= (4/3)\pi I_0 \\
h_2 &= (\partial \ln p/\partial \ln T)_0 & b_1 &= 4(h_2/h_1)\beta\xi
\end{aligned} \quad [1.2]$$

I have dealt in (3) with the physical meanings of m, X, Θ and Z, and of the symbols appearing therein; Z is the reciprocal of Boltzmann's constant if we take as the characteristic speed the adiabatic speed of sound c_0; X is the reciprocal of the generalized Reynolds number referred to c_0 and to the adiabatic wave length. These might be called the reciprocals of the Boltzmann and Reynolds wave numbers. Also, γ is the ratio of the specific heats, and ξ is the ratio of the radiation pressure p_{R0} to the pressure p_0 in the unperturbed medium.

The $X^{(j)}$ are related to the frequency $\sigma/2\pi$ and to the state of the medium

$$X^{(0)}\int_0^\infty \frac{\partial B_\nu}{\partial T}\,d\nu = \int_0^\infty \frac{\partial B_\nu}{\partial T}\,w_\nu\left(1 - \frac{1}{2q_\nu}\ln\frac{1+q_\nu}{1-q_\nu}\right)d\nu$$

$$X^{(1)}\int_0^\infty \frac{\partial B_\nu}{\partial T}\,d\nu = \int_0^\infty \frac{\partial B_\nu}{\partial T}\,w_\nu \ln\frac{1+q_\nu}{1-q_\nu}\,d\nu$$

$$X^{(2)}\int_0^\infty \frac{\partial B_\nu}{\partial T}\,d\nu = \int_0^\infty \frac{\partial B_\nu}{\partial T}\,w_\nu\frac{1}{q_\nu}\left(1 - \frac{1}{2q_\nu}\ln\frac{1+q_\nu}{1-q_\nu}\right)d\nu \quad [1.3]$$

in which B_ν is Planck's function; the other symbols are

$$q_\nu = \frac{m}{w_\nu + ic^\circ} \qquad w_\nu = \frac{c_0 w_{\nu e}}{\sigma} \qquad \omega_{\nu 0} = \rho\alpha_{\nu e} \qquad c^\circ = \frac{c_0}{c} \quad [1.4]$$

in which $\omega_{\nu 0}$ is the volume absorption coefficient for thermal radiation. These quantities can have any values in classical mechanics, but in relativistic mechanics they must be less than 1. The numbers Z, ξ and c° are related by

$$Z = 12\beta\xi/c^\circ \quad [1.5]$$

Again, w_ν may be called the spectral Bouger wave number because (apart from a factor $1/2\pi$) it is the same as the ordinary Bouger wave number if we take as the characteristic dimension the adiabatic wave length $l_0 = 2\pi c_0/\sigma$ and as the opacity factor the volume absorption coefficient for the frequency ν. The reciprocal v_ν of that number is proportional to frequency and is equal to 2π times the adiabatic wave length expressed in mean free paths for radiation of frequency in the range from ν to $\nu + d\nu$ (of spectral frequency ν). The parameter q_ν is complex; it can be expressed in the form

$$q_\nu = q_{\nu r} + iq_{\nu i} = \pm(\alpha_{\nu\tau} + in_\nu) \qquad |q_{\nu r}| = \alpha_{\nu\tau} = \frac{|a_r|}{\omega_{\nu 0}}$$

$$|q_{\nu i}| = n_\nu = \frac{|a_i|}{\omega_{\nu 0}} = \frac{\sigma}{\omega_{\nu 0}c_a} = \frac{2\pi}{\omega_{\nu 0}l} = \frac{2\pi}{l_{\nu\tau}} \quad [1.6]$$

The real part of q_ν equals the absorption (attenuation) coefficient $\alpha_{\nu\tau}$ for a mean free path $\tau_\nu = 1/\omega_{\nu 0}$ at optical frequency ν. The imaginary part equals the wave number n_ν referred to the wave length $l_{\nu\tau}$ expressed in units of mean free path for the optical frequency ν. Further, c_a is the actual speed of the wave, and l is the wave length; Eq. 1.1 implies that q_ν is an even function, which explains the double sign in Eqs. 1.6.

The optical absorption coefficient is determined by the nature and state of the medium and is a complicated function of frequency having many sharp peaks superimposed on a smooth curve Under normal conditions the continuous absorption, represented by the smooth curve, is negligible or zero within the range of interest, so the curve consists simply of a set of peaks. Therefore, the integrals over the whole spectrum for $X^{(j)}$ may be replaced by the sums of the integrals for the peaks, i.e., by the sum of a finite number of terms.

Further, X, Θ, Z, ξ, and c° are small over an extensive range of frequencies for liquids and gases under conditions close to normal; for example, for air at zero deg C and 760 mm Hg we have

$$X = 1.60\cdot10^{-10}\sigma \qquad \Theta = 2.26\cdot10^{-10}\sigma \qquad Z = 6.07\cdot10^{-6}$$
$$\xi = 1.38\cdot10^{-12} \qquad c^\circ = 1.105\cdot10^{-6} \quad [1.7]$$

These values are typical as regards order of magnitude for all gases in the normal state; they all increase with temperature. For example, for a perfect gas having fixed specific heats the ratios for two different sets of conditions are

$$\frac{X_2}{X_1} = \frac{\theta_2}{\theta_1} = \frac{p_1}{p_2}\left(\frac{T_2}{T_1}\right)^n \qquad \frac{Z_2}{Z_1} = \frac{p_1}{p_2}\left(\frac{T_2}{T_1}\right)^{7/2}$$

$$\frac{\xi_2}{\xi_1} = \frac{p_1}{p_2}\left(\frac{T_2}{T_1}\right)^4 \qquad \frac{c_2^\circ}{c_1^\circ} = \left(\frac{T_2}{T_1}\right)^{1/2} \quad [1.8]$$

It is assumed here that the viscosity and thermal conductivity are proportional to T^n (it is usual to take $1/2 \le n \le 1$ in gasdynamics) and that the Stokes' relation applies to the viscosities. Then X and Θ remain small except at very high frequencies, but at those frequencies the wave length becomes comparable with the mean free path for the radiation (6),

and the mechanics of continuous media cease to be applicable. It is possible to have a case such that

$$\xi \ll 1, \quad Z = 0(1): \quad \xi \ll 1, Z \gg 1; \quad \xi = 0(1), Z = 0(1)$$
$$\xi = 0(1), Z \gg 1; \quad \xi \gg 1, Z \gg 1$$

at high temperatures, in which X and Θ remain small at all acoustic frequencies allowed by the ultimate structure of the medium. Again, c° may approach 1, but only at temperatures far above the range considered here; and ξ can be large only at very low pressures combined with very high temperatures. Such conditions shall not be dealt with; X (and hence θ) shall be taken small (except in certain limiting cases), i.e., small perturbations having large Reynolds wave numbers shall be considered.

2. Limiting Frequencies

The $|q_\nu|$ will be large for any spectral region of the thermal radiation for a compression wave whose phase velocity lies between the isothermal and adiabatic speeds of sound or is of the order of those speeds if w_ν and c° are both small simultaneously. The first condition will be complied with for any medium in a certain range of frequencies; that range is controlled by the state and nature of the medium and begins at not very low audio frequencies if the medium is highly transparent. The second is satisfied in all cases, except at very high temperature (when relativistic effects become appreciable).

If $|q_\nu| > 1$, the $X^{(j)}$ may be expanded as an absolutely convergent series

$$X^{(j)} = -\sum_{k=0}^{\infty} \frac{1}{2k-1} \left(\int_0^\infty \frac{\partial B_\nu}{\partial T} w_\nu q_\nu^{-2k+s_j} \, d\nu \right) \times$$
$$\left(\int_0^\infty \frac{\partial B_\nu}{\partial T} \, d\nu \right)^{-1} \mp \pi i (-1)^j 2^{-k_1} \int_0^\infty \frac{\partial B_\nu}{\partial T} w_\nu q_\nu^{-k_2} \, d\nu \qquad [2.1]$$

where

$$s_j = \frac{(-1)^j \cdot j}{j!}$$

$$k_1 = (1+j)^j$$

$$k_2 = (1-j)^j j! \quad (j = 0,1,2)$$

We take only the first terms and get

$$X^{(0)} \approx w_1$$

$$X^{(1)} \approx \pm \pi i w_1 + (2/m)(w_2^2 + ic^\circ w_1)$$

$$X^{(2)} \approx \frac{1}{m}(w_2^2 + ic^\circ w_1)$$

$$w_n^n \int_0^\infty \frac{\partial B_\nu}{\partial T} \, d\nu = \int_0^\infty \frac{\partial B_\nu}{\partial T} w_\nu^n d\nu$$

. . . . . [2.2]

The first equation in 2.2 gives us the rule for determining the mean optical absorption coefficient for large $|q_\nu|$; here we need not the Rosseland mean (the one often used) but another mean ω_1, whose weight is $\partial B_\nu/\partial T$, because

$$w_1 \int_0^\infty \frac{\partial B_\nu}{\partial T} \, d\nu = \int_0^\infty \frac{\partial B_\nu}{\partial T} w_\nu \, d\nu \qquad [2.3]$$

This equation also defines the numerical factor that is introduced in averaging the radiation transport equation with respect to direction. Comparison with the characteristic equation given previously (3) shows that the coefficients are $g = (1/3)^{1/2}$ and $g' = 1/2$ or $g = g' = 1/2$, i.e., Eddington's and Schwarzchild's means, respectively. But these factors and that mode of forming the mean are suitable only for calculations based solely on the main terms in the expansion, and then for two cases only, namely if we take c° as zero and we take frequencies so high that $w_\nu \ll c^\circ$, i.e., such that $c\omega_{\nu_0}/\sigma \ll 1$, which is equivalent to the requirement that the lifetime of the front for any optical frequency must exceed the period of oscillation of the wave. If the latter terms are taken, or if we do not have $w_\nu \ll c^\circ$ (with $c^\circ \neq 0$), it becomes impossible to use only one factor and one averaging coefficient in determining w.

All three functions in $X^{(j)}$ tend to zero when the oscillation frequency increases indefinitely, whereas X and θ, which represent the effects of viscosity and conductivity, increase; when they become large, the characteristic equation splits up into two equations

$$(i - Xm^2)(i - \theta m^2) = 0 \qquad [2.4]$$

representing the motions of the viscosity wave and thermal conductivity wave, respectively, as when radiation is neglected entirely (7). The radiation field appears only in small corrections to the absorption coefficient and to the wave velocity, which in this case is large relative to the adiabatic velocity. Although $|m|$ is small, it is without effect on the foregoing estimates, because $|m|/w_\nu$ is directly proportional to the square root of the oscillation frequency. The remarks made previously on the limits to the applicability of hydrodynamic theory for X and θ large must be borne in mind.

Only one factor b_1, which contains the radiation pressure, remains in the frequency equation when $w_\nu \to 0$ and $|m|$ is bounded; if the Bouger wave numbers tend to zero on account of a reduction in transparency, the terms representing viscosity and molecular conductivity may be small. It can happen that all the dissipative terms are small; the absorption and the dispersion they cause are dealt with in Section 3. On the other hand, if X and Θ are of the order of 1, the result is analogous to that for X and θ large.

The other limiting case (of very large Bouger wave numbers—very low frequencies and very strong optical absorption) corresponds to q_ν having small absolute value, subject to restriction on the value of the root to the characteristic equation. If $|q_\nu| < 1$ we have

$$X^{(0)} \int_0^\infty \frac{\partial B_\nu}{\partial T} d\nu = -\sum_{n=1}^{\infty} \frac{1}{2n+1} \int_0^\infty \frac{\partial B_\nu}{\partial T} w_\nu q_\nu^{2n} \, d\nu$$

$$X^{(1)} \int_0^\infty \frac{\partial B_\nu}{\partial T} \, d\nu = 2 \sum_{n=1}^{\infty} \frac{1}{2n-1} \int_0^\infty \frac{\partial B_\nu}{\partial T} w_\nu q_\nu^{2n-1} \, d\nu$$

$$X^{(2)} \int_0^\infty \frac{\partial B_\nu}{\partial T} \, d\nu = -\sum_{n=1}^{\infty} \frac{1}{2n+1} \int_0^\infty \frac{\partial B_\nu}{\partial T} w_\nu q_\nu^{2n-1} \, d\nu$$

. . . . . [2.5]

We take only the first terms and get

$$X^{(0)} \approx -\frac{m^2}{3w_R} \qquad X^{(1)} \approx 2m \qquad X^{(2)} \approx -\frac{m}{3} \qquad [2.6]$$

The first equation defines the rule for calculating the capacity coefficient for $|q_\nu| \ll 1$ (the Rosseland mean is required)

$$\frac{1}{\omega_R} \int_0^\infty \frac{\partial B_\nu}{\partial T} \, d\nu = \int_0^\infty \frac{\partial B_\nu}{\partial T} \frac{d\nu}{\omega_{\nu_0}} \qquad [2.7]$$

It also defines the method of averaging with respect to direction; the coefficients suitable here are $g = (1/3)^{1/2}$ and $g' = 1/2$ or $g = g' = 2/3$ [see (8 and 4)]. We may average with respect to frequency also if we allow for the mechanical effects of the radiation, although then still further coefficients must be introduced in averaging with respect to direction.

3. Nearly Adiabatic Waves

The characteristic equation has a single root corresponding to undamped waves propagating with the Laplace speed of sound when dissipation is absent. The speed of a compression wave in a real, and hence dissipative, fluid is close to the adiabatic speed, and the attenuation factor is small. Let us consider such waves since they are the ones of greatest interest under conditions not deviating greatly from normal; in the next section nearly isothermal waves (ones propagating with the Newtonian speed of sound) shall be discussed. Let the root of the characteristic equation take the form

$$m = \pm i m_0 (1 + \epsilon_1 + \epsilon_2 + \dots) \qquad [3.1]$$

in which m_0 is a real number to be determined and the ϵ are small quantities whose orders are indicated by the subscripts. $X^{(j)}$ are

$$(-1)^k X^{(j)} = a_0^{(j)} + a_1^{(j)}\epsilon_1 + a_2^{(j)}\epsilon_2 + a_3^{(j)}\epsilon_1^2 + \dots \qquad (k = j/j!) \qquad [3.2]$$

The first coefficients in the expansion take the form

$$a_0^{(0)} \int_0^\infty \frac{\partial B_\nu}{\partial T}\,d\nu = \int_0^\infty \frac{\partial B_\nu}{\partial T}\,w_\nu\left[1 + \frac{i}{2}(w_\nu' + ic^{\circ\prime})a_{11}^{\circ}\right]d\nu$$

$$a_1^{(0)} \int_0^\infty \frac{\partial B_\nu}{\partial T}\,d\nu = -\frac{1}{2}\int_0^\infty \frac{\partial B_\nu}{\partial T}\,w_\nu(w_\nu' + ic^{\circ\prime}) \times \left[ia_{11}^{\circ} + \frac{2(w_\nu' + ic^{\circ\prime})}{1 + (w_\nu' + ic^{\circ\prime})^2}\right]d\nu$$

$$a_0^{(1)} \int_0^\infty \frac{\partial B_\nu}{\partial T}\,d\nu = \int_0^\infty \frac{\partial B_\nu}{\partial T}\,w_\nu a_{11}^{\circ} d\nu$$

$$a_1^{(1)} \int_0^\infty \frac{\partial B_\nu}{\partial T}\,d\nu = 2i\int_0^\infty \frac{\partial B_\nu}{\partial T}\,w_\nu \frac{w_\nu' + ic^{\circ\prime}}{1 + (w_\nu' + ic^{\circ\prime})^2}\,d\nu$$

$$a_0^{(2)} \int_0^\infty \frac{\partial B_\nu}{\partial T}\,d\nu = -i\int_0^\infty \frac{\partial B_\nu}{\partial T}\,w_\nu(w_\nu' + ic^{\circ}) \times \left[1 + \frac{i}{2}(w_\nu' + ic_\nu^{\circ\prime})a_{11}^{\circ}\right]d\nu$$

$$a_1^{(2)} \int_0^\infty \frac{\partial B_\nu}{\partial T}\,d\nu = i\int_0^\infty \frac{\partial B_\nu}{\partial T}\,w_\nu(w_\nu' + ic^{\circ\prime}) \times \left[1 + i(w_\nu' + ic^{\circ\prime})a_{11}^{\circ} + \frac{(w_\nu' + ic^{\circ\prime})^2}{1 + (w_\nu' + ic^{\circ\prime})^2}\right]d\nu \qquad [3.3]$$

Here

$$a_{11}^{(0)} = \frac{1}{2}\ln\frac{w_\nu'^2 + (1 + c^{\circ\prime})^2}{w_\nu'^2 + (1 - c^{\circ\prime})^2} + i \arctan\frac{2w_\nu'}{[w_\nu'^2 - (1 - c^{\circ\prime 2})]}$$

$$w_\nu' = \frac{w_\nu}{m_0}$$

$$c^{\circ\prime} = \frac{c^{\circ}}{m_0} \qquad [3.4]$$

The main interest is in the case when c° is small, so we expand the $a_i^{(k)}$ in powers of the small quantity $c^{\circ\prime}$

$$a_i^{(k)} = a_{i,0}^{(k)} + a_{i,1}^{(k)}c^{\circ\prime} + a_{i,2}^{(k)}c^{\circ\prime 2} + \dots$$

$$a_{0,0}^{(0)} \int_0^\infty \frac{\partial B_\nu}{\partial T}\,\partial\nu = \int_0^\infty \frac{\partial B_\nu}{\partial T}\,w_\nu(1 - w_\nu' \operatorname{arc\,cotan} w_\nu')d\nu$$

$$a_{0,1}^{(0)} \int_0^\infty \frac{\partial B_\nu}{\partial T}\,d\nu \equiv ib_{0,1}^{(0)} \int_0^\infty \frac{\partial B_\nu}{\partial T}\,d\nu = i\int_0^\infty \frac{\partial B_\nu}{\partial T}\,w_\nu\left(\frac{w_\nu'}{1 + w_\nu'^2} - \operatorname{arc\,cotan} w_\nu'\right)d\nu$$

$$a_{1,1}^{(0)} \int_0^\infty \frac{\partial B_\nu}{\partial T}\,d\nu \equiv ib_{1,1}^{(0)} \int_0^\infty \frac{\partial B_\nu}{\partial T}\,d\nu = i\int_0^\infty \frac{\partial B_\nu}{\partial T}\,w_\nu \times \left(\operatorname{arc\,cotan} w_\nu' - \frac{w_\nu'(3 + w_\nu'^2)}{(1 + w_\nu'^2)^2}\right)d\nu$$

$$a_{1,2}^{(1)} \int_0^\infty \frac{\partial B_\nu}{\partial T}\,d\nu = 2\int_0^\infty \frac{\partial B_\nu}{\partial T}\,w_\nu \frac{1 - w_\nu'^2}{(1 + w_\nu'^2)^3}\Big)\,d\nu$$

$$a_{0,0}^{(1)} \int_0^\infty \frac{\partial B_\nu}{\partial T}\,d\nu \equiv 2ib_{0,0}^{(1)} \int_0^\infty \frac{\partial B_\nu}{\partial T}\,d\nu = \int_0^\infty \frac{\partial B_\nu}{\partial T}\,w_\nu \operatorname{arc\,cotan} w_\nu' d\nu$$

$$a_{0,1}^{(1)} \int_0^\infty \frac{\partial B_\nu}{\partial T}\,d\nu = 2\int_0^\infty \frac{\partial B_\nu}{\partial T}\,\frac{w_\nu d\nu}{1 + w_\nu'^2}$$

$$a_{0,2}^{(1)} \int_0^\infty \frac{\partial B_\nu}{\partial T}\,d\nu = -2i\int_0^\infty \frac{\partial B_\nu}{\partial T}\,\frac{w_\nu w_\nu' d\nu}{(1 + w_\nu'^2)^2}$$

$$a_{1,0}^{(1)} \int_0^\infty \frac{\partial B_\nu}{\partial T}\,d\nu \equiv 2ib_{1,0}^{(1)} \int_0^\infty \frac{\partial B_\nu}{\partial T}\,d\nu = 2i\int_0^\infty \frac{\partial B_\nu}{\partial T}\,w_\nu \frac{w_\nu' d\nu}{1 + w_\nu'^2}$$

$$a_{1,1}^{(1)} \int_0^\infty \frac{\partial B_\nu}{\partial T}\,d\nu = -2\int_0^\infty \frac{\partial B_\nu}{\partial T}\,w_\nu \frac{1 - w_\nu'^2}{(1 + w_\nu'^2)^2}\,d\nu$$

$$a_{1,2}^{(1)} \int_0^\infty \frac{\partial B_\nu}{\partial T}\,d\nu = 2i\int_0^\infty \frac{\partial B_\nu}{\partial T}\,w_\nu w_\nu' \frac{3 - w_\nu'^2}{(1 + w_\nu'^2)^3}\,d\nu$$

$$a_{0,0}^{(2)} \int_0^\infty \frac{\partial B_\nu}{\partial T}\,d\nu = -ib_{0,0}^{(0)} \int_0^\infty \frac{\partial B_\nu}{\partial T}\,d\nu = -i\int_0^\infty \frac{\partial B_\nu}{\partial T}\,w_\nu w_\nu'(1 - w_\nu' \operatorname{arc\,cotan} w_\nu')d\nu$$

$$a_{0,1}^{(2)} = 2a_{0,0}^{(0)} - \tfrac{1}{2}a_{0,1}^{(1)}$$

$$a_{1,0}^{(2)} = -2a_{0,0}^{(2)} - \tfrac{1}{2}a_{1,0}^{(1)}$$

$$a_{0,2}^{(2)} \int_0^\infty \frac{\partial B_\nu}{\partial T}\,d\nu = -i\int_0^\infty \frac{\partial B_\nu}{\partial T}\,w_\nu \times \left(\operatorname{arc\,cotan} w_\nu' - \frac{w_\nu'(2 + w_\nu'^2)}{1 + w_\nu'^2}\right)d\nu$$

$$a_{1,1}^{(2)} \int_0^\infty \frac{\partial B_\nu}{\partial T}\,d\nu = -\int_0^\infty \frac{\partial B_\nu}{\partial T}\,w_\nu \times \left[\frac{1 + 7w_\nu'^2 + 4w_\nu'^4}{(1 + w_\nu'^2)^2} - 4w_\nu' \operatorname{arc\,cotan} w_\nu'\right]d\nu$$

$$a_{1,2}^{(2)} \int_0^\infty \frac{\partial B_\nu}{\partial T}\,d\nu = -i\int_0^\infty \frac{\partial B_\nu}{\partial T}\,w_\nu \times \left[\frac{7 + 5w'^2 + 2w_\nu'^4}{(1 + w_\nu'^2)^3}\,w_\nu' - 2 \operatorname{arc\,cotan} w_\nu'\right]d\nu \qquad [3.5]$$

This expansion applies for all w_ν' in the range from zero to ∞; all the $a_i^{(k)}$ tend to zero as w_ν' tends to zero. If we neglect terms containing c in the denominator (c° is small), we find (as we shall see in the following) that the coefficient $a_{0,0}^{(0)}$ is the one that brings in the effects of radiation in the absorption of almost adiabatic compression waves. That

coefficient increases from the low value $m_0 u_1$ for w_ν small to a maximum value $0.2299 m_0$ when $w_\nu = 0.6601$, decreases monotonically to $m_0/3w_R$ for $w_\nu \gg 1$, and then tends to zero; that is, tends to zero when $\lambda w_\nu \to 0$ and $w_\nu \to \infty$.

The following are necessary and sufficient conditions for almost adiabatic waves to exist for X and Θ small:

1 The speed differs little from c_0

$$m_0 = 1 \qquad [3.6]$$

if we have

$$\xi \ll 1 \qquad Z\,|a_0^{(0)}| \ll 1 \qquad [3.7]$$

This will be so in circumstances such that $Z \ll 1$, i.e., for any fluid in a state close to normal; it is so also for Z large (if ξ is small) for w_ν sufficiently small and sufficiently large (by virtue of the behavior of $a_0^{(0)}$).

2 The speed differs little from the second adiabatic speed, corrected for the radiation pressure

$$m_0 = \sqrt{\gamma/(\gamma + b_1)} \qquad [3.8]$$

if

$$Z|a_0^{(0)}| \ll 1 \qquad \beta\xi|a_0^{(1)}| \ll 1 \qquad \beta\xi\,|a_0^{(2)}| \ll 1 \qquad [3.9]$$

These inequalities reduce to Eqs. 3.7 if $\xi \ll 1$; all three are satisfied for any ξ and Z at sufficiently high frequency. The latter two cease to be satisfied at sufficiently low frequency (as determined by ξ, or, strictly, for sufficiently large w_ν).

This second speed appears at first sight nonsensical, for in a medium that is completely transparent and does not interact with radiation we have an effect of a radiation field on an elastic wave. The following argument partly disposes of this paradox. If $w_\nu = 0$ because the optical absorption coefficient is zero, then Kirchhoff's law implies that the emission coefficient is also zero, so the radiation intensity in the unperturbed fluid (if we consider only the fluid's own radiation) is zero; i.e., there are no radiation sources; hence, by definition, the radiation pressure is zero, i.e., $b_1 = 0$. In what follows it shall be assumed that the optical absorption coefficients are not zero.

3 The speed differs little from the adiabatic speed of sound in a space filled by a gas and by blackbody radiation

$$m_0 = \sqrt{\frac{\gamma h_1 h_2(1 + 12\beta\xi)}{\gamma h_1 h_2 + 4[(\gamma - 1)h_1 + (3h_1 + h_2)h_2\beta]\xi + 16h_2\beta\xi^2}} \qquad [3.10]$$

if $w_\nu \gg 1$ and X and Θ are small. The principal values of the $a_0^{(k)}$ for large Bouger numbers and for any physically feasible c^{e} are

$$a_0^{(0)} = \tfrac{1}{3}m_0^2/w_R \qquad a_0^{(1)} \approx 2m_0 i \qquad a_0^{(2)} \approx -\tfrac{1}{3}i m_0 \qquad [3.11]$$

i.e., only the first of the inequalities in 3.9 is satisfied if ξ is not small, because w_R is large and m_0 is bounded.

The conditions for the wave propagation with the first adiabatic speed, which is defined by the root of Eq. 3.10, are

$$Z/w_R \ll 1 \qquad w_1 \gg 1 \qquad [3.12]$$

which can be satisfied at low frequencies for any Z and ξ for an optically dense and very hot fluid; these parameters determine w_ν. This is the case which has been dealt with in Section 2 if we take X and Θ to be large; if X and Θ are of the order of 1, the speed will depend on the frequency and may reach the adiabatic speed within certain narrow frequency ranges.

We see that there are two distinct speeds for small amplitude waves in a medium having a temperature sufficient to make ξ no longer negligible (X and Θ remaining small), those speeds being given by Eqs. 3.10 and 3.8 as

$$c_{a0} = c_0\sqrt{\frac{\gamma h_1 + 4[(\gamma - 1)h_1 + (3h_1 + h_2)\beta h_2]\xi + 16h_2\beta\xi^2}{\gamma h_1 h_2(1 + 12\beta\xi)}}$$

$$c_{a\infty} = c_0\sqrt{1 + b_1/\gamma} \qquad [3.13]$$

The second speed occurs for any medium above some frequency, that limiting frequency being lower the higher the optical absorption. This speed is the high frequency adiabatic speed of sound. The first speed applies to fairly low frequencies covering a range that is wider the stronger the optical absorption is; it is the low frequency adiabatic speed of sound and is the speed of sound for a completely opaque medium. The two speeds are the same if one of these conditions holds

$$\gamma = 1 \qquad \gamma = \tfrac{4}{3} \qquad \xi = 0 \qquad [3.14]$$

In the last case the two speeds are the adiabatic speed of sound uncorrected for radiation pressure; if $\xi \neq 0$, the first speed is higher than the second if $1 < \gamma < \frac{4}{3}$, the converse being true if $\gamma > \frac{4}{3}$.

The two adiabatic speeds can be accommodated within the framework of the relaxation theory, namely relaxation involving a finite lifetime $\tau_{R\nu} = 1/\omega_{\nu 0}c$ for photons; if the period of oscillation $\vartheta_a = 2\pi/\sigma$ greatly exceeds that lifetime (low frequencies or strong optical absorption) or the lifetime referred to the integral absorption $\tau_R = 1/\omega_0 c$, then local equilibrium is set up between the gas and the radiation within the wave, so the speed for small amplitude waves is

$$c_{a0}^2 = [\partial(p + p_R)/\partial\rho]_{0s}$$

in which the derivative is taken for constant entropy. This formula is equivalent to Eq. 3.13. On the other hand, $\tau_R \gg \vartheta_a$ if the frequency is high enough or the optical absorption is weak enough; then the mean free path of a photon is much greater than the wave length. This means that the photon concentration does not change during one cycle of oscillation; the energy equation, which becomes the equation of conservation of entropy if we neglect the contributions from viscosity and conductivity, then gives us the adiabatic speed of sound as

$$c_{a\infty}^2 = \left[\frac{\partial(p + p_R)}{\partial\rho}\right]_{0s,\,p_R} = c_0^2\left(1 + \frac{b_1}{\gamma}\right)$$

which is exactly the second expression in 3.13; here the derivative is taken for constant entropy and for constant photon concentration (fixed radiation pressure).

High Frequency Waves

The root of the characteristic equation takes the following form when 3.9 is satisfied, the small parameters being X, Θ and the parameters of 3.9

$$\pm m = m_0\left\{i + \frac{1}{2(\gamma + b_1)}\left[(\gamma - m_0^2)\Theta + \gamma X + (\gamma + b_1 - 1)Za_0^{(0)} + 6(\gamma + b_1 - 1)\frac{\beta\xi a_0^{(1)}}{m_0} + \frac{12}{h_2}(\gamma + b_1 - 1)\frac{\xi a_0^{(2)}}{m_0}\right]\right\} +$$
$$\frac{im_0}{8(\gamma + b_1)^2}\left\{\left[(\gamma - m_0^2)\Theta + \gamma X + (\gamma + b_1 - 1)Za_0^{(0)} + \frac{6\xi}{m_0}(\gamma + b_1 - 1)\left(\beta a_0^{(1)} + \frac{2}{h_2}a_0^{(2)}\right)\right]\times\right.$$
$$\left[3\gamma\Theta - (6\gamma + 6b_1 - 7)m_0^2\Theta - 3\gamma X + (\gamma + b_1 + 3)Za_0^{(0)} - 2(\gamma + b_1 - 1)Za_1^{(0)} + \frac{6\beta\xi}{m_0}[(3\gamma + 3b_1 + 1)a_0^{(1)} -\right.$$
$$\left.\left.2(\gamma + b_1 - 1)a_1^{(1)}] - \frac{12}{m_0 h_2}(\gamma + b_1 - 1)\xi(a_0^{(2)} + 2a_1^{(2)})\right] - 4(\gamma + b_1)\gamma X\left(Za_0^{(0)} + m_0^2\Theta + \frac{6\beta\xi}{m_0}a_0^{(1)}\right)\right\} + \ldots \qquad [3.15]$$

in which m_0 is given by Eq. 3.8. Here all terms up to those of the second order of smallness for any bounded values of ξ and c° have been included; the real and imaginary parts of $a_0^{(k)}$ must be inserted to find the absorption and the dispersion. The form this root takes for ξ small (in which case Eqs. 3.6 and 3.7 apply) is

$$\pm m = i + \frac{1}{2\gamma}\left[(\gamma-1)\Theta + \gamma X + (\gamma-1)(Za_0^{(0)} + 6\beta\xi a_0^{(1)}) + \frac{12}{h_2}(\gamma-1)\xi a_0^{(2)}\right] - i\,\frac{b_1}{2\gamma} - \frac{b_1}{4\gamma^2}\left[(3\gamma-5)\Theta + 3\gamma X + (\gamma-1)Za_1^{(0)} + (\gamma-3)Za_0^{(0)} + 6(\gamma-1)\beta\xi a_1^{(1)} - 12\beta\xi a_0^{(1)} + \frac{12}{h_2}(\gamma-1)\xi a_1^{(2)} - \frac{24}{h_2}\xi a_0^{(2)}\right] - \frac{i}{8\gamma^2}\left\{\left[(\gamma-1)\Theta + \gamma X + (\gamma-1)(Za_0^{(0)} + 6\beta\xi a_0^{(1)}) + \frac{12}{h_2}(\gamma-1)\xi a_0^{(2)}\right]\left[(3\gamma-7)\Theta + 3\gamma X + 2(\gamma-1)Za_1^{(0)} - (\gamma+3)Za_0^{(0)} - 6(3\gamma+1)\beta\xi a_0^{(1)} + 12(\gamma-1)\beta\xi a_1^{(1)} + \frac{12}{h_2}(\gamma-1)\xi(2a_1^{(2)} + a_0^{(2)})\right] - 3b_1^2 + 4\gamma^2 X(\Theta + Za^{(0)} + 6\beta\xi a_0^{(1)})\right\} + \ldots \quad [3.16]$$

Here $a_k^{(j)}$ terms are taken for $m_0 = 1$; for $Z = 0$ (and so $\xi = 0$) we get a root corresponding to the waves examined by Rayleigh, Kirchhoff, Langevin and (more recently and more generally) by Truesdell (7). With $c^\circ = 0$ (that is, $\xi = 0$) we get a root that describes the attenuation and dispersion of almost adiabatic compression waves propagating in a not very strong radiation field

$$\pm m = i + \frac{1}{2\gamma}\left[(\gamma-1)(\Theta + Za_{00}^{(0)}) + \gamma X\right] - i\,\frac{\gamma-1}{4\gamma^2}\left[\gamma XZ + (\gamma-1)\Theta Z + (\gamma-1)Z^2 a_{00}^{(0)}\right]a_{10}^{(0)} + i\left[-\frac{3}{8}X^2 + \frac{(\gamma-1)(7-3\gamma)}{8\gamma^2}\Theta^2 - \frac{5(\gamma-1)}{4\gamma}X\Theta - \frac{3}{4}\frac{\gamma-1}{\gamma}a_{0,0}^{(0)}XZ + \frac{(5-\gamma)(\gamma-1)}{4\gamma^2}a_{00}^{(0)}\Theta Z + \frac{(\gamma-1)(\gamma+3)}{8\gamma^2}(a_{00}^{(0)})^2 Z^2\right] + \ldots \quad [3.17]$$

in which $a_{00}^{(0)}$ and $a_{10}^{(0)}$ are taken for $m_0 = 1$. We see that the absorption coefficient [referred to unit length (3)] varies in general in a complicated way with the oscillation frequency, whereas that coefficient is simply proportional to the square of the frequency if radiation exchange is neglected.

The linear real part of Eq. 3.17 is the same as that part in Eq. 3.16 if the values are small, so the fact that c is finite has no effect on the absorption of $c^\circ \ll 1$ and $\xi \ll 1$, but it does affect the dispersion very substantially if, as our measure of the dispersion, we take the relative deviation from the adiabatic speed of sound; in fact, the imaginary part of Eq. 3.16 (for $c^\circ \ll 1$) takes the form

$$2\gamma(m_i - 1) = \xi\left\{12(\gamma-1)\beta b_{10}^{(1)} - \frac{12}{h_2}(\gamma-1)b_{00}^{(2)} - \frac{b_1}{\xi} - \frac{b_1}{2\gamma}\left[12(\gamma-1)\beta(b_{12}^{(0)} + b_{10}^{(1)}) + 12(\gamma-3)\beta a_{01}^{(0)} - 24\beta b_{00}^{(1)} + \frac{24}{h_2}b_{00}^{(2)}\right]\right\} - \frac{1}{4\gamma}\left\{\left[(\gamma-1)\Theta + \gamma X + (\gamma-1)Za_{00}^{(0)}\right]\times\left[(3\gamma-7)\Theta + \frac{24}{h_2}\xi a_{10}^{(2)} + 3\gamma X + 2(\gamma-1)Za_{10}^{(0)} - (\gamma+3)a_{00}^{(0)}\right] - 3b_1^2 + 4\gamma^2 X(\Theta + Za_{00}^{(0)})\right\} + \ldots \quad [3.18]$$

The deviation is small, but the effect of radiation exchange is equal to the effect of viscosity and conductivity at high audio frequencies, the first effect actually exceeding the second at medium audio frequencies.

Condition 3.9 is satisfied for w_ν small, provided the frequency is high enough; then Eq. 3.15 can be simplified by replacing the $a_i^{(k)}$ terms by the first terms in the expansion in powers of w_ν'. For example, for $c^{\circ\prime}$ small we have $a_0^{(1)}$ and $a_0^{(0)}$ of the first order of small quantities, and $a_0^{(2)}$, $a_1^{(1)}$, $a_1^{(2)}$ and $a_1^{(0)}$ of the second order. Therefore the principal value of the real part of Eq. 3.15 takes the form

$$m_r = [1/2(\gamma + b_1)][(\gamma - m_0^2)\Theta + \gamma X + (\gamma + b_1 - 1)Zw_1] \quad [3.19]$$

The expression for the dispersion is

$$m_0 r = 1 + \frac{1}{8(\gamma+b_1)^2}\{3\gamma^2 X^2 - [3\gamma - m_0^2(6\gamma + 6b_1 - 7)](\gamma - m_0^2)\Theta^2\} - \frac{6}{\gamma}\xi w_2^2(\gamma + b_1 - 1)\left(\beta + \frac{1}{h_2}\right) + \frac{5\gamma^2}{4(\gamma+b_1)^3}(\gamma + b_1 - 1)X\Theta + \frac{w_1 Z}{8(\gamma+b_1)^2}\times\{6(\gamma - 1 + b_1)\gamma X + [4\gamma(\gamma+b_1) - 6m_0^2(\gamma + b_1 - 1)^2 - 4m_0^2]\Theta + (\gamma + b_1 - 1)(\gamma + b_1 + 3)Zw_1\} + \ldots \quad [3.20]$$

We see that the radiation pressure decreases the attenuation coefficient when w_ν is small; it is sufficient to use the mean absorption coefficient ω_1 to calculate the attenuation, whereas for the small (second-order) deviation from the first adiabatic speed of sound we must use the mean square absorption coefficient, which appears in the expression for w_2.

Low Frequency Waves

If 3.12 is satisfied, if X and Θ are small, and if ξ and c° take some bounded values, the root of the equation takes the form

$$m = \pm m_0[i + h_1(F_1/F_2)] \qquad [3.21]$$

$$F_1 = m_0^2[(\gamma - m_0^2)(\Theta + Z/3w_R) + \gamma X(1 + 12\beta\xi)] + (4\xi c^\circ/h_2 w_R)[3\gamma h_2 - (3h_2 + \gamma - 1 + b_1)m_0^2]$$

$$F_2 = h_1\gamma(3m_0^2 - 1) + 4\beta\xi\{m_0^2[2 + 3h_2 + 3h_1 + 3(\rho_0 h_3/p_0) + 12\xi] - 4\gamma h_1\}$$

Then for $\xi \ll 1$ we have

$$\pm m_0 = i + \frac{\gamma - 1}{2\gamma}\left(\theta + \frac{1}{3}\frac{Z}{w_R}\right) + \frac{1}{2}X - \frac{2\xi i}{\gamma}\left[(\gamma - 1)\left(\frac{1}{h_2} - 3\beta\right) + \frac{h_2}{h_1}\beta\right] + \frac{6(\gamma - 1)}{\gamma}\beta c^\circ\xi + \ldots \qquad [3.22]$$

which gives us the speed and attenuation coefficient; a measure of the dispersion resulting from radiation pressure in a perfect gas is

$$2(\gamma - 1)(5 - 3\gamma)\xi/\gamma \qquad [3.23]$$

which becomes zero (to quantities of the first order of smallness) when $\gamma = \frac{5}{3}$, being positive for $\gamma < \frac{5}{3}$.

4. Nearly Isothermal Waves

The speed of a weak compression wave in a real gas under conditions not too far from normal is equal, to within quantities of the second order of smallness, to the adiabatic speed, which is related to the isothermal (Newtonian) speed by

$$c_0 : c_T = \sqrt{\gamma} \qquad [4.1]$$

Waves propagating at the latter speed do not exist under normal conditions, but conditions can be stated so that this speed applies for a certain range of frequencies; outside that range, the speed will be the adiabatic one (there are two such speeds to consider if radiation pressure is included), the transition from one speed to the other occurring smoothly and fairly rapidly. This situation can occur only for Z large (when X and Θ are small), and the larger Z is, the wider that range. An intermediate case occurs when Z is of the order of 1; there is then a range in which the actual speed differs by a finite amount from both of the limiting speeds.

Now Eq. 1.1 implies that the waves will be almost isothermal if the following requirements are satisfied. Firstly X must be small; this is the usual situation for most gases and liquids, and must be so if the mechanics of continuous media are to be applicable, hence we shall assume that it holds. This implies that Θ is also small if the Prandtl number is of the order of 1. Secondly, b_1 must be small or of the order of 1, which means that ξ cannot be large, with the result that $\xi|a_0^{(2)}|$ and $\xi|a_0^{(1)}|$ are also bounded. Thirdly, $Z|a_0^{(0)}|$ must be large; now $a_0^{(0)}$ is bounded and becomes zero at frequencies of 0 and ∞, so this is equivalent to two requirements, namely that Z must be large, and that the frequency must be neither too high nor too low, the exact range being dependent on Z.

This requirement may be replaced by the condition that Θ must be large (for X small), i.e., that the Prandtl number must be small. Then $Za_0^{(0)}$ can have any value. However, it is doubtful whether such conditions can actually occur; in what follows then it shall be assumed that Θ does not exceed 1.

A necessary and sufficient condition for there to be almost isothermal waves is that the following inequalities apply

$$Z|a_0^{(0)}| \gg 1 \qquad \xi \ll 1 \qquad [\text{or } \xi = 0(1)] \qquad [4.2]$$

The isothermal speed is not affected by either neglecting or including the radiation pressure; the ratio of the speed of sound to that of light will be small if inequalities 4.2 apply, and only at the limits of the applicability of 4.2 will it cease to be of the order of $1/Z$. We expand the root in terms of powers of the small quantities X and $[Za_0^{(0)}]^{-1}$ for values of ξ and Θ not larger than 1

$$\pm\frac{m}{\sqrt{\gamma}} = i + \frac{1}{2}\left[\gamma X + \frac{\gamma - 1 + b_1}{Za_0^{(0)}}\left(1 + \frac{12i\xi a_0^{(2)}}{\sqrt{\gamma}\,h_2}\right)\right] + \frac{i}{4}\left\{\gamma X\left[\frac{1}{2}\gamma X + (Za_0^{(0)})^{-1}\left(2\gamma\theta + \frac{c^\circ}{\sqrt{\gamma}}\,a_0^{(1)} - \gamma - 1 - b_1\right)\right] + (Za_0^{(0)})^{-2}\left[-\frac{1}{2}(\gamma - 1 + b_1)(3\gamma + 3b_1 + 1) + \frac{12\xi}{h_2\sqrt{\gamma}}\,a_0^{(2)}(\gamma - 1 + b_1)\left(\frac{6\xi}{h_2}(\gamma - 1 + b_1) \times \left(\frac{a_0^{(1)}}{\sqrt{\gamma}} + 2a_1^{(2)}\right) - 2\gamma\Theta - c^\circ a_0^{(1)}\right)\right]\right\} + \frac{1}{4}\left\{\gamma X(Za_0^{(0)})^{-1}\left[\frac{12}{h_2}(\gamma - 1 + b_1)\xi a_1^{(2)} - 2\gamma\Theta - c^\circ a_0^{(2)} - 2\right] + (\gamma - 1 + b_1)(Za_0^{(0)})^{-2}\left[\frac{12}{h_2}(\gamma - 1 + b_1)\xi\left(\frac{2a_0^{(2)}}{\sqrt{\gamma}} + a_1^{(2)}\right) - 2\gamma\Theta - c^\circ a_0^{(1)} + \frac{24\xi\,a_0^{(2)}}{h_2\sqrt{\gamma}}\right]\right\} + \ldots \qquad [4.3]$$

This formula enables us to express the attenuation coefficient and speed in explicit form. Here the m_0 term appearing in the $a_i^{(k)}$ terms is $\gamma^{1/2}$; substituting for $a_i^{(k)}$, the attenuation coefficient is found as

$$m_r = \frac{1}{2}\gamma^{3/2}X + \frac{(\gamma - 1 + b_1)A_{00}}{2Z(A_{00}^2 + B_{00}^2)} + \frac{12(\gamma - 1 + b_1)\xi}{2h_2 Z}\,\frac{A_{02}B_{00} + A_{00}B_{02}}{A_{00}^2 + B_{00}^2} + \ldots \qquad [4.4]$$

where

$$A_{00}\int_0^\infty \frac{\partial B_\nu}{\partial T}\,d\nu = \int_0^\infty \frac{\partial B_\nu}{\partial T}\,w_\nu'\left[1 - \frac{1}{2}w_\nu' \arctan\frac{2u_\nu'}{[w_\nu'^2 - 1 + c^{\circ\prime 2}]} - \frac{1}{4}c^{\circ\prime}\ln\frac{w_\nu'^2 + (1 + c^{\circ\prime})^2}{w_\nu'^2 + (1 - c^{\circ\prime})^2}\right]d\nu$$

$$B_{00}\int_0^\infty \frac{\partial B_\nu}{\partial T}\,d\nu = \frac{1}{2}\int_0^\infty \frac{\partial B_\nu}{\partial T}\,w_\nu'\left[\frac{1}{2}w_\nu'\ln\frac{w_\nu'^2 + (1 + c^{\circ\prime})^2}{w_\nu'^2 + (1 - c^{\circ\prime})^2} - \frac{1}{4}c^{\circ\prime}\arctan\frac{2w_\nu'}{[w_\nu'^2 - 1 + c^{\circ\prime 2}]}\right]d\nu$$

$$A_{02}\int_0^\infty \frac{\partial B_\nu}{\partial T}\,d\nu = \int_0^\infty \frac{\partial B_\nu}{\partial T}\,w_\nu'\left[c^{\circ\prime} + \frac{1}{4}(w_\nu'^2 - c^{\circ\prime 2})\ln\frac{w_\nu'^2 + (1 + c^{\circ\prime})^2}{w_\nu'^2 + (1 - c^{\circ\prime})^2} - c^{\circ\prime}w_\nu'\arctan\frac{2w_\nu'}{[w_\nu'^2 - 1 + c^{\circ\prime 2}]}\right]d\nu$$

$$B_{02}\int_0^\infty \frac{\partial B_\nu}{\partial T}\,d\nu = \int_0^\infty \frac{\partial B_\nu}{\partial T}\,w_\nu'\left[w_\nu' - \frac{1}{2}(w_\nu'^2 - c^{\circ\prime 2})\arctan\frac{2w_\nu'}{[w_\nu'^2 - 1 + c^{\circ\prime 2}]} - \frac{c^{\circ\prime}w_\nu'}{2}\ln\frac{w_\nu'^2 + (1 + c^{\circ\prime})^2}{w_\nu'^2 + (1 - c^{\circ\prime})^2}\right]d\nu \qquad [4.5]$$

For c° small this becomes

$$m_r = \pm\left[\frac{1}{2}\gamma\sqrt{\gamma}\,X + \frac{2(\gamma - 1 + b_1)}{Z a_{00}^{(0)}} \times \left(1 + \frac{12\xi}{h_2}\frac{a_{00}^{(1)}}{a_{00}^{(0)}}\right)\right] + \ldots \quad [4.6]$$

in which the $a_{ij}^{(k)}$ terms differ from those of the previous section only in that $w_\nu/\gamma^{1/2}$ replaces w_ν. The attenuation is controlled by the viscosity, the radiative transfer and the radiation pressure; the last of these drops out if ξ is small (the term is of the second order of small quantities). Then

$$\pm m_r = \frac{1}{2}\gamma\sqrt{\gamma}\,X + \frac{2(\gamma - 1)}{Z a_{00}^{(0)}} + \ldots \quad [4.7]$$

The absorption coefficients are complicated functions of frequency.

The contribution to the dispersion (the deviation from the isothermal speed)

$$\frac{c_a}{c_T} - 1 = \frac{\sqrt{\gamma}}{2}\frac{\gamma - 1 + b_1}{Z}\frac{B_{00}}{A_{c0}^2 + B_{00}^2} - \frac{6(\gamma - 1 + b_1)\xi}{h_2 Z}\frac{A_{00}A_{c2} - B_{00}B_{02}}{A_{00}^2 + B_{00}^2} + \ldots \quad [4.8]$$

is of the first order of small quantities only if $c^\circ = 0(1)$; if $c^\circ \ll 1$ (as may be expected), this contribution to the dispersion is of the second order of small quantities and combines additively with the other contributions, as found from Eq. 4.3.

5. Small Bouger Wave Numbers

Let the Bouger number be small, but not infinitely small (in the latter case the conclusions of Sections 2 and 3 apply), and let us suppose that the conditions

$$w_\nu \ll 1 \qquad X,\Theta \ll 1 \qquad Z\,|a_0^{(0)}| = 0(1) \quad [5.1]$$

are satisfied; the last of these takes the form

$$Zw_1 = O(1) \quad [5.2]$$

when w_ν is small; here w_1 (for the optical absorption defined by Eq. 2.3) is small, so Z is large. Then the root of the characteristic equation (for any c° and for any ξ having an upper bound) becomes

$$\frac{1}{m^2}\ln\frac{ic^\circ + m}{ic^\circ - m} = \frac{\gamma + (\gamma + b_1)m^2 - i(\gamma + m^2)Zw_1 - 12ih_2^{-1}(\gamma + b_1 - 1)\,\xi c^\circ w_1}{6\xi w_1 h_2^{-1}[2c^{\circ 2}m(\gamma + b_1 - 1) + (\gamma + m^2)\beta(2m_0 - ic^\circ)h_2]} \quad [5.3]$$

In what follows it is assumed that c° is small; then

$$m_0^2 = -\frac{\gamma}{\gamma + b_1}\frac{1 - iZw_1}{1 - iZw_1/(\gamma + b_1)} \quad [5.4]$$

The speed is

$$\frac{c_a}{c_0} = \frac{\sqrt{2}\Psi_1}{\Psi_2}\Psi_3(\gamma + b_1) \quad [5.5]$$

where

$$\Psi_1 = \frac{1}{(\gamma + b_1 - 1)Zw_1}$$

$$\Psi_2 = \frac{\sqrt{\gamma}}{\sqrt{(\gamma + b_1)^2 + Z^2w_1^2}} \quad [5.6]$$

$$\Psi_3 = \sqrt{\sqrt{1 + Z^2w_1^2}\,\sqrt{(\gamma + b_1)^2 + Z^2w_1^2} - (\gamma + b_1 + Z^2w_1^2)} \quad [5.7]$$

That speed changes monotonically from $c_0/\gamma^{1/2}$ (the isothermal speed) when Zw_1 is small to the second adiabatic speed when Zw_1 is large. The attenuation coefficients resulting from radiation are

$$\alpha_a^1 = = (\omega_1/\sqrt{2}\,w_1)\Psi_2\Psi_3$$

$$\alpha_a^\circ = \pi\sqrt{2}\Psi_2\Psi_3$$

$$\alpha_a = 2\pi\Psi_1\Psi_3^2 \quad [5.8]$$

The coefficients α_a^1 (per unit length) and α_a°/ω_1 (per unit mean free path of the radiation) are monotonically increasing functions of frequency which for large values of Zw_1 tend asymptotically to

$$\alpha_a^{1}{}_{\max} = \frac{\pi\omega_1}{2}\sqrt{\frac{\gamma}{\gamma + b_1}}\frac{\gamma + b_1 - 1}{\gamma + b_1}Z \quad [5.9]$$

which does not depend on frequency. (The attenuation coefficients related to the viscosity and thermal conductivity are simply added on to these.) The attenuation coefficient per unit adiabatic wave length and the true attenuation coefficient per wave length have maximum values in this region

$$\alpha_a^\circ{}_{\max} = \pi\frac{\gamma + b_1 - 1}{\sqrt{2(\gamma + b_1 + 1)}} \quad \text{for } Zw_1 = (\gamma + b_1)\sqrt{\frac{\gamma + b_1 + 3}{3\gamma + 3b_1 + 1}}$$

$$\alpha_{a\,\max} = 2\pi\frac{\sqrt{\gamma + b_1} - 1}{\sqrt{\gamma + b_1} + 1} \quad \text{for } w_{1\max} = \frac{\sqrt{\gamma + b_1}}{Z} \quad [5.10]$$

The maximum true attenuation coefficient increases monotonically from $2\pi(\sqrt{\gamma} - 1)/(\sqrt{\gamma} + 1)$ for $\xi \to 0$ to 2π as ξ increases without limit.

We can use Eqs. 3.5 to get the following approximation for the root; that approximation enables us to extend the range of frequencies described by that root for c° small

$$m = \pm m_0\left\{i + \frac{(\gamma - m_0^2)\Theta + (1 - iZu_1)\gamma X m_0^2}{(\gamma - 3m_0^2)iZw_1 + 3m_0^2(\gamma + b_1) - \gamma} + \ldots\right\} \quad [5.11]$$

in which m_0 is defined by Eq. 5.2. Radiation transfer appears only as a second-order quantity if the viscosity and conductivity are neglected.

6. Large Bouger Wave Numbers

There is another case which is of interest in obtaining a general picture of the behavior of harmonic waves. Let the oscillation frequency be low, and let the optical absorption be strong, then the Bouger wave numbers are large for all spectral ranges involved in radiation transfer. We may then expand Eqs. 3.3 in power series in terms of $1/w_\nu$; as before, scattering is neglected and c° is assumed small. Moreover (and here with even better reason than before) X and Θ are assumed small, but $Z\,|a_0^{(0)}|$ is assumed to be of the order of 1, as in the previous section; that is, Z is fairly large; i.e., we have

$$X,\Theta \ll 1 \qquad Z\,|a_0^{(0)}| = 0(1) \qquad w_\nu \gg 1 \quad [6.1]$$

Now Eqs. 3.11 imply that, for the arge w_r envisaged here, the equation assumes the form

$$Z\,|a_0^{(0)}\,| \approx \frac{m_0^2}{3}\,\frac{Z}{w_R} = 0(1) \qquad [6.2]$$

in which w_R is the Bouger wave number formed from the Rosseland mean of Eq. 2.7; clearly, it is large here. The equation for the principal values of the real and imaginary parts of the root is an algebraic biquadratic

$$\frac{iZ}{3w_R}\,m_0^4 - \left(\beta_1 + \frac{\gamma iZ}{3w_R}\right) m_0^2 + \gamma\beta_4 = 0 \qquad [6.3]$$

where

$$\beta_1 = \gamma + 4\left[\frac{\gamma - 1}{h_2} + \left(3 + \frac{h_2}{h_1}\right)\beta\right]\xi + \frac{16}{h_1}\,\beta\xi^2$$

$$\beta_4 = 1 + 12\beta\xi \qquad [6.4]$$

This equation implies that in this case the waves tend to become adiabatic as the frequency decreases, their speed being the $c_{\infty 0}$ of Eqs. 3.13; they tend to become isothermal as the frequency increases (Z large). The equation describes the transition between the two modes of propagation; the curve $r(\sigma)$ has an inflection in this region. Again, Eq. 6.3 implies that the attenuation coefficient per unit length increases with frequency, whereas that coefficient has a maximum if taken per wave length or per adiabatic wave length. We may expand the root in power series about the value defined by Eq. 6.3 to find the corrections to the dispersion and to the attenuation coefficients, these corrections being calculated for w_r close to the values corresponding to this transition region. Then we have

$$m = \pm m_0 i\left\{1 - i\left[(\gamma - m_0^2)\,\Theta m_0^2 + \gamma X m_0^2\left(1 - \frac{iZm_0^2}{3w_R} + 12\beta\xi\right) - \frac{4c^\circ\xi m_0^2(\gamma + b_1 - 1)}{h_2 w_R} + 4(\gamma - m_0^2)\,\beta\xi\left(\frac{3c^\circ}{w_R} - \frac{2im_0^2}{w_{-2}{}^2}\right) - \frac{\gamma - m_0^2}{5w_{-3}{}^3}\,Zm_0^2(m_0^2 + 5c^{\circ 2})\right]\left[3m_0^2(\gamma + b_1) - \gamma + \frac{12}{h_2}\,(\gamma + b_1 - 1)\,\xi m_0^2 + i\,\frac{Zm_0^2}{w_R}\left(\gamma - \frac{5}{3}\,m_0^2\right) - 12\beta\xi\,(\gamma - 3m_0^2)\right]^{-1}\right\} + \ldots \qquad [6.5]$$

Neglecting viscosity, conductivity and radiation pressure we have

$$m = \pm m_0 i\left(1 - \frac{3}{5}\,i\,\frac{w_R}{w_{-3}{}^3}\,\frac{m_0^2(m_0^2 - 1)(m_0^2 - \gamma)}{2\gamma + m_0^2(5m_0^2 - 3\gamma - 7)}\right) + \ldots \qquad [6.6]$$

in which m_0 is obtained from Eq. 6.3 (in the latter case for $\xi = 0$).

7. Conclusions

The following picture can now be drawn. X, Θ, Z, ξ and c° are small for not too high temperatures (e.g., for gases under normal conditions); small amplitude waves are then almost adiabatic sound waves. The attenuation coefficient per unit length is a monotonically increasing function of frequency and is controlled by radiative transfer at low frequencies; by viscosity, conductivity and radiative transfer at medium frequencies; and by viscosity and conductivity alone at high frequencies, because the relative role of radiative transfer tends to zero (the radiative transfer rises asymptotically with frequency to a frequency independent value). The attenuation coefficient per wave length due to radiative heat transfer has only a single maximum at medium frequencies and tends monotonically to zero at very high and very low frequencies.

At higher temperatures (Z of the order of 1), with X and Θ still small, the speed becomes nearly adiabatic for very high and very low frequencies; at medium frequencies, it approaches (but not attains) isothermal speed.

At very high temperatures Z can be large, while X, Θ, ξ and c° are small; in that case the speed falls monotonically from adiabatic speed at low frequencies to isothermal speed at medium frequencies, the transition from one speed to the other occurring in the region in which $Z/w_R = 0(1)$. Higher frequencies, up to about the limit $Zw_1 = 0(1)$, have isothermal speed; that limit specifies the transition from isothermal speed to adiabatic speed. Further increase in frequency gives waves whose speed is adiabatic, while X and Θ remain small.

If at high temperatures Z is large while ξ is not negligibly small (X and Θ remaining small), then low frequency waves have the low frequency adiabatic speed of sound as their speed (radiation pressure is allowed for), whereas high frequency waves have the high frequency adiabatic speed of sound as their speed (also constant). Otherwise, main features of velocity variation are the same as those for small ξ but large Z: Near $Z/w_R = 0(1)$ we have a transition from the low frequency adiabatic speed to the isothermal speed, and near $Zw_1 = 0(1)$ we have a transition from the isothermal speed to the high frequency adiabatic speed.

The attenuation coefficient per wave length (due to thermal radiation) has two maxima and one minimum for Z large; that is, there are two anti-resonant systems and one resonance, which may be described in terms of the corresponding relaxation times. The phase velocity of the waves becomes larger than the adiabatic speed of sound if X and Θ are large.

—*Received Feb. 18, 1957*

References

1 Stokes, G., "An Examination of the Possible Effect of Radiation Heat on the Propagation of Sound," *Phil. Mag.*, 1851, Series 4, vol. 1, p. 305.

2 Lord Rayleigh (J. W. Strutt), *The Theory of Sound*, Vol. 1.

3 Prokof'ev, V. A., "Effects of Radiation on the Propagation of Small Perturbations in a Viscous Conducting Fluid (Hydrodynamic Theory)," *Izv. Akad. Nauk SSSR, Otdel. Tekh. Nauk*, 1957, no. 7.

4 Prokof'ev, V. A., "Allowance for Radiation in the One-Dimensional Steady-State Motion of a Monatomic Gas," *Uch. Zap. Mosk. Gos. Univ.*, 1954, no. 172, *Mekhanika* issue 5.

5 Prokof'ev, V. A., "Allowance for Radiation for Small-Amplitude Waves in a Compressible Fluid," *Prikl. Matematika i Mekhanika*, 1957, vol. 21, no. 6.

6 Prokof'ev, V. A., "Absorption and Dispersion of Weak Forced Waves as Influenced by Radiative Transfer at Very Low and Very High Frequencies," *Izv. Akad. Nauk SSSR, Otdel. Tekh. Nauk*, 1958, no. 12.

7 Truesdell, C., "Precise Theory of the Absorption and Dispersion of Forced Plane Infinitesimal Waves According to the Navier-Stokes Equations," *J. Rat. Mech. Anal.*, 1953, vol. 2, no. 4.

8 Unsold, A., *Physics of Stellar Atmospheres*, IL, 1949.

Reviewer's Comment

This paper continues the author's earlier researches on the effect of radiation on the propagation of sound. These, in turn, generalized my complete analysis of the effects of viscosity and heat conduction in 1953. In this paper Prokof'ev starts from a more general mathematical description of the radiation process and effects. The frequency equation is complicated, and he makes no attempt to solve it exactly or to give an analytical theory of its solutions. Instead, the

paper is devoted to a discussion of the limit cases arising in various different physical problems. The results indicate what a variety of circumstances may be taken into account by suitable analysis of a sufficiently general continuum theory.

In contrast to the more "physical" approach favored by American specialists in this field, Prokof'ev attempts to derive all results from a single, embracing theory. For a summary of American research, see the book *Absorption and Dispersion of Ultrasonic Waves*, by K. Herzfeld and T. A. Litovitz (Academic Press, N.Y., 1959).

—C. TRUESDELL
Graduate Institute for Applied Mathematics
Indiana University

Solution of Several Problems of Air Motion in the Presence of Dissociation and Ionization

S. S. KVASHINA and
V. P. KOROBEINIKOV

IN VARIOUS problems of modern gasdynamics we encounter air flows in which zones of high temperature and various ranges of pressure occur.

Under these conditions, the effects of dissociation and ionization begin to play an important role (1–6).[1]

For temperatures lower than 1000 K and moderate pressures, the characteristics of air are well described by the equation of state of an ideal gas

$$p = (R/\mu)\rho T \qquad (\gamma = c_p/c_v)$$

for constant heat capacities, where γ = constant 1.4, and for constant molecular weight μ. For higher temperatures, the equation of state and the thermodynamic functions of an ideal gas are no longer suitable for solving problems of gasdynamics. At temperatures higher than 1000 K, the dependence of heat capacity on temperature begins to affect the calculations, and at $T > 2000$ K, processes of dissociation of molecules and ionization of atoms take place which have an important effect on all thermodynamic factors. In addition, the internal energy, enthalpy and speed of sound depend not only on temperature, but also on density or pressure. In this paper, we propose equations which approximate the table for air (2,7) and we also give the solution for several problems of gasdynamics taking into account both dissociation and ionization.

A method of calculating the thermodynamic functions of air over the range of temperatures from 1000 to 20,000 K and pressures from 0.001 to 1000 atm was developed by a group of workers of the Power Institute of the Academy of Sciences, USSR (2).

The results of the calculations were published in the form of tables of thermodynamic functions and air compositions over the given interval of temperatures and pressures (2,7). (Recently tables have been published covering a range of temperatures from 6000 to 12,000 K.) In the following, when we examine problems of gasdynamics, we will consider the processes of dissociation and ionization as being equal; in the calculation we will employ the tables given in (7).

Translated from *Izvestiia Akademii Nauk SSSR, Mekhanika i Mashinostroenie* (*Bulletin of the Academy of Sciences USSR, Mechanics and Machine Building*), 1960, no. 2, pp. 34–41. Translated by Research Information Service, New York.

[1] Numbers in parentheses indicate References at end of paper.

R. P. Arofonova and L. C. Balashova participated in performing the calculations for this paper.

The authors sincerely thank L. I. Sedov for his valuable advice, G. G. Chernov for evaluating the results of this work, and E. V. Samuelov for his useful comments.

The authors also express their gratitude to workers of the Combustion Physics Laboratory of the Power Institute for permitting us to use their tables of air properties for the entire range of temperatures from 1000 to 20,000 K.

1. Basic Thermodynamic Equations

The work which we did on the approximation of the tables, given in (2 and 7), over the temperature interval 1000 to 20,000 K by means of simple equations, turned out to be convenient for calculating flow at constant entropy.

For calculating such flows it is sufficient to know the dependence of enthalpy h on the speed of sound a.

For a temperature of less than 1000 K, let us consider that

$$h = [1/(\gamma - 1)]a^2$$

For a temperature interval of 1000 to 20,000 K, the dependence of h on a can be represented by

$$i = \alpha(s)c^{\beta(s)} \quad \text{or} \quad i = \sigma(s)c^2 + J(s) \qquad [1.1]$$

Here

$$i = \frac{h}{h_*} \qquad c = \frac{a}{a_*} \qquad s = \frac{S}{S_*} \qquad [1.2]$$

and α, β, σ and J are functions of s, the forms of which are found from the conditions of approximation of the tables of data; h_*, a_* and S_* are the values of h, a and S at T = 1000 K, p = 1 atm (h_* = 250.1 cal per gm, a_* = 618.9 m per sec, S_* = 1.943 cal/gm/deg).

However, use of a single equation of the form of Eqs. 1.1 for a given s is not always possible over the entire temperature interval, since the relative maximum error of Eqs. 1.1 as compared with the tables of data can attain 15–20%. For this reason it is sometimes necessary to divide the interval of changes a for a given entropy into a series of parts (in this paper, the interval has been divided into two parts) and to find separately the factors α, β, σ and J for each part. The

Table 1

ε	α	β	c	T, K	δ, %
0.936	1.000	2.407	1.000–1.443	1000–2190	0.4
1.063	1.000	2.472	1.007–1.922	1015–4270	1.3
1.090	1.000	2.486	1.016–2.123	1035–4780	1.5
1.193	1.000	2.600	1.064–1.864	1140–3750	2.9
	1.462	2.059	1.864–2.471	3750–5930	0.7
1.287	0.888	2.989	1.047–1.910	1050–3800	2.4
	1.428	2.151	1.910–3.155	3800–8880	0.9
1.390	0.755	3.686	1.295–1.606	1770–2840	2.7
	1.490	2.193	1.606–3.631	2840–10390	1.3
1.441	1.043	3.047	1.381–1.772	2180–3210	2.3
	1.562	2.181	1.772–3.876	3210–11040	2.0
1.493	1.446	2.497	1.456–1.879	2390–3385	2.8
	1.687	2.140	1.879–4.132	3385–11690	3.1
1.544	2.206	1.793	1.537–2.433	2550–5280	2.1
	2.156	1.972	2.433–4.397	5280–12370	2.7
1.595	2.080	1.963	1.635–2.585	2720–5890	3.6
	2.723	1.815	2.585–4.693	5890–13170	2.5
1.647	1.136	2.749	2.000–2.702	3490–6145	1.3
	3.507	1.650	2.702–5.015	6145–14180	1.7
1.801	1.802	2.395	2.167–2.946	4360–6490	0.5
	4.540	1.517	2.946–5.921	6490–18250	1.7
1.904	3.065	1.926	2.312–3.526	4640–7800	1.8
	5.135	1.468	3.526–6.225	7800–19330	1.8
2.059	5.211	1.531	2.522–3.962	4930–8600	1.8
	4.263	1.618	3.962–6.454	8600–19365	0.7
2.162	7.581	1.249	2.584–4.306	5100–10040	1.0
	4.441	1.618	4.306–6.582	10040–19180	0.3
2.316	5.550	1.531	2.923–4.547	5440–10840	2.3
	7.209	1.332	4.547–7.048	10840–19910	0.4
2.573	4.928	1.675	3.711–5.419	7730–12920	0.4
	8.651	1.347	5.419–7.597	12920–15160	0.3
2.831	8.844	1.374	4.169–5.549	8750–12430	0.7
	10.556	1.282	5.549–8.013	12430–19655	0.7
3.088	8.723	1.445	4.595–5.988	9330–12800	0.2
	18.696	1.021	5.988–8.319	12800–19050	0.7
3.345	12.813	1.305	5.020–6.529	9820–13430	0.4
	32.915	0.762	6.529–8.974	13430–19780	0.6
3.603	19.001	1.077	5.476–6.452	10340–12520	0.2
	39.387	0.685	6.452–8.727	12520–18630	0.7
3.860	60.237	0.474	6.100–8.261	11180–15880	0.5

results of the approximation based on the first equation in 1.1 are given in Table 1, and the results based on the second equation in 1.1 are given in Table 2. These tables show the average error of the approximation, $\delta\%$. The maximum error at individual points for the first equation in 1.1 attains 5%; for the second equation it is 7%. Using the first equation in 1.1 and the well-known thermodynamic relationship

$$dh = T\,dS + (1/\rho)dp \qquad [1.3]$$

we find

$$R = R_0(s) \exp\left[\frac{i^n}{n}\,\alpha^{2/\beta}\right] \text{ for } \beta \neq 2$$

$$R = R_0(s) i\alpha \text{ for } \beta = 2 \qquad \left(n = \frac{\beta - 2}{\beta},\ R = \frac{\rho}{\rho_*}\right)$$

$$\pi = R_0(s) \int \exp\left[\frac{i^n}{n}\,\alpha^{2/\beta}\right] di + \pi_0(s) \text{ for } \beta \neq 2$$

$$\pi = R_0(s) \frac{i^{a+1}}{\alpha + 1} + \pi_0(s) \text{ for } \beta = 2 \qquad \left(\pi = \frac{p}{\rho_* h_*}\right)$$

.....[1.4] .....[1.5]

$$T = \frac{1}{\rho}\left[\frac{\partial p}{\partial S}\right]_h \qquad [1.6]$$

Here ρ is the value for the density at $T = 1000$ K, $p = 1$ atm. The arbitrary functions $R_0(s)$ and $\pi_0(s)$ in Eqs. 1.4 and 1.5 may be selected from the approximation conditions of the tables. For an ideal gas, $R_0 =$ constant, $\pi_0 = 0$. From the second equation in 1.1 and from Eq. 1.3 we obtain the follow-

ing relationships

$$R = \theta(s)[i - J]^{\sigma/\tau}$$

$$\pi = \frac{\tau}{\sigma + \tau}\,\theta(s)\left(\frac{R}{\theta(s)}\right)^{\frac{\tau}{\sigma}+1} + \varphi(s)$$

$$T = \left(\frac{dh}{dS}\right)_p \qquad \left(\tau = \frac{a_*^2}{h^*}\right)$$

.....[1.7]

where $\theta(s)$ and $\varphi(s)$ are entropy functions. With the help of Eqs. 1.1 to 1.7, we can construct an analytical analog of the tables in (7) for the determination of thermodynamic parameters and the solution of problems of gasdynamics. We will examine several such problems.

2. Riemann Waves in the Dissociation of a Gas

Let s = constant everywhere in the region of flow. For uniform flows with flat waves, a partial solution is known for gasdynamic equations having the arbitrary functionalities $p = p(\rho)$ or $h = h(\rho)$ [see, for example, (8)]. This solution describes the so-called Riemann waves and can be represented in the form

$$v = \pm \int \frac{dh}{a(h)} \qquad r = t(v \pm a) + f(a) \qquad [2.1]$$

Here

$f(a)$ = arbitrary function
v = velocity
r = coordinate

Let us examine the solution of Eqs. 2.1 for the functionality $h(a)$ determined by the first equation in 1.1.

If the functionality $a(h)$ is a smooth function divided into parts, then it is necessary to divide the region of integration into a series of intervals. For example, if there are sectors in the flow of gas where $T < 1000$ K, then upon transition into the high temperature region we must take into consideration the change in the functionalities $a(h)$ in Eqs. 2.1.

For an ideal gas we have

$$v(c) = \pm[2a_*/(\gamma - 1)](c - c_0) \qquad (c_0 = \text{const})$$

In the presence of dissociation, and using the first equation in 1.1, we obtain

$$v(c) = \pm \frac{\alpha\beta}{\beta - 1}\,\frac{h_*}{a_*}\,[c^{\beta-1} - c_0^{\beta-1}] \qquad [2.2]$$

The functionalities $\rho(a)$ and $p(a)$ may be found by using the tables or Eqs. 1.4 and 1.5.

As in the case of the ideal gas, where there is a dissociation and ionization reaction in the air a compression wave may be transformed into a shock wave. The time of appearance of

Table 2

s	σ	J	c	T, K	δ, %
0.936	1.302	−0.3164	1.000–1.443	1000–2190	0.9
1.063	1.344	−0.3683	1.007–1.509	1015–2410	1.5
	1.685	−1.1350	1.509–1.922	2410–4270	0.4
1.090	1.294	−0.3085	1.016–1.396	1035–2080	0.57
	1.709	−1.172	1.396–2.123	2080–4780	0.72
1.193	1.614	−0.7186	1.064–1.732	1140–3300	4.10
	1.570	−0.1781	1.732–2.471	3300–5930	0.67
1.287	1.566	−0.6400	1.023–1.552	1050–2690	6.73
	1.831	−0.8974	1.552–3.155	2690–8880	2.20
1.390	2.217	−1.690	1.295–2.084	1770–4100	5.28
	1.838	−0.7260	2.084–3.631	4100–10390	4.20
1.493	1.895	−0.1556	1.456–2.416	2390–5380	4.31
	1.983	0.3798	2.416–4.132	5380–11690	1.89
1.595	2.183	−0.4825	1.635–2.585	2720–5100	4.12
	1.879	3.231	2.585–4.693	5100–13170	2.30
1.801	2.963	−2.423	2.167–2.946	4360–6490	1.34
	1.623	10.700	2.946–5.921	6490–18250	2.06
1.904	3.296	−2.601	2.312–2.895	4460–6120	0.72
	1.659	12.320	2.895–6.225	6120–19330	1.21
2.059	2.698	3.998	2.522–3.322	4930–6860	1.05
	1.835	11.400	3.322–6.454	6860–19365	0.86
2.162	2.194	9.950	2.584–3.488	5100–7020	0.84
	1.905	12.120	3.488–6.582	7020–19180	0.67
2.316	2.024	12.940	2.923–4.406	5440–10350	1.38
	1.879	18.150	4.406–7.048	10350–19910	0.80
2.573	2.725	6.560	3.711–4.544	7730–10305	0.23
	1.837	28.950	4.544–7.597	10305–15160	1.86
2.831	2.723	13.57	4.169–4.981	8750–10880	0.26
	1.757	40.50	4.981–8.013	10880–19655	1.49
3.088	2.671	22.57	4.595–5.280	9330–11010	0.15
	1.602	55.48	5.280–8.319	11010–19050	1.64
3.345	2.473	35.53	5.020–5.951	9820–12150	0.36
	1.127	87.91	5.951–8.974	12150–19780	1.50
3.603	1.955	60.23	5.476–6.452	10340–12860	0.36
	0.813	109.93	6.452–8.727	12860–18630	0.77
3.860	0.7669	112.88	6.099–8.261	11180–15880	0.74

a shock wave t_b and its coordinate at that instant r_b is found from the conditions

$$\left(\frac{\partial r}{\partial a}\right)_t = 0 \qquad \left(\frac{\partial^2 r}{\partial a^2}\right)_t = 0 \qquad [2.3]$$

From Eqs. 2.1 to 2.3 for a wave propagating in a positive direction, we find that

$$r_b = t_b[v(c_b) + a_* c_b] + f(c_b)$$

$$t_b = -\frac{f'(c_b)}{\alpha\beta(h_*/a_*)c_b^{\beta-2} + a_*}$$

$$\frac{f''}{f'} = \frac{\alpha\beta(\beta-2)c_b^{\beta-3}}{\alpha\beta c_b^{\beta-2} + \tau}$$

..... [2.4]

where the derivatives are calculated for the point $c = c_b$. The last equation in Eqs. 2.4 may be used to determine the factor c_b. When $\beta = 2$, the conditions in 2.4 are analogous to the conditions for an ideal gas.

If the compression wave borders on an unmoving gas and the shock wave forms at the boundary, then the conditions of Eqs. 2.4 are written

$$t_b = -\frac{f'(c_0)}{\alpha\beta(h_*/a_*)c_0^{\beta-2} + a_*}$$

$$r_b = ta_* c_0 + f(c_0)$$

..... [2.5]

Example: Let a flat piston move according to the rules

$$r_n = (k/2)t^2 \qquad dr_n/dt = U = kt$$

and let it either move into ($k > 0$) a tube of adequate length containing air, or move out of it ($k < 0$). Let us consider that the initial (at $t = 0$) temperature of the air in the tube is $T_0 \geqslant 1000$ K. Determine the velocity of flow of the gas.

We find the arbitrary function $f(c)$ from the boundary conditions at the piston

$$v = U \qquad f(c) = -\frac{v(c)}{k}\left[\frac{v(c)}{2} + a_* c\right]$$

Here the function $v(c)$ is known from Eq. 2.2. When $k > 0$, the coordinate and the instant of formation of the shock wave are found from Eqs. 2.5.

We now write the results of calculation of Δ, the ratio of t_b in air to t_b in an ideal gas for several initial temperatures T_0 and entropies

s	= 0.936	1.090	1.287	2.059
$T°$	= 1000	1040	3800	8600
Δ	= 1.317	1.372	1.853	2.229

Naturally, in the course of time when $k < 0$, the temperature will drop as a result of adiabatic expansion. For this reason, in that portion of air lying close to the piston, a recombination of atoms into molecules will occur, and the air will undergo transition into a state in which it may be considered an ideal gas with $\gamma = 1.4$.

When $k \to -\infty$, we obtain flow of the gas into empty space, accompanied by a process of recombination. In the solution of Eqs. 2.1, we must postulate $f(a) = 0$ for this case, and break up the interval of integration into parts corresponding to the fact that the air is initially considered a dissociated gas and then becomes an ideal gas. A numerical computation of the speed of flow into empty space and the distribution of the temperature along the length of the tube was carried out for the initial data: $a_0 = 1300$ m per sec, $S = 2.118$ cal/gm/deg. For $T < 1000$ K, air is considered an ideal gas. The results of calculation and comparison with an ideal gas (the dashed curves) are shown in Fig. 1. For the speed of flow into empty space, $v(0) = -8780$ m per sec in air and $v(0) = -6490$ m per sec in an ideal gas.

3. Calculating the Parameters at the Point of Deceleration

Using the thermodynamic functions given in Eqs. 1.1 to 1.7 or the tables, we can calculate the parameters of the primary shock wave and determine the factors T_0, p_0, ρ_0 at the point of deceleration for a blunt body in air traveling at supersonic speed. Calculation of the flow parameters behind the shock wave for values of temperature in front of the shock wave of $T_1 = 200$, 300 and 400 K is given in (9).

Calculations of the parameters behind the shock wave and at the deceleration point were carried out for the case of motion of a body at various speeds v_1 at sea level and at altitudes of 16 and 100 km, in air and in an ideal gas. For the

Table 3

	Air			Ideal gas		
T_1	288	217	240	288	217	240
T_2	3175	8585	10160	3940	23150	103150
T_0	3250	8675	10180	4060	23820	106100
p_1	1	0.1	$5.5\cdot10^{-7}$	1	0.1	$5.5\cdot10^{-7}$
p_2	80	70	$1.62\cdot10^{-3}$	76	63	$1.42\cdot10^{-3}$
p_0	95	79	$1.67\cdot10^{-3}$	85	70	$1.56\cdot10^{-3}$
ρ_1	$0.1226\cdot10^{-2}$	$0.1628\cdot10^{-3}$	$0.8000\cdot10^{-9}$	$0.1226\cdot10^{-2}$	$0.1628\cdot10^{-3}$	$0.8000\cdot10^{-9}$
ρ_2	$0.8848\cdot10^{-2}$	$0.1982\cdot10^{-2}$	$0.1813\cdot10^{-7}$	$0.6834\cdot10^{-2}$	$0.9682\cdot10^{-3}$	$0.4789\cdot10^{-8}$
	$0.1031\cdot10^{-1}$	$0.2211\cdot10^{-2}$	$0.1855\cdot10^{-7}$	$0.7374\cdot10^{-2}$	$0.1040\cdot10^{-2}$	$0.5139\cdot10^{-8}$
ρ_0 [a]	$0.9434\cdot10^{-2}$	$0.2056\cdot10^{-2}$	$0.1854\cdot10^{-7}$			
h_1	69.10	52.10	58.25	69.10	52.10	58.25
h_2	957.3	5679	25510	945.2	5558	25035
h_0	974.6	5717	25565	974.3	5719	25750
a_1	340.5	295.4	312.6	340.5	295.4	312.6
a_2	1058	2047	3200	1259	3051	6480
	1066	2058	3205	1278	3094	6572
a_0 [a]	1066	2084	3214			
v_1	2750	6880	14665	2750	6880	14665
v_2	381.5	565.0	647.0	493.8	1158	2450

[a] The first column corresponds to values determined from tables in (7), the second from Eqs. 1.1, 1.7.

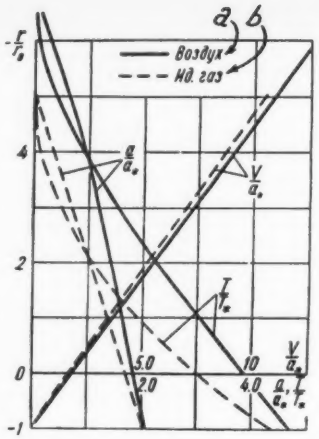

Fig. 1 [a] Air; [b] ideal gas

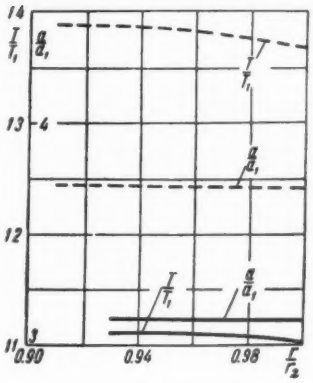

Fig. 2

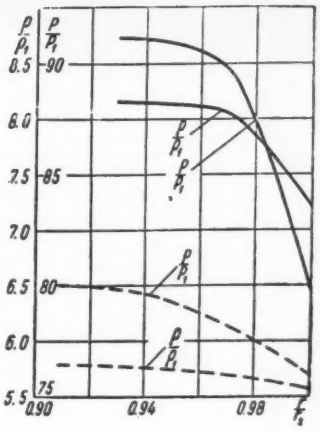

Fig. 3

calculation, we made use of the Bernoulli integral, thermodynamic Eqs. 1.1 to 1.7, and the tables in (7); the results of the calculations are given in Table 3.

As can be seen from the tables, dissociation and ionization lead to a considerable reduction in temperature behind the shock wave and at the deceleration point, as compared with calculations for the ideal gas. In addition, there is an increase in pressure and density. However, the density undergoes relatively little change.

The values for speed of sound a and density ρ were calculated from the second equation in 1.1 and from 1.7; for purposes of comparison, they were also found from the tables in (7). Calculations from the equations show good conformity with data from the tables.

4. Broadening of the Piston in Still Air With Constant Speed

A system of equations for the motion of air behind the front of a shock wave may be written

$$\frac{dv}{dt} + \frac{\partial h}{\partial r} = 0 \qquad \frac{\partial v}{\partial r} + (\nu - 1)\frac{v}{r} = -\frac{1}{\rho}\frac{d\rho}{dt}$$

$$d\rho = \frac{\rho}{a^2}\,dh \qquad h = h_* \alpha \left(\frac{a}{a_*}\right)^{\beta} \qquad [4.1]$$

In order to make an automatic model of the problem in (10), the system of Eqs. 4.1 may be transformed into a system of ordinary differential equations by introducing new dimensionless variables

$$\lambda = \frac{r}{Dt} \qquad V = \frac{t}{r}v \qquad H = \frac{h}{D^2}$$

where D is the speed of the shock wave. This system has the form

$$V' = -\frac{V}{\lambda}\,\frac{H^{2/\beta}\nu - A\lambda^2(V-1)^2}{H^{2/\beta} - A\lambda^2(V-1)^2}$$

$$H' = -\lambda V(V-1)\,\frac{(1-\nu)H^{2/\beta}}{H^{2/\beta} - A\lambda^2(V-1)^2}$$

$$\left(A = \left[\frac{\alpha h_*}{a_*^{\beta}}\,D^{5-2}\right]^{2/\beta}\right)$$

The values $\nu = 1, 2, 3$ correspond respectively to a flat, cylindrical and spherical piston. At the front of the shock wave $\lambda = 1$, and V, H are factors known from the calculations of the primary shock wave (9).

A concrete calculation was carried out for the case $\nu = 2$, $D/a_1 = 8.085$, $p_1 = 1$ atm, $T_1 = 288$ K. The results of the calculation are given in Figs. 2 and 3.

Also carried out was a comparison with the calculated results for the motion of a piston in an ideal gas ($\gamma = 1.4$), using the same values for D/a_1, T_1 and p_1 (dashed curves in Figs. 2 and 3). Comparison shows that pressure and density behind the shock wave in air are higher and temperature is lower than in the ideal gas. The effect of dissociation on the distribution of velocities is small.

5. Flow About a Cone at Zero Angle of Attack

As the next application of the first equation in 1.1, let us examine the problem of flow around a cone in air approaching it at high velocities.

As in the case of an ideal gas, the problem of flow about a cone at zero angle of attack may be solved by calculation of the shock wave and integration of the equation

$$vv'' = 1 + v'^2 - (u + vv')^2/a^2 \qquad [5.1]$$

with the boundary conditions

$$u_k + v_k v_k' = 0 \qquad \text{at surface of cone} \qquad [5.2]$$

$$v = v_2 \quad \text{when } u = u_2,\ v' = -\operatorname{cotan}\omega_2 \text{ at shock wave} \qquad [5.3]$$

where

u = component of the velocity along the axis of the cone
v = component perpendicular to the axis of the cone
ω_2 = angle of the shock wave
k = factors at the surface of the cone

In Equation 5.1, a is a known function of u; v is known from Eqs. 1.1 and the Bernoulli integral

$$h + \frac{u^2 + v^2}{2} = h_1 + \frac{u_1^2 + v_1^2}{2}$$

In performing the calculations, the angle of the shock wave and the parameters in front of the shock wave were considered as given, and the factors ω_k, u_k and v_k were determined by numerical integration.

A comparative calculation was made in which the speed

of sound was calculated not from Eqs. 1.1 but directly from the tables.

In the process, it became clear that use of Eqs. 1.1 introduces practically no error in the determination of $v(u)$, and consequently of factors h, p and ρ.

Calculations were carried out for $M_1 = 14$, $\omega_2 = 30$ deg, $p_1 = 1$ atm, $T_1 = 288$ K.

A comparison using the flow of an ideal gas (11) for equal M_1 and ω_2 shows that the value of the temperature at the cone taking dissociation into consideration is approximately 1.5 times smaller than in the ideal gas. Here, the calculated values for cone angle differ by 3%: For the ideal gas $\omega_k = 26°36'$, for air it is $27°28'$.

Calculations also show that the speed of sound behind the shock wave changes extremely little. This is true even where dissociation and ionization are absent, i.e., for relatively small M_1 and small cone angles—which follows from the tables of Kopal (11).

The density in the flow behind the shock wave front changes much more strongly than the speed of sound, especially in the presence of dissociation and ionization.

These peculiarities of flow are apparently general for the isentropic flow of air behind the shock wave, which is confirmed by the examples given in Sections 3 and 4.

Several approximation methods have been worked out for calculating flow around a cone. One of these is a method of calculating the motion of a gas in which constant gas density is assumed between the shock wave and the cone. In this case, Eq. 5.1 is simplified and can be integrated in its final form (12).

We could propose a more precise approximation method, where the speed of sound in the flow behind the shock wave is considered constant and equal to a_2. Here the accuracy of the calculation is increased, and the time is relatively the same.

Calculations have been performed in which it was assumed that a = constant; these were then compared with accurate calculations. The comparison showed that for $M_1 = 3$, $\omega_2 = 28°11'$ (dissociation is absent), the relative error in determining the angle of the cone amounted to 0.08%, the speed at the cone was 0.2%, the pressure on the cone was 0.04%. In the presence of dissociation, the coincidence of the results was still better: For normal conditions in front of the shock wave ($T_1 = 288$ K, $p_1 = 1$ atm), $M_1 = 14$, $\omega_2 = 30°$, the relative error in the determination of ω_k was equal to 0.06%, and in the determination of speed V_k was 0.002%.

The values given here show that calculation of flow about a cone according to the proposed method results in negligible error for the broad region of factors M_1.

It is to be noted that for a = constant, Eq. 5.1 in dimensionless variables

$$v - a = f \qquad u/a = x$$

takes the form

$$ff'' = 1 + f'^2 - (x + ff')^2$$

Using various values of f_k for a selected ω_k, we can integrate Eq. 5.1 for any desired a and obtain a whole series of curves corresponding to various systems of flow about the cone. Knowledge of the adiabatics of shock and, consequently, of the relations between f_2, x_2, f_2', makes it possible to derive an integral curve corresponding to the given conditions in front of the shock wave and to determine the conditions directly behind the shock wave.

The supposition of small change in the speed of sound behind the shock wave front can also be utilized in solving other gasdynamic problems which take dissociation and ionization into consideration.

—Submitted July 17, 1959

References

1 Zel'dovich, Ya. B. and Raizer, Yu. P., "Shock Waves of Large Amplitude in Gases," *Usp. Fiz. Nauk*, 1957, vol. LXIII, no. 3.

2 Stupochenko, E. V., Stakhanov, I. P., Samuelov, E. V., Pleshanov, A. S. and Rozhdestvenski, I. B., "Thermodynamic Properties of Air Over the Temperature Interval 1000 to 12,000°K and the Pressure Interval 0.001 to 1000 atm," *Physical Gas Dynamics*, collection of articles published by Akad. Nauk SSSR, 1959.

3 Nemchinov, I. V., "The Effect of Dissociation and Ionization of Air in Several Problems of Gas Dynamics," Trans. Physical-Technical Institute, Investigation in Mechanics and Applied Mathematics, Oborongiz, 1958, no. 1.

4 Selivanov, V. V. and Shlyapintokh, I. Ya., "Thermodynamic Properties of Air in the Zone of High Temperature and Shock Waves," *J. Phys. Chem.*, 1958, vol. 32, no. 3.

5 Bond, J., "Plasma Physics and Hypersonic Flight," JET PROPULSION, 1958, vol. 28, no. 4. (Russian translation in collection "Problems of Rocket Technology," 1959, no. 1.)

6 Feldman, S., "Some Shock Tube Experiments on the Chemical Kinetics of Air at High Temperatures," *J. Fluid Mech.*, 1957, pt. 3. (Russian translation in collection "Problems of Rocket Technology," 1959, no. 1.)

7 Predvoditeleyev, A. S., Stupochenko, E. V., Samuelov, E. V., Stakhanov, I. P., Pleshanov, A. S. and Rozhdestvenski, I. B., "Tables of Thermodynamic Functions of Air for Temperatures from 6000 to 12,000°K and Pressures from 0.001 to 1000 atm," Akad. Nauk SSSR, 1957.

8 Landau, L. D. and Lifshitz, E. M., *Mechanics of Dense Media*, Gostekhizdat, 2nd ed., 1954.

9 Rozhdestvenski, I. B., "Thermodynamic and Gas Dynamic Properties of a Flow of Air Behind the Primary Densification Shock Wave Considering Dissociation and Ionization of the Air," *Physical Gas Dynamics*, collection of articles published by Akad. Nauk SSSR, 1959.

10 Sedov, L. I., *Similarity and Regularity Methods in Mechanics*, Gostekhizdat, 4th ed., 1957.

11 Kopal, Z., "Tables of Supersonic Flow Around Cones," vol. 1, MIT, Rep., 1947.

12 Feldman, S., "Hypersonic Conical Shock for Dissociated Air in Thermodynamic Equilibrium," JET PROPULSION, 1957, vol. 27, no. 12.

Reviewer's Comment

In this paper some classical problems of gasdynamics are reinvestigated for air with consideration of dissociation and ionization, instead of a perfect gas. Before this can be done, the chemistry of air at high temperatures must be worked out and the pertinent values tabulated, as in Tables 1 and 2 of this work. Comparison of these values and the formulas upon which they are based with results of similar studies in this country (e.g., in NASA Tech. Rep. no. R-50, 1959, by C. F. Hansen) will be of interest. The same is certainly true of the results obtained here for simple waves, flow past cones, etc. It might be emphasized, however, that these are equilibrium calculations; a more difficult and sometimes more pertinent problem is to determine the flow field in a dissociating and ionizing gas with consideration of time lags, i.e., chemical kinetics.

—W. R. SEARS
Department of Aeronautical Engineering
Cornell University

Digest of Translated Russian Literature

The following abstracts have been selected by the Editor from translated Russian journals supplied by the indicated societies and organizations, whose cooperation is gratefully acknowledged. Information concerning subscriptions to the publications may be obtained from these societies and organizations. Note: Volumes and numbers given are those of the English translations, not of the original Russian.

BULLETIN OF THE ACADEMY OF SCIENCES USSR, GEOPHYSICS SERIES (Izvestiia Akademii Nauk SSSR, Seriia Geofizicheskaia). Published by American Geophysical Union, Washington, D. C.

No. 5, May 1959.

Modeling of Some Geophysical Phenomena on Electrical Grids, B. N. Ivakin, pp. 480–485.

Abstract: The author discusses the possibilities of modeling the nonlinear processes occurring in earthquake foci and in the vicinity of explosions (phenomena of continuity disruption of an elastic medium), as well as the wave phenomena associated with such processes, by means of electrical grid models.

He investigates also the possibilities of modeling electromagnetic waves propagating in a conductive medium by means of an electrical grid model. A model is found which reproduces the "scalar process" of electromagnetic wave propagation.

Approximate Equations for Radiation Transfer, K. Ya. Kondrat'ev and I. L. Senderikhina, pp. 508–512.

Abstract: The question of the applicability of approximate equations for radiant energy transfer to the calculation of short wave length radiation flux in the atmosphere is considered. It is shown that approximate treatment of the rigorous integro-differential equations for the radiation transfer as ordinary differential equations for the radiation flux is not justified.

The Character of the Free Oscillations of Piezo Pickups Used in Modeling Seismic Phenomena, V. M. Prosvirnin and L. N. Rykunov, pp. 528–530.

Introduction: The method of modeling seismic phenomena under laboratory conditions is now being utilized to an ever increasing degree. Piezoelectric crystals—most often crystals of Seignette's salt—are ordinarily used as emitters and receivers for elastic waves.

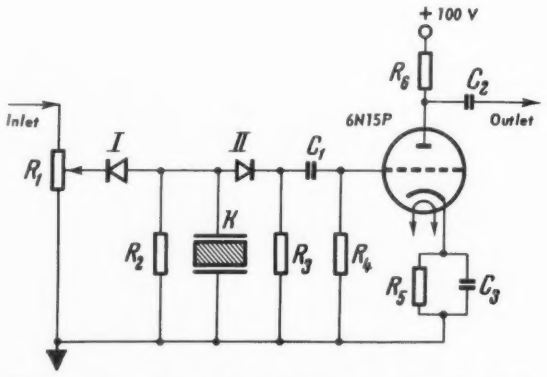

Fig. 1. Diagram of the device for observing the free oscillations of piezocrystals

R_1 = 200 kilo-ohms; R_2 = 1.5 kilo-ohms; R_3 = 4.3 kilo-ohms; R_4 = 70 ohms; R_5 = 1.1 megohm; R_6 = 20 kilo-ohms; C_1 = 0.05 microfarad; C_2 = 0.05 microfarad; C_3 = 0.1 microfarad; I and II - DG-Ts7, K - crystal.

To model sources of elastic waves similar to natural ones, we must obtain both short elastic impulses (imitating earthquakes) as well as quite long trains of waves of a nearly sinusoidal form (imitating microseisms). For this purpose we made an experimental study of the oscillations of a cubic package of ten plates of Seignette's salt 45° X-section, excited by rectangular electric impulses.

The Spectrophotometry of Dawn and Evening Glow, A. Kh. Darchia, pp. 559–565.

Conclusions:

1 Visual evaluations of glow types cannot be considered subjective; they conform well to the types of spectral curves which differ from each other by the ratio of brightness in the short wave and long wave segment of the spectrum. This ratio, on its part, is related to the size and nature of the aerosol particles present in the atmosphere.

2 The spectral type of a glow does not depend upon the latitude of the site and the underlying surface along the direction of observation.

3 An air mass, uniform along a considerable distance in the horizontal and vertical directions, insures the constancy of the spectral type of a glow and also a monotonous decrease in its brightness with the increasing $Z_\odot$. The changes of the spectral type of a glow, its premature extinction and a jump-like decrease in the brightness with the increase of $Z_\odot$, are caused by the non-uniformity of the air masses.

4 The occurrence of changes in the spectral characteristics of glows in the absence of any changes in the visible sphere, enables us to contend that the atmospheric layers (cloudforming up to the height of 3–5 km) beyond the observer's horizon (up to a distance of the order of 600 km) take part in producing dawn and evening glow phenomena.

No. 6, June 1959.

Hydroxyl Radiation in the Upper Atmosphere, N. I. Fedorova, pp. 591–598.

Abstract: The paper gives the results of measuring the relative and absolute intensities of the hydroxyl bands in the near infrared region, from 8200 to 11,200 Å, from night sky spectra obtained in southern latitudes. There are substantial discrepancies from the intensities calculated by Roach. The density of the different vibration levels was determined from the absolute intensities of the OH bands. Density increases smoothly as V' diminishes. The rotation temperature, which apparently varies from night to night, is determined from the intensity distribution in the P-branch. The mean value is 233 ± 16 K.

Doppler Contours and Brightness Distribution Curves for Hydrogen in Aurorae Polares, B. A. Bagaryatsky, pp. 605–608.

Abstract: Formulas are derived for the brightness distribution curves and Doppler contours of the hydrogen emission lines, on the assumption that the beam of protons is monokinetic. The integral expressions for the brightness curves and the zenith contour coincide with those obtained earlier when the meaning of the angular proton distribution function $N(\theta)$ is made more precise. A new formula is given for the horizontal Doppler contour.

Spectral Studies of the Twilight Sky in the Infrared Region, T. G. Megrelishvili, pp. 645–653.

Introduction: An important result of the spectral studies of the twilight sky which have been systematically carried on for more

than 20 years is the discovery of luminescence in the higher layers of the atmosphere, which appear when the lower layers are in Earth's shadow. In 1936 Chernyaev and Wuchs discovered a flare of the yellow sodium doublet; Garrigue observed an intense excitation of the red line of atomic oxygen. Later, excitation of N_2^+ ions was observed, and intensification of the O_2 band, $\lambda = 8669$ Å as well as the OH bands $\lambda = 8431$ and 8780 Å; excitation of atomic nitrogen, $\lambda = 5200$ Å; and apparently also occasional excitation of Ca^+ ions and a lightening of the twilight sky in the 1μ region.

The present paper sets out some of the results obtained by processing twilight sky observations made in the years 1952–1957 at the Abastuman astrophysical observatory. These results gave us grounds for assuming the existence of twilight luminescence of the thin atmospheric layers at altitudes of 35–40 and 90–100 km in the spectral region around $\lambda = 9400$ Å, as we had already indicated elsewhere. These investigations form part of the program of systematic observations in the infrared region begun in the Autumn of 1952 with the photoelectric photometer invented by Rodionov and his co-workers.

JOURNAL OF PHYSICAL CHEMISTRY (Zhurnal Fizicheskoi Khimii). Published by The Chemical Society, London.

Vol. 33, no. 11, Nov. 1959.

The Application of the Variational Method to the Calculation of the Distribution Functions of Molecules in a Liquid, V. V. Vatollo, pp. 445–446.

Introduction: In recent years many views have been put forward on the so-called variation theory of systems of interacting particles, which, unlike other theories, is self-consistent. Even the strict Bogolyubov-Born-Green theory is based on Kirkwood's "superposition approximation," the accuracy of which is doubtful for small distances. The binary distribution function calculated theoretically thus leads to considerable errors in the thermodynamic quantities.

Summary:

1 The "superposition approximation" is not applicable to all possible liquid models, but only when the density is low or when the interaction energy is small, i.e., only under these conditions does the average force potential $\Phi(1, 2)$ become the interaction potential for a pair of molecules, and Eq. 11 becomes the Bogolyubov-Born-Green equation.

2 Generalization of the "superposition approximation" leads to an integral equation for the binary distribution function. It is to be expected that this equation should give a more accurate description of the behavior of the distribution function at comparatively small distances, than the equations based on the "superposition approximation" theories.

3 An advantage of the present method is that the difficulties associated with the divergence of the integrals in the limit $N \to \infty$, $V \to \infty$ in Richardson's theory are automatically eliminated by the appropriate normalization of the correlative distribution functions.

Liquid-Vapor Equilibrium. An Explicit Expression for the Equilibrium Composition of the Phases in Multicomponent Systems, E. Hála, pp. 463–467.

Introduction: The present paper provides an explicit expression for the mutual dependence of the equilibrium compositions of the phases in real systems with any number of components, which takes the form

$$\alpha_{ij\ldots w} = \frac{y_i}{x_i}\frac{x_j}{y_j} = \frac{1 + \sum\limits_{\substack{w \\ r\neq i}} a_{ir}x_r + \sum\limits_{\substack{w \\ r\neq i}}\sum\limits_{\substack{w \\ s\neq i}} a_{irs}x_r x_s + \sum\limits_{\substack{w \\ r\neq i}}\sum\limits_{\substack{w \\ s\neq i}}\sum\limits_{\substack{w \\ t\neq i}} a_{irst}x_r x_s x_t + \ldots}{1 + \sum\limits_{\substack{w \\ r\neq j}} a_{jr}x_r + \sum\limits_{\substack{w \\ r\neq j}}\sum\limits_{\substack{w \\ s\neq j}} a_{jrs}x_r x_s + \sum\limits_{\substack{w \\ r\neq j}}\sum\limits_{\substack{w \\ s\neq j}}\sum\limits_{\substack{w \\ t\neq j}} a_{jrst}x_r x_s x_t + \ldots} \quad [1]$$

where x_i, x_j and x_r are the mole fractions of the constituents i, j and r in the liquid phase; y_i and y_j are the mole fractions of components i and j in the gaseous phase; and a is a constant characteristic of the system. The summations indicate the sum of all terms of the given type with the exception of that term indicated by the lower suffix; for example, for the four-component system we have

$$\sum_{\substack{w \\ r\neq i}} a_{ir}x_r = a_{ij}x_j + a_{ik}x_k + a_{il}x_l \quad [2]$$

If the relative volatilities of the components are known as a function of the composition of one phase, the composition of the other phase is easily calculated from the equation

$$y_i = \frac{\alpha_{iw\ldots}\dfrac{x_i}{x_w}}{\sum\limits_{j=i}^{w}\alpha_{jw\ldots}\dfrac{x_i}{x_w}} \quad [3]$$

where the suffixes $i, j, \ldots, w$ indicate the components of the w – component system.

The right-hand side of Eq. 1 is the ratio of two series having $(w - 1)$ terms, where w is the number of components of the system.

Summary: By using Eq. 1 it is possible to express rationally the mutual relationship between the equilibrium compositions of liquid and gaseous phases in real systems with any number of components to any degree of accuracy; the greater the accuracy required, the larger the number of constants which must be included in the corresponding equations.

The practical significance of the equation is that it limits the amount of experimental data required to characterize a system; most of the constants (or in two-suffix equations, all of them) can be determined from experimental data for binary systems. The advantage of this method is that it can be used even for systems in which both phases are non-ideal.

Vol. 33, no. 12, Dec. 1959.

Thermal Explosion and Isothermal Decomposition of Explosives. I. Activation Energy for the Decomposition of Glycerol Trinitrate, A. I. Serbinov, pp. 559–562.

Summary: Both the results of the present work on the thermal explosion of glycerol trinitrate and published data on its unimolecular isothermal decomposition and thermal explosion, covering a range of decomposition velocities differing by a factor of 10^7, are very satisfactorily represented by Eq. 8 for the temperature dependence of the rate constant for unimolecular decomposition, with the normal value of the pre-exponential factor equal to the characteristic frequency of the valency vibrations of the NO_2 group in nitric-acid esters and with an activation energy equal to the energy of rupture of the —O—NO_2 bond.

Effect of Rate of Initiation of Active Centers on the Kinetics of Chain Reactions With Degenerate Branching and Second-Order Chain Termination, D. G. Knorre, V. L. Pikaeva and N. M. Emanuel', pp. 568–571.

Introduction: Chain reactions with degenerate chain branching occur in a number of processes which are autocatalytic and, like any self-accelerating process, are characterized by a more or less distinct induction period (the time during which the reaction products do not accumulate in measurable amounts in the system).

In the present work, devoted to an analysis of the kinetics of oxidations with molecular oxygen in the liquid phase, the induction period is taken to be the time required for the concentration of hydroperoxides to reach 0.001%, a concentration which is at the limit of sensitivity of the iodometric determination.

Summary:

1 A solution has been obtained for a system of differential equations representing the kinetics of the accumulation of hydroperoxide and stable reaction products with first-order and

second-order chain branching and second-order chain termination. The solution has been obtained without assuming a steady-state concentration of RO_2 radicals.

2 Decrease in the rate of initiation and increase in the proportion of second-order branching lead to kinetic curves of more markedly autocatalytic character.

3 Even at rates of initiation $w_0 \cong 10^{10}$ radicals per cm³ sec, the condition of a steady-state concentration of RO_2 radicals leads to an incorrect solution. In particular, the steady-state approximation indicates that at $w_0 < 10^{10}$ the induction period ceases to depend on w_0, which is not supported by a semi-stationary approximation.

The Influence of Pressure in the Gas-Phase Oxidation of Hydrocarbons, A. S. Badrian, N. S. Enikolopyan and M. S. Furman, pp. 580–585.

Summary:

1 A study has been made of the effect of pressure and temperature on the oxidation of a propane-air mixture containing 50 mole % C_3H_8, 3 mole % O_2, and 47 mole % N_2. Experiments were carried out at pressures of 5, 10 and 15 atm and temperatures of 325, 350 and 375 C under flow conditions with the gaseous mixture remaining for only short periods (4–8 sec) in the reaction zone.

2 The relative yield of hydroperoxide (or acetone) increases linearly with rise in the pressure of the reaction mixture and falls with rise in temperature with an activation energy of about 10 kcal.

3 The relative yield of alcohols α increases with rise in pressure (or hydrocarbon concentration) and falls with rise in temperature. The variation of α with pressure is represented by a curve which approaches asymptotically the value $\alpha = 1$.

4 The ratio between the rates of formation of ethyl and methyl alcohols is practically independent of the pressure of the reaction mixture and of the hydrocarbon concentration; the relative proportion of ethyl alcohol increases with rise in temperature.

5 These results are explained in terms of the effects of change in pressure and temperature on the competition between individual reaction stages in the gas-phase oxidation of hydrocarbons.

MEASUREMENT TECHNIQUES (*Izmeritel'naia Tekhnika*). Published by Instrument Society of America, Pittsburgh, Pa.

No. 10, Oct. 1959.

Measurements of Half-Widths of Spectral Lines by Means of a Fabry-Perot Interferometer With Photoelectric Recording, Yu. P. Efremov, pp. 756–760.

Conclusions: The lines of the near infrared region of the spectrum of Kr^{86} can be successfully used for interference measurements of length, especially for difference rates exceeding 500 mm in cases when measurements by means of visible lines of the spectrum become difficult or altogether impossible.

OPTICS AND SPECTROSCOPY (*Optika i Spektroskopiia*). Published by Optical Society of America, Washington, D. C.

Vol. 9, no. 1, July 1960.

The Scattering of Light by Dielectric Ellipsoids Comparable With the Wavelength. I. A General Expression for the Indicatrix of Scattering of an Ellipsoidal Particle, A. V. Shatilov, pp. 44–47.

Abstract: The problem of the diffraction of an electromagnetic wave by an anisotropic nonabsorbing ellipsoid is solved in first approximation. Expressions for the indicatrix and coefficient of scattering of particles with refractive indexes which are not large are obtained. The dependence of the form of the indicatrix on the dimensions, eccentricity and orientation of the scattering ellipsoids is clarified.

New Recursion Formulas in the Theory of Multilayer Optical Coatings, P. G. Kard, pp. 49–51.

Introduction: The appearance of the recursion formulas of Vlasov may be considered as the beginning of the development of multilayer optical coating theory. In spite of the fact that since that time the theory has advanced considerably, these formulas have remained important. They are widely used in theoretical investigations as well as in practical computations. A combination of the Vlasov method with other methods is usually the most fruitful.

In this work we shall obtain new recursion formulas, outwardly somewhat similar to the Vlasov formulas, however, in essence, different from them. It seems probable that in certain cases application of the new formulas may prove to be more convenient than the use of other methods. Moreover, it will be shown how some of the Vlasov formulas can be substantially simplified.

We shall make use of the following notation: N is the number of layers; $n_1, n_2, \ldots, n_N$ are the indexes of refraction of the layers (the numbers increase in the direction of light propagation); n_0 is the index of refraction of the original medium from which light is incident on the coating; $n_{N+1} \equiv n$ is the index of refraction of the final medium (substrate). Normal incidence will be taken for simplicity, although all conclusions, with the appropriate modifications, are applicable also in the case of oblique incidence. Further, let k denote the wave number in vacuum, h_m the thickness of the mth layer, and

$$\alpha_m = kn_m h_m \qquad [1]$$

Finally, let us take

$$a_m = \frac{1}{2}\ln\frac{n}{n_m} \qquad m = 0, 1, \ldots, N \qquad [2]$$

The indexes of refraction of the layers and the bounding media can be complex; i.e., the corresponding substances are absorbing. We shall limit ourselves here to the case of isotropic substances.

Threshold Sensitivity of Radiation Receivers, E. S. Ratner, pp. 52–55.

Abstract: The relationship of the sensitivity threshold of radiation receivers, as determined by the fluctuations in the effectively absorbed quanta, to the magnitude of the steady background and certain properties of the receiver-amplifier-indicator system are considered.

High Sensitivity Modulation Photometer, A. Yu. Borisov, pp. 60–61.

Abstract: The present note describes a photometer in which a direct current flowing through a photomultiplier (*PM*) is changed, by means of a low frequency voltage applied to one of the dynodes, into an alternating current of twice the applied frequency. This frequency doubling allows the signal to be filtered from stray induced currents.

Vol. 9, no. 2, Aug. 1960.

The Scattering of Light by Dielectric Ellipsoids Comparable With the Wavelength. II. Dependence of the Indicatrix of the Scattering on the Size, Form and Orientation of the Ellipsoid. The Scattering Coefficient, A. V. Shatilov, pp. 123–127.

Introduction: From an expression obtained earlier

$$I = I_0 \frac{k}{\epsilon_1''} \cdot \frac{P_{0^2\perp}}{E_0^2} v^2 f^2(q) \qquad [1]$$

where

$$f(q) = (3/q^3)(\sin q - q\cos q)$$
$$q = 2\rho \sin(\beta/2)\sqrt{1 + \sigma\alpha_1^2}$$
$$I_0 = \frac{c}{8\pi}\sqrt{\epsilon_1}E_0^2\frac{1}{r^2}$$
$$\sigma = \frac{\epsilon^2}{1 - \epsilon^2}$$
$$\rho = 2\pi(b/\lambda)$$

the scattering indicatrix is determined by the parameters $P_{0\perp}$ and q, whose dependence on the dimensions, form, dielectric properties and orientation of the scattering ellipsoid must be found (here v is the volume of the ellipsoid, ϵ is its eccentricity, b is the semi-axis which is not the axis of symmetry, β is the scattering angle, α_1 is the cosine of the angle between the normal to the scattering layers and the symmetry axis of the ellipsoid, $\mathbf{k}$ is the wave vector, and $\mathbf{r}$ the distance to the particle). We recall that $\mathbf{P}_{0\perp}$ is determined by the polarization of the ellipsoid and q by the number of waves contained within the dimensions of the particle in a direction normal to the "reflecting" layers.

Determination of the Size of Particles by the Scattering of Light. Nomograms for the Determination of the Size of Rod-Shaped Particles, I. Ya. Slonim, pp. 127–128.

Theory of Increasing the Transparency of Metallic Coatings, P. G. Kard, pp. 129–131.

Introduction: Semitransparent metallic coatings (usually monolayers) are widely used in optics. Among their defects is that of considerable absorption. Therefore the problem of improving the optical properties of such coatings arises. Depending on the specific objective, the change of optical properties of a metallic layer can proceed in different directions; however, in any case it is possible to formulate the problem as follows: The absorption coefficient A must be as small as possible, and the ratio R/D (of the reflection coefficient to the transmission coefficient) must initially have a given value. Thus the basic problem consists of clarifying a metallic coating; we understand "clarifying" to mean a decrease in the absorption coefficient whether it results in an increase in D or in R.

In this paper we will examine theoretically the problem of clarifying a metallic layer with the help of multilayer dielectric films. It is conceivable that in this way better results will be obtained than by the application of additional metallic layers.

The dielectric film can be deposited on the outside of the metallic layer or introduced between the substrate and the layer. In the first case, clarification is possible only accompanying an increase in the reflection coefficient. In the second case, the magnitude of the ratio R/D can take large or small values depending principally on the way in which the parameters of the dielectric film are chosen. Also, the magnitude of the ratio A/D is constant in the first case, whereas in the second case it can be significantly decreased. The second case consequently contains more possibilities, and so we will give it our principal attention.

In our theory we will use simplified Vlasov formulas.

We will make use of the following designations

$$a = r/d \qquad b = 1/d \qquad [1]$$

where r and d are the amplitude reflection and transmission coefficients

$$\alpha = knh \qquad \beta = kxh \qquad [2]$$

where K is the wave number in vacuum, n is the index of refraction or its real part, x is the imaginary part of the refractive index, and h is the thickness of the layer. The subscripts used with the magnitudes a, b, n, x, h, α and β will show to which coating, layer or lumped sub-assembly of coatings they are related.

The incidence of the light will be assumed normal throughout.

RADIO ENGINEERING (*Radiotekhnika*). Published by Pergamon Institute in conjunction with Massachusetts Institute of Technology.

Vol. 14, no. 11, 1959.

Study of Methods of Maintaining a High Precision of Scale Graduation Using Mechanical Correctors and the Frequencies of a Heterodyne Oscillator, M. Ye. Movshovich, pp. 44–53.

Abstract: The optimum conditions for the use of simple and complex correcting methods are investigated. In deriving the optimum correction conditions the Chebyshev theorem of least deviations is employed. In conclusion, the effect on the optimum correction conditions of instabilities in the frequencies of the reference oscillator and the intermediate frequency amplifier are determined

Conclusion: We have described the basic theory and calculation of the methods whereby mechanical correctors are employed to maintain the initial high precision of the graduation of the scales of superheterodyne-type receivers. The relationships obtained determine the position of the reference marks, the limits of change of the correctors and the values of the possible relative errors of the scale graduations in these circumstances. The equalities which have been derived allow us to determine both the maximum possible and the most probable magnitudes of the relative errors of the scale graduations. For this purpose we must employ the expressions which determine the coefficients β.

The Influence of Input Pulse Rise Time in Pulse Transformers, L. Z. Gogolitsyn, pp. 68–72.

Abstract: This paper is concerned with the influence of the rate of rise of the input pulse leading edge on the leading edge of the output pulse in pulse transformers. Formulas and graphs are given for the selection of the design parameters of pulse transformers which secure the requirements demanded of an output pulse depending upon the duration of the input pulse rise time which varies exponentially.

Conclusion: A more accurate result will be obtained when determining the rise time and the "overshoot" of a voltage at the peak of an output pulse if we take into account the rate of rise of the input pulse leading edge.

The formulas and graphs may be employed when calculating those parameters of the pulse transformer which must satify the requirements demanded of the output pulse leading edge.

Vol. 15, no. 3, 1960.

The Principles of the Construction of a Machine for Pattern Recognition, V. S. Fain, pp. 16–23.

Abstract: The problems of the construction of a machine which operates by the "parallel" method are analyzed; the theoretical considerations which determine the most advantageous design trend are developed, and a circuit constructed on the basis of these considerations is examined. The circuit is compared with the living visual apparatus.

The Dynamic Properties of Automatic Pulse Rangefinders With Two Integrators, Ye. P. Nikitin and A. G. Saibel', pp. 33–41.

Abstract: Pulse rangefinders with automatic range tracking with two integrators are examined. Formulas and graphs are derived which permit the determination of the stability of a system, its behavior under transient conditions and also the calculation of the systematic dynamic errors.

Single-Stage Selective Amplifier With an Amplified Negative Selective Feedback, A. I. Belichenko, pp. 75–81.

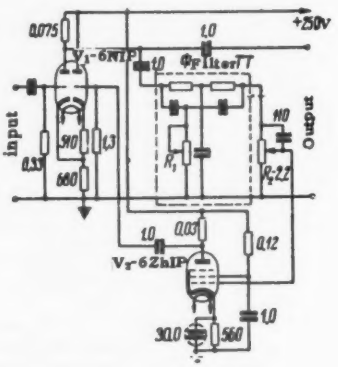

Abstract: A means is proposed for increasing the selectivity of a single-stage amplifier with negative selective feedback by including after the band stop filter an additional single valve amplifier in the feedback circuit and by feeding a negative signal to the cathode of the first valve through the cathode follower. The theoretical formulas and the practical circuit are given.

The Measurement of the Nonlinearity of Pulse Instruments by a Comparison Method, I. F. Ivanov, pp. 96–108.

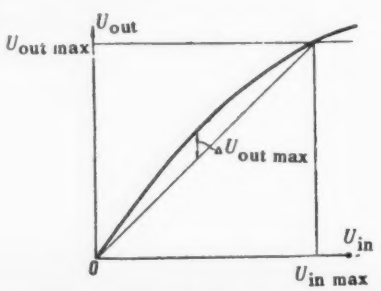

Fig. 1

Abstract: The possibility of measuring the nonlinearity of pulse instruments by comparing taken input and output voltages is examined.

Introduction: When measuring the nonlinearity of pulse instruments used in television, radar and experimental physics, it is of interest to know the nonlinearity of the amplitude characteristic of these instruments. We can judge the degree of nonlinearity of an amplitude characteristic from a knowledge of the nature of the change of the differential amplification factor in the prescribed input voltage limits or by determining the maximum relative deviation of the amplitude characteristic from a straight line drawn between two points on the characteristic. In the latter case the quantity

$$\xi = (\Delta U_{\text{out max}}/U_{\text{out max}})\ 100\% \qquad [1]$$

is the criterion of nonlinearity (the straight line drawn from the origin to the end point of the characteristic, Fig. 1.).

We describe the measurement of the nonlinearity by the comparison method which allows the quantity ξ to be determined with a high degree of accuracy.

Conclusions: The method which has been described for the measurement of the nonlinearity of the pulse devices by the method of the comparison of the voltages taken from the input and output of the device under investigation permits the following conclusions to be drawn:

1 The nonlinearity of the pulse devices is measured with the help of signals of the same form as the working signals of the device.

2 The comparison method permits the measurement of the nonlinearity with an error which does not exceed 3–7 % of the quantity being measured.

3 The error involved in the measurement of the nonlinearity is determined mainly by the nonlinearity of the components of the device which stand before the comparison circuit; to obtain a high accuracy, the nonlinearity of these elements must not exceed 0.5–1 %, in which case the nonlinearity of the elements of the instrument which stand after the comparison circuit may reach several parts in a hundred (2 %).

RADIO ENGINEERING AND ELECTRONICS (*Radiotekhnika i Electronika*). Published by Pergamon Institute in conjunction with Massachusetts Institute of Technology.

Vol. 4, no. 8, 1959.

Test of Probe Method Applicability to the Measurement of Charge Concentration in High Frequency Discharges, S. M. Levitskii and I. P. Shashurin, pp. 8–16.

Introduction: A fairly large number of papers have been published in which probe methods have been applied to the study of high frequency gas discharges. A portion of these studies was carried out by a method using a single probe and counter probe, a part by a double-probe method. However in the majority of these studies these methods, developed for d-c discharge, were applied to the hf discharge without any analysis and experimental verification.

In the present work a test was carried out of the applicability of probe methods for measuring change concentrations existing in an hf discharge.

Conclusions: The investigations carried out permit considering that the classical single-probe method is fully applicable to charge concentration measurement in high frequency discharge plasma.

Concerning the double-probe method, it is subject to some distortion due to stray probe capacitance which could not be eliminated before the end of this work; therefore, from our point of view, the double-probe method in the existing form may be recommended for use in hf discharges only in those cases where the single probe is not possible for some reason or other.

The difficulties encountered in using the probe method for investigating hf discharge plasmas (the effects of stray capacitance, insufficient probe isolation), were essentially of a "circuit character" and did not affect the essential character of the probe method.

Utilization of High Frequency Electromagnetic Fields for Plasma Investigation, S. Brown, pp. 17–29.

Introduction: The study of interaction between a gas discharge plasma and electromagnetic waves leads to the understanding of certain essential physical properties of the discharge studied.

In the majority of cases considered, this interaction is characterized by two quantities, attenuation and phase shift of the electromagnetic wave in its passage through the plasma. Without regard to this limitation in the number of observable quantities, experiments may be proposed giving the possibility of determining such important parameters as the electron density, the cross sections of electron-atom, electron-ion, ion-atom collisions, electron temperature, electron energy losses in collisions, the rate of loss of electrons in diffusion and recombination.

The purpose of the present report is to give a survey of work undertaken in the U.S.A. during the last period, containing methods of measuring these parameters in isotropic plasmas and plasmas located in constant magnetic fields.

Discharge Ignition in Inhomogeneous Fields at Low Gas Pressure, L. G. Guseva, pp. 42–50.

Abstract: It has been found that on the left branch of a Paschen curve, discharge ignition occurring in inhomogeneous fields varies strongly with change in electrode polarity. In the general case, the ignition field intensity is found higher than that corresponding to the longest flux line between electrodes. An explanation is given on the basis of an analysis of the differing characters of ion and electron motion in a rarefied gas.

Introduction: The existing literature on igniting discharges in the left branch of the Paschen curve relates basically to homogeneous fields. There remains unexplained a complex of questions connected with the role of the shape of non-plane electrodes and their polarities.

In the present work the ignition potential of the discharge was investigated in five different types of inhomogeneous fields with various relationships among the geometric parameters for each of the types. The effect of electrode polarity on the ignition voltage in these fields was also determined.

Some Peculiarities of Arc Discharge in Inert Gases, V. N. Kolesnikov and N. N. Sobolev, pp. 79–82.

Introduction: In studying low precision arc discharges formed at normal pressure between clean carbon electrodes in a helium or argon atmosphere with controlled admixtures of hydrogen and neon, together with V. N. Egorov, we have previously established that the absolute population of various atomic levels of hydrogen, helium and neon corresponds to temperatures of 10,000–11,000 K. The relative population of these levels corresponds to a quasi-Boltzmann distribution with temperature 3000–4000 deg. Employing "transverse images" it was found that in a single point of the arc column at sufficiently intense excitation not only atoms of He, Ar, Ne, H but also molecules of H_2, C_2, CH, CN are excited. On the basis of these results it is possible to conclude that thermal equilibrium is absent from the arc column studied.

Under the same conditions the intensity distribution in the region of CN 3883 Å was studied with unresolved rotary structure and the excitation temperature of oscillating levels of this molecule was determined from pyrometric graphs. It was found to be $\backsim (3 \times 10^3)$ K independently of the arc regime and atmosphere composition, which is very close to the value (3.5×10^3) K previously obtained from atomic spectra. This may indicate that the mechanism of excitation in the investigated arc column is the same for all particles and connected with certain features common to all inert gases.

The Use of Oscillations at a Small Anode to Measure Vapor or Gas Density, A. V. Rubchinskii, F. S. Kobelev and V. M. Mantrov, pp. 115–122.

Abstract: A method is described for measuring mercury vapor pressure in the range 10^{-1}–10^3 Hg, based on voltage oscillations arising on a small anode having an amplitude dependence on the vapor density.

Calibration curves are presented for mercury vapor and for the inert gases. A method is given for oscillographic determination of vapor density in gas discharge devices in the reverse and forward half periods.

Vol. 4, no. 10, 1959.

The Significance of Optimum Criteria and A Priori Distributions in the Theory of Signal Reception, L. S. Gutkin, pp. 1–18.

Introduction: An analysis is given of the significance of optimum criteria for receivers and the form of a priori distributions of messages in the reception of signals with a background of fluctuation noise.

It is proved that with high requirements on the accuracy

(reliability) of message reproduction the structure of the optimum receiver and its properties are practically independent of the form of a priori distribution and of the selected optimum criterion for a broad class of these distributions and criterion. Therefore, in seeking a precise optimum receiver and investigation of its properties, it is permissible in many cases to start from the simplest (uniform) a priori message distribution and one of the simplest optimum criteria.

From this it also follows that the broad results obtained for high signal to noise ratio by a number of authors and, in the first place, V. A. Kotel'nikov, starting from a uniform a priori distribution and the simplest optimum criterion, may be extended to broad classes of more complicated a priori distributions and optimum criteria.

The Probability of Distortion Caused by Spurious Currents and Gaussian Noise, V. I. Bunimovich and V. A. Morozov, pp. 19–33.

Abstract: Signal distortions caused by the excitation of spurious currents and receiver noise in pulse signal transmission over communications lines are considered. The line inhomogenities leading to the spurious currents are assumed lumped and located at approximately equal distances from each other. Expressions are obtained for the mean probability of distortion in pulse signal reception and the dispersion of this probability. A knowledge of the mean probability of distortion is found sufficient for practical estimation of the probability that the distortion probability does not exceed a pre-assigned value.

Properties of a Wave Guide Matrix with $2(P + 1)$ Terminals, R. A. Silin, pp. 92–98.

Abstract: The properties of wave guide matrices with $2(P + 1)$ terminals are found as a function of their reversibility, horizontal and circular symmetry, the absence of loss and the absence of reactance. The scattering properties of the wave guide matrix are found as a function of the circular symmetry of the $2(P + 1)$ terminals.

Radiation of a Modulated Beam of Charged Particles in Passage Through a Round Opening in an Ideally Conducting Plane Screen, Iu. N. Dnestrovskii and D. P. Kostomarov, pp. 122–137.

Abstract: The electromagnetic radiation arising in the passage of a modulated electron beam through an opening in an ideally conducting plane screen is investigated. The problem is reduced to a Fredholm integral equation of the first kind, which is solved numerically on an electronic computer in the range of velocities from $\beta = 0.1$ to $\beta = 0.99$.

Vol. 5, no. 2, 1960.

The Statistical Properties of Large Ionospheric Inhomogenities, V. D. Gusev, pp. 1–13.

Abstract: The statistical and correlational properties of the phases of waves reflected from an ionosphere containing large inhomogeneities are considered. The analysis is carried out on the basis of solution of the eikonal equations. It is demonstrated that only with a normal distribution of angles of incidence of the wave the distribution of rate of change of phase with respect to time is independent of the distance to the ionosphere. The statistical character of focusing phenomena by large ionospheric inhomogenities, which may have substantial significane in the phase method for studying these inhomogeneities, is investigated.

Approximate Method for Calculating the Detection Characteristics of Multichannel Systems With Correlated Noise and Selection of Largest Amplitude, Iu. B. Cherniak, pp. 29–40.

Abstract: An approximate method of calculating the magnitude of false alarm is considered for an n-channel system with correlated noise and solution of maximum amplitude.

An asymptotic expression is obtained for the integral two-dimensional distribution of envelope amplitudes at the output of a linear detector.

Conclusion: We have derived relations enabling us to find the probability of false alarm in multichannel systems with correlated noise and choice of maximum envelope amplitude. We have obtained also the asymptotic expression for the integral distribution of the envelope amplitudes of a two-dimensional normal process and have proved that the influence of correlation in the given method of processing signals rapidly decreases with increase of threshold level.

The Optimum Method of Determining the Time Position of Pulses, B. N. Mitiashev, pp. 41–52.

Introduction: There are several methods of determining the time position of pulse signals, providing the theoretically attainable precision under low noise conditions. In the majority of cases an indispensable condition for obtaining the limiting precision is the use of filters with frequency characteristics complex-conjugate to the spectrum of the pulse signals. At the same time with sufficiently low noise level the limiting precision or close to it is realized even without the application of these filters. The attraction of using these filters consists in that they are optimal as well in the problem of detecting weak signals, and therefore with optimal filtering the possibility appears of defining exactly the time position of pulses at increased noise level. However, this is not obtained in all methods of measurement, requiring optimum filtering to provide the limiting precision in the case of low signal to noise ratio.

In the present work it is clarified in which methods of determining the time position of pulses the limiting precision at low noise level is combined with maximum limiting resistance to noise.

Interaction Between Electron Stream and Plasma, E. V. Bogdanov, V. Ia. Kislov and Z. S. Chernov, pp. 75–89.

Abstract: The problem of interaction of a bounded electron stream with plasma is considered. The dispersion equation is obtained and the conditions for an increasing hf signal are analyzed. A system in which a modulated electron stream interacts with a gas discharge plasma located in a longitudinal magnetic field is experimentally investigated. In the range from 30 to 3 cm plasma amplification up to 40 db was obtained.

SOVIET PHYSICS-JETP (Zhurnal Eksperimental'noi i Teoreticheskoi Fiziki). Published by American Institute of Physics, New York.

Vol. 11, no. 2, Aug. 1960.

Energy Distribution of Sputtered and Scattered Ions in the Bombardment of Tantalum and Molybdenum by Positive Cesium Ions, V. I. Veksler, pp. 235–242.

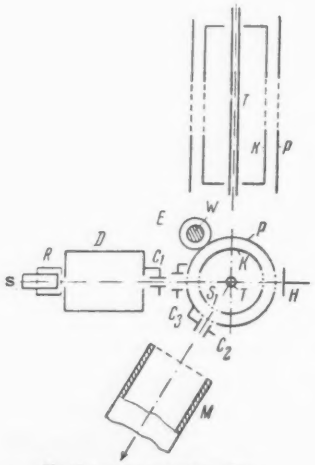

FIG. 1. Diagram of the apparatus: S – primary-ion source, S–R–D – ion gun, C_1, C_2, C_3 – deflection capacitors, T – target, K – cylinder of the energy analyzer, P – accelerating cylinder, M – mass-spectrometer tube, H – collector for "straight-through" ions, E – shield, W – traverse, S_1 – screen.

Abstract: A method is described for studying the energy spectra of scattered and sputtered ions produced in the bombardment of metals by positive ions. The energy spectra of the Cs^+, Mo^+ and Ta^+ ions obtained by bombarding molybdenum and tantalum targets ($T \sim 1600 - 1800$ K) with Cs^+ ions with energies $U = 900$–2150 ev have been investigated. The sputtering and scatter-

ing components have been separated from the secondary emission ion spectra which have been described earlier; the result is a considerable reduction in the limiting energy in the spectrum of Cs^+ scattered on molybdenum. The width of the energy spectrum for the sputtered ions is found to be 30–35 ev for Mo^+ and 35–50 ev for Ta^+; these values are much higher than the value of 5 ev which is quoted in the literature. These results indicate that the probability of ionization of a sputtered atom which escapes from the surface increases as its energy increases.

Investigation of a High Energy Interaction Event in Photographic Emulsion, Kh. P. Babayan, M. G. Sarinyan and É. R. Tumanyan, pp. 227–230.

Abstract: A star of the 5 + 21 p-type produced by a primary particle of $\sim 10^{12}$ ev was investigated. The measured angular distribution of the secondary shower particles exhibits two maxima. The event was interpreted as a peripheral collision of two nucleons. The ratio of the number of neutral π mesons to the total number of charged shower particles was found to be of the order of 0.4. A secondary interaction of the 0 + 6 p-type, which is probably due to a single π-N collision in a peripheral collision of nucleons, was detected.

type. The conformal invariance of the nonlinear equations of the meson and spinor fields is discussed.

Internal Structure of Super Dense Stars, D. A. Kirzhnits, pp. 365–368.

Abstract: The peculiarities of a "condensed state plasma" transition in ultra-compressed matter are considered, and it is concluded that the cores of dense white dwarfs may be in a condensed state. As a result, the nuclear processes have much lower rates than in a plasma, and the possible hydrogen concentration in the matter of white dwarfs may be much higher.

The Motion of a Conducting Piston in a Magnetohydrodynamic Medium, I. A. Akhiezer and R. V. Polovin, pp. 383–386.

Abstract: The types of waves excited in a magnetohydrodynamic medium by a uniformly moving conducting plane (piston) are investigated. The question of the resolution of an initial discontinuity is discussed.

Vol. 11, no. 3, Sept. 1960.

Interaction of an Electron Beam With a Plasma, I. F. Kharchenko, Ya. B. Fainberg, R. M. Nikolaev, E. A. Kornilov, E. A. Lutsenko and N. S. Pedenko, pp. 493–498.

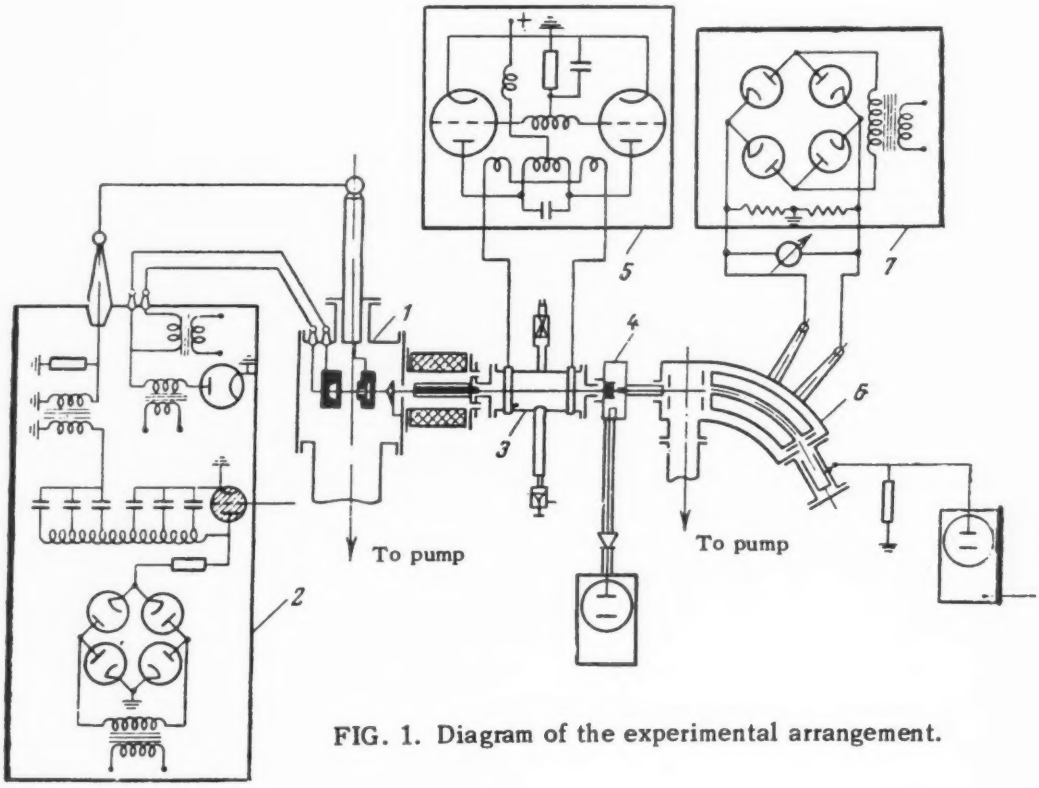

FIG. 1. Diagram of the experimental arrangement.

The Nonlinear Theory of Elementary Particles, D. F. Kurdgelaidze, pp. 339–346.

Abstract: The energies and momenta of spinor fields in theories with pseudovector and scalar nonlinear terms are calculated on the basis of a number of new exact solutions of the wave type. By a semiclassical quantization the mass of the nucleon is determined as $k_0 l = 2^{1/2}\pi^{3/2} \approx 7.84$. The dependence of the energy of the field on the degree of nonlinearity is established. The method of fusion is used to derive from the nonlinear spinor equation a nonlinear undor equation, which on certain assumptions reduces to a nonlinear meson equation of the Klein-Gordon

Abstract: The results of an experimental investigation of the interaction of modulated and unmodulated high energy electron beams with the plasma in a high frequency discharge are presented. It is shown that the passage of an unmodulated beam through a plasma results in the production of plasma oscillations in the beam at a frequency close to the plasma frequency. The dependence of oscillation amplitude on frequency and the plasma parameters is determined. The coherent energy losses of electrons in modulated and unmodulated beams moving through a plasma have also been studied.

Experimental Investigation of the Energy Spectrum of the

Penetrating Component of Extensive Air Showers, E. L. Andronikashvili and R. E. Kazarov, pp. 507–510.

Abstract: The energy spectrum of the μ-meson component of extensive air showers was measured in the range from 0.4 to 37 Bev. The investigations were carried out for three groups of showers with mean number of particles equal to 1.4×10^4, 7×10^4 and 2.9×10^5. The energy spectrum has been plotted for the three shower groups at a mean distance of ~ 28 m from the axis. The energy spectrum of the shower as a whole has also been determined. For all three shower groups, the power exponent of this spectrum is approximately equal to 1.

The Significance of Strange Particles in Fermi's Statistical Theory, V. I. Rus'kin and P. A. Usik, pp. 669–672.

Abstract. It is shown that account of resonance interaction of two π-mesons in Fermi's statistical theory permits one to explain a number of experimental facts which remained inexplicable by the statistical theory which takes into account only the nucleonic "isobar" ($\frac{3}{2}$, $\frac{3}{2}$). Such facts are the mean multiplicity of π and K mesons in pp annihilations, mean multiplicity of strange particles in meson-nucleon collisions, and angular correlations between π-mesons in π^-p interactions at an energy of 1.0 Bev.

A Variational Principle for the Calculation of a Correction, Quadratic With Respect to the Magnetic Field Intensity, to the Electron Energy in a Molecule, T. K. Rebane, pp. 694–695.

Abstract: A variational principle is formulated for the calculation of the diamagnetic correction to the ground state energy of an electron in a molecule. The method is based on the variation of the gage transformation functions of the vector potential.

Contribution to the Theory of Absorption of Ultrasound in Metals, V. P. Silin, pp. 703–707.

Abstract: The absorption of sound is considered in the low temperature region, where absorption is due to electrons, and for frequencies sufficiently high so that the acoustic wave length is small in comparison with the mean free path. The anisotropy of Fermi surface is taken into account, as are interactions due to the electromagnetic field and to the variation in electron energy as a result of lattice deformations. The acoustic absorption is determined. In the region of wave lengths close to the thickness of the anomalous skin layer at the acoustic frequency, it is shown that a decrease in the ratio of the absorption coefficient to the frequency should be observed with increasing frequency.

Vol. 11, No. 4, Oct. 1960.

Disintegration of Cosmic-Ray Nuclei by Solar Photons, N. M. Gerasimova and G. T. Zatsepin, pp. 899–904.

Abstract: A calculation is made of the effect of disintegration of cosmic-ray nuclei in the field of solar photons, leading to the production of correlated showers in the atmosphere The energy of the disintegrated nuclei is found to be of the order of 10^{16} ev per nucleon, and their flux of the order of 10^{-4} to 10^{-3} km^{-2} hr^{-1} sr^{-1}. As a result of the divergence of the photonuclear disintegration products before they enter the atmosphere, the distances between the shower cores turn out to be approximately of the order of 1 km.

Renormalization in Parity-Nonconservation Theory, B. L. Ioffe, pp. 911–919.

Abstract: A method is proposed for the renormalization of mass, charge and wave functions in the parity-nonconservation theory. The method is checked in the case in which the "three-Γ approximation" equation is used for the vertex part.

Distribution of the Transverse Momentum of Shower Particles in Jets, É. G. Boos and Zh. S. Takibaev, pp. 920–926.

Abstract: Experimental data are presented on the distribution of the transverse momenta of secondary shower particles in jets produced by cosmic rays. Transverse momentum distributions that follow from various theories and also from various phenomenological descriptions of multiple production of mesons are analyzed and systematized. Comparison with the experiments narrows the possible choice of a scheme for description of the elementary process of multiple meson production.

Contribution to the Theory of Electron Gas Conductivity in a Strong Magnetic Field, V. G. Skobov, pp. 941–945.

Abstract: The conductivity of an electron gas in perpendicular electric and magnetic fields is investigated for $\omega\tau >> 1$ (τ is the electron relaxation time, ω is the cyclotron frequency). Elastic scattering of electrons on fixed short range force centers is considered. Interaction between the electrons and the scatterers is treated without the aid of perturbation theory. In the final result the conductivity is expressed as a function of the magnetic field and the exact amplitude for scattering of a zero energy electron on a single center in the absence of a magnetic field.

Buildup of Electromagnetic Waves in a Plasma Moving in a Nondispersive Dielectric in the Presence of a Constant Magnetic Field, G. G. Getmantsev and V. O. Rapoport, pp. 871–875.

Abstract: We have obtained a dispersion relation that determines the propagation of plane electromagnetic waves in a plasma beam moving in a fixed plasma along the lines of force of a constant and uniform magnetic field. We have found the damping (or buildup) coefficients of the rarefied plasma moving along the magnetic field in a nondispersive dielectric.

Vol. 11, no. 5, Nov. 1960.

Energy Spectra of the Electron-Photon Component in Extensive Atmospheric Showers Near the Shower Axis, O. I. Dovzhenko, S. I. Nikol'skiĭ and I. V. Rakobol'skaya, pp. 981–986.

Abstract: A cloud chamber with lead plates was employed to investigate the electron-photon component of extensive atmospheric showers at sea level. Showers containing on the average 8×10^3, 1.2×10^4 and 3×10^4 particles and passing at distances of 0–3 m from the chamber were selected. Energy spectra of the electron-photon component were derived, and the fraction of high energy electrons and photons at distances of 0–3 m and 0–0.3 m from the shower axis were determined. The lateral distribution of high energy electrons and photons at distances of 0–0.3 m from the axis was also obtained.

Observation of Ion Oscillations in a Plasma, M. D. Gabovich, L. L. Pasechnik and V. G. Yazeva, pp. 1033–1035.

Abstract: Ion oscillations have been observed against the noise background of a discharge plasma (charge density approximately 10^{10} cm^{-3}). The results which have been obtained can be interpreted if it is assumed that the probe selectively detects oscillations characterized by a wave length approximately equal to the radius of the ion sheath which surrounds the probe.

Anisotropy of Surface Tension at the Boundary Between the Superconducting and Normal Phases of Tin, Yu. V. Sharvin and V. F. Gantmakher, pp. 1052–1062.

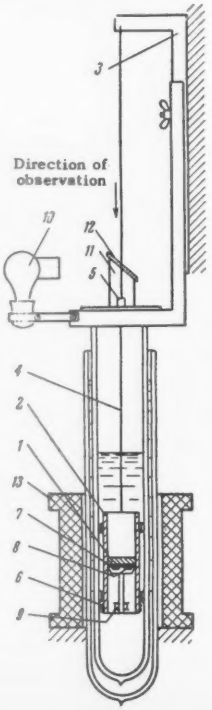

FIG. 1. Diagram of apparatus: 1 – specimen; 2 – lead tube, hung from the stand 3 by two threads 4, passing through the seal 5; 6 – lead resistance thermometer for monitoring the temperature of the tube; 7 – carbon thermometer; 8 – bismuth for measuring the field; 9 – heater; 10 – lamp; 11 – glass tube; 12 – flat window; 13 – solenoid.

Abstract: The anisotropy of surface tension at the boundary between the *s* and *n* phases of tin was investigated by two methods. In the first, the structures of the intermediate state, revealed by using a ferromagnetic powder, were observed in specimens with different crystal orientations. In the second method, the moment of the forces acting on a spherical specimen in a magnetic field was measured. There was agreement between the results obtained by both methods. The form of the dependence of surface tension on the direction of the normal to the phase interface, the absolute order of magnitude of the effect and its temperature dependence were determined.

The Einstein Statics in Conformal Space, V. A. Fock, pp. 1067–1072.

Abstract: A new definition is proposed for a three-dimensional spatial metric that corresponds to a given four-dimensional space-time metric. The space with a metric so defined is called conformal space. It is shown that the equations of the Einstein statics in conformal space are simple in form and lead to definite expressions for the energy density and for the gravitational tensions. Cases of spherical and axial symmetry are considered. It is pointed out that the concept of conformal space can be useful in the general nonstatic case as well.

The Theory of Nuclear Matter, G. M. Vagradov and D. A. Kirzhnits, pp. 1082–1086.

Abstract: A simple method is proposed for quantitative description of the ground state of nuclear matter. It is shown that the gas approximation with a modified nucleon dispersion law can be employed. The error of the method does not exceed that of the empirical quantities.

The Motion of a Piston in a Conducting Medium, R. V. Polovin, pp. 1113–1120.

Abstract: We consider magnetohydrodynamic waves which arise when a piston moves in a perfectly conducting medium in the presence of a magnetic field. If the transverse velocity component of the piston exceeds the velocity of sound in the undisturbed medium, then a magnetic field is generated; in this case, the magnetic pressure becomes comparable with the hydrostatic pressure. At supersonic velocities, a vacuum is formed between the piston and the medium (cavitation). Compared with ordinary hydrodynamics, additional cases of cavitation appear when the piston moves with supersonic velocity in the direction perpendicular to the normal, and also when the piston moves in, if the angle between its velocity vector and the normal to its surface exceeds 70 deg (for an ideal gas with $\gamma = 5/3$). Increase of the piston velocity component perpendicular to the normal decreases the drag. When cavitation occurs, the drag is four times less than in the case of motion of the piston in the direction normal to its surface.

Magnetic Bremsstrahlung of a Confined Plasma, K. N. Stepanov and V. I. Pakhomov, pp. 1126–1129.

Abstract: Magnetic bremsstrahlung of a high temperature plasma located in a strong magnetic field is considered.

The Amount of Accelerated Particles in an Ionized Gas Under Various Accelerating Mechanisms, A. V. Gurevich, pp. 1150–1157.

Abstract: The kinetic equation is solved for a system of particles interacting according to Coulomb-law conditions where the presence of the accelerating mechanism makes the distribution function nonstationary in the high velocity range, i.e., when the accelerating mechanism leads to continuous acceleration of particles whose energy is greater than the injection energy. The value of the particle flux is determined.

Super-Heavy Isotopes of Hydrogen and Helium, V. I. Gol'danskii, pp. 1179–1180.

Instability of an Induction Pinch, I. F. Kvartskhava, K. N. Kervalidze and Yu. S. Gvaladze, pp. 1182–1183.

New Strange Particles, B. Pontecorvo, pp. 1192–1193.

SOVIET PHYSICS-SOLID STATE (Fizika Tverdogo Tela). Published by American Institute of Physics, New York.

Vol. 2, no. 2, Aug. 1960.

Distribution of Losses and the Efficiency of Different Processes in Photoelectric Converters of Solar Energy, V. K. Subashiev, pp. 181–186.

Abstract: Since the appearance of high efficiency silicon photoelements, a number of authors have conducted theoretical and experimental investigations aimed at finding out ways of further improvement of photoelectric converters and at determining their optimum working conditions. The problem cannot, as yet, be regarded as fully solved for the following reasons. The losses in the photoelements are, in the majority of cases, considered qualitatively or only an estimate is given of the possible losses on the basis of the known average parameters of the substance. In all the cited works losses were computed in one operation by some process in which they were referred to the total input energy. It seems to us that in a number of cases the characteristic of each separate process showing the degree of its perfection is of no less interest. Apart from that, examinations made by a number of authors were limited to the case of monochromatic light. Such a situation, to a certain degree, arose from the fact that because of the variety of processes taking place in the photoelement, for a fuller and more definite quantitative analysis of the losses it was necessary to have the data which became known only recently. In this work an attempt is being made to give a fuller analysis of the processes which are essential to the functioning of a photoelectric converter of solar energy from the point of view of quantitative distribution of losses and of the efficiency of individual processes.

Energy Diagram of a Real Silicon Photocell, V. K. Subashiev and É. M. Pedyash, pp. 194–201.

Abstract: A means is described of constructing the energy diagram of a real photocell with its carrier concentration, under equilibrium conditions, utilizing experimental data obtained from measurements on the photocell and on the starting material, and parameters characterizing the particular method of preparation of the photocell. The diagrams of two silicon photocells obtained by diffusion of Sb in p-Si are presented to illustrate the necessity for considering the field and the potential drop in the diffusion layers during analysis of the work of such photocells.

Photosensitivity Spectrum of p-Type Indium Antimonide, D. N. Nasledov, M. P. Pronina and Yu. S. Smetannikova, pp. 219–221.

Introduction: The photosensitivity spectrum of p-type InSb was studied by several workers. Because these investigations were carried out by different people and under different conditions they cannot be used to deduce dependence of photosensitivity of InSb on the acceptor concentration.

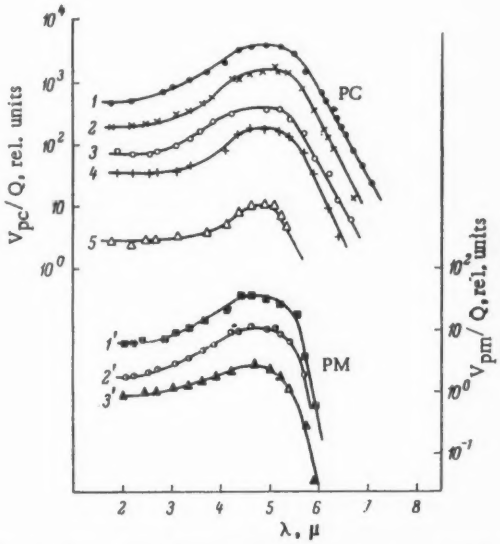

Fig. 1. The response spectra of photoconductivity (PC) and photomagnetic effect (PM) of p-type InSb samples with different acceptor concentrations. 1 and 1') $p = 10^{13}$ cm^{-3}; 2 and 2') $p = 3 \times 10^{13}$ cm^{-3}; 3 and 3') $p = 10^{14}$ cm^{-3}; 4) $p = 5 \times 10^{14}$ cm^{-3}; 5) $p = 2 \times 10^{15}$ cm^{-3}.

The present paper reports measurements of the response spectra of photoconductivity and photomagnetic effect of p-type samples with acceptor concentrations from 10^{13} to 10^{15} cm.$^{-3}$. For this purpose InSb monocrystals, prepared by zone melting, were employed. Dimensions of the samples were $4 \times 1 \times 0.1$ mm^3. Sample surfaces were ground and etched.

Vol. 2, no. 5, Nov. 1960.

Thermal Conductivity of Semiconductor Solid Solutions, A. V. Ioffe and A. F. Ioffe, pp. 719–728.

Introduction: The quality of a thermocouple increases as the value of the ratio of charge carrier mobility to phonon thermal conductivity in the material increases. By noting that the scattering depends on the ratio of the wave length to the dimensions of the scattering defects, and that the electron wave length is larger by orders of magnitude than the wave length of the fundamental phonons, we suggested the use of solid solutions with atomically dispersed scattering centers. The fact is, that when solid solutions of semiconductor materials were used in place of the materials themselves, the thermal conductivity was lowered by a larger amount than the mobility.

It can also be expected that, for a sufficiently high impurity concentration approaching 50%, the phonthermal conductivity decreases to very small values.

This paper is devoted to an examination of the basic rules governing the thermal conductivity of semiconductor solid solutions, based on a very wide range of experimental materials, and especially to the problem of the scattering of phonons by impurities.

Influence of the Electric Field on the Electrical Conductivity, Hall Coefficient and Magnetoresistance of n-Type InSb at Low Temperatures, Lien Chih-ch'ao and D. N. Nasledov, pp. 729–733.

Introduction: It is well known that the increase in electrical conductivity resulting from an increase of electric field may be caused by the current carriers increasing either their mobility or their concentration. Recently, the influence of the electric field on electrical properties of germanium at low temperatures has been investigated. Conwell and others assumed that the increase of σ was connected with the increase of mobility. They reasoned that, at low temperatures, current carriers are scattered principally by ionized impurities, and, since the drift velocity of electrons increases with the increase of the electric field, the probability of scattering should, therefore, decrease, and the mobility increase with an increase of field. At the present time, the experiments of some authors show that the increase of σ is caused by the increase in current carrier concentration. According to their data, the Hall coefficient decreases strongly with an increase of the electric field, and the mobility shows little change. The mechanism of the action of the electric field is considered to consist of impact ionization of neutral impurities by the free electrons.

As yet, the dependence of the electrical properties of n-type InSb on the electric field at liquid helium temperatures has been little investigated. Some authors have observed that, at very weak fields, deviations from Ohm's law begin to take place. Putley assumes that the increase in electrical conductivity is connected with the increase in mobility. In the present work, we have investigated the electric field dependence of the electrical conductivity, Hall coefficient and resistance variations of samples at low temperatures and in the presence of a magnetic field. According to our data, these effects may be interpreted by assuming that electrons in the impurity band are excited into the conduction band under the influence of the applied electric field. Since the effective mass of electrons and the activation energy of donors of n-type InSb are very small, we assume that the action of the electric field causes tunnel passage of electrons, from the impurity band into the conduction band.

The Equation of State of Metals by a Statistical Method, V. P. Trubitsyn, pp. 820–823.

Abstract: On the basis of a modified statistical method, an approximate equation of state is found for metals for pressures from zero to a million atmospheres and $T = 0$ K. In the statistical expression for the energy, the electron density used for the ion core is that found by the Hartree-Fock method, and approximated by an exponential function. An explicit analytical expression is obtained for the dependence of the energy and pressure on the volume for metals. The method is illustrated by the example of magnesium.

The Existence of Entropy for Dynamical Systems, V. Kh. Kozlovskii, pp. 841–846.

Introduction: The proof of the existence of entropy in certain classes of systems of material point moving according to the laws of mechanics has been one of the main problems of the dynamic theory of heat. A large number of papers was devoted to this problem; we shall mention here only the most important ones. In Helmholtz's theory, it was proved that monocyclic systems have an entropy. In the papers of Boltzmann, Loschmidt and Clausius, the existence of entropy for large molecular aggregates was proved, but these proofs were based on particular model representations, so that they should be considered as physical proofs, not mechanical proofs. In our opinion, the most thorough proofs were those of Szily, Mikhel'son and Clausius, which were carried out from a consistent mechanical point of view; however, the discussions were not complete enough to permit the formulation of the conditions dynamical systems must satisfy in order to have an entropy.

The present paper is concerned with a further examination of the problem in question; from this examination the limitations which must be imposed on dynamical systems will emerge very clearly.

Vol. 2, no. 6, Dec. 1960.

The Calculated and Empirical Values of the Lifetime of Metals and Alloys Under a Load, B. Ya. Pines and A. F. Sirenko, pp. 942–949.

Abstract: The empirical data on the lifetimes of Sn, Pb, Al, Pt, Ag and Cu under load were compared with the values calculated using Eq. 1 and good agreement was obtained. It was found that Eq. 1 was not valid for alloys unless the pre-exponential multiplier was modified.

The Question of the Scattering of Energy in Matter, V. T. Troshchenko, pp. 958–967.

Summary:

1 On the basis of the assumption that the scattering of energy in a vibrating material is caused basically by microplastic deformation, and taking account of the inhomogeneity of the stress distribution in grains by the method of mathematical statistics, an analytical expression for the energy scattered per unit volume of the material in one vibration cycle is found. The relation thus found agrees well with the hypothesis proposed by Davidenko.

2 It is shown that the energy scattered in the material in one cycle depends very essentially on the properties and structure of the material, the dimensions of the sample, the form of the stress state, and so on. A procedure is noted by which one may take account of some of these factors.

3 On the basis of the results obtained the relations for the relative cyclical viscosity for different forms of the stressed state are found, which relations agree well with experimental data.

Technical Notes

Surface Temperatures of High Speed, Radiation Cooled Bodies in Dissociating Atmospheres[1]

DANIEL E. ROSNER[2]

AeroChem Research Laboratories Inc., Princeton, N. J.

THE surface temperature of an object traveling at high speed through a planetary atmosphere will seek a value at which the rate of heat input by convective processes exactly balances that lost by thermal radiation (1,2).[3] When the gaseous medium through which the object moves undergoes thermochemical change (e.g., dissociation-recombination, or ionization-recombination) this causes the surface temperature to depart from that expected for the aerodynamically equivalent motion through a chemically "inert" atmosphere (3). The magnitude of this departure is briefly examined here for the case of molecular dissociation-atom recombination reactions under the assumption of no surface melting or vaporization. In particular, for continuum flow we ask: Under what conditions can the steady-state surface temperature *exceed* (4) that attained in an inert environment at the same velocity and density in the presence of radiation energy loss from the solid surface?

Simple Approximate Treatment

Let $\dot{q}_\epsilon = \epsilon\sigma T_w^4$ denote the energy flux due to radiation loss from an element of the body surface. The input heat flux due to boundary layer convective processes may be written $\dot{q}_\lambda + \dot{q}_D$ where the first term, $\dot{q}_\lambda$, represents the contribution due to ordinary heat conduction (convection), including the effects of viscous dissipation of kinetic energy, and the term $\dot{q}_D$ represents the contribution due to thermochemical changes within the gas phase boundary layer and at the gas/solid interface (5). When all of the chemical reaction occurs at the gas/solid interface each of these contributions may be expressed in terms of its respective nondimensional transfer coefficient and driving force (5), as follows

$$\dot{q}_\lambda = \mathrm{St}_\lambda G\bar{c}_p(T_r - T_w) \qquad [1]$$

$$\dot{q}_D = \mathrm{St}_D G(\alpha_e - \alpha_w)Q \qquad [2]$$

where the symbols are defined in the nomenclature. In what follows, the gas-dynamic recovery temperature T_r will be approximated by the stagnation temperature $T_e + (1/2)u_e^2/\bar{c}_p$, and for the present, the binary gas phase boundary layer will be considered to be chemically frozen, i.e., compositional changes within the layer are assumed to be induced by surface catalyzed reactions alone (6).

The steady-state surface temperature satisfies the basic heat balance equation $\dot{q}_\epsilon = \dot{q}_\lambda + \dot{q}_D$. Before proceeding it is convenient to introduce the following notation

$$T^0 \equiv T_e + (1/2)u_e^2/\bar{c}_p + \alpha_e Q/\bar{c}_p \qquad [3a]$$

$$r_D \equiv \mathrm{St}_D/\mathrm{St}_\lambda \cong (\mathrm{Le}_f)^{2/3} \qquad [3b]$$

$$\phi \equiv (\alpha_e - \alpha_w)/\alpha_e \qquad [3c]$$

$$\theta \equiv T_w/T^0 \qquad [3d]$$

$$Q_* \equiv 1 + [r_D\phi - 1]\frac{\alpha_e Q}{\bar{c}_p T^0} \qquad [3e]$$

$$\mathfrak{R} \equiv \epsilon\alpha(T^0)^3/(\mathrm{St}_\lambda G\bar{c}_p) \qquad [3f]$$

The basic heat balance equation then assumes the nondimensional form

$$\mathfrak{R}\theta^4 + \theta - \theta_* = 0 \qquad [4]$$

In the "inert" case (subscript I) the steady-state value θ_I of θ would satisfy the quartic equation

$$\mathfrak{R}\theta_I^4 + \theta_I - 1 = 0 \qquad [5]$$

since the temperature T^0 would apply equally well to both cases (by energy conservation, if the chemically frozen specific heat $\bar{c}_p$ is not appreciably changed). Eqs. 4 and 5 can be reduced to the same form by noting that the reduced temperature $\tau \equiv \theta/\theta_*$ satisfies the same equation as θ_I if $\mathfrak{R}$ is replaced by $\theta_*^3\mathfrak{R}$.

Discussion

From Eqs. 4 and 5 it can be seen that the condition $\theta > 1$ is both necessary and sufficient for a temperature "overshoot," i.e., $\theta > \theta_I$. Moreover it can be shown that if the discriminant θ_* were a constant then the extent of this overshoot could not exceed that achieved in the *absence* of radiation loss. In actual fact, however, θ_* will itself be a function of the dimensionless surface temperature θ and hence, implicitly, a function of the convection-radiation parameter $\mathfrak{R}$. Qualitatively speaking, the nature of this dependence usually makes an overshoot impossible when $\mathfrak{R} = 0$ but possible for large values of $\mathfrak{R}$, provided the surface is an active catalyst for atom recombination *and* the ratio of diffusivities Le_f exceeds unity.

This can be seen as follows. In the absence of gas phase chemical reaction the rate of convective diffusion of atoms to the gas/solid interface must be identically equal to the interfacial rate of recombination. Using the reversible chemical rate law discussed in (7) this can be written

$$\mathrm{St}_D G(\alpha_e - \alpha_w) = k_w\rho_w\left\{\alpha_w - \alpha_{eq}(\theta)\left[\frac{1 + \alpha_w}{1 + \alpha_{eq}(\theta)}\right]\right\} \qquad [6]$$

where k_w is related to the recombination probability γ and atomic mass m_1 by $k_w = [kT_w/(2\pi m_1)]^{1/2}\gamma$. Defining a dimensionless catalytic parameter $\mathfrak{C} \equiv k_w\rho_w/(\mathrm{St}_D G)$ and solving for the extent of recombination $\phi \equiv (\alpha_e - \alpha_w)/\alpha_e$

[1] This research was supported by the U. S. Air Force through AFOSR and ARDC under contract no. AF 49(638)-300.

[2] Research scientist. Member ARS.

[3] Numbers in parentheses indicate references at end of paper.

EDITOR'S NOTE: The Technical Notes and Technical Comments sections of ARS JOURNAL are open to short manuscripts describing new developments or offering comments on papers previously published. Such manuscripts are usually published without editorial review within a few months of the date of receipt. Requirements as to style are the same as for regular contributions (see masthead page).

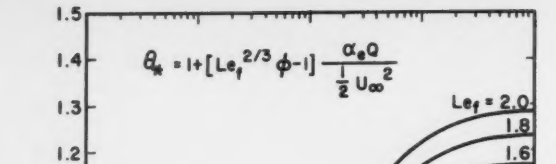

Fig. 1 The discriminant θ_* (see Eq. 3e) as a function of the catalytic parameter $\mathcal{C}$ for strongly cooled surfaces $[\alpha_{eq}(T_w) \ll \alpha_e]$ in the forward stagnation region; $\alpha_e Q/(\frac{1}{2}U_\infty^2) = 0.5$, $\frac{1}{2}U_\infty^2 \gg \bar{c}_p T_\infty$.

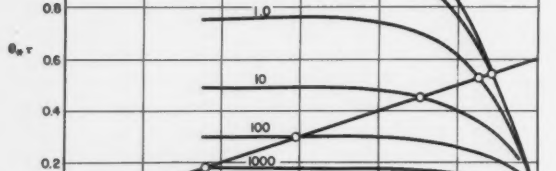

Fig. 2 Graphical solution for the steady-state surface temperature in equilibrium hydrogen; $p_e = 0.1$ atm, $T_e = 3000$ K, $u_e = 0$

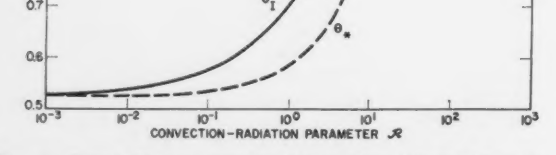

Fig. 3 Comparison of steady-state surface temperatures in dissociating and inert atmospheres as a function of the convection-radiation parameter $\mathcal{R}$; hydrogen, $p_e = 0.1$ atm, $T_e = 3000$ K, $u_e = 0$

we find

$$\phi = \frac{\mathcal{C}}{1 + \mathcal{C} + \alpha_{eq}(\theta)} \cdot \left[1 - \frac{\alpha_{eq}(\theta)}{\alpha_e}\right] \qquad [7]$$

where $\mathcal{C}$ will often be a relatively weak function of the surface temperature T_w and hence of θ, but α_{eq} will be a strong function of θ (when α_{eq} is neither small compared to unity nor very close to unity). As the surface temperature decreases with increased radiation loss it is seen that $\alpha_{eq}(\theta)$ will eventually become negligible with respect to α_e and *ipso facto* negligible with respect to unity. In this extreme we have the familiar result (4,8,9) for the extent of recombination

$$\phi \to \frac{\mathcal{C}}{1 + \mathcal{C}} \qquad [8]$$

On the other hand, if we consider the stagnation region with the atom concentration α_e at the outer edge of the boundary layer in equilibrium at the local temperature T_e, it is apparent from Eq. 7 that ϕ will vanish when $T_w = T_e$ regardless of the magnitude of the catalytic parameter $\mathcal{C}$ since in this case $\alpha_{eq}(T_w) = \alpha_e$. Thus we have a realistic situation for which, in the absence of radiation loss, there could be no temperature "overshoot" even for a "perfect" catalyst. Combining these observations, it may be said that a temperature overshoot can occur for the motion of an active catalyst ($\mathcal{C} \gg 1$) through an initially undissociated atmosphere only if the average Lewis-Semenov number Le_f for atom diffusion is greater than unity and the radiation loss is sufficient to cool the surface to the extent that the equilibrium degree of dissociation α_{eq} corresponding to the steady state surface temperature is small compared to the atom concentration α_e established at the outer edge of the boundary layer. In this extreme the behavior of the discriminant θ_* with $\mathcal{C}$ will be as shown in Fig. 1, where we have assumed $\alpha_e Q/[(1/2)U_\infty^2] = 0.5$ and $(1/2)U_\infty^2 \gg \bar{c}_p T_\infty$ for purposes of illustration. In general the dependence of θ_* and hence θ on $\mathcal{R}$ for any given set of conditions can be obtained from a graphical or numerical solution of Eq. 4. A general procedure for carrying this out is illustrated below for the opposite extreme of gas phase reassociation of atoms at equilibrium within the boundary layer.

Local Thermochemical Equilibrium

If one considers surface temperatures achieved in the forward stagnation region the foregoing analysis (through Eq. 5) should be approximately correct when the atom recombination alternatively occurs at quasi-equilibrium within the gas phase boundary layer (5,10). In this case the catalytic activity of the body surface will play a very minor role but, again, the extent of recombination ϕ will depart from zero only if the surface temperature departs from T_e, i.e., only in the presence of finite radiation loss. Here a knowledge of the equilibrium thermodynamic and transport properties of the reacting binary mixture alone enables the approximate determination of the steady state surface temperature $\theta(\mathcal{R})$ in accord with Eq. 4. This may be accomplished graphically as shown in Fig. 2. First $\theta_* \tau(\theta_*{}^3\mathcal{R})$ is plotted against θ itself for several values of the convection-radiation parameter $\mathcal{R}$. Where these curves intersect the straight line whose ordinates are everywhere equal to θ the equation $\theta = \theta_* \tau(\theta_*{}^3\mathcal{R})$ is satisfied and the corresponding values of $\theta(\mathcal{R})$ can be read off the abscissa. This particular example was drawn for equilibrium hydrogen (11) at the following conditions: stagnation pressure = 0.1 atm, $T_e = 3000$ K (stagnation enthalpy = 27.8 kcal/gm). The resulting $\theta(\mathcal{R})$ values can then be compared to the corresponding "inert" values $\theta_I(\mathcal{R})$ as determined from Eq. 5. Fig. 3 shows this comparison in the form of the ratio θ/θ_I as a function of the convection-radiation parameter $\mathcal{R}$. In this particular case it is noted that the surface temperature is significantly lower than that pertaining to an inert atmosphere except at large values of the convection-radiation parameter $\mathcal{R}$. For

values of $\mathcal{R}$ in excess of about 20, the nondimensional surface temperature θ *exceeds* θ_I, however, the maximum "overshoot" in this example is only about 3 %. Within the framework of the approximations it is clear from Eq. 7 that results for the case of local thermochemical equilibrium apply equally well to the chemically frozen case if the catalytic parameter $\mathcal{C}$ is very large compared to unity.

By comparing Eqs. 4 and 5 it has already been noted that, in general, $\theta \gtrless \theta_I$ according as $\theta_* \gtrless 1$. Thus, so long as the quantity $r_D\phi - 1$ is negative, the surface temperature will be *less* than that corresponding to aerodynamically similar motion through an inert atmosphere. For the equilibrium case this is certainly true in the limit of no radiation loss ($\mathcal{R} \to 0$) since $\phi \to 0$. In the other extreme ($\mathcal{R} \to \infty$) the extent of recombination ϕ approaches unity so that the actual surface temperatures can *exceed* those in an inert atmosphere if the average Lewis-Semenov number for atom diffusion through the mixture is greater than unity.

Conclusions

On the basis of this brief examination of radiation cooled surface temperatures it is concluded that operating surface temperatures in an initially undissociated environment can *exceed* those encountered in an inert environment at the same stagnation enthalpy but only if the average Lewis-Semenov number Le_f exceeds unity. This condition is, however, not sufficient. A temperature overshoot is found to be possible both for (a) catalytically active radiation cooled solids in the chemically frozen (nonequilibrium) boundary layer regime, and (b) radiation cooled solids of arbitrary activity in the local thermochemical equilibrium boundary layer regime only if, in addition, the nondimensional convection-radiation parameter $\mathcal{R}$ is sufficiently large to cause the equilibrium atom concentration corresponding to the interface temperature to be negligible compared to the atom concentration at the outer edge of the boundary layer. Thus the temperature "overshoot" phenomenon should be considered the exception rather than the rule. If noncatalytic, high temperature coatings are available, and the boundary layers are in practice (12,13) chemically frozen, then operating surface temperatures of radiation cooled vehicles can be considerably lower than would be encountered in an inert atmosphere for all values of the convection-radiation parameter.

Acknowledgment

It is a pleasure to thank Mr. F. Kuehner for his assistance in the computation of the transport and thermodynamic properties of partially dissociated hydrogen (11) and constructing graphical solutions to Eq. 4.

Nomenclature

$\bar{c}_p$ = chemically frozen specific heat, assumed constant
$\mathcal{C}$ = nondimensional catalytic parameter
D = atom-molecule binary diffusion coefficient
G = mass velocity $\rho_e u_e$ at the outer edge of the boundary layer
k_w = interfacial reaction rate constant (velocity)
k = Boltzmann constant
Le_f = Lewis-Semenov number = $D/[\lambda_f/(\rho\bar{c}_p)]$
m_1 = atomic mass
Pr_D = Prandtl number for diffusion (Schmidt number) = $(\mu/\rho)/D$
Pr_λ = Prandtl number for heat conduction = $(\mu/\rho)/[\lambda_f/(\rho\bar{c}_p)]$
$\dot{q}$ = heat flux at gas/solid interface
Q = heat of the recombination reaction (assumed constant)
$\mathcal{R}$ = dimensionless convection-radiation parameter (see Eq. 3f)
r_D = recovery factor for chemical energy $\equiv St_D/St_\lambda$
St = Stanton number (nondimensional transfer coefficient)
T = absolute temperature
T^0 = "total" temperature (defined by Eq. 3a)
u = local gas velocity parallel to element of surface
U_∞ = velocity of object with respect to the undisturbed medium
α = mass fraction of atoms in the mixture
β = inviscid velocity gradient at the nose of the body (see Fig. 1)
γ = recombination probability (coefficient)
ϵ = total hemispheric emissivity
θ = nondimensional surface temperature (see Eq. 3d)
θ_* = discriminant defined by Eq. 3e
λ_f = chemically frozen thermal conductivity of the gas mixture
μ = absolute viscosity of the gas mixture
ρ = mass density of the gas mixture
σ = Stefan-Boltzmann radiation constant
τ = reduced surface temperature variable θ/θ_*
ϕ = extent of recombination (see Eq. 3c) (fraction recombined)

Subscripts

D = pertaining to concentration (Fick) diffusion
e = at outer edge of the boundary layer
eq = pertaining to the condition of thermochemical equilibrium
f = chemically frozen
I = inert
r = recovery (adiabatic wall) in absence of chemical reaction
w = at the wall (gas/solid interface)
ϵ = pertaining to radiation
λ = pertaining to heat conduction
∞ = at upstream infinity

References

1 Lighthill, M. J., "Contributions to the Theory of Heat Transfer Through a Laminar Boundary Layer," *Proc. Roy. Soc. (London)*, vol. A202, 1950, p. 359.

2 Rosner, D. E., "Theory of Radiation Cooling at High Mach Numbers," AeroChem Research Laboratories TM-18, November 1959.

3 Rosner, D. E., "Steady State Surface Temperatures of Radiation Cooled Bodies in Dissociating Atmospheres," AeroChem Research Laboratories, TP-26, Feb. 1961.

4 Rosner, D. E., "Steady State Surface Temperatures in Dissociated High Speed Gas Flows," *J. Aero/Space Sci.*, vol. 26, 1959, p. 384.

5 Rosner, D. E., "Convective Heat Transfer With Chemical Reaction-I.Theoretical Development of Correlation Formulae for the Prediction of Heat Fluxes in High Performance Rocket Motors and Related Systems," AeroChem Research Laboratories TP-22, Jan. 1961 (to appear as WADC Report).

6 Rosner, D. E., "Diffusion and Chemical Surface Catalysis in Flow Systems," AeroChem Research Laboratories TP-14, AFOSR TN-60-887. Sept. 1959.

7 Rosner, D. E., "Boundary Conditions for the Flow of a Multi-component Gas" JET PROPULSION, vol. 28, 1958, pp. 555–556.

8 Goulard, R. J., "On Catalytic Recombination Rates in Hypersonic Stagnation Heat Transfer," JET PROPULSION, vol. 28, 1958, pp. 737–745.

9 Rosner, D. E., "Similitude Treatment of Hypersonic Stagnation Heat Transfer," ARS JOURNAL, vol. 29, 1959, pp. 215–216.

10 Rosner, D. E., "Effects of Diffusion and Chemical Reaction on Convective Heat Transfer," ARS JOURNAL, vol. 30, 1960, pp. 114–115.

11 Rosner, D. E., "Properties of Equilibrium Dissociating Hydrogen for Predicting Convective Heating in Nuclear-Thermal Rockets," AeroChem Research Laboratories TP-27, February 1961.

12 Goodwin, G., and Chung, P. M., "Effects of Non-equilibrium Flows on Aerodynamic Heating During Entry into the Earth's Atmosphere from Parabolic Orbits," Second International Congress of the Aeronautical Sciences, Zurich, Switzerland, Sept. 1960.

13 Whalen, R. J., "Viscous and Inviscid Non-equilibrium Gas Flows," IAS Paper No. 61-23, 29th Annual Meeting, Jan. 23–25, 1961.

Satellite Life Duration[1]

THOMAS L. VINCENT[2]

University of Arizona, Tucson, Ariz.

Received Nov. 14, 1960.

[1] This paper is based on a thesis presented by the author at Oregon State College, January 1960, in partial fulfillment of the requirement for the degree of Master of Science.

[2] Instructor, Department of Mechanical Engineering, College of Engineering. Student Member ARS.

Satellites orbiting near Earth are influenced by atmospheric drag. After a sufficiently long time, the drag dissipates the total energy initially possessed by the satel-

lite, thereby forcing the vehicle to return to Earth. The orbital decay time is determined by solving the general equation of motion using certain simplifying assumptions. The total life duration for initially elliptical orbits with eccentricities less than 0.2 and perigee heights up to 600 miles is presented in graphical form. The accuracy of the solution is estimated by comparing predicted and actual lifetimes of several recent Earth satellites.

IN THE past few years, a number of papers have been written on the subject of satellite lifetime. For example, Petersen (1)[2] calculated the lifetime for satellites in elliptical orbits. Henry (2) has calculated the total number of revolutions a satellite would make before returning to Earth. Both of these papers, and others concerned with satellite life duration, have made approximations that enabled them to obtain expressions for the lifetime of a satellite. The most important of these approximations are that the satellite experiences drag retardation only in the vicinity of perigee and that the drag coefficient for the satellite remains at a constant value 2.

It is the purpose of this paper to obtain a solution for lifetime directly from the equations of motion using these approximations, and then to compare the results with actual lifetimes of some recent satellites. The assumed atmospheric density variation used in the analysis is composed of three regions, as shown in Fig. 1. The upper and lower regions are expressed analytically by the barometric formula, and between these regions densities inferred from satellite motion are used (3).

The motion of an Earth satellite may be described using Newton's Second Law of Motion.

$$\Sigma \bar{F} = m\ddot{\bar{R}} \qquad (R = r\bar{R}_1) \qquad [1]$$

[2] Numbers in parentheses indicate References at end of paper.

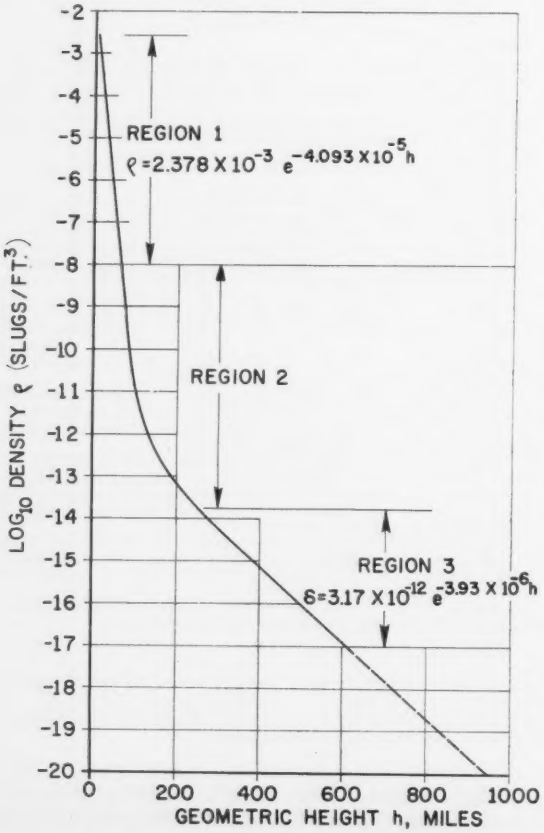

Fig. 1 Earth's atmospheric density variation

Two forces are assumed to act on the satellite: the atmospheric drag force and Earth's gravitational force as given by Newton's Law of Gravitation. The drag force is given by the relation $\rho A v^2$. (This is obtained by assuming thermal velocity negligible and free molecule flow with 100% diffused reflection.)

Eq. 1 is rewritten as

$$\ddot{\bar{R}} = -\frac{KM}{r^2}\bar{R}_1 - \rho\frac{A}{m}v^2\bar{T} \qquad [2]$$

The total lifetime of a satellite in an elliptical orbit is assumed to be composed of two distinct time intervals. The first time interval is obtained from Eq. 2 by assuming that the perigee altitude remains fixed while the apogee altitude decreases, due to drag, until a circular orbit is obtained. The second time interval is obtained from Eq. 2 by assuming that the satellite spirals in from its circular orbit until motion is terminated by the ground.

Elliptical Decay

If there were no atmosphere, the last term in Eq. 2 could be set equal to zero. The equation would then reduce to the well-known expression for particle motion under an inverse square force of attraction

$$\ddot{\bar{R}} = -\frac{KM}{r^2}R_1 \qquad [3]$$

From this equation, the following expressions can be obtained

$$r = \frac{b^2/KM}{1 + \epsilon\cos\theta} = \frac{a(1-\epsilon^2)}{1+\epsilon\cos\theta} \qquad [4]$$

$$\frac{1}{2}mv^2 - \frac{KMm}{r} = -\frac{KMm}{2a} \qquad [5]$$

$$\frac{1}{2}mv_p^2 - \frac{KMm}{r_p} = -\frac{KMm}{2a} \qquad [6]$$

$$r^2\frac{d\theta}{dt} = b \qquad [7]$$

$$P = \frac{2\pi a^{3/2}}{\sqrt{KM}} \qquad [8]$$

Eqs. 4 to 8 will approximate the actual motion predicted by Eq. 2 for one or two revolutions. The drag term becomes important when long time periods are involved.

The change in velocity at perigee due to drag during one revolution can be determined. This is accomplished by using dot product multiplication with the unit tangent vector on Eq. 2, and then dropping from the resulting equation the term which describes the periodic variation in acceleration as the satellite moves in orbit

$$\frac{dv}{dt} = -\rho v^2\frac{A}{m} \qquad [9]$$

Eqs. 4, 5 and 7, together with the expression for density given by $\rho = \rho_0 e^{-\beta h}$ (region 3, $\beta = 3.93 \times 10^{-6}$), are substituted into Eq. 9, and $\cos\theta$ is expanded by using $\cos\theta = 1 - \theta^2/2$. (This is a small angle assumption, which is justifiable since density varies very rapidly with altitude and the greatest change in velocity will occur near perigee.) After rearranging and dropping terms of order higher than θ^2, an expression for dv is obtained in which the terms b, ϵ, a, and θ appear. For one revolution b, ϵ, and a may be assumed to be constant and the expression can be integrated with respect to θ. Negligible error is introduced if integration is carried out between the limits $-\infty$ and $+\infty$ instead of the "small" values of θ. Neglecting higher order terms in the expansion of $\cos\theta$ eliminates any periodicity in θ. Integration gives the following result

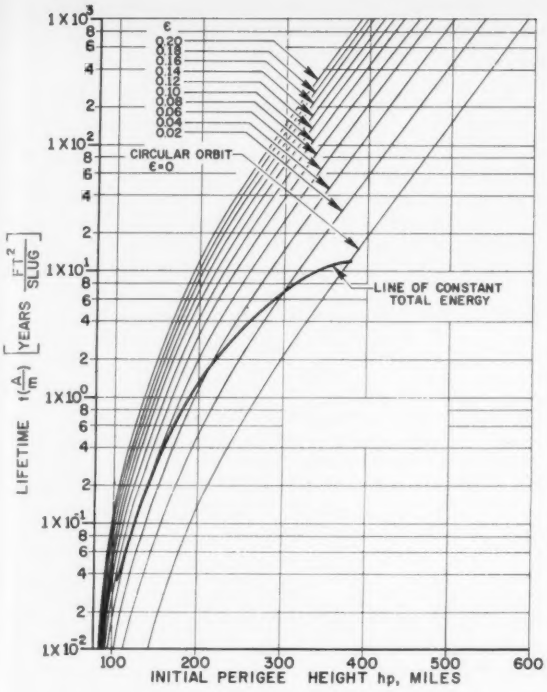

Fig. 2 Total artificial Earth satellite life duration

$$(\Delta v)_p = -\rho_p r_p \frac{A}{m} \frac{2KM}{b} \left(1 - \frac{r_p}{2a}\right) \sqrt{\frac{2\pi(1+\epsilon)}{\beta r_p \epsilon}} \quad [10]$$

Eq. 6 is used to relate the change in perigee velocity to the semimajor axis

$$dv_p = \frac{\sqrt{KMr_p}}{\sqrt{8a^4}\sqrt{1 - r_p/2a}}\, da \quad [11]$$

If the incremental velocity change at perigee due to drag per period of revolution is set equal to the time rate of change of velocity at perigee, the resulting expression may be solved for elliptical decay time.

$$\frac{(\Delta v)_p}{P} = \frac{dv_p}{dt} \quad [12]$$

Substituting Eqs. 8, 10 and 11 for P, $(\Delta v)_p$ and dv_p, and then integrating with respect to a gives

$$t = \frac{\sqrt{\pi\beta r_p}}{4\rho_p (A/m)\sqrt{KM}} \left\{ 1.086 \sqrt{r_p} \left(\sqrt{\frac{\epsilon}{1-\epsilon}} - \tan^{-1} \sqrt{\frac{\epsilon}{1-\epsilon}} \right) + \sqrt{\epsilon^3 \frac{r_p}{1-\epsilon}} \left[0.902 + 0.311(1-\epsilon) + 0.123(1-\epsilon)^2 + 0.038(1-\epsilon)^3 + \ldots \right] \right\} \quad [13]$$

Eq. 13 expresses the time required for a satellite to decay from an initially established elliptical orbit of eccentricity ϵ and perigee distance r_p to circular orbit of radius r_p.

Spiral Decay

The radius of curvature of the flight path for the near circular orbit is given approximately by

$$\delta = r/\sin\phi \quad [14]$$

Combining this equation with the scalar equations obtained from Eq. 2 by first dot product multiplication with the unit normal vector and then multiplication with the unit tangent vector and then integrating gives

$$t = \frac{2(\sqrt{r} - \sqrt{r_1})}{\sqrt{KM}\,(A/m)\bar{\rho}} \quad [15]$$

where $r - r_1$ represents a small increment in height. The density is taken as an average over this height interval. The total time spent in the circular orbit is obtained by summing up the time spent in each segment $(r - r_1)$ starting with r_p.

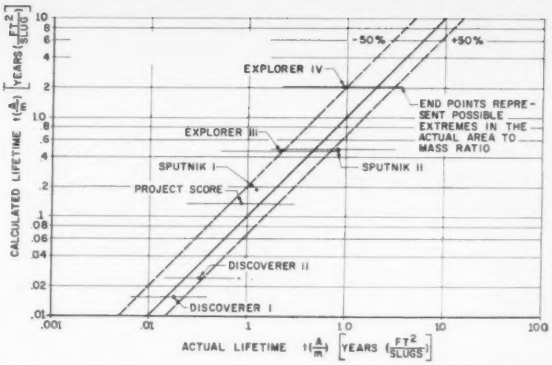

Fig. 3 Accuracy curves for several Earth satellites

Satellite Lifetime

The total lifetime is the sum of the solutions of Eqs. 13 and 15. These equations were used to compute the ordinates of Fig. 2. The lifetime in years is evaluated by dividing the ordinate value as read from the figure by the area to mass ratio (A/m). The overall accuracy of these curves is estimated by comparing actual lifetimes for several Earth satellites with their measured lifetimes (Fig. 3). An average value of (A/m) was used for each satellite. For the seven satellites illustrated, the lifetime predictions are on the average 5% low with a maximum deviation amounting to ±50% of lifetime.

Nomenclature

a = semimajor axis
A = satellite area projected to free stream
b = a constant
g = local acceleration of gravity
h = height measured from Earth's surface
K = universal gravitation constant
m = satellite mass
M = mass of Earth
P = period of revolution
r = magnitude of radius vector from Earth's center to satellite
r_1 = radial distance
r_p = radius to satellite at perigee
$\bar{R}$ = radius vector from Earth's center to satellite
$\bar{R}_1$ = unit vector in direction of $\bar{R}$
t = time
$\bar{T}$ = unit vector tangent to satellite flight path
v = speed of satellite
v_p = speed at perigee

V = velocity of satellite
β = slope of logarithmic density curve
δ = radius of curvature of satellite flight path
ϵ = eccentricity of satellite orbit
θ = angle measured between ray from focus to perigee and focus to satellite
ρ = density of atmosphere
ρ_0 = initial value of density
ρ_p = atmospheric density at perigee
ϕ = included angle between unit radius and unit tangent vector

References

1 Petersen, N. V., "Lifetimes of Satellites in Near-Circular and Elliptic Orbits," JET PROPULSION, vol. 26, 1956, pp. 341–351.
2 Henry, I. G., "Lifetimes of Artificial Satellites of the Earth," JET PROPULSION, vol. 27, 1957, pp. 21–24.
3 Sterne, T. E., "High-Altitude Atmospheric Density," *Phys. Fluids* vol. 1, May-June, 1958, pp. 165–170.

High Energy, Low Thrust Jupiter Missions[1]

ROBERT H. FOX[2]

University of California, Lawrence Radiation Laboratory, Livermore, Calif.

Calculations have been carried out on Jupiter round trip missions using low thrust and high energy coasting orbits. The initial period of acceleration away from Earth's orbit was accomplished using tangential thrust. This was followed by a period of coasting until the proper moment arrived for commencing the orbit matching maneuver. This terminates when the velocity and spatial coordinates of Jupiter's orbit are matched. Best results for the final maneuver were obtained with the thrust vector approximately normal to the velocity vector. It is shown that the round trip Jupiter mission requires only four and a half years with 0.10 kw/kg specific power and 16% payload. The acceleration is about 0.12 cm/sec² Increasing the specific power by a factor of 2 does not materially affect the time. The total power-on time is typically three to four years.

PREVIOUS studies have been made of the relationship among acceleration, specific power, payload fraction and travel time for many interplanetary missions (1,2,3).[3] These utilized tangential thrust and correspond to the high thrust Hohmann transfer orbits. In addition, a complete optimization of the one way Mars mission has been accomplished (4). Since the minimum Jupiter round trip time was six and a half years for tangential thrust, calculations were carried out using higher energy transfer orbits. These transfer orbits necessitate the use of large thrust angles.

In all cases, constant acceleration was assumed. The justification for this is contained in the earlier reports. In this report we consider only the interplanetary part of the voyage. That is, we start in Earth's orbit about the sun and with Earth's velocity. The distance from the Earth itself is assumed to be large enough so that only the sun's gravitational field need be considered. Similar conditions apply upon arriving in Jupiter's orbit. The return trip is assumed to be the "mirror image" of the outgoing trip. The waiting time at Jupiter is chosen so that the return trip terminates in the vicinity of Earth rather than at some other point on Earth's orbit. The outgoing trip is broken up into three phases.

First, during phase 1, we accelerate from Earth's orbital velocity to some coasting velocity. Second, we coast for a precalculated length of time (phase 2). Third, phase 3 is the orbit matching maneuver which terminates when the velocity vector matches that of Jupiter's orbit. For an example, see Fig. 1.

With the high energy coasting orbits we wish to use, it is of course no longer possible to use tangential thrust exclusively. Consider the E-e diagram shown in Fig. 2. The points E_1 and E_2 represent the circular orbits of the two planets. Any transfer trajectory must connect these two points. The heavy lines show the result for high thrust directed tangentially. The Hohmann coasting orbit is indicated. The corresponding low thrust trajectories will traverse regions I, II, III. If phase 3 is carried out using constant acceleration with the thrust directed at constant angle to the velocity vector, the resulting trajectories will lie entirely in regions II or III.

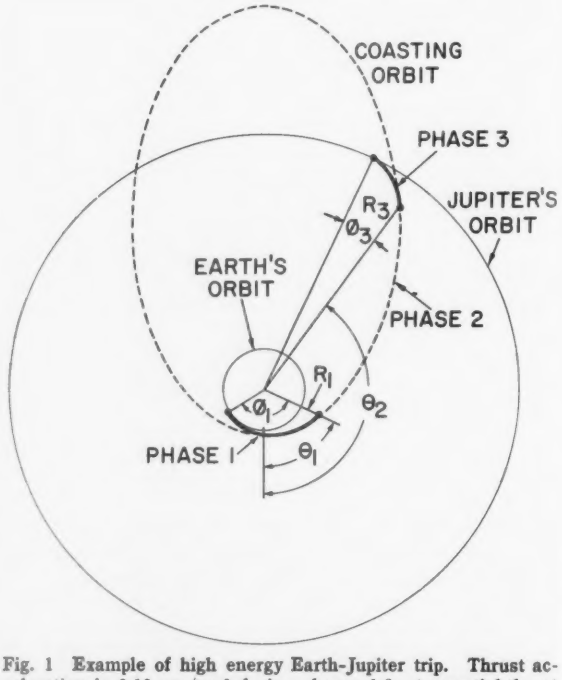

Fig. 1 Example of high energy Earth-Jupiter trip. Thrust acceleration is 0.10 cm/sec² during phases 1,3; tangential thrust for 130 days used for phase 1; phase 2 coasting orbit—A_0 = 5.208 A.U., ϵ_0 = 0.7875, time is 391 days; phase 3 uses perpendicular thrust (ψ = 90 deg) for 145.5 days. Waiting in Jupiter's orbit for 0.52 years permits return to Earth by a symmetrical route

Presented at the ARS Annual Meeting, Washington, D. C., Dec. 5–8, 1960.

[1] This work performed under the auspices of the United States Atomic Energy Commission.

[2] Assistant Division Leader, Reactor Research and Advanced Concepts.

[3] Numbers in parentheses indicate References at end of paper.

For the thrust magnitudes considered, the intersection with the tangential thrust orbits starting from Earth will lie close to the right boundary. Thus, the coasting orbits have high energy (high mean velocity) and high eccentricity (reduced flight path distance).

In order to achieve the coasting energy rapidly, phase 1 is carried out with tangential thrust. This maximizes the instantaneous rate of change of total energy (kinetic energy plus potential energy). At the proper moment, thrust ceases, and phase 2 (coasting) is carried out for the required duration of time. Phase 3 is then initiated with the same acceleration and with the thrust vector arbitrarily kept at a constant angle ψ with respect to the velocity vector. For values of coasting orbit energy between minimum energy (Hohmann) and the energy of Jupiter's orbit we have

region II:

$$0 \leq \psi \leq \pi/2$$

For higher values of coasting energy

region III:

$$\psi \geq \pi/2$$

In the latter case the required tangential thrust component is negative. The same acceleration is used for both powered phases since earlier analyses indicate that this nearly maximizes the payload.

A similar analysis has been given by Rodriguez (5) using the $E - h$ diagram. He considers various types of trajectories and determines the required acceleration to achieve matching conditions. Here the problem was that of determining the trajectories for fixed acceleration with emphasis on reducing the time. For this purpose it is helpful to be able to visualize the size and shape of the coasting orbits easily. E and e give these parameters directly. A more general discussion of the interorbital transfer problem has also been given by Levin (6).

The problem of determining the proper moments for thrust shutdown and startup was determined in the manner described previously (1). For each value of thrust acceleration a tangential thrust problem was run on the computer starting from Earth's orbit about the sun. Initial conditions were as described earlier. Each problem was terminated when escape energy relative to the sun was achieved. The computer output consisted of spatial and time coordinates, velocity components, and the eccentricity and semimajor axis of the osculating orbit. Using the latter two quantities, the locus of the total energy and eccentricity of the osculating orbits was plotted in the $1/A$, ϵ coordinate system (note that $E = -GM/2A$). Similarly, problems using various values of ψ were run starting from Jupiter's orbit and descending toward the sun. These were terminated when the osculating orbit eccentricity became nearly unity. The loci of the osculating orbits were plotted in the same manner and the intersections for phase 1 and phase 3 determined. Fig. 3 shows the results for $a = 0.10$ cm/sec.^{2} The numbers are the values of tan ψ for the descending orbits. For phase 3, outgoing, symmetry conditions show that the loci are the same; only the sign of tan ψ is changed. Each intersection determines A_0, ϵ_0 for the phase 2 coasting orbit. R_1, ϕ_1, R_3, ϕ_3, τ_1 and τ_3 were then obtained from the computer output. θ_1 and θ_2 were calculated from

$$\cos \theta_1 = \frac{A_0}{R_1}\left(\frac{1 - \epsilon_0^2}{\epsilon_0}\right) - \frac{1}{\epsilon_0}$$

$$\cos \theta_2 = \frac{A_0}{R_3}\left(\frac{1 - \epsilon_0^2}{\epsilon_0}\right) - \frac{1}{\epsilon_0} \quad \ldots\ldots\ldots\ldots\ldots\ldots\ldots\ldots\ldots\ldots [1]$$

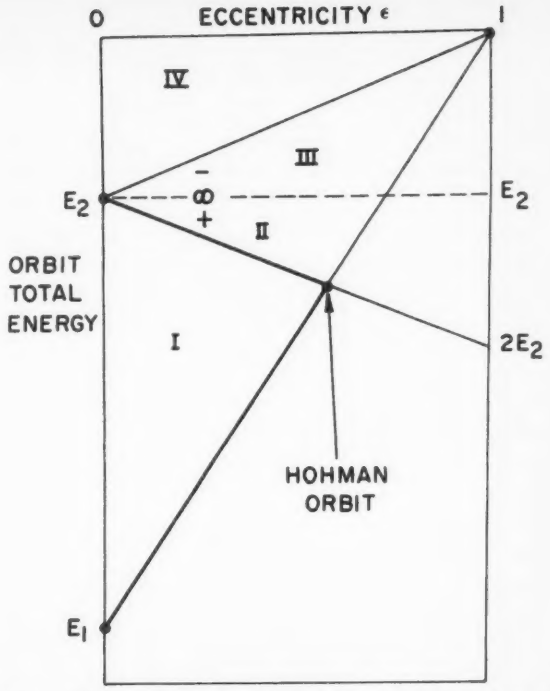

Fig. 2 Energy-eccentricity diagram for osculating orbits of powered trajectories; used for determining elements of the coasting orbit connecting powered trajectories

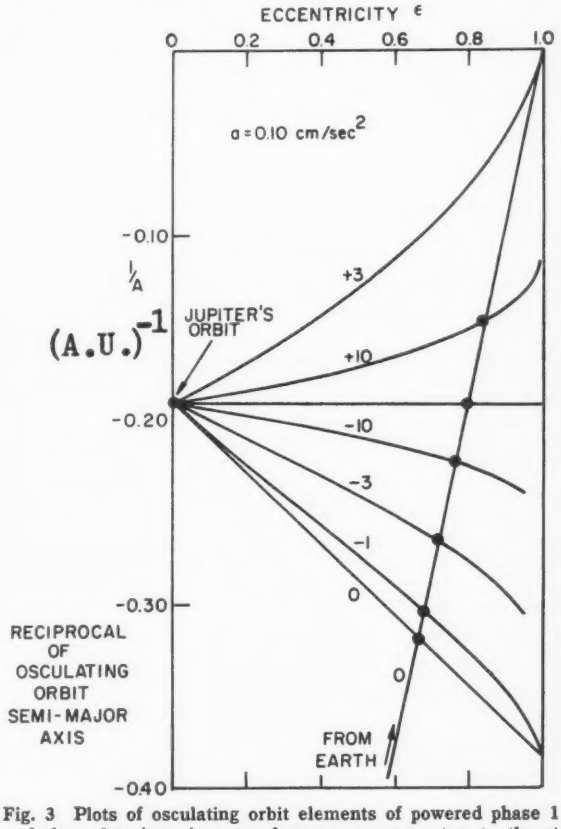

Fig. 3 Plots of osculating orbit elements of powered phase 1 and phase 3 trajectories; numbers on curves are tan ψ; thrust acceleration is 0.10 cm/sec^2 for all curves; ordinate is proportional to total energy of orbit

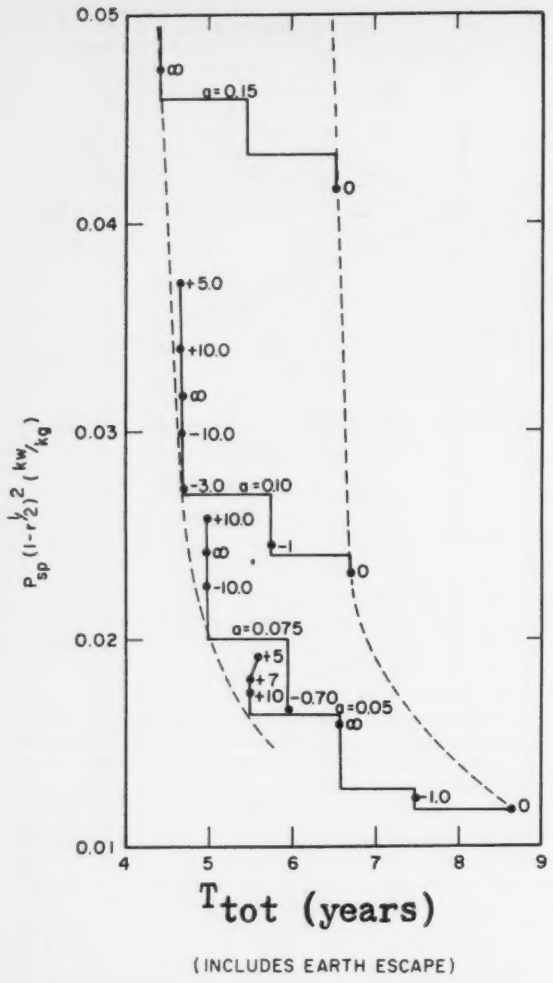

Fig. 4 Relationship among specific power, payload fraction, total mission time and phase 3 thrust angle for Earth-Jupiter missions; numbers give tan ψ

This in turn permitted the calculation of the coasting time T_2 from

$$T_2 = \frac{1}{\sqrt{GM}} A_0^{3/2}\sqrt{1-e_0^2}\left|\frac{-\epsilon_0 \sin\theta}{1+\epsilon_0\cos\theta} + \frac{2}{\sqrt{1-\epsilon_0^2}}\tan^{-1}\left(\frac{1-\epsilon_0^2\tan\theta/2}{1+\epsilon_0}\right)\right|_{\theta_1}^{\theta_2} \quad [2]$$

The transit angle and transit time are determined from

$$\theta_t = \phi_1 + (\theta_2 - \theta_1) + \phi_3$$
$$T_t = \tau_1 + T_2 + \tau_3 \quad \ldots\ldots\ldots\ldots\ldots\ldots\ldots\ldots\ldots\ldots [3]$$

Finally, the required waiting time before starting the return trip is calculated from

$$T_w = T_s(N - n)$$

where

$$n = 2\left(\frac{T_t}{T_E}\right) - \frac{\theta_t}{\pi} \quad [4]$$

and N is an integer satisfying $N \geq n \geq N-1$. T_s and T_E are the length of the synodic year and the period of revolution of Earth.

Physically, n is the number of half revolutions Earth makes *relative* to the space vehicle during its transient. In contrast to Mars and Venus missions where $N = 1$ for reasonable values of acceleration (0.025 cm/sec$^2 \leq a \leq 0.20$ cm/sec^2), here N had values ranging from 2 to 6. Consequently, in plotting round trip time vs. ψ for fixed acceleration, several jumps one synodic year in magnitude occurred. These jumps occur for integral values of n.

It should be pointed out that earlier results of a generalized calculation (7) for low thrust powered trajectories are not directly applicable to the problem solved. From the solution of Perkins' Eqs. 31 and 32 in (7) we could obtain R_1, R_2, τ_1, τ_2, A_0, e_0, θ_1 and θ_2, but we could not obtain ϕ_1 and ϕ_3 without performing, in addition, integrations of the form

$$\phi_1 = \int_0^{T_1} \frac{1}{X}\sqrt{Y^2 - (\dot{X})^2}\, dT \quad [5]$$

(Perkins' notation is used for X, Y and T.) Also, since $aR^2/GM > 10^{-2}$ in all cases considered here, the number of curves and hence computational effort is not reduced. Finally, no results for nontangential thrust have yet been published in that form. In any case, the machine calculations involved for our purposes required only a few minutes.

It has been shown earlier (1) that the quantity aV_c associated with a particular trajectory provides an index of the specific power required for a specified payload fraction. The relationship is

$$P_{sp}(1 - r^{1/3})^2 = aV_c/2 \quad [6]$$

Here, since a is constant

$$V_c = a\sum_i \tau_i$$

τ_i is the time required for the ith phase of powered flight.

In Fig. 4 we show a plot of the left side of Eq. 6 vs. round trip time. Escape from a low altitude orbit about Earth and return to such an orbit is taken into account by adding 1.58×10^6 cm/sec to the calculated V_c and $(1.58 \times 10^6$ cm/sec$)/a$ sec to the calculated T_{tot}. Points with the same value of acceleration are connected to form each curve. The locations of the horizontal discontinuities have been estimated by plotting n vs. V_c. The locus of tangential thrust missions ($\psi = 0$) has been drawn as well as the locus of minimum total time missions using a normal thrust component for phase 3. We see that for similar values of P_{sp}, r the latter program gives approximately a two year reduction in total mission time. For

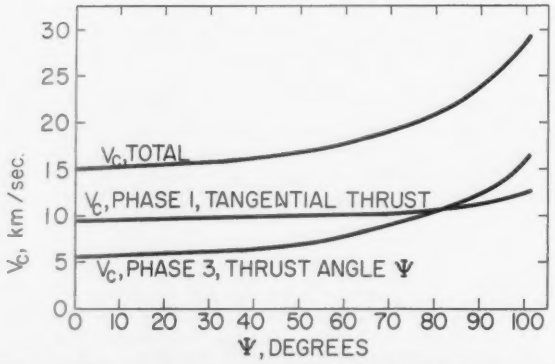

Fig. 5 Effect of phase 3 thrust angle upon both phase 1 and phase 3 characteristic velocity; thrust acceleration is 0.10 cm/sec^2

example, from the figure we find that the entire mission could be carried out in four and one-half years with 16% payload and 0.10 kw/kg specific power ($aV_e/2 = 3.6 \times 10^5$ cm²/sec³). The corresponding approximate values of a, ψ are

$$a \simeq 0.12 \text{ cm/sec}^2$$
$$\psi \simeq 90 \text{ deg}$$

Further increase in specific power did not materially affect the time. Naturally, a price must be paid for the use of higher energy transfer orbits. It takes the form of increased V_e (and hence energy expended) for both phase 1 and 3 with increased ψ. This is shown in Fig. 5 for an acceleration of 0.10 cm/sec². An interesting observation may be made considering the eccentricity of the most desirable coasting orbits. In Fig. 4, these are the orbits on the minimum total time locus. These were the cases giving lowest integral n for each value of acceleration. Over the acceleration range from 0.05 to 0.15 cm/sec², these values of eccentricity were nearly constant at $\epsilon_0 = 0.71 \pm 0.01$.

Now, it has already been shown that a specific power value of approximately 0.10 kw/kg is desired for a manned Mars mission. Apparently it is also adequate for the much more difficult Jupiter mission. The difference, of course, lies in the much greater power-on time of the powerplant in the latter case. For the specific Jupiter mission mentioned, the total powered flight time is 28,600 hr (including Earth escape). Needless to say, this represents a considerable increase in the reliability problem over that associated with Mars missions.

References

1 Fox, R. H., "Ionic Propulsion," *Astro. Sci. Rev.*, vol. 1, no. 3, July–Sept. 1959, pp. 7-12.

2 Moeckel, W. E., "Trajectories with Constant Tangential Thrust in Central Gravitational Fields," NASA Tech. Rep. R-53, 1959.

3 Fox, R. H., "Powered Trajectory Studies for Low Thrust Space Vehicles," ARS JOURNAL, vol. 31, no. 1, Jan. 1961, pp. 28–32.

4 Irving, J. H. and Blum, E. K., "Comparative Performance of Ballistic and Low-Thrust Vehicles for Flight to Mars," *Vistas in Astronautics*, vol. II, Pergamon Press, N. Y., 1959, pp. 191–218.

5 Rodriguez, E., "Method of Determining Steering Programs for Low Thrust Interplanetary Vehicles," ARS JOURNAL, vol. 29, no. 10, Oct. 1959, pp. 783–788.

6 Levin, E., "Low Acceleration Transfer Orbits," Rand Corp. Rep., July 1960, p. 2038.

7 Perkins, F. M., "Flight Mechanics of Low-Thrust Spacecraft," *J. Aero/Space Sci.*, vol. 26, no. 5, May 1959, pp. 291–297.

Maximum Error in Total Emissivity Measurements Due to Non-Grayness of Samples[1]

D. K. EDWARDS[2] and K. E. NELSON[3]

University of California, Los Angeles, Calif.

PRECISE measurements of total emissivity are required for the design of space vehicle temperature-control systems. Materials used on spacecraft exteriors may be designed to have long wavelength spectral selectivity, in order to have a compensating form of temperature control. Such compensation results from the emissivity increasing with increasing temperature. This note shows that accurate total emissivity measurements for such materials cannot be made unless the surrounds, including the detector, are much colder than the sample.

Jakob (1)[4] classifies total emissivity measurement techniques as emitter methods or receiver methods. Both types are susceptible to error due to long wavelength spectral selectivity, but for the sake of brevity only the receiver method will be discussed. The reader may show that the results hold for the emitter method as well.

In the receiver method of total emissivity measurement [for example, see (1–4)], the sample is heated to temperature T_S while the surrounds are maintained at temperature T_0. A detector views the sample and gives an output V_S which is linearly dependent on the radiant flux from the sample [see (2, 3), for example]. Since the detector is part of the surrounds of the sample, the detector, too, should be black and at temperature T_0. These requirements are particularly important when the view factor from the sample to the detector is large or when the sample has particular directional characteristics.

Received May 12, 1961.

[1] This note is based upon a part of a report to the National Science Foundation under Grant G 9505.

[2] Assistant Professor, Department of Engineering.

[3] Assistant Research Engineer, Department of Engineering.

[4] Numbers in parentheses indicate Reference at end of paper.

The radiant flux from the sample to the detector is

$$\int_{A_D} \int_{A_S} I_S \frac{\cos \theta_S \cos \theta_D}{r_{SD}^2} \, dA_S dA_D$$

where

A = area
θ = angle between the line-of-sight r_{SD} and the surface normal
I = intensity in the direction of r_{SD}
S, D = sample and detector, respectively

Since the sample is irradiated by the surrounds, which should be a hohlraum, the sample intensity I_S is

$$I_S = \epsilon_S(T_S)[\sigma T_S^4/\pi] + \rho_S(T_S, T_0)[\sigma T_0^4/\pi] \qquad [1]$$

where

$\epsilon_S(T_S)$ = (by definition) the sample emissivity in the direction of I_S
$\rho_S(T_S, T_0)$ = sample reflectivity for the direction of I_S when irradiated from the surrounds at T_0
σ = Stefan-Boltzmann constant

The detector output is then given by

$$K(V_S - V_0) = \bar{\epsilon}_S(T_S)\sigma T_S^4 + \bar{\rho}_S(T_S, T_0)\sigma T_0^4 - \sigma T_0^4 \qquad [2]$$

where K is a proportionality constant determined by calibration, and the overscore denotes the averaging over the solid angle of the sample viewed from the detector; for example

$$\bar{\epsilon}_S = \frac{\int_{A_D} \int_{A_S} \epsilon_S \frac{\cos \theta_S \cos \theta_D}{r_{SD}^2} \, dA_S dA_D}{\int_{A_D} \int_{A_S} \frac{\cos \theta_S \cos \theta_D}{r_{SD}^2} \, dA_S dA_D} \qquad [3]$$

The detector, of course, must have a response independent of the wavelength and the direction of the intensity of irradiation within Ω.

Only for a nonselective or gray sample is the emissivity $\epsilon_S(T_S)$ equal to the absorptivity $\alpha_S(T_S, T_0)$ where

$$\alpha_S(T_S, T_0) = 1 - \rho_S(T_S, T_0) \qquad [4]$$

Table 1 Error for a non-gray sample

Temp. ratio, T_0/T_S	Emissivity, $\bar{\epsilon}_S$	Discrepancy, $(\bar{\epsilon}_S' - \bar{\epsilon}_S)$	Error, $(\bar{\epsilon}_S' - \bar{\epsilon}_S)/\bar{\epsilon}_S$, %
0.6	0.41	0.046	11
0.7	0.36	0.072	20
0.8	0.32	0.096	30
0.9	0.28	0.129	46
1.0	0.25	0.165	66

The total absorptivity is defined in terms of the monochromatic absorptivity as

$$\alpha_S(T_S, T_0) = (1/\sigma T_0^4) \int_0^\infty \alpha_\lambda(T_S) E_{b\lambda}(T_0) d\lambda \qquad [5]$$

and from Kirchoff's law

$$\epsilon_S(T_S) = (1/\sigma T_S^4) \int_0^\infty \alpha_\lambda(T_S) E_{b\lambda}(T_S) d\lambda \qquad [6]$$

where $E_{b\lambda}$ is the Planck black body monochromatic emissive power at wave-length λ. For convenience we define $\Delta\alpha$ by the relation

$$\alpha_S(T_S, T_0) = \epsilon_S(T_S) + \Delta\alpha_S(T_S, T_0) \qquad [7]$$

The apparent emittance $\bar{\epsilon}'_S$ is obtained from Eq. 2 under the assumption that $\Delta\bar{\alpha}_S$ is zero.

$$\bar{\epsilon}'_S = K(V_S - V_0)/(\sigma T_S^4 - \sigma T_0^4) \qquad [8]$$

However, the actual emissivity may be obtained by Eqs. 2 through 8 as

$$\bar{\epsilon}_S = \bar{\epsilon}_S' + [\sigma T_0^4/(\sigma T_S - \sigma T_0^4)]\Delta\alpha_S \qquad [9]$$

Since $\Delta\bar{\alpha}_S$ is bounded certainly by unity, it is at once obvious that when $T_S^4 \gg T_0^4$ a true measurement of $\bar{\epsilon}_S$ is obtained. However, when T_S and T_0 are nearly the same, as in the arrangements of (1–4), large errors are possible for non-gray samples.

The above source of error was not considered in (1, 2, 4). Eckert, et al. (3) discussed it qualitatively but reached the erroneous conclusion that it disappears as T_0 approaches T_S. In order to evaluate the maximum error, hypothetical spectral characteristics can be chosen to maximize $\Delta\bar{\alpha}_S$ when T_0 is close to T_S

$$\bar{\alpha}_\lambda = 0 \qquad \lambda > \lambda_0$$

$$\bar{\alpha}_\lambda = 1 \qquad \lambda < \lambda_0 \qquad [10]$$

where λ_0 is such that

$$(1/2)(\lambda_0 T_0 + \lambda_0 T_S) = 5215\mu R \qquad [11]$$

The true maximum $\Delta\bar{\alpha}_S$ would be obtained when λ_0 is such that

$$E_{b\lambda_0}(T_0)/\sigma T_0^5 = E_{b\lambda_0}(T_S)/\sigma T_S^5$$

but the value above gives the same answer when T_0 is close to T_S and is more convenient to use. For the spectral variation in Eq. 10 there follows from Eqs. 5 through 7

$$\Delta\bar{\alpha}_S = -\int_{\lambda_0 T_0}^{\lambda_S T_S} (E_{b\lambda}/\sigma T^5) d(\lambda T) \qquad [12]$$

With Eqs. 9 through 12 and Dunkle's tables (5) the discrepancy $(\bar{\epsilon}'_S - \bar{\epsilon}_S)$ due to sample spectral selectivity can be evaluated. A few values are shown in Table 1.

It is emphasized that the above values are for a sample with extreme spectral selectivity. For most materials encountered in technology the discrepancy would be much smaller. However, an appreciable error would exist in measured emissivities of surfaces designed to have long wavelength spectral selectivity, unless the surrounds were considerably colder than the sample.

References

1 Jakob, M., *Heat Transfer, Vol. II*, John Wiley & Sons, Inc., N. Y., 1959, pp. 85–88.

2 Snyder, N. W., Gier, J. T. and Dunkle, R. V., "Total Normal Emissivity Measurements on Aircraft Materials between 100 and 800 F," *Am. Soc. Mech. Engr. Trans.*, 1955, vol. 77, p. 1011.

3 Eckert, E. R. G., Hartnett, J. P. and Irvine T, F., Jr., "Measurement of Total Emissivity of Porous Materials in Use for Transpiration Cooling," JET PROPULSION, vol. 26, 1956, p. 280.

4 Herrington, L. P., "Theory of, and Appropriate Methods for Measurement of Surface Emittance," Am. Soc. Test. Mat. Special Pub. no. 119.

5 Dunkle, R. V., "Thermal-Radiation Tables and Applications," *Am. Soc. Mech. Engr. Trans.*, vol. 76, 1954, p. 549

Hypersonic Viscous Effects in Wind Tunnels[1]

ROBERT H. JOHNSON[2]

General Electric Research Laboratory, Schenectady, N. Y.

Some strong influences of fluid viscosity on Mach 30 operation of a low density helium tunnel are described. Thick boundary layers characteristic of this flow not only change with pressure level, but they are affected by model and passage geometry so that: 1 Model shock wave strength and shape affect the test section flow, necessitating the use of calibrating impact probes with the same shape as the model to be studied; and 2 These thick boundary layers are utilized in "viscous contouring" in a conical nozzle; i.e., uniform test section flow is achieved without the use of contoured nozzles.

Received April 24, 1961.

[1] This research was supported in part by the Ballistic Missile Division, U. S. Air Force, under Contract AF 04(647)–269.

[2] Mechanical Engineer. Member ARS.

MANY OF the problems of high velocity flight stem from the strong effects of fluid viscosity in producing very thick boundary layers with the subsequent modification of flow fields over body surfaces. These thick viscous layers govern some of the flow characteristics of flight simulating wind tunnels and must be accounted for in the design and operation of such tunnels. It has been found that many conventional wind tunnel procedures in calibration, starting, model mounting, and measurements cannot be directly adapted to low density, very high Mach number tunnels.

Strong feedback upstream through thick boundary layers on the tunnel walls with the resulting inability of shock waves to reflect from the walls adds to problems already associated with the very large pressure drop and recovery needed to attain the desired flow. Some of these problems have been resolved in the General Electric Research Laboratory helium tunnel during its development toward operation at Mach numbers up to 36 and densities simulating Earth altitudes above 100,000 ft (1)[3]. Models are supported in a 3.6-in. diameter test section by means of a cone-cylinder-cone sting which also acts as part of the central body diffuser arrangement in a cylindrical passage having the same diameter as the test section.

[3] Numbers in parentheses indicate References at end of paper.

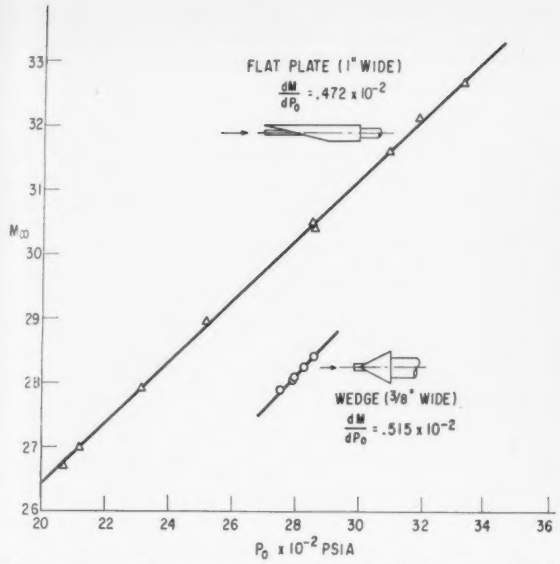

Fig. 1 Stagnation pressure dependence of test section Mach number

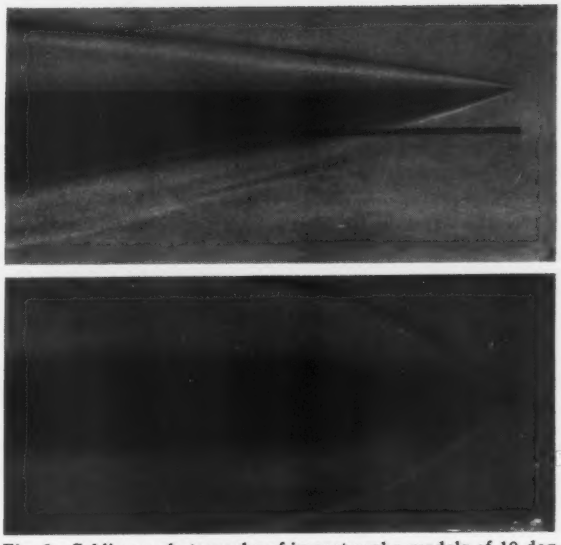

Fig. 2 Schlieren photographs of impact probe models of 10 deg semi-wedge and 60 deg wedge

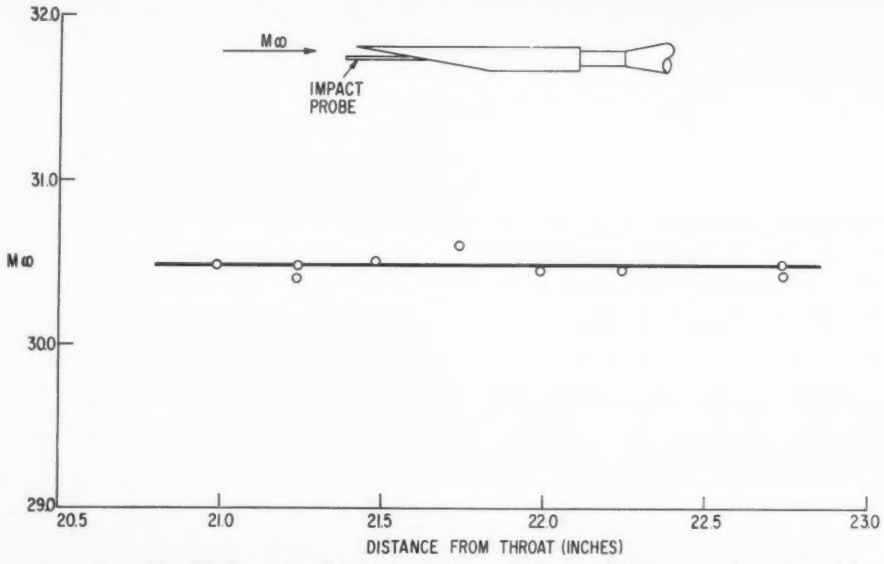

Fig. 3 Centerline Mach number distribution for $P_0 = 2855$ psia with 10 deg semi-wedge model

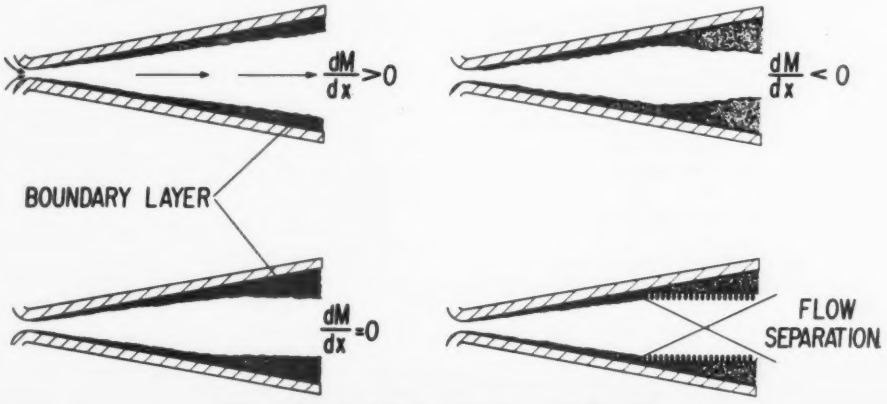

Fig. 4 Boundary layer growth in a conical nozzle

Boundary layer thickness changes with tunnel density level as caused by changes in tunnel stagnation pressure. This pressure dependency of free stream Mach number is shown with the upper curve in Fig. 1 for a 10 deg sharp semi-wedge model mounted at a single location on the centerline of the test section. As would be expected, these data show an increase in Mach number with P_0.

Since the shock wave system associated with the model is generally stronger than any produced in the diffuser section, a dependence of tunnel operation and flow characteristics on model geometry might be expected. In Fig. 1 the P_0 dependency curve for the wide (1 in.) 10 deg semi-wedge is compared with the Mach numbers obtained for a narrower ($\frac{3}{8}$ in.) wedge with a 30 deg half angle. The stronger shock system seen on the more blunt model in the schlieren photographs in Fig. 2 intersecting the boundary layer further upstream causes more feedback and thereby thickens the boundary layer in the nozzle to give rise to the measured lower Mach number level.

From the above observations it was seen that the tunnel flow was strongly influenced by the model shape and size. Care must be exercised when stagnation pressure surveys for calibrating the tunnel are made with conventional rakes; the probes should be shaped as closely as possible to that of the model subsequently studied.

Because a conical nozzle was used, one would in general expect an axial Mach number gradient to exist. This has been the case in the G.E. helium tunnel and in other helium tunnels (2). However, with some combinations of stagnation pressures and model geometries, the usual axial gradients have been observed to vanish. For example, Fig. 3 shows a centerline Mach number of 30.5 measured along the entire length of the test section for a stagnation pressure of 2855 psia with the sharp 10 deg semiwedge model. This surprisingly uniform test section flow results from the fact that the boundary layer growth along the nozzle wall together with the 10 deg wall divergence, yields an effective idealized flow boundary contour (see Fig. 4).

"Viscous contouring" may be obtained for other Mach numbers with other combinations of models and stagnation pressures. Thus a limited number of uniform test section Mach numbers may be realized without the use of conventional contoured nozzles.

Acknowledgment

The assistance of E. C. Bigelow in operating the helium tunnel and in reducing the data is gratefully acknowledged. Stimulating discussions have been held with R. A. Alpher.

References

1 Johnson, R. H., "A Hypersonic Helium Tunnel for Mach Numbers Above Twenty," Gen. Elec. Research Lab. Rep. no. 58-RL-2089, Sept. 1958.

2 Henderson, A., Jr. and Johnston, P. J., "Fluid-Dynamic Properties of Some Simple Sharp- and Blunt-Nosed Shapes at Mach Numbers from 16 to 24 in Helium Flow," NASA Memo 5-8-59L, June 1959.

On "Numerical Comparison Between Exact and Approximate Theories of Hypersonic Inviscid Flow Past Slender Blunt-Nosed Bodies"[1]

H. K. CHENG[2] and A. L. CHANG[3]

Cornell Aeronautical Laboratory, Inc., Buffalo, N. Y.

FELDMAN (1)[4] presents numerical results, based on the method of characteristics for an inviscid hypersonic flow in local thermal equilibrium about a long hemisphere cylinder. The energy in the cross flow field based on the numerical calculation is found to be radically different from that predicted by the blast wave theory (2–4); thus, it is concluded that the validity of the latter theory cannot be justified on rational or theoretical grounds. On the other hand, the structure of the flow field as revealed by the results for the pressure, the temperature, the density and the velocities are generally in accord with that predicted by the blast wave theory (2–5). In view of this, the conclusion reached in (1) is rather surprising. The purpose of this note is to point out that the increase of cross flow energy when correctly calculated from the flow quantities provided by the characteristics methods does remain essentially constant and does agree within the expected degree of accuracy with that required by blast wave theory.

The basic requirements underlying blast wave theory for blunt nosed slender bodies are that the perturbation in the streamwise velocity component $\Delta u \equiv u - U_\infty$ be small in comparison with the free stream velocity U_∞, and that the region in which the theory is applied be far from the blunt nose region, i.e., $x/R_0 \gg 1$. The first condition is essential for the small disturbance assumption, and the second is required in order that the point blast concept be applicable. When these requirements are met, the approximations and the solutions obtained are consistent with the full equations governing the hypersonic inviscid flow. The errors incurred in these approximations are chiefly related to the ratio $\Delta u/U_\infty$. In the "entropy layer" close to the afterbody, most of the gas particles have come from the strongest portion of the shock near the nose; hence, the enthalpy is rather high. Therefore, the ratio $\Delta u/U_\infty$, according to the Bernoulli relation, may not be extremely small. The magnitude of this ratio and the error of the blast wave theory may be estimated (5) in terms of the shock slope dR_s/dx under the assumption of a sufficiently strong shock and a constant specific heat ratio γ as

$$\frac{\Delta u}{U_\infty} \lesssim \frac{1}{2}\left(\frac{dR_s}{dx}\right)^2 \frac{\gamma-1}{\gamma} \qquad [1]$$

It is noted that the error becomes more and more critical as γ approaches unity. Nevertheless, for a given γ, no matter how close to unity, the ratio $\Delta u/U_\infty$ will be small at points sufficiently far downstream.

It is essential, however, to inquire whether the domain of validity of the blast wave theory is large enough for practical application. This question can best be answered by a direct comparison of the theory with numerical solutions carried out for particular cases. The specific, detailed analysis of (1) is of value in this respect.

The main results of (1) for a hemisphere cylinder are obtained from numerical computations based on the method of characteristics. The flow field is assumed to be in local chemical equilibrium with a free stream velocity of 17,500 ft/sec and

Received April 20, 1961.

[1] The present paper was sponsored by U. S. Air Force through the Office of Scientific Research, Contract No. AF 49(638)-952.

[2] Principal Engineer, Aerodynamic Research Dept.

[3] Junior Mathematician, Aerodynamic Research Dept.

[4] Numbers in parentheses indicate References at end of paper.

a free stream condition given by a standard atmosphere at 60,000 ft altitude (6). The flow field in the subsonic region around the nose is determined by an approximate integral method employed previously by Belotserkovskii (refer to 1). The numerical results were compared with corresponding values given by the second-order blast wave theory of Lees and Kubota based on a perfect gas with constant specific heats (3). In spite of the different gas models assumed, the two analyses agree rather well in both surface pressure and in shock shape. The characteristic features of the flow field revealed by the results of (1) also agree reasonably well with those predicted by the blast wave theory, as already pointed out. However, according to Feldman's computation, the increase of cross flow energy per unit length ΔE differs radically from that required by the blast wave theory (2–5). The gain of cross flow energy ΔE may be defined for the present problem as

$$\Delta E \equiv 2\pi \int_{R_0}^{R_s} \left[\rho \left(e + \frac{v^2}{2} \right) - \rho_\infty e_\infty \right] r dr \qquad [2]$$

where ρ, e and v are, respectively, the density, the specific internal energy and the velocity normal to the axis. According to the analyses of (2–5) ΔE will remain constant and equal to the nose drag D. The comparison in ΔE is, therefore, a direct check on the validity of the blast wave theory, which is independent of the specific gas model assumed. Feldman's result, reproduced in Fig. 1, shows a variation of -40 to $+40\%$ from the value $\Delta E/D = 1$ for $x/R_0 \geq 8$.

On the other hand, application of the conservation laws of mass and momentum to the flow field over the afterbody gives the integral relation

$$\frac{\Delta E}{D} = 1 + \frac{2}{C_D} \int_{R_0}^{R_s} \frac{\rho}{\rho_\infty} \left(1 - \frac{u}{U_\infty} \right)^2 \frac{r dr}{R_0^2} + \frac{4 h_\infty}{C_D U_\infty^2} \int_{R_0}^{R_s} \frac{\rho}{\rho_\infty} \left(1 - \frac{u}{U_\infty} \right) \frac{r dr}{R_0^2} \qquad [3]$$

where h_∞ is the specific enthalpy in the free stream and C_D is the nose drag coefficient ($= 2D/\rho_\infty U_\infty^2 \pi R_0^2$) which is taken to be unity in (1). The analysis of (1) shows that $u < U_\infty$, as is

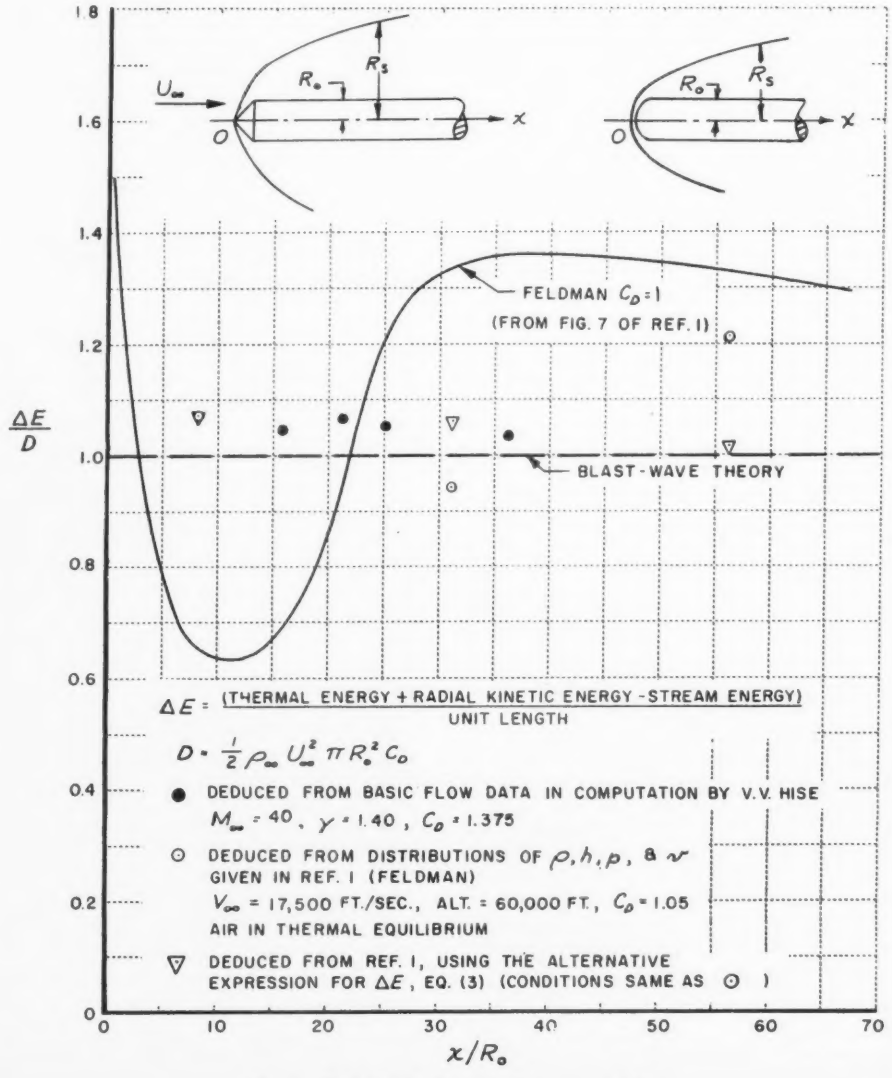

Fig. 1 Variation of the cross flow energy ΔE

to be expected. According to Eq. 3 then, $\Delta E/D$ cannot fall below one, and the large discrepancy between $\Delta E/D$ and unity in Feldman's result is clearly incorrect. Furthermore, with Eq. 3 and the aid of the Bernoulli relation, the ratio of the integrals on the right of Eq. 3 to $\Delta E/D$ is seen to be of the same order as $\Delta u/U_\infty$; meanwhile, the smallness of $\Delta u/U_\infty$ is indeed borne out by the analysis of (1). Hence, there is apparently a contradiction between the results obtained and conclusion reached in Feldman's work.

Using the basic flow data presented in Figs. 2–4 of (1) three values of $\Delta E/D$ have been recalculated which pertain to $x/R_0 = 8$, 31 and 56 where the shock location, streamline pattern, as well as the profiles of velocity, pressure and temperature have been adequately defined. These new calculations were carried out using Eq. 2 and the gas table from (6). The results are presented as open circles in Fig. 1. It must be pointed out that a nose drag coefficient of 1.05 has been used, which is slightly larger than that suggested in (1). Results of (1) which are reproduced in Fig. 1 are based on $C_D = 1$. The present value of 1.05 was determined by application of the conservation relation Eq. 3 at station $x/R_0 = 8$. This value is presumably more reliable for the purpose because the supersonic flow field provided by (1) does not correspond exactly to that downstream of a spherical nose due to the approximate nature of the method used for the nose region. The deviations from the blast wave theory, that is, from $\Delta E/D = 1$, as revealed by the new calculation, are rather small, certainly much smaller than that reported by Feldman. The discrepancy between the present calculation and the blast wave theory at the most downstream station $x/R_0 = 56$ possibly results from the insufficient accuracy in the basic flow data used for the evaluation based on Eq. 2. In view of this, an alternative calculation of $\Delta E/D$ is made, utilizing the integral relation, Eq. 3, based on the density and velocity data. These alternative calculations are presented in Fig. 1 as open triangles; they show that the deviation from unity is small.

To further ascertain the validity of the blast wave concept, the ratio $\Delta E/D$ based on Eq. 2 has been evaluated from another source of data. These are taken from the original numerical computations of V. V. Hise for a different nose shape with different gas properties.[5] In the case analyzed by Hise, an ideal gas with a constant specific heat ratio $\gamma = 1.40$ is assumed, the free-stream Mach number is 40, and a nose cone of 53 deg half-cone angle is used. These data are presented as full circles (black dots) in Fig. 1. The surface pressure and the shock shape which resulted from this numerical calculation have been presented by Hise in (7). In this case, also, the blast wave theory was shown to agree well with the calculation based on the method of characteristics.

The comparison made for both cases has demonstrated the accuracy of the blast wave theory and its applicability to a gas with $\gamma = 1.40$ as well as a dissociative gas in local thermal equilibrium. In all instances, the error incurred by application of the blast wave theory is indeed small; except for the most downstream station where the accuracy of calculation is uncertain, the discrepancy is generally of the order of 6% for $x/R_0 \geq 8$.

References

1 Feldman, S., "Numerical Comparison Between Exact and Approximate Theories of Hypersonic Inviscid Flow Past Slender Blunt Nosed Bodies," ARS JOURNAL, vol. 30, no. 5, May 1960, p. 463.

2 Lin, S. C., "Cylindrical Shock Waves Produced by Instantaneous Energy Release," *J. Appl. Phys.*, vol. 25, 1954, p. 54.

3 Lees, L. and Kubota, T., "Inviscid Hypersonic Flow Over Blunt-Nosed Slender Bodies," *J. Aero/Space Sci.*, vol. 24, 1957, p. 195.

4 Cheng, H. K., "Similitude of Hypersonic Real-Gas Flows Over Slender Bodies with Blunted Noses," *J. Aero/Space Sci.*, vol. 26, no. 9, Sept. 1959, p. 575.

5 Cheng, H. K., Hall, J. G., Golian, T. C. and Hertzberg, A., "Boundary-Layer Displacement and Leading-Edge Bluntness Effects in High-Temperature Hypersonic Flow," *J. Aero/Space Sci.*, vol. 28, no. 5, May 1961, p. 353.

6 Feldman, S., "Hypersonic Gas Dynamic Charts for Equilibrium Air," AVCO Res. Rep. 40, Jan. 1957.

7 Hise, V. V., "Analytic Study of Induced Pressure on Long Bodies of Revolution with Varying Nose Bluntness at Hypersonic Speeds," NASA TR R-78, 1960.

[5] The basic flow data obtained in V. V. Hise's calculation were made available to the writers through Mr. M. H. Bertram of Langley Research Center, NASA, and Mr. A. Burke of Cornell Aeronautical Laboratory.

Effect of Acoustic Environment on the Burning Rate of Double-Base Solid Propellants

J. E. CRUMP[1] and E. W. PRICE[2]

U. S. Naval Ordnance Test Station, China Lake, Calif.

DURING unstable combustion in solid propellant rocket motors, the oscillatory combustion is ordinarily accompanied by a net change in burning rate of the propellant. This change in burning rate is ordinarily inferred from the accompanying change in equilibrium pressure in the rocket motor and is further evidenced by observations of propellant samples recovered after interruption of burning. Recent notes in ARS JOURNAL have described observations of two different types of burning rate response to oscillatory combustion (1, 2 and 3),[3] and in each instance it was observed that the details of how the burning rate changed during oscillatory combustion were linked with the details of the acoustic environment at the particular point on the burning surface. In this respect, it should be pointed out that the gas oscillations during oscillatory combustion occur in characteristic modes of the combustion chamber cavity, so that the details of the acoustic environment vary systematically as a function of location in the cavity (and hence as a function of location on the propellant burning surface). This detailed dependence of local burning rate on the local acoustic environment cannot be inferred from observation of pressure-time curves because they reflect only the surface-average burning rate. However, some quantitative data have recently been obtained by the authors from interrupted burning of propellants which reveal decisively some of the details of local dependence of burning rate on acoustic environment. The purpose of this note is to present this data and to point out with respect to it that the effect of acoustic environment on burning rate is considerably more complex than is generally believed and cannot be inferred from observations of pressure-time curves alone.

The type of burning rate behavior to be discussed here was reported earlier (1 and 3 through 6), and the general arrangement of the experiments here is based on the arrangement described previously (3). The type of burning rate response is reflected in the orthodox manner by the pressure-time records[4] in Figs. 1, which show the changes in chamber pres-

Received March 10, 1961.

[1] Physicist, Research Dept. Member ARS.

[2] Head, Aerothermochemistry Group. Member ARS.

[3] Numbers in parentheses indicate References at end of paper.

[4] A high frequency response pressure transducer was used for the measurements. The lower trace is the mean pressure obtained by low pass filtering of the transducer output; the upper trace is the oscillatory pressure obtained by high pass filtering of the transducer output. Since the propellant charge has a cylindrical internal perforation, a pressure-time curve with no oscillatory burning would be progressive.

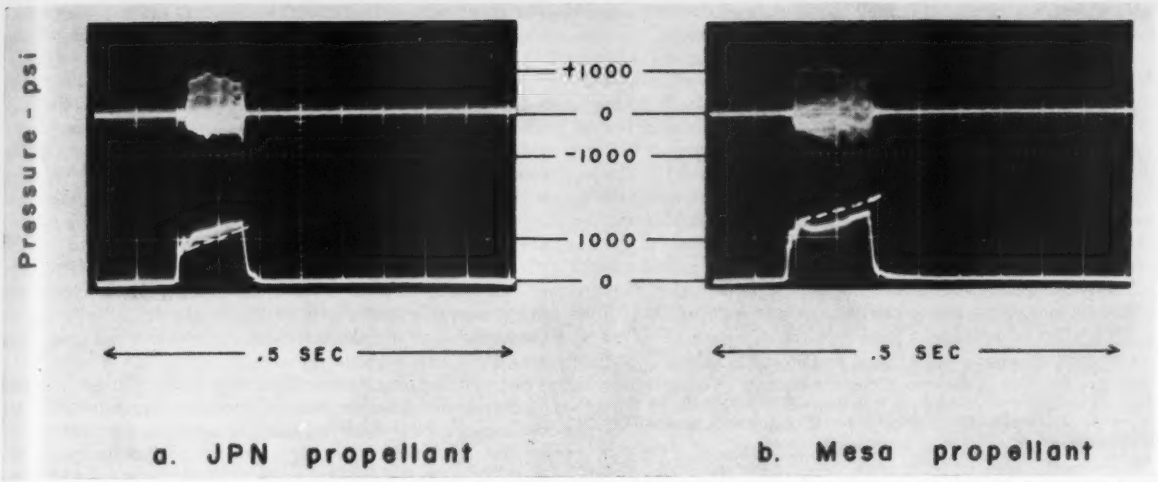

Figs. 1 Pressure-time curves showing pressure change due to effect of oscillatory combustion on burning rate of double-base propellants for—a JPN propellant; b mesa propellant. Dashed lines indicate approximate pressure-time relations without oscillatory combustion

sure (lower traces) coincident with the onset of oscillatory combustion (upper traces). The information derived from the traces of Figs. 1 is the effect of the burning rate change integrated over the entire propellant burning surface. In Fig. 1a, this surface-averaged burning rate was increased during oscillatory burning as indicated by the increase in mean pressure (lower trace). In Fig. 1b, the opposite effect is observed; the surface-averaged burning rate was decreased during oscillatory burning. Both tests used extruded, double-base propellant. The propellant in Fig. 1a was JPN (7); the propellant in Fig. 1b was a mesa propellant of comparable burning rate and energy content.

Interpretation of test results in this program has progressed through three successive eras of increasing refinement. In the first era, inferences regarding burning rate behavior during oscillatory combustion were made as stated previously, i.e., the change in surface-average burning rate was inferred from irregularities in the pressure-time curve. Such interpretations were reported in (3 and 8). In the second era, interruption of burning made it possible to determine on a *relative basis* the variation in rate as a function of location on the charge and hence as a function of details of the acoustic environment. Such interpretations were reported in (1, 4 and 9) and showed that burning rates were always higher at the velocity antinode than at the pressure antinode of the unstable acoustic mode. Interrupted burning tests did not provide any reference point which could be called "burning rate without oscillatory behavior," for comparison with the partially burned charge. Strand burning rate data were not accurate enough for this purpose. The third era of this program occurred when the present experimental technique was developed for simultaneous partial burning of a test sample and a non-oscillating control sample. Only with the advent of this latter technique was it possible to be sure of the absolute change in burning rate during oscillatory combustion. Interpretations based on this method were reported previously in (5 and 6).

The apparatus for the present experimental technique is shown in Figs. 2. Two propellant charges are burned simultaneously in different sections of the burner. One section is arranged to be dynamically unstable in the fundamental longitudinal acoustic mode and the other to be stable in all modes. The gas evolved from both charges exhausts through the same sonic nozzle. Thus, the two charges, when ignited simultaneously and later extinguished simultaneously, experience the same mean pressure-time history, but one "sees" oscillatory flow while the other does not. After

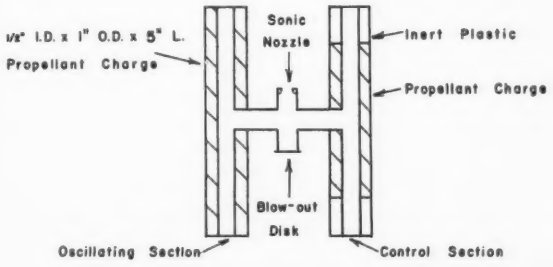

a. Internal Arrangement of Double Burner

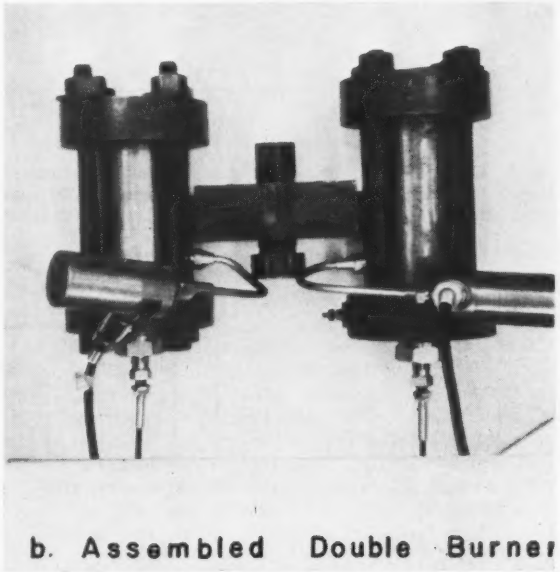

b. Assembled Double Burner

Figs. 2 Basic double burner arrangement—a internal arrangement of double burner; b assembled double burner

interruption of burning, the web thicknesses of the two are compared as a function of distance along the charge.[5]

Examples of the reduced data are shown in Fig. 3. The data shown in Fig. 3 for JPN propellant are typical of the data obtained from nine tests and for the mesa propellant, from two tests. The abscissa has been normalized by dividing the distance along the charge by the charge length (which is half the wave length of the first longitudinal acoustic mode). The dominant oscillation frequency in these tests was approximately 4200 cps corresponding to the first longitudinal mode. For sinusoidal oscillations in the first longitudinal mode of the cavity, the amplitude of the oscillations in pressure and gas velocity would vary with position along the propellant sample in the manner shown above the burning rate curves in Fig. 3.

[5] The non-oscillating charge shows no variation in web thickness as a function of distance along the charge. This indicates that no oscillatory combustion was present and also shows that there is no steady state erosive burning present to confuse interpretation.

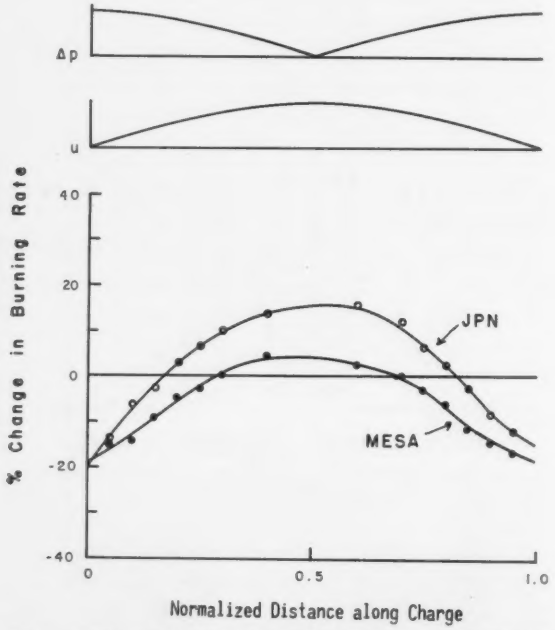

Fig. 3 Graph showing change in burning rate as function of acoustic environment for combustion oscillations at 4200 cps; upper curve is for JPN double-base propellant, lower curve is for double-base mesa propellant

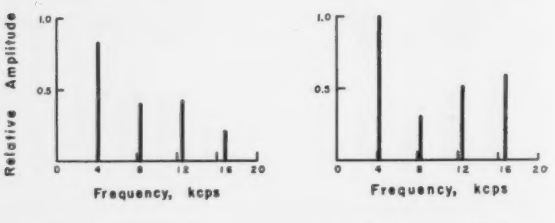

Figs. 4 Harmonic analyses of pressure oscillations showing relative strength of longitudinal modes for—a JPN propellant test; b mesa propellant test

The upper curve indicates the amplitude of the pressure oscillations, and the lower curve indicates the amplitude of the velocity oscillations.

Thus, for "pure" first longitudinal mode oscillations, the reduced data could be correlated with: pressure oscillations which occur with negligible gas velocity oscillations at the ends of the propellant sample (near the zero and 1 points on the abscissa scale); and with gas velocity oscillations which occur with negligible pressure oscillations at the midpoint of the propellant sample (around the 0.5 point on the abscissa scale). To summarize briefly, the effect of oscillating pressure and the effect of oscillating velocity on the burning rate of the propellant are separated in this experiment; in addition, the interaction of these two effects can be studied by considering the region between the ends and midpoint of the propellant sample.

Interpreting the burning rate data in Fig. 3 first in terms of the idealized assumption of pure first mode longitudinal oscillations, it is evident that the acoustic environment of oscillating pressure (also temperature and density) at the ends of the propellant sample leads to a substantial reduction in burning rate. On the other hand, the acoustic environment of gas oscillating parallel to the burning surface near the midpoint of the sample leads to increases in burning rate, but to larger increases with the conventional propellant than with the mesa propellant.

One may reasonably inquire whether these effects might be anticipated on the basis of the steady state burning characteristics of the propellant alone Applying the known pressure dependence of burning rate under steady state conditions to the variation in pressure during one cycle of oscillation, it was determined that the mean burning rate of the JPN propellant would have been reduced by 1.9% whereas the rate of the other propellant would not have changed at all. Comparing this with the actual changes in burning rate at the ends of the propellant sample as indicated in Fig. 3, it is clear that the changes in burning rate cannot be explained in terms of steady state burning behavior. This should not be surprising, considering that the rates of change of pressure during a cycle of oscillation exceeded 10^7 psi/sec.

A similar calculation was made for the JPN data in order to compare the observed change in burning rate at the midpoint of the sample with the change predicted by the steady state erosive burning rate law (the erosive burning law for the mesa propellant is not known). This calculation indicated that the burning rate would have been increased by 52%, whereas the observed increase was about 19%. However, these results must be viewed with reservations, since the oscillatory behavior in the system included appreciable energy in higher longitudinal modes (Figs. 4). Although this condition does not seriously complicate interpretation of the burning rate effects at the ends of the propellant samples (since the ends correspond to pressure antinodes for all modes involved), it leads to rather complicated acoustic environments at other points on the sample. Since the first mode is the dominant one, the authors believe that the burning rate change at the midpoint of the charge is due primarily to the acoustic velocity and that the behavior really deviates from the steady state erosive law in the way implied by the aforementioned results; however, too little is known about the combined effects on burning rate of acoustic pressure and acoustic velocity acting concurrently to be certain of this belief. Efforts in this program are continuing to minimize the energy in higher modes in order to yield unequivocal information on the effect of acoustic velocity.

The results to date can hardly be said to elucidate the mechanisms of change of burning rate by acoustic environment, but they provide a much less speculative starting point for future work than was available heretofore. Successful elucidation of these mechanisms will undoubtedly reveal much about rate controlling processes in solid propellant burning, and the methods used in the present investi-

gation seem to hold considerable promise in this problem area. However, rather than speculate about mechanisms we return to the implications of the previously indicated results in terms of observations of pressure-time curves. Referring to the JPN data in Fig. 3, integration of the area between the curve and the zero value abscissa indicates that there should have been an increase in surface-average rate. This is in agreement with the interpretation of the mean pressure-time curve (Fig. 1a) which reflects the space integrated effect of the burning rate changes. Similarly, in Fig. 3, with the mesa propellant, the integration indicates a decrease in surface-average burning rate, which is in agreement with Fig. 1b (1 and 3). In this respect, the present experiments point out an important fact—the changes in pressure observed during oscillatory combustion cannot be correlated in any simple way to a change in the burning rate of the propellant; the pressure changes can be correlated only to the surface-averaged effect of a wide range of changes in burning rate related to the space distributed variation in acoustic environment in which the propellant is burning.

In light of these experimental results and interpretations, see the notes by Nachbar and Green (10 and 11) and by McClure, Hart and Bird (12) regarding burning rate changes during oscillatory combustion. Note that the references of the aforementioned authors to experimentally obtained information on irregular burning pertain almost exclusively to observations of pressure-time curves, and hence are relevant only to the changes in surface-average burning rate during oscillatory combustion. Although in the phenomenological arguments advanced they recognize the space-wise nonuniformity of acoustic environment over the burning surface, their comparison of theory with observed pressure-time curves does not include any serious attempts to "surface-average" the corresponding local burning rate effects as would be required to explain pressure-time curves. This point was raised earlier (9) about the Green-Nachbar work and is reiterated here regarding the remarks of McClure et al. Although the present authors agree with McClure "that the major factor responsible for the mean pressure level changes observed during severe oscillatory combustion has been uncovered" (12), it is suggested that the argument in the preceding paragraph does a more complete job of explaining the major factors. The experimental results cited show that, in looking at the space-wise variation of burning rate changes, the decrease in burning rate noted in Fig. 3 cannot be lightly dismissed in an attempt, such as McClure's, designed to correlate burning rate during oscillatory behavior with steady state erosive burning behavior. In fact, it appears that the decrease in pressure during oscillatory burning of mesa propellants is due primarily to the decrease in burning rate in the vicinity of pressure antinodes, rather than a rate decrease in the region of velocity antinodes as hypothesized by McClure et al. The "erosive rectification" suggested by McClure is undoubtedly a major factor in the effect of acoustic velocity on local burning rate, but it seems doubtful that a steady state erosive burning law is applicable, and it is clear that the effects explained by McClure in terms of such a law are due substantially to the contribution of the acoustic pressure (and temperature and density) instead.

References

1 Price, E. W., "Combustion Instability in Solid Propellant Rocket Motors," ARS JOURNAL, vol. 30, no. 6, June 1960, pp. 574–576.

2 Crump, J. E. and Price, E. W., " 'Catastrophic' Changes in Burning Rate of Solid Propellants During Combustion Instability," ARS JOURNAL, vol. 30, no. 7, July 1960, pp. 705–707.

3 Price, E. W. and Sofferis, J. W., "Combustion Instability in Solid Propellant Rocket Motors," JET PROPULSION, vol. 28, no. 3, March 1958, pp. 190–192.

4 Price, E. W., Mathes, H. B., Crump, J. E. and McGie, M. R., "Experimental Research in Combustion Instability of Solid Propellants," accepted for publication in *Combustion and Flame*.

5 Price, E. W., "Effect of Acoustic Environment on the Burning Rate of Solid Propellants," contribution to the Round Table on Acoustic Instability, Eighth Symposium (International) on Combustion, Calif. Inst. of Tech., Pasadena, Calif., Aug. 29–Sept. 2, 1960.

6 Price, E. W., "Analysis of Results of Combustion Instability Research on Solid Propellants," *Progress in Astronautics and Rocketry. Vol. 1: Solid Propellant Rocket Research*, Academic Press, N. Y., 1960, pp. 561–602.

7 Wimpress, R. N., *Internal Ballistics of Solid-Fuel Rockets*, McGraw-Hill Book Co., Inc., N. Y., 1950.

8 Price, E. W., "Combustion Instability in Solid Propellant Rocket Motors," *Astronautica Acta*, vol. V, no. 1, 1959, p. 63.

9 Price, E. W., "Combustion Instability in Solid Propellant Rocket Motors," U. S. Naval Ordnance Test Station, China Lake, Calif., NAVORD Rep. 7023 (NOTS TP 2389), Dec. 21, 1959.

10 Green, L., Jr. and Nachbar, W., "A Comment on Combustion Instability in Solid Propellant Rocket Motors," JET PROPULSION, vol. 28, no. 11, Nov. 1958, p. 769.

11 Nachbar, W. and Green, L., Jr., "Closure by W. Nachbar and L. Green, Jr.," ARS JOURNAL, vol. 30, no. 6, June 1960, pp. 576–577.

12 McClure, F. T., Hart, R. W. and Bird, J. F., "Acoustic Instability in Solid Fuel Rockets," ARS JOURNAL, vol. 30, no. 9, Sept. 1960, pp. 908–910.

Advanced Ignition System for Solid Propellant Rocket Motors

J. J. PRIAPI[1]

United Technology Corp., Sunnyvale, Calif.

THIS paper is concerned with an advanced system for the ignition of solid propellant rocket motors. The system utilizes a liquid that is hypergolic with solid propellants and that upon contact with the propellant surface initiates an exothermic interfacial reaction which results in motor ignition. The hypergolic ignition phenomena and the tests which demonstrated the feasibility of the system are discussed. Based upon the reaction theories and test results presented in the paper the hypergolic system appears to be ideal for the ignition of large solid propellant boosters.

Received Feb. 15, 1961.

[1] Project Engineer, Solid Propellant Rocket Branch. Member ARS.

Hypergolic Ignition

In conventional ignition systems, the total rocket chamber pressure at ignition is the sum of the pressure developed by the igniter and that due to the burning propellant ignited by hot particles and gases from the igniter. This type of reaction can easily result in over-ignition. In the hypergolic system the surface area of the propellant, and therefore the amount of fuel available to react with the hypergolic oxidizer, is fixed by the grain design. Since the operating pressure of the motor is directly dependent upon the propellant surface area, peak pressures developed during ignition will be limited essentially to the operating pressure of the motor. However, there are two primary conditions necessary in order that this be true. The first of these is that the flame temperature of the propellant burning with the liquid oxidizer be approximately of the same magnitude as the flame temperature of the propellant burning alone. This parameter is necessary since any significant increase in flame temperature will also increase the burning rate, which will in turn increase the initial operating pressure. Excessive ignition flame temperatures should not be encountered in contemporary and advanced pro-

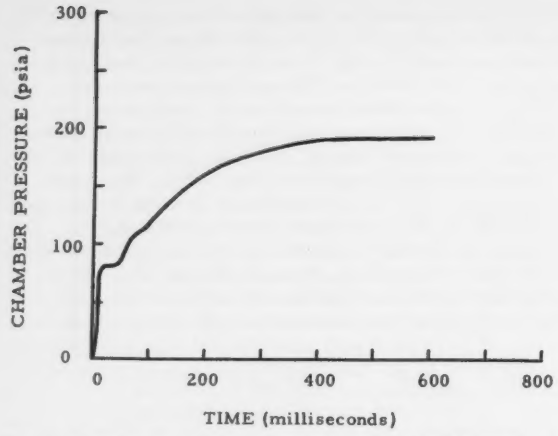

Fig. 1 Pressure vs. time curve for hypergolic ignition test of polyurethane propellant, using chlorine trifluoride

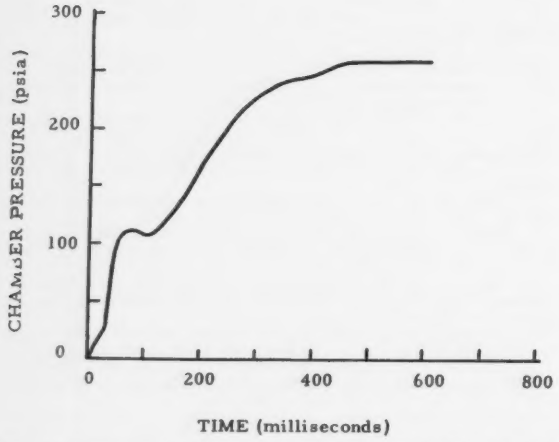

Fig. 2 Pressure vs. time curve for hypergolic ignition test of polybutadiene-acrylic acid propellant, using chlorine trifluoride

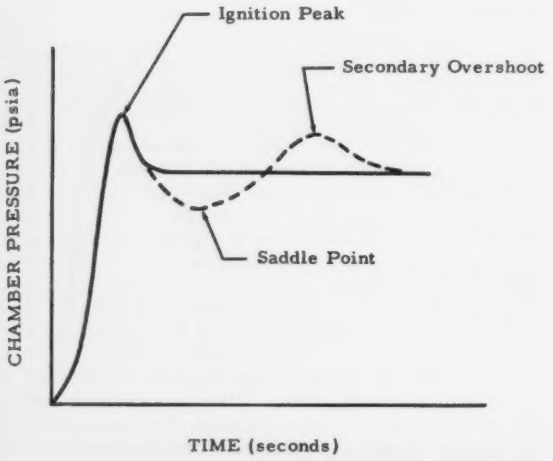

Fig. 3 Typical pressure vs. time curves for non-optimized conventional ignition systems

pellant systems since the flame temperature of a high performance propellant closely approximates the flame temperature of the same propellant system plus a halogen fluoride oxidizer.

The second condition, and undoubtedly the one which will have the greatest effect on the ignition transient pressure, is that the time from injection of liquid to propellant ignition should not be excessive. If this time is too great, the burning rate, and therefore the initial operating pressure, will increase as a result of an increase in propellant temperature prior to ignition, which is caused by a low order exothermic reaction between the liquid and the propellant. However, in order to cause an excessive ignition delay, the flow rate of the liquid oxidizer entering the motor must be extremely low. This low flow rate is most improbable in the normal ignition process of a hypergolic system. On the other hand, any liquid oxidizer in excess of the minimum amount necessary for ignition has only a negligible effect on ignition transients. Consequently, the hypergolic system will operate efficiently over a wide range of ignition flow rates, thereby precluding the possibility of ignition peak pressures. Such a feature is not found in any conventional ignition system.

The hypergolic ignition system affords several basic advantages as a result of its capability to eliminate the possibility of excessive peak pressures during the ignition phase. The first advantage is that the required development cycle of the ignition system can be markedly reduced since hypergolic ignition is inherently smooth and the possibility of motor case failure caused by excessive pressures is precluded. Elaborate igniter research and development programs utilizing costly special ignition test motors and equipment should no longer be required and the ignition system can be used with confidence in the full scale motor, early in the program. This is an important consideration in very large solid propellant boosters where the cost of ignition test motors are prohibitive and a failure at ignition could be catastrophic.

The second basic advantage is in reliability. Conventional igniters require the maintenance of stringent quality control standards and precise processing techniques. The hypergolic system stresses simplicity, since it is essentially a mechanical device containing a liquid oxidizer. Statistical reliability can be readily demonstrated, since the system is not destroyed by testing.

The third advantage is in system storability and the elimination of many of the problems associated with motor storage. Fuel rich propellant surfaces caused during casting and aging, and decomposed and deteriorated propellant surfaces often tax the capability of current ignition systems while the action of the hypergolic system should not be affected by these conditions. Also, failure can result from a cracking of a deteriorated surface layer, which may open up during ignition and produce severe peak pressures or motor failure. Hypergolic ignition shocks are markedly reduced since the liquid itself does not contribute additive pressure. Conventional ignition materials are temperature sensitive and subject to deleterious decomposition even under ambient storage. The hypergolic system should have an indefinite storage life because halogen fluorides form passive fluoride films with their containers and do not undergo further reaction for an indefinite period of time.

The final advantage stems from igniter accessibility and consequent safety in transportation and handling. Because of the configuration and location of conventional ignition systems and the increasing size of solid propellant rocket motors, the igniter is often virtually inaccessible once the missile is assembled making it almost mandatory to handle and transport engines with the ignition system in place. Also, if the ignition system is required to be removed or replaced, the missile would have to be disassembled. Because the hypergolic system utilizes a liquid as its ignition material, the primary igniter assembly may be located at or near the surface of the flight vehicle, thereby making the ignition system read-

ily accessible from the outside. This allows the missile to be handled or transported without the ignition system in place, and thus reduces the hazard of accidental ignition.

Demonstration of Feasibility

The feasibility of the hypergolic ignition system has been demonstrated in a series of tests conducted at United Technology Corporation. In the initial tests, samples of both polyurethane and polybutadiene-acrylic acid propellants were ignited by sprays of chlorine trifluoride. The test firings were photographed with a high speed movie camera operating at 1000 frames per sec. Ignition was demonstrated at ambient conditions with resulting times to ignition being approximately 80 millisec.

The second phase of the demonstration was successfully conducted in solid propellant motors. The motors contained 5 lb of solid propellant in the configuration of an internal burning cylinder and a splash plate type injector was utilized. The first motor contained an aluminized polyurethane propellant and chlorine trifluoride was utilized as the ignition liquid. Even though this was the initial test firing of a hypergolic system, ignition was smooth and the ignition peak pressure was negligible, as can be seen in the pressure-time curve in Fig. 1. The pressure-time curve of a motor containing an aluminizing polybutadiene-acrylic acid propellant and ignited by chlorine trifluoride is shown in Fig. 2. As in the first firing the rate of pressure rise was smooth and the ignition peak pressure was negligible.

In the two motor firings discussed, zero time is not defined in accordance with military specifications, since an exceptionally long line was utilized between the remotely operated ignition valve and the injector, and a standard definition would be meaningless. Instead, zero time is defined as the time at which there is a first indication of pressure in the motor. However, if the results of the first phase of the demonstration are incorporated with the above results, it can be seen that ignition delays of approximately 90 to 115 millisec are attainable.

A comparison of hypergolic and pyrotechnic ignition may be made if Figs. 1 and 2 are viewed in relation to Fig. 3, which shows typical pressure-time curves for pyrotechnic igniters that have not been perfectly tailored to the propellant. If the igniter is too large or if it burns too rapidly, an ignition peak will occur. This peak is evidenced as a hard start and can lead to failure if the mechanical design cannot sustain the higher pressure. Another type of malfunction is evidenced by the existence of the saddle point region where the motor operates below design pressure for a short period of time. Such a condition generally occurs if the igniter has not supplied sufficient heat to the propellant to result in steady-state burning. This phenomenon can contribute to hang-fires and secondary pressure peaks, resulting in combustion instability or bursting of the pressure vessel. In fundamental terms, the existence of a saddle region is associated with the fact that when the igniter burns out, the temperature contour within the solid propellant is not matched with that which existed during steady-state burning. Thus, it can be seen that if an igniter is employed which creates normal solid propellant burning as part of the ignition process itself, these types of ignition failures will be eliminated.

These initial tests have successfully demonstrated the feasibility of the hypergolic ignition system. They have shown that polyurethane and polybutadiene-acrylic acid type propellants can successfully be ignited, with resulting ignition peak pressures being negligible. The rate of pressure rise was relatively low and the ignition delay was in the range of 100 millisec and the ignition time was in the range of 200 millisec. Because of the limited number of firings, the reproducibility could not be ascertained.

NASA also has successfully ignited motors containing composite and double-base solid propellants with hypergolic liquids, at their Lewis Research Center.[2] Chlorine trifluoride, bromine trifluoride, and bromine pentafluoride were investigated as hypergolic ignition liquids, and several different injector configurations were evaluated. These motor firings were made over a range of simulated altitudes in order to determine the effect of altitude on ignition transients.

The tests conducted at NASA demonstrated that composite and double-base solid propellant rocket motors can be ignited by reaction with a hypergolic fluid. Of the hypergolic liquids evaluated, chlorine trifluoride was found to be the most promising because of its high degree of reactivity and relative reliability over the range of test conditions. The ignition characteristics of the composite propellant were unaffected by extreme altitude, while double-base propellant ignition became progressively more difficult as the simulated altitude was increased. In these tests the ignition delay obtained with the hypergolic system was greater than that obtained with a conventional pyrotechnic igniter and the peak pressure developed by the hypergolic system was higher than that produced by the pyrotechnic igniter. However, the rate of motor pressure rise produced by both systems was approximately equal. The high ignition pressures produced by the hypergolic system are attributed directly to the fact that low flame temperature propellants were utilized, and very low injection rates were used. High propellant flame temperature and reasonable flow rates are primary parameters in order that ignition pressure be limited essentially to motor operating pressure.

Although there was a difference in the test results obtained by NASA and United Technology Corporation, the results indicated that a smooth pressure rise and a negligible ignition peak pressure can be obtained with a hypergolic ignition system. They have also shown that the outstanding problem area associated with hypergolic ignition is that of excessive ignition delay. However, the open air tests conducted at United Technology Corporation, in which samples of propellant were sprayed with chlorine trifluoride, produced times to ignition on the order of 80 millisec. The conditions encountered in the open air are more adverse to ignition than those encountered in a closed motor and therefore it is strongly indicated that the ignition delay of a motor could be less than 80 millisec.

Conclusions

The hypergolic system is an interesting and novel approach to solid propellant ignition and while it does not represent a major break through in the field of ignition, it does represent a potential advancement in the state-of-the-art. The tests conducted by NASA and United Technology Corporation indicate that this system can be used in practical solid propellant igniting applications. Ignition delays produced by the hypergolic system are comparatively long, making the system inadequate where very short ignition delays are required. In applications where long ignition delays can be tolerated and when the advantages accrued by inherently smooth ignition and negligible peak pressures can be utilized, the hypergolic system would be ideal.

[2] Ciepluch, C. C., Allen, H., Jr. and Fletcher, E. A., "Ignition of Solid Propellant Rocket Motors by Injection of Hypergolic Fluids," ARS JOURNAL, vol. 31, no. 4, 1961, pp. 514–518.

Secular Gravitational Torque on a Satellite in a Circular Orbit

RUSSELL A. NIDEY[1]

Kitt Peak National Observatory, Tucson, Ariz.

The secular gravitational torque on an inertially oriented satellite in a circular orbit is normal to the geocentric angular velocity and is a function not only of the differences in the principal moments of inertia but also of the square of the angular velocity and of the orientation of the satellite relative to the axis of the orbit.

THE AUTHOR has previously shown (1)[2] that the torque on a satellite of arbitrary shape can be represented by the following expression (in vector notation)

$$\mathbf{M} = 3\omega^2[(\mathbf{j}\cdot\mathbf{I})(\mathbf{k}\cdot\mathbf{I})(I_3 - I_1) + (\mathbf{j}\cdot\mathbf{J})(\mathbf{k}\cdot\mathbf{J})(I_3 - I_2)]\mathbf{i} - 3\omega^2[(\mathbf{i}\cdot\mathbf{I})(\mathbf{k}\cdot\mathbf{I})(I_3 - I_1) + (\mathbf{i}\cdot\mathbf{J})(\mathbf{k}\cdot\mathbf{J})(I_3 - I_2)]\mathbf{j} \quad [1]$$

where

$\mathbf{M}$ = gravitational torque
ω = numerically the geocentric angular velocity characteristic of the circular orbit corresponding to the instantaneous geocentric distance
$\mathbf{i}, \mathbf{j}, \mathbf{k}$ = a right-hand orthogonal set of unit vectors, $\mathbf{k}$ in the direction of local vertical
$\mathbf{I}, \mathbf{J}, \mathbf{K}$ = a right-hand orthogonal set of unit vectors parallel to the principal axes of inertia of the satellite
I_1, I_2, I_3 = corresponding principal moments of inertia

But

$$(\mathbf{j}\cdot\mathbf{I})\mathbf{i} - (\mathbf{i}\cdot\mathbf{I})\mathbf{j} = (\mathbf{I}\times\mathbf{k}) \quad [2]$$

and

$$(\mathbf{j}\cdot\mathbf{J})\mathbf{i} - (\mathbf{i}\cdot\mathbf{J})\mathbf{j} = (\mathbf{J}\times\mathbf{k}) \quad [3]$$

Hence

$$\mathbf{M} = -3\omega^2[(I_3 - I_1)(\mathbf{k}\cdot\mathbf{I})(\mathbf{k}\times\mathbf{I}) + (I_3 - I_2)(\mathbf{k}\cdot\mathbf{J})(\mathbf{k}\times\mathbf{J})] \quad [4]$$

or

$$\mathbf{M} = 3\omega^2\mathbf{k}\times[I_1(\mathbf{k}\cdot\mathbf{I})\mathbf{I} + I_2(\mathbf{k}\cdot\mathbf{J})\mathbf{J} + I_3(\mathbf{k}\cdot\mathbf{K})\mathbf{K}] \quad [5]$$

since

$$\mathbf{k}\times[(\mathbf{k}\cdot\mathbf{I})\mathbf{I} + (\mathbf{k}\cdot\mathbf{J})\mathbf{J}] = \mathbf{k}\times[\mathbf{k} - (\mathbf{k}\cdot\mathbf{K})\mathbf{K}] = -(\mathbf{k}\cdot\mathbf{K})(\mathbf{k}\times\mathbf{K}) \quad [6]$$

Secular Torque

Let $\mathbf{n}$, $\boldsymbol{\mu}$ and $\boldsymbol{\nu}$ be a right-hand orthogonal set of unit vectors fixed in space with $\mathbf{n}$ in the direction of the geocentric angular velocity. Then, since $\mathbf{k}$ is always normal to $\mathbf{n}$ and in the case of a circular orbit varies in direction at the uniform rate ω

$$\mathbf{k} = -\boldsymbol{\mu}\sin\omega t + \boldsymbol{\nu}\cos\omega t. \quad [7]$$

Also if the satellite is inertially oriented for an entire orbit period $\mathbf{I}$, $\mathbf{J}$, and $\mathbf{K}$ as well as $\boldsymbol{\omega}$ are constant. Thus, substituting Eq. 7 in Eq. 4, integrating over an orbit, and dividing by the orbit period, we have

$$\begin{aligned}\mathbf{M}_{avg} &= (\omega/2\pi)\oint \mathbf{M}\,dt \\ &= (-3\omega^2/2\pi)(I_3 - I_1)\oint \{(-\boldsymbol{\mu}\cdot\mathbf{I})(-\boldsymbol{\mu}\times\mathbf{I})\sin^2\omega t + (\boldsymbol{\nu}\cdot\mathbf{I})(\boldsymbol{\nu}\times\mathbf{I})\cos^2\omega t + [(-\boldsymbol{\mu}\cdot\mathbf{I})(\boldsymbol{\nu}\times\mathbf{I}) + (\boldsymbol{\nu}\cdot\mathbf{I})(-\boldsymbol{\mu}\times\mathbf{I})]\sin\omega t\cos\omega t\}\,\omega dt + \\ &\quad (-3\omega^2/2\pi)(I_3 - I_2)\oint \{(-\boldsymbol{\mu}\cdot\mathbf{J})\times(-\boldsymbol{\mu}\times\mathbf{J})\sin^2\omega t + (\boldsymbol{\nu}\cdot\mathbf{J})(\boldsymbol{\nu}\times\mathbf{J})\cos^2\omega t + (-\boldsymbol{\mu}\cdot\mathbf{J})(\boldsymbol{\nu}\times\mathbf{J}) + (\boldsymbol{\nu}\cdot\mathbf{J})\times(-\boldsymbol{\mu}\times\mathbf{J})]\sin\omega t\cos\omega t\}\,\omega dt \\ &= (-3\omega^2/2)\{I_3 - I_1)[(\boldsymbol{\mu}\cdot\mathbf{I})(\boldsymbol{\mu}\times\mathbf{I}) + (\boldsymbol{\nu}\cdot\mathbf{I})(\boldsymbol{\nu}\times\mathbf{I})] + (I_3 - I_2)[(\boldsymbol{\mu}\cdot\mathbf{J})(\boldsymbol{\mu}\times\mathbf{J}) + (\boldsymbol{\nu}\cdot\mathbf{J})(\boldsymbol{\nu}\times\mathbf{J})]\} \\ &= (3/2)[(I_3 - I_1)(\boldsymbol{\omega}\cdot\mathbf{I})(\boldsymbol{\omega}\times\mathbf{I}) + (I_3 - I_2)(\boldsymbol{\omega}\cdot\mathbf{J})(\boldsymbol{\omega}\times\mathbf{J})]\end{aligned} \quad [8]$$

since

$$\begin{aligned}[(\boldsymbol{\mu}\cdot\mathbf{I})\boldsymbol{\mu} + (\boldsymbol{\nu}\cdot\mathbf{I})\boldsymbol{\nu}]\times\mathbf{I} &= \{\mathbf{I} - [\mathbf{n}\cdot\mathbf{I}]\mathbf{n}\}\times\mathbf{I} \\ &= -(\mathbf{n}\cdot\mathbf{I})(\mathbf{n}\times\mathbf{I}) \\ &= (-\omega^{-2})(-\boldsymbol{\omega}\cdot\mathbf{I})(\boldsymbol{\omega}\times\mathbf{I})\end{aligned} \quad [9]$$

and

$$[(\boldsymbol{\mu}\cdot\mathbf{J})\boldsymbol{\mu} + (\boldsymbol{\nu}\cdot\mathbf{J})\boldsymbol{\nu}]\times\mathbf{J} = -\omega^{-2}(\boldsymbol{\omega}\cdot\mathbf{J})(\boldsymbol{\omega}\times\mathbf{J}) \quad [10]$$

or

$$\mathbf{M}_{avg} = (-3/2)\boldsymbol{\omega}\times[I_1(\boldsymbol{\omega}\cdot\mathbf{I})\mathbf{I} + I_2(\boldsymbol{\omega}\cdot\mathbf{J})\mathbf{J} + I_3(\boldsymbol{\omega}\cdot\mathbf{K})\mathbf{K}] \quad [11]$$

since

$$\boldsymbol{\omega}\times[(\boldsymbol{\omega}\cdot\mathbf{I})\mathbf{I} + (\boldsymbol{\omega}\cdot\mathbf{J})\mathbf{J}] = -\boldsymbol{\omega}\times(\boldsymbol{\omega}\cdot\mathbf{K}) \quad [12]$$

Body of Revolution

Furthermore, if $I_3 = I_2$ as for a body with cylindrical symmetry, then

$$\mathbf{M}_{avg} = (-3/2)\Delta I(\boldsymbol{\omega}\cdot\mathbf{I})(\boldsymbol{\omega}\times\mathbf{I}) \quad [13]$$

where

$\mathbf{I}$ = axis of symmetry

and

ΔI = longitudinal principal moment of inertia reduced by the transverse principal moment of inertia

This expression is equivalent to Eq. 22 of (1), but is more useful than the latter since all of the terms used are explicit.

If we define β as the inclination of the longitudinal axis to the orbital plane

$$|\mathbf{M}_{avg}| = (3/4)\omega^2\Delta I\sin 2\beta \quad [14]$$

Note the correction in this expression of the typographical error in Eq. 23 of (1).

Conclusions

The secular gravitational torque on any inertially oriented satellite in a circular orbit is inversely proportional to the orbital period and directly proportional to the differences in the principal moments of inertia. Furthermore, if the principal moments of inertia are constant, the secular torque is normal to the orbital angular velocity. Hence, to eject angular momentum parallel to the orbital velocity, the shifting of weights as proposed by Newton (2) would have to be done at least twice per orbit period; whereas, to eject angular momentum normal to the orbital velocity, a single shifting might well suffice, particularly if several orbit periods can be used.

It is also quite interesting to note that either the instantaneous or the secular torque (Eqs. 5 and 11, respectively) can be considered to be the vector sum of the torques exerted individually on each of three cylindrical bodies corresponding to the three principal moments of inertia, assuming, in each body, the transverse moments of inertia to be zero.

References

1 Nidey, R. A., "Gravitational Torque on a Satellite of Arbitrary Shape," ARS JOURNAL, vol. 30, Feb. 1960, pp. 203–204.

2 Newton, R. R., "Method of Stabilizing an Astronomical Satellite," ARS JOURNAL, vol. 29, Sept. 1959, pp. 665–666.

[1] Systems Manager, Space Division. Member ARS.

[2] Numbers in parentheses indicate References at end of paper.

New Patents

George F. McLaughlin, *Contributor*

Release mechanism (2,967,482). J. B. Toomey Jr., Alexandria, Va., assignor to the U. S. Navy.

Ring for clamping a missile to a booster rocket. The ring is automatically unlocked and released as acceleration forces decrease to zero value.

Flare mounting (2,967,484). J. Q. Tabor Jr. and F. L. Haake, Oxnard, Calif.

Combination of mount and missile having a stabilizing fin mounted on a boattail of the missile.

Satellite demonstration model (2,967,358). F. S. Fay and G. W. Nichols, Eastlake, Ohio, assignors to the Standard Oil Co.

Rotatable globe supported at the lower pole. An elliptically shaped plane surface depicting a satellite orbit surrounds the globe, pivotally supported on a rotatable equatorial band.

Apparatus for launching balloons (2,967,677). O. C. Winzen (ARS member) and R. C. Hawkins, Minneapolis, Minn., assignors to Winzen Research, Inc.

A collapsed parachute and balloon stowed above a cylindrical gas tank are released by timed explosions which also open a gas valve to inflate the balloon.

Monopropellent for rocket motors (2,698,145). I. A. Kanarek, W. Los Angeles Calif., assignor to North American Aviation, Inc. (ARS corporate member).

Miscible mixture of a liquid fluorine compound as an oxidizer, and a liquid fluorinated saturated lower alkyl hydrocarbon as a fuel.

Supersonic diffuser (2,968,147). R. H. Truly Jr., L. P. Bonifaci and B. F. Beckelman (ARS members), Kirtland, Wash., assignors to Boeing Airplane Co. (ARS corporate member).

Air flow through a ram jet engine diffuser becomes sonic as the normal shock advances rearward to a position incipient to the formation of undesired oblique shock waves.

Spinning rocket (2,968,245). G. P. Sutton, P. Albanese, J. R. Convers, H. H. Isaacs (ARS members) and N. W. Pion, Los Angeles Calif., assignors to North American Aviation, Inc. (ARS corporate member).

Spin cartridge attached to a ring on the after end of a rocket adapted to fly off when the cartridge leaves the launcher.

Rocket control system (2,968,454). R. Youngquist, I. R. Barr (ARS members) and H. W. Merrill, Towson, Md., assignors to the Martin Co. (ARS corporate member).

Valves in a rocket housing actuate jets to produce guidance forces upon cessation of power plant operation after a predetermined period.

High altitude power supply systems (2,968,916). C. F. Taylor and J. C. Livengood, So. Lincoln, Mass., assignors to Special Purpose Engine Co., Inc.

Airborne apparatus for using the sun's radiation as a source of energy. Heat engine bodily orients heat collector in a direction facing the sun.

Rocket motor shell (2,968,918). F. G. Denison Jr., Pasadena, Calif. assignor to California Institute Research Foundation.

Hollow archways disposed longitudinally within the shell to define liquid-circulating passages; radial inner surfaces of archways exposed to burning gases.

Variable area nozzle (2,968,919). L. E. Hughes and P. J. Stevens (ARS member), Los Angeles, Calif., assignors to Hughes Aircraft Co. (ARS corporate member).

Reduced cross-sectional area throat inserts secured to the discharge end of a propellant container. Vanes in the inserts move to control fluid flow in response to changes in container pressure.

Engine mounting arrangement (2,968,920). C. J. Wayne, D. P. Edkins and R. L. Cleveland, Lynnfield, Mass., assignors to General Electric Co. (ARS corporate member).

Structure for multiple engines permitting relative movement between the aircraft and the mounting structure laterally and longitudinally, affording differential thermal expension of the mounting.

Aerodynamic jet deflecting nozzle (2,968,921). C. V. David, San Diego, Calif., assignor to Ryan Aeronautical Co. (ARS corporate member).

Vanes extend upstream edges into jet stream so part of stream is deflected through throat to provide a boundary layer flow parallel to nozzle surface.

Integrating accelerometer (2,968,949). H. A. Lassen (ARS member), Los Angeles, Calif., assignor to Hughes Aircraft Co (ARS corporate member).

Magnetic circuits provide a signal proportional to an integral of accelerations perpendicular to a reference axis nonsensitive to accelerations.

Accelerometer (2,968,950). L. E. Dunbar and V. Vacquier, La Jolla, Calif., assignors to Sperry Rand Corp. (ARS corporate member).

Pair of filaments connecting to a rigid frame a member responsive to a force. Force measured by change in tension and related frequencies of vibration of the filaments.

Stabilizing system correcting mechanism (2,968,953). G. Agins, Brooklyn, N. Y., assignor to American Bosch Arma Corp. (ARS corporate member).

Pendulum suspended for movement about a horizontal axis on a stabilized frame on an unstable support. The relation between inductive windings on the gyroscope and the frame is modified by pendulum movement.

Air-supported spherical gyroscope (2,968,954). F. K. Mueller (ARS member), Huntsville, Ala., assignor to the U. S. Army.

Gaseous film between the casing and rotor in which the force on the rotor from any semispherical part of the film is balanced by the force from the complimentary semispherical part of the film.

Centripetal acceleration compensation computer for stable platform (2,968,957). M.A. Condie and L. S. Reel (ARS member), San Diego, Calif, assignors to Ryan Aeronautical Co (ARS corporate member).

Vehicle heading and velocity inputs provide output signals combined with output signals of heading and drift accelerometers.

Fin stabilized, center-rotated rocket (2,968,996). R. I. Strickland and W. C. McCorkle Jr., Huntsville, Ala., assignors to the U. S. Army.

Power-transmission, on the rotatable part of a missile, spins the missile at nongyroscopic speed prior to launching from a conventional straight-rail launcher.

Stabilizers for jet-propelled vehicles (2,969,017). Dr. R. B. Kershner (ARS member), Silver Spring, Md., assignor to the U. S. Navy.

Vane pivotally mounted in a jet orifice. A trailing vane outside the missile moves the jet vane in a direction to return the missile to its proper orientation.

Quadrant homing system (2,969,018). S. J. Erst and G. E. Bowden, Plainview, N. Y., assignors to I.T. & T. Corp. (ARS corporate member).

Two pairs of planar photocells orthogonally arranged in the nose of a missile. A mechanism coupled to a divider circuit moves the control surfaces in response to the ratio voltaged generated.

High altitude sounding projectile (2,973,712). Y. Sekella, J. J. Digby and R. J. Covert, Montour Falls, N. Y., assignors to The Bendix Corp. (ARS corporate member).

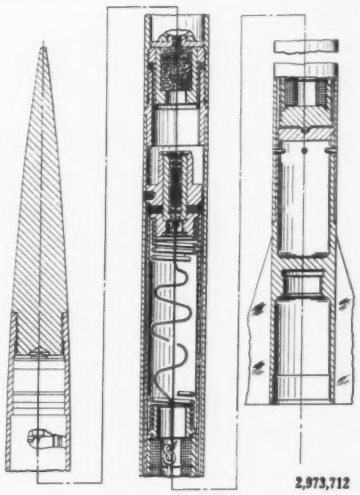

Meterological projectile which ejects at the top of its trajectory a well-spread but not too widely dispersed mass of chaff forming a radar target.

EDITOR'S NOTE: Patents listed above were selected from the Official Gazette of the U. S. Patent Office. Printed copies of patents may be obtained from the Commissioner of Patents, Washington 25, D. C., at a cost of 25 cents each; design patents, 10 cents.

Inflatable-wing rocopter (2,969,211). F. G. von Saurma (ARS member), Huntsville, Ala.

Space vehicle with deflated hollow rotor vanes shielded from the air while being propelled to the stratosphere. Pressurized gas inflates the vanes for rotation upon re-entry to the denser levels of the atmosphere.

Solid propellant and burning rate catalyst system (2,969,638). G. D. Sammons (ARS member), Bartlesville, Okla., assignor to Phillips Petroleum Co.

Inorganic oxidizing salt as an oxidizer, and a suitable binder. Catalyst system consists of base propellants of amonium dichromate, and finely divided copper metal, chromate and oxides.

Gyroscope with inverted hydrodynamic bearings (2,969,680). S. S. Linn and O. H. Bauschinger (ARS member), Ridgewood, N. J., assignors to Sperry Rand Corp., Ford Instrument Div. (ARS corporate member).

Trunnions extend into bearing sleeves with air space between. Sleeves rotate in opposite direction at same rpm, providing air film journal bearings without applying torque to the precession axis.

Gyroscopic apparatus (2,969,681). T. J. Beasley, Canoga Park, Calif., assignor to Lear Inc. (ARS corporate member).

Means, responsive to angular accelerations of a casing supporting a stabilizing means, torque the gimbal as required to reduce the accelerations to zero.

Gyro erection cut-out method (2,969,683). F. V. Sulmer, Baltimore, Md., assignor to Westinghouse Electric Corp. (ARS corporate member).

Erection of the spin-axis-defining means is prevented when the gyro may be subjected to acceleration forces other than gravity, irrespective of the direction of such forces.

Book Notes

Fatigue Testing and Analysis of Results, W. Weibull, Pergamon Press, N. Y., 1961, 305 pp. $12.

Chapters: 1. Symbols and Nomenclature; 2. Fatigue Testing Methods; 3. Fatigue Testing Machines and Equipments; 4. Instruments and Measuring Devices; 5. Test Pieces: Design, Preparation, Measurement and Protection; 6. Factors Affecting Test Resuls; 7. Planning of Test Programs; 8. Presentation of Results; 9. Analysis of Results.

This volume, published for AGARD, is intended as a thorough and authoritative reference source of information in this field. (Included is a 55 page bibliography.) It represents the work of the Structures and Materials Panel of AGARD under the guidance of the late Deryck C. Smith, to whom the book is dedicated. The book will especially interest the aircraft industry, and will also be of great interest to all engineers and research workers who are concerned with fatigue in metals and metal structures.

High Altitude Aircraft Equipment, L. T. Bykov, M. S. Yegorov and P. V. Tarasov, translated from Russian by W. J. Fiedler, edited by O. J. Marstrand, Pergamon Press, N. Y., 1961, 430 pp. $15.

Chapters: 1. The Atmosphere and the Physiological and Medical Conditions of High-Altitude Flying; 2. Technical Means of Protecting Personnel in High-Altitude Flight; 3. Cabin Pressurization; 4. Cabin Sealing; 5. Thermal Systems in Pressurized Cabins; 6. The Cleaning and Regeneration of Air in Pressurized Cabins; 7. The Control of Conditions in a Pressurized Cabin; 8. Regulation of Air Supply; 9. The Control of Air Pressure in Pressurized Cabins; 10. The Control of Air Temperature in Pressurized Cabins; 11. Safety Devices and Regulating Apparatus; 12. Oxygen Equipment and Pressure Suits.

This book deals with the problem of achieving the correct physiological conditions for maintaining the normal functioning and efficiency of the crew during high-altitude flight. Intended as a textbook for higher technological institutes, it can also be used by specialists concerned with the production and use of high-altitude equipment.

Transmission of Information: A Statistical Theory of Communications, Robert M. Fano, (Professor of Electrical Communications, Massachusetts Institute of Technology), MIT Press and John Wiley & Sons, Inc., N. Y., 1961, 387 pp. $7.50.

Chapters: 1. The Transmission of Information; 2. A Measure of Information; 3. Simple Message Ensembles; 4. Discrete Stochastic Sources; 5. Transmission Channels; 6. Channel Encoding and Decoding; 7. Encoding for Binary Symmetric Channels; 8. Multinomial Distributions; 9. Encoding for Discrete, Constant Channels. *Appendix:* Problems; Entropy Tables; Gaussian Distribution Function.

This book presents the foundations and major results of information theory. It is primarily an account of the work of C. E. Shannon, and of work inspired by him, either directly or indirectly. It has evolved out of a graduate course taught by the author over the past ten years, and includes some previously unpublished research. Problems are provided for every chapter to meet the requirements of a graduate course in electrical engineering. The author presupposes a mathematical background that includes the foundations of probability theory and of Fourier analysis. The book provides an up-to-date treatment of coding theory that emphasizes those formulations and mathematical techniques that have proved to be of greatest engineering significance.

An Introduction to the Theory and Practice of Transistors, J. R. Tillman, and F. F. Roberts, (Post Office Research Station), John Wiley & Sons, Inc., N. Y., 1961 and Sir Isaac Pitman & Sons, Ltd., London, 1961, 340 pp. $8.

Chapters: 1. The Relevant Basic Properties of Semiconductors; 2. The *p-n* Junction; 3. The Monority Carrier Junction Transistor; 4. Technology; 5. The Electrical Properties of Transistors and of Semiconductor Diodes and Their Measurement; 6. Applications.

The aim of the authors of this book is to present to newcomers to the subject of transitors and related semiconductor devices a wide treatment in one volume. It was not the intention of the authors to write a handbook for the designer of either devices or circuits, but rather to help the student of the subject to obtain a confident quantitative understanding of all the primary physical effects on which minority-carrier transistors depend for their electrical behavior and an insight into the potentialities and limitations of the devices as circuit elements.

Atlas of the Other Side of the Moon, edited by N. P. Barabashov, A. A. Mikhailov and Yu. N. Lipskiy, translated from Russian by Leon Ter-Oganian, Pergamon Press, Inc., N. Y., 1961, (orig. publ. by the Academy of Sciences of the USSR), 141 pp + 30 photographs. $7.

Contents: 1. Introduction; 2. Results of a Reconstruction of the First Photographs of the Other Side of the Moon: features of the materials used and photographs taken, methods of improving the deciphering properties of the photographs transmitted by the automatic interplane-

---

The books listed here are those recently received by the ARS from various publishers who wish to announce their current offerings in the field of astronautics. The order of listing does not necessarily indicate the editors' opinion of their relative importance or competence.

tary station, photometric cross-sections of photographs of the other side of the moon, reconstruction of the material; 3. Catalog of Formations Found on the Other Side of the Moon: objects of first degree of reliability, objects of second degree of reliability, objects of third degree of reliability; 4. Photographs of the Other Side of the Moon; 5. Supplement: map of the other side of the moon.

This book consists of some results of studies made of photographs taken from the Russian cosmic rocket launched on Oct. 4, 1959, of the part of the moon's surface that is invisible from Earth. The methods used in studying these photographs in order to reveal the details of the lunar surface, to compile the catalog of the newly discovered objects, to fix coordinates, and to draw up a map of the moon, were formulated in Moscow jointly in P. K. Sternberg's State Astronomical Institute and in the Central Scientific Institute of Geodesy, Air Photography and Cartography. Simultaneously and independently the same work was done in the Main Astronomic Observatory of the Academy of Science of the USSR and in the Astronomic Observatory at the Kharkov Gorky's State University.

A Collection of Tables and Nomograms for the Processing of Observations Made on Artificial Earth Satellites, I. D. Zhongolovich, and V. M. Amelin, (Institute of Theoretical Astronomy, Academy of Sciences of the USSR), translated from Russian by Prasenjit Basu, Pergamon Press, Inc., N. Y., 1961 (orig. publ: Moskow, 1960), 195 pp. $15.

Contents: Method of Compilation of the Tables and Nomograms and Rules for Using Them; Table 1—Period of Revolution and Semi-Axis of the Orbit Calculated from the Mean Diurnal Motion of the Artificial Earth Satellite; Table 2—Values of r/a and $v - M$; Table 3—Auxiliary Tables for the Calculation of the Geocentric Equatorial and Local Geocentric Coordinates of the Earth Satellite; Table 4—Approximate Values of Secular Perturbations of the Earth Satellite Caused by the Oblateness of the Earth; Nomograms; Appendix—Auxilary Table for Interpolation with Second Differences.

This book, intended for specialist astronomers and certain amateur astronomers, is designed to facilitate work connected with the compilation of ephemerides and with the processing of observations made on artificial Earth satellites. It is composed of tables and nomograms which permit the calculation, by an observer situated at any point on Earth's surface, of the local topocentric coordinates of the satellite in accordance with the elements of its movement. The tables have been worked out for a wide range of values of the elements of possible artificial Earth satellites.

Gas Sampling and Chemical Analysis in Combustion Processes, G. Tiné, (Professor, Institute of applied Mechanics, University of Naples), Pergamon Press, N. Y., 1961, 94 pp. $17.50.

Chapters: Ideal and Practical Sampling Systems; 2. Properties of the Fluid being Sampled; 3. Flow Problems; 4. Quenching; 5. Catalytic Effects on the Sampling Tube Wall; 6. Sample Handling and Storage; 7. Location of Sampling Probes; 8. Probe Shapes and Mechanical Design; 9. Summary and Recommendations on Sampling Procedure; 10. General Survey of Gas Analysis; 11. The essential features of analysis of Combustion Gases; 12. Analysis of the Main Components; 13. Analysis of Exhaust gases; 14. Summary and Recommendations; 15. Conclusion.

This AGARDograph is devoted to a review of an experimental technique—gas sampling and chemical analysis—as applied to combustion phenomena of interest in aeronautics. The book summarizes the various problems involved. The author, appointed by the Combustion and Propulsion Panel of AGARD to prepare this review, visited 28 of the outstanding scientific laboratories in the world to accumulate data for the book.

Technical Literature Digest

M. H. Smith, *Associate Editor*
The James Forrestal Research Center, Princeton University

Propulsion and Power (Combustion Systems)

Wissenschaftliche Gesellschaft für Luftfahrt e.v. (WGL), Jahrbuch, 1959, Herausgegeben von Hermann Blenk, Braunschweig, Friedr, Wieweg & Sohn, 1960, 442 pp.

A Possible Application of Ramjet Propulsion, by R. Feraud and R. Alder, pp. 175–183. (In German)

Quarterly Progress Report on Engineering Research, *Rohm & Haas Co., Redstone Arsenal Res. Div., Rep.* no. P-60-23, March 20, 1961, 23 pp.

Design and Evaluation of a Rotating Nozzle for Use in a Thrust Vector Control System, by R. M. Sanders, pp. 18–23.

The Measurement of the Performance of Liquid Propellant Rocket Engines, by A. W. T. Mottram, *J. Brit. Interplanet. Soc.*, vol. 18, no. 1, Jan.–Feb. 1961, pp. 28–32.

Propulsion and Power (Non-Combustion)

Theory of the Magnetohydrodynamic Homopolar Generator Part I. Liquid Mediums, by Coleman du P. Donaldson, Bernard B. Hamel, James E. McCune and Richard S. Snedeker, *Aeron. Res. Associates of Princeton, Inc. Rep.* 20, Sept. 1959, 43 pp.

Theory of the Magnetohydrodynamic Homopolar Generator, Part II. Gaseous Mediums, by James E. McCune, *Aeron. Res. Associates of Princeton, Inc. Rep.* 25, June 1960, 85 pp.

Survey of State-of-the-Art Fuel Cell Development, by Joseph S. Smatko, J. B. Chrisney and Charles C. Cook, *Hoffman Labs. Div.*, Dec. 1959, 166 pp., 366 refs. (*ASTIA AD* 248,428)

Bibliography on Unconventional Sources of Electrical Power, by John B. Forlini, *Army Corps Engrs., Info. Resources Branch, Logistical Tech. Info. Section, LTIS Bibliography* 1, Nov. 1959, 24 pp. (*ASTIA AD* 231,326)

Bibliography on Unconventional Sources of Electrical Power (Supplement to LTIS Bibliography 1), by John B. Forlini, *Army Corps Engrs., Info. Resources Branch, Logistic Tech. Info. Section, LTIS Bibliography* **5,** Jan. 1961, 51 pp. (*ASTIA AD* 248,615)

Synthesis of Current Waveforms by Type C Networks, by D. Rigney, L. Kraus and H. Malamud, *Republic Aviation Corp., Plasma Propulsion Lab.*, PPL-TR-61-4 (258), Jan. 1961, 19 pp.

Electromagnetic Acceleration of a Plasma Slug, by Philip M. Mostov, Joseph L. Neuringer and Donald S. Rigney, *Republic Aviation Corp., Plasma Propulsion Lab.*, PPL-TR-61-5, Feb. 1961, 24 pp.

The Minta Martin Aeronautical Student Fund, First Award Student Papers, *Inst. Aeron Sci.*, 1960, 216 pp.

Optimization of the Power to Weight Ratio of a Brayton Cycle for a Space Vehicle, by Roy Scott Hickman, pp. 76–81.

EDITOR'S NOTE: Contributions from Professors E. R. G. Eckert, E. M. Sparrow and W. E. Ibele of the Heat Transfer Laboratory, University of Minnesota, are gratefully acknowledged.

International Institute of Refrigeration. Problems of Low Temperature Physics and Thermodynamics, Proceedings of the Meeting of Commission of the International Institute of Refrigeration, Delft, 1958, Pergamon Press, N. Y., 1959, 341 pp.

Some Remarks on Thermoelectricity, by J. W. Leech and D. K. C. MacDonald, pp. 307–310.

Nuclear Flight; the United States Air Force Programs for Atomic Jets, Missiles and Rockets, Kenneth F. Gantz, ed., Duell, Sloan and Pearce, N. Y., 1960, 216 pp.

Nuclear Propulsion and Aerospace Power, by Thomas D. White, pp. 4–8.

The Payoff in Nuclear Propulsion, by Roscoe C. Wilson, pp. 9–14.

The USAF Nuclear Propulsion Programs, by Donald J. Kearn, pp. 15–19.

Manned Aircraft Nuclear Propulsion Program, by Williams A. Tesch, pp. 20–25.

Nuclear Missile, Rocket and Auxiliary Power Programs, by Jack L. Armstrong, pp. 26–36.

Power-Reactor Fundamentals, by Thomas L. Jackson, pp. 37–58.

Thrust and Power Production from Nuclear Energy, by John P. Wittry, pp. 59–62.

Heat Transfer and Coolant Systems, by John P. Wittry, pp. 63–72.

Reactor Materials, by John J. Connelly Jr., pp. 73–78.

The Shield, by Frederick R. Westfall, pp. 79–92.

Direct-Cycle Nuclear Propulsion, by D. R. Shoults, pp. 93–102.

Indirect-Cycle Nuclear Propulsion, by Kenneth K. Klingensmith and Carl D. Lingenfelter, pp. 102–111.

Nuclear Reactors for Ramjet Propulsion, by Theodore C. Merkle, pp. 112–119.

Design of a Nuclear Ramjet, by Alan R. Gruber, pp. 119–127.

Nuclear-Rocket Propulsion, by Raemer E. Schreiber, pp. 128–137.

Radioisotopic Power Sources, by Jerome G. Morse, pp. 138–145.

Nuclear Reactors as Auxiliary Power Sources, by Joseph R. Wetch, pp. 146–156.

Testing Radiation Effects on Aircraft Systems—the USAF Support Program, by William C. Shiel, pp. 157–166.

Propellants and Combustion

On the Evaporation and Decomposition of Droplets of Liquid Ozone-Oxygen Mixtures in a Hot Oxygen Atmosphere, by R. Sandri, *Canada, National Res. Council, Div. Mech. Engng., NRC MP*-19, Dec. 1960, 18 pp.

Thermodynamic Charts for the Decomposition Products of 80, 85, and 90 per cent w/w Hydrogen Peroxide (R.T.P.), by Enid Carter, *Gt. Brit. Aero. Res. Council, R&M* no. 3158, Apr. 1958, 9 pp., 5 figs.

Critical Conditions for Drop and Jet Shattering, by Gerald Morrell, *NASA Tech. Note* D-677, Feb. 1961, 13 pp.

Investigation of the Nitroglycerin-Sodium Hydroxide Reaction, by William M. Ayres, Gerald C. Whitnack and Raymond T. Marrow, *Bur. Naval Weapons, NAVWEPS Rep.* 7608, Jan. 1961, 14 pp.

Ionization in Laminar Flames, by N. N. Inozemtsev, *The Johns Hopkins Univ., Appl. Physics Lab.,* TG 230-T112 (transl. from *Izvestiia Akademii Nauk SSSR, Otdelenie Tekhnicheskikh Nauk, Energetika i Avtomatika,* no. 2, March–Apr. 1960, pp. 59–66), Oct. 1960, 13 pp.

Transfer of Cryogenic Fluids by an Expulsion-Bag Technique, by Paul J. Sirocky, *NASA Tech. Note* D-849, April 1961, 11 pp.

Storage, Transfer, and Servicing Equipment for Liquid Hydrogen, by B. M. Bailey, et al., *Wright Air Dev. Center, Tech. Rep.* 59-386, July 1959, 772 pp. (*ASTIA AD* 231-635)

Handbook for Hydrogen Handling Equipment, (Arthur D. Little, Inc.) *Wright Air Dev. Center, Tech. Rep.* 59–751, Feb. 1960, 584 pp. (*ASTIA AD*-235,123)

Summary Report—Phase I. Study and Preliminary Experimental Evaluation of Missile Fuel Systems and Components Using Liquid Hydrogen (Borg-Warner Corp., Pesco Products Div.), *Wright Air Dev. Center, Tech. Rep.* 59-426, July 1959, 135 pp., 56 figs. (*ASTIA AD* 234,109)

Theoretical Performance of Propellants Suitable for Electrothermal Jet Engines, by John R. Jack, *NASA Tech. Note* D-682, April, 1961, 25 pp.

Some Considerations for the Selection of Upper-Stage Propellants, by J. A. Orr, *Calif. Inst. Tech., Jet Propulsion Lab. Tech. Rep.* 32-26, April 1960, 11 pp.

Air-Fuel Mixture Preparation, by Malcolm A. Weiss, *The Johns Hopkins Univ., Appl. Physics Lab* TG 370-7, Aug. 1958, 130 pp. (124 refs., Ramjet Tech.)

An Experimental Investigation on the Chemistry and Interconversion of Boron Hydrides, by Riley Schaeffer, *Air Force Res. Div. ARL-TR*-60-334, Dec. 1960, 28 pp.

Freely Expanding Gaseous Detonation Waves Initiated by Electrical Discharges, by Elton L. Litchfield, *Proj. Squid Tech. Rep.* BUM-32-P, Jan. 1961.

Gaseous Detonations, XV. Expansion Waves in Gaseous Detonations, by Hajime Miyama and Paul Kydd, *Harvard Univ., Dept. Chemistry* [Contract Nonr-1866 (36)], Feb. 17, 1961, 43 pp.

Gaseous Detonations, XIV. The CH Radical in Acetylene Oxygen-Detonations, by Richard K. Lyon and Paul H. Kydd, *Harvard Univ., Dept. Chemistry* [Contract Nonr-1866 (36)], Feb. 17, 1961, 3 pp.

Theoretical Studies for a Problem in Electro-Magnetically Induced Detonations, by W. Chinitz, K. M. Foreman and L. W. Levin, *Republic Aviation Corp., Plasma Propulsion Lab. Rep.* 121, Nov. 1959. (*AFOSR TN* 60-85)

The Evaporation of Fuel Sprays, I—Theoretical Treatment, by G. W. Benson, *Canada, National Aeron. Establ.,* NAE LR-181, Nov. 1956, 44 pp., 4 figs.

Evaporation of Fuel Sprays, II—Experimental Work, by G. W. Benson and R. J. Brisebois, *Canada, National Aeron. Establ.,* NAE LR-182, Nov. 1956, 15 pp., 8 figs.

A Literature Survey of Combustion Flames, by S. L. Woodbridge, G. K. Strather and H. D. Rix, *Haller, Raymond and Brown, Inc., State College, Pa. Rep.* 98-F, vol. I, April 1957, 384 pp. (*ASTIA AD* 117,102)

Wissenschaftliche Gesellschaft für Luftfahrt e. V. (WGL), Jahrbuch, 1959, Herausgegeben von Hermann Blenk, Braunschweig, Friedr, Wieweg & Sohn, 1960, 442 pp.

Performance Limits of Chemical Propellants Compared with Newer Possibilities for Propulsion, by A. Dadieu, pp. 322–326. (In German)

Kinetics and Mechanism of the Interaction of Ethyl Radicals with Molecular Oxygen, by L. I. Avramenko and R. V. Kolesnikova, *The Johns Hopkins Univ., Appl. Physics Lab.* TG 230-T215 (Transl. Series), Feb. 1961, 8 pp. (transl. from *Izvestiia Akademii Nauk SSR Otdelenie Khimicheskikh Nauk,* no. 5, May 1960, pp. 806–811).

The Stark Effect in Lithium, by R. G. Breene, Jr., *Gen. Electric Co., Missile & Space Vehicle Dept.,* T.I.S. R60SD477, March 1961, 16 pp.

The Minta Martin Aeronautical Student Fund, First Award Student Papers, *Inst. Aeron. Sci.,* 1960, 216 pp.

A Theoretical and Experimental Investigation of a High Speed Light Gas Gun, by David L. Kohlman, pp. 82–93.

Development of a High Velocity Air Gun, by John W. Gresham Jr., and Thomas P. Tytula, pp. 65–75.

International Institute of Refrigeration Problems of Low Temperature Physics and Thermodynamics, Proceedings of the Meeting of Commission of the International Institute of Refrigeration, Delft, 1958, Pergamon Press, N. Y., 1959, 341 pp.

The M.I.T. Helium-Hydrogen Liquefier, by S. C. Collins, pp. 15–20.

A Heat Exchanger Combined with a Helium-Recovery System for Producing Liquid Hydrogen from Liquid Helium, by J. O. Linde and K. Svensson, pp. 39–44.

Some Problems of the Liquefaction of Hydrogen and the Storage of Liquid Hydrogen and Helium, by M. P. Malkov, pp. 61–70.

Solubility of Oxygen, Nitrogen and Argon in Liquid Hydrogen, by L. Weil and P. Petit, pp. 271–274. (In French)

The Electrical Breakdown in Liquid Helium and Liquid Nitrogen, by B. S. Blaisse, A Van Den Boogaert and F. Erne, pp. 333–340.

The Effect of Fuel Distribution on Reaction Rates, by M. V. Herbert, *Aeron. Quarterly,* vol. 12, pt. I, Feb. 1961, pp. 41–50.

Lithium and Sodium for Underwater Propulsion, by W. D. White, *Astronautica Acta,* vol. 6, no. 5, 1960, pp. 38–39, 78–79.

Thermal Radiation from Fluorine-Ammonia Flames, by R. Eulner, J. Mertens and R. L. Potter, *Combustion and Flame,* vol. 5, no. 1, March 1961, pp. 1–6.

Burning Velocities of Hydrogen-Air and Hydrogen-Oxygen Mixtures, Determination by Burner Method with Schlieren Photography, by D. A. Senior, *Combustion and Flame,* vol. 5, no. 1, March 1961, pp. 7–10.

The Theory of Steady Laminar Spherical Flame Propagation: Analytical Solutions, by D. B. Spalding and V. K. Jain, *Combustion and Flame,* vol. 5, no. 1, March 1961, pp. 11–18.

The Theory of Steady Laminar Spherical Flames Propagation: Analogue Solutions, by D. B. Spalding, V. K. Jain and M. D. Samain, *Combustion and Flame,* vol. 5, no. 1, March 1961, pp. 19–26.

Perturbation Studies of Flames by Changes in Composition, by Rose L. Schalla, *Combustion and Flame,* vol. 5, no. 1, March 1961, pp. 45–54.

The High Temperature Pyrolysis of Acetylene 1 400° to 2 500°K, by C. F. Aten and E. F. Greene, *Combustion and Flame,* vol. 5, no. 1, March 1961, pp. 55–64.

Evidence for Carbon Suboxide, C_3O_2, as an Intermediate Product in the Cool Flame Oxidation Products of Diethyl

"WEATHER EYE" IN SPACE

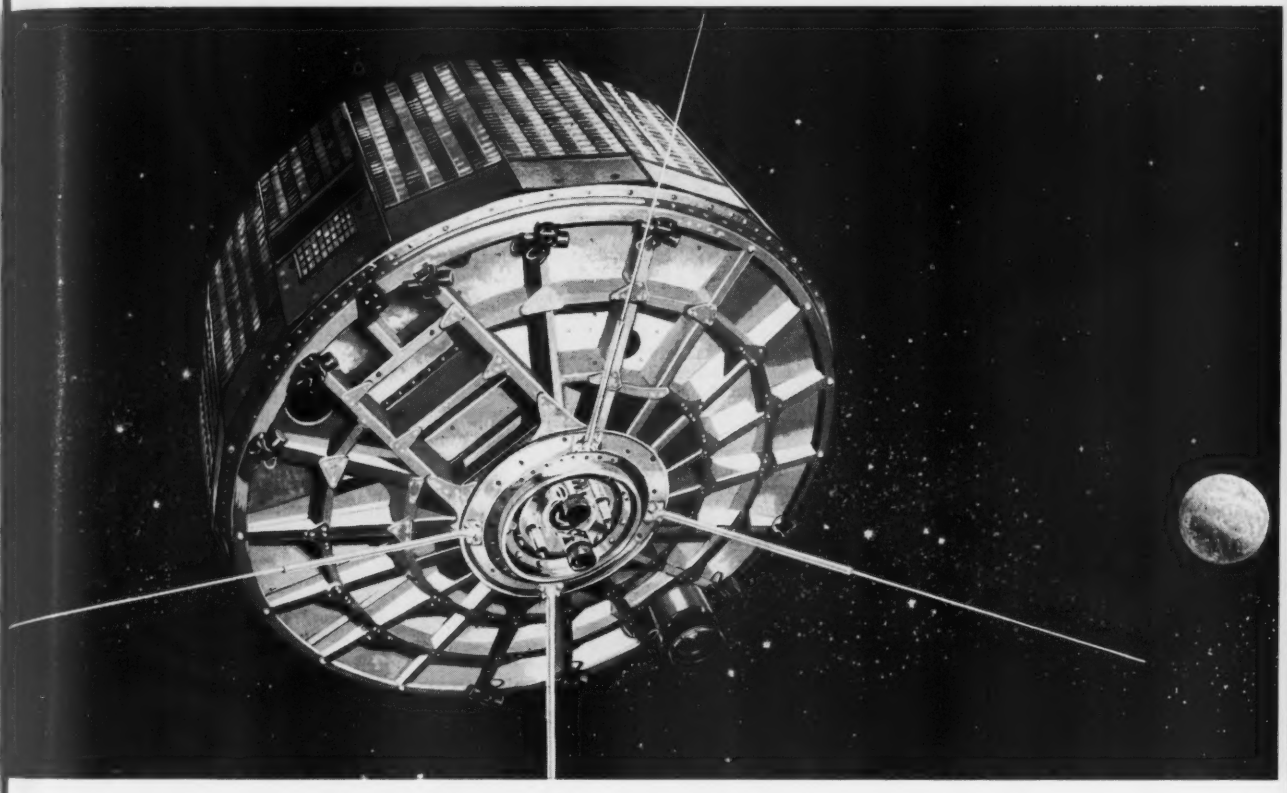

RCA-NASA Development of TIROS Advances Progress in Worldwide Weather Forecasting

From its vantage point in space, TIROS is sending down to earth new, more definite pictures and data of the world's everchanging weather patterns to aid man in his ageless efforts to control the elements.

Incorporating revolutionary and advanced electronic equipment, TIROS was designed, developed and built by RCA's Astro-Electronics Division for National Aeronautics and Space Administration. Within its small circumference are miniature TV cameras, tape recorders, TV transmitters, command receivers, timing mechanisms, beacons and telemetry equipment. In addition, it carries new scanning and non-scanning Infra-red Sensing Devices, developed by NASA, to measure and record the heat radiation of the earth and its cloud cover, and a revolutionary new Magnetic Orientation Device to capitalize on the effects of the earth's magnetic field and maintain favorable orientation of the satellite for long periods.

RCA developments in miniaturization, reliability, computing and overall electronic activities are contributing to many of the nation's leading space and missile projects. For information describing new RCA scientific developments, write Dept. 434, Defense Electronic Products, Radio Corporation of America, Camden, N. J.

RCA®

The Most Trusted Name in Electronics

RADIO CORPORATION OF AMERICA

Ether, by L. H. S. Roblee Jr., J. T. Agnew and K. Wark Jr., *Combustion and Flame*, vol. 5, no. 1, March 1961, pp. 65–70.

Inhibition of Combustion Reactions by Inorganic Lead Compounds, by J. Bardwell, *Combustion and Flame*, vol. 5, no. 1, March 1961, pp. 71–76.

The Relationship Between Burning Velocity and Space Velocity of a Spherical Combustion Wave in a Closed Spherical Chamber, by S. D. Raezer, *Combustion and Flame*, vol. 5, no. 1, March 1961, pp. 77–80.

The Quenching Diameter of Ozone Flames, by A. G. Streng and A. V. Grosse, *Combustion and Flame*, vol. 5, no. 1, March 1961, pp. 81–86.

Light Scattering Measurements on Particles Condensed From Boron-Containing Flames, by W. E. Kaskan, *Combustion and Flame*, vol. 5, no. 1, March 1961, pp. 93–98.

The Oscillations of a Viscous Liquid Drop, by W. H. Reid, *Quarterly Appl. Math.*, vol. 18, no. 1, April 1960, pp. 86–88.

Fluid Dynamics, Heat Transfer and MHD

On the Interaction Between Stream and Body in a Free-Molecule Flow, Part III: Relations Between the Interation Coefficients and the Sitting Time of the Molecules on the Surface, by Silvio Nocilla, *Torino, Politecnico, Laboratorio di Meccanica Applicata*, Oct. 1960, 11 pp. (*AFOSR TN* 60-914: *part* 3)

Steady Magnetohydrodynamic Flow Through a Channel of Circular Section, by Frank Fishman, *Avco-Everett Res. Rep.* 97, AFBMD TR-61-13, Dec. 1960, 19 pp.

Ionization Effects of Precursor Radiation From Shocks in Air, by Peter Hammerling, *Avco-Everett Res. Rep.* 98, June 1960, 17 pp.

Shock Wave-Laminar Boundary Layer Interaction on a Convex Wall, by Isaac Greber, *Mass. Inst. Tech., Fluid Dynamics Res. Group, Tech. Rep.* 58-4, July 1958, 29 pp.

Ionization and Deionization Processes as in Low-Density Plasma Flows, by Raymond L. Barger, *NASA Tech. Note* D-470, April 1961, 21 pp.

The Effects of Magnetic Fields on the Flow of Partially Ionized Gases, by J. B. Wilkinson, *Aero Chem Res. Labs., Inc.* TM-32, *Second Semi-annual Progress Rep.*, Nov. 1960, 13 pp.

Experiments on the Propagation of Weak Disturbances in Stationary Supersonic Nozzle Flow of Chemically Reacting Gas Mixtures, by Peter P. Wegener and Julian D. Cole, *Calif. Inst. Tech., Jet Propulsion Lab. Rep.* 20-134, April 1960, 28 pp.

Rate Chemistry and Flow of an Air-Like Mixture, by Harold Rosenbaum and Martin H. Bloom, *Brooklyn, Polytech. Inst., Dept. Aerospace Engng. Appl. Mech. PIBAL Rep.* 533, Aug. 1960, 30 pp.

Analytic Formulation for Radiating Fins with Mutual Irradiation, by E. R. G. Echert, T. F. Irvine Jr. and E. M. Sparrow, *Air Force Res. Div., ARL Tech. Note* 60-160, Dec. 1960, 15 pp.

Ballistic Range Measurements of Stagnation-Point Heat Transfer in Air and in Carbon Dioxide at Velocities up to 18,000 Feet per Second, by Layton Yee, Harry E. Bailey and Henry T. Woodward, *NASA Tech. Note* D-777, March 1961, 36 pp.

The Thermal Protection of a Re-entry Satellite, by Sinclaire M. Scala, *Gen. Electric Co., Missile and Space Vehicle Dept.*, T.I.S. R59SD336, March 1959, 21 pp., 10 figs.

Near-Field and Far-Field Noise Measurements for a Blow-Down-Wind-Tunnel Supersonic Exhaust Jet Having About 475,000 Pounds of Thrust, by William H. Mayes, Philip M. Edge Jr. and James S. O'Brien Jr., *NASA Tech. Note* D-517, April 1961, 22 pp.

The Behavior of the Wall Law Constants in Turbulent Pipe Flow, by David L. Murphree, *Mississippi State Univ., Aerophys. Dept. Res. Note* 13, Jan. 1961, 27 pp.

Effect of Periodic Oscillations of Velocity and Density of a Medium on Disintegration of Liquid Jets, by I. F. Dityakin and V. I. Yagodkin, *NASA Tech. Transl.* F-63, April 1961, 11 pp. (Transl. from *Akademiia Nauk SSSR, Izvestiia, Otdelenie Tekhnicheskikh Nauk*, no. 4, 1957, pp. 115–120.)

Elementary Mechanics of Turbulent Fluid Motion, by Max M. Munk, *Inst. Aerospace Sci., Sherman M. Fairchild Publ. Fund Paper* FF-28, Aug. 1960, 146 pp.

Laminar Mixing in the Presence of Axial Pressure Gradients, by Luigi G. Napolitano and A. Pozzi, *Naples, Univ. Inst. di Aeron. Rep.* 22 (*Final Rep. Part III*) Oct. 1960, 71 pp. (*AFOSR TR* 60-123: *part* 2)

Turbulent Mixing of Streams of Different Gases, by Luigi G. Napolitano, *Naples, Univ., Inst. di Aeron. Rep.* 18 (Final Rep, Part I) July 1960, 50 pp. (*AFOSR TR* 60-123: *part* 1)

Hot-Wire Measurement in Low Reynolds Number Hypersonic Flows, by C. Forbes Dewey, *Calif. Inst. Tech., Guggenheim Aeron. Lab.* (presented at the ARS Annual Meeting, Washington, D. C., 1960), 40 pp.

Notes on Magneto-Hydrodynamics, VII, Fluid Dynamical Analogies, by A. A. Blank and Harold Grad, *Atomic Energy Commission*, NYO 6486, July 1958, 15 pp.

Ultra-High Frequency Oxide Induction-Heating Furnance, by Martin H. Leipold and Jack L. Taylor, *Calif. Inst. Tech., Jet Propulsion Lab. Tech. Rep.* 32-32, March 1961, 4 pp.

Calcuation of Transient Ablation, by Martin Zlotnick and Bruce Nardquist, *Avco Corp., Res. Adv. Dev. Div. Tech. Memo* RAD-9-7 M-60-83, Jan. 1961, 16 pp.

Numerical Integration of the Navier-Stokes Equations, by J. Gillis, *Weizmann Inst. Sci., Dept. Appl. Math. Rech. Rep.* 1, Jan. 1961, 32 pp. (*AFOSR* 322)

Radiation Losses From Hydrogen Plasmas, by John W. Benoit and James E. McCune, *Aeron. Res. Associates of Princeton, Inc. Rep.* 27, July 1960, 21 pp.

Impurity Radiant Energy Loss, by S. M. Berman, *Space Tech. Labs., Physical Res. Lab.*, STL/TR-60-0000-GR 435, Nov. 1960, 20 pp.

Electromagnetic Diffusion into a Cylindrical Plasma Column During the Early Stages of Pinch Formation, by Joseph L. Neuringer, Lester Kraus and Herbert Malamud, *Republic Aviation Corp., Plasma Propulsion Lab.* PPL-TR-61-1, Jan. 16 1961, 38 pp. (*AFOSR TN* 320)

Magnetoacoustics in a Three Component Plasma, by D. A. Frank-Kamevetskii (transl. from *Magnitnyi Zvuk v. Trekhkomponentnoc Plazma*, Order of Lenin Inst. of Atomic Energy, named for I. V. Kurchatov, Moscow, 1960), *Atomic Energy Commission*, AEC TR-4183, 1960, 8 pp.

A DC Glow Model of the Formation of the Magnetic Piston, by L. Aronowitz and P. Mostov, *Republic Aviation Corp., Plasma Propulsion Lab.*, PPL-TR-60-21 (241), Dec. 1960, 12 pp. (*AFOSR* 319)

Vibrational Relaxation in Carbon Dioxide, by W. J. Witteman, *Univ. of Maryland, Inst. Fluid Dynamics Appl. Math Tech.* Note BN-226, Jan. 1961, 37 pp. (*AFOSR* 410)

The Free-Free Continuum of Nitrogen, by R. G. Breene Jr. and Maria Nardone, *Gen. Electric Co., Missile Space Vehicle Dept.* T.I.S. R60SD 476, March 1961, 3 pp.

Heat Engineering and Thermodynamics, M. A. Sturikovich, G. E. Kholodovskii and M. S. Fomichev, eds. (transl. from *All-Union Conference on the Use of Isotopes and Nuclear Radiation*, Moscow, April 1957, *Proc.*, vol. 4), *Atomic Energy Commission, Transl.* AEC-tr-4206, Sept. 1960, 94 pp.

Measuring the Volumetric Content of Steam Generating Elements by Means of Gamma Radiation, by Z. L. Miropol'skii and R. I. Shneerova, pp. 1–7.

Utilization of Gamma Radiation in the Study of the Bubbling Process, by G. G. Bartolomei, Ya. G. Vinokus, V. A. Kolokol'tsev and V. I. Petukhov, pp. 8–11.

Utilization of the Gammascope Method of Studying the Hydrodynamic Regime of a Liquid-liquid System, by S. S. Kutateladze and V. N. Moskvichev, pp. 12–15.

Tagged Atom Method of Investigating Water and Steam Content During Surface Boiling of Liquids, by P. G. Poletavkin and N. A. Shapkin, pp. 16–20.

Radioactive Methods of Studying the Processes of a Liquid Flow in a Porous Medium, by D. I. Leipushinskaya and Ya. A. Pruslin, pp. 65–69.

The Minta Martin Aeronautical Student Fund, First Award Student Papers *Inst., Aeron. Sci.*, 1960, 216 pp.

On the Use of the Cyanogen-Oxygen Flame for Simulation of the Electron Concentration Encountered by a Body During Entry to a Planetary Atmosphere, by Anthony J. Russo Jr., pp. 170–184.

Liquid Spray Response to High Frequency Sonic Oscillations, by Imants Reba, pp. 159–184.

Non-Equilibrium Molecular Dissociation of Air in a Hypersonic Nozzle, by John N. Perkins, pp. 117–127.

Nearly Free Molecular Flow Through an Orifice, by Roddam Narashimha, pp. 110–116.

The Effect of a Variable Thickness Insulating Wall on the Aerodynamic Heating of a Composite Slab, by Herbert Fox, pp. 41–57.

International Institute of Refrigeration Problems of Low Temperature Physics and Thermodynamics, Proc. of the Meeting of Commission of the International Institute of Refrigeration, Delft, 1958, Pergamon Press, N. Y., 1959, 341 pp.

The Effect of Fast Neutron Bombardment on the Thermal Conductivity of Silica Glass at Low Temperature, by J. H. Crawford Jr. and A. F. Cohen, pp. 165–172.

Low Temperature Thermal Conductivity of Lithium Fluoride Crystal Upon Irradiation by Thermal Neutrons and 60CoOy-Rays, by A. F. Cohen, pp. 173–180.

The Influence of the Density on the Thermal Diffusion in Gas Mixtures of Gases at Low Temperatures, by H. Van EE, A. Van Itterbeek and J. J. M.

Beenakker, pp. 275–280.

Viscosity Measurements of Gases Between 20 and 80°K, by J. M. J. Coremans, J. J. M. Beenakker, A. Van Itterbeek and P. Zandbergen, pp. 281–288.

Measurements on the Velocity of Sound in Liquid Oxygen and Nitrogen and Mixtures of Nitrogen and Oxygen Under High Pressures, by A. Van Itterbeek and W. Van Dael, pp. 295–306.

Film Boiling of Liquefied Gases, Especially of Liquid Helium 1, by T. Frederking and P. Grassman, pp. 317–322.

The Vibration of Air in a Duct with a Subsonic Mean Flow, by D. S. Whitehead, *Aeron. Quarterly*, vol. 12, pt. 1, Feb. 1961, pp. 34–40.

Investigation on the Theory of Plane Waves of Finite Amplitude in Ideal Gases with Friction and Heat Transfer, by W. Werner, *Annalen der Physik*, vol. 7, no. 1–2, 1961, pp. 28–44. (In German)

On Boundary Layers Associated with Oscillating Streams, by J. Kestin, P. F. Maeder and H. E. Wang, *Appl. Sci. Res.*, section A, vol. 10, no. 1, 1961, pp. 1–22.

A Unified Theory of Turbulent Flow, III, by William Squire, *Appl. Sci. Res.*, section A, vol. 10, no. 1, 1961, pp. 23–44.

Taylor Instability in a Thin Fluid Layer, by J. N. Hunt, *Appl. Sci. Res.*, section A, vol. 10, no. 1, 1961, pp. 45–58.

Instability in a Spherical Fluid Shell, by J. N. Hunt, *Appl. Sci. Res.*, section A, vol. 10, no. 1, 1961, pp. 59–80.

A Note on Heat Transfer in Laminar Flow Through a Gap, by S. Pahor and J. Strnad, *Appl. Sci. Res.*, section A, vol. 10, no. 1, 1961, pp. 81–84.

A Variational Principle for Fully Developed Laminar Heat Transfer in Uniform Channels, I, by S. C. Gupta, *Appl. Sci. Res.*, section A, vol. 10, no. 2, 1961, pp. 85–101.

Momentum and Energy Balances for Dispersed Two-Phase Flow, by J. J. van Deemter and E. T. van der Laan, *Appl. Sci. Res.*, section A, vol. 10, no. 2, 1961, pp. 102–108.

Time Dependent Temperature Distribution in Radiating Solids, by Saul S. Abarbanel, *J. Math. Phys.*, vol. 39, no. 4, Dec. 1960, pp. 246–257.

On Meteor Ablation in the Atmosphere, by F. Verniani, *Nuovo Cimento*, vol. 19, no. 3, Feb. 1, 1961, pp. 415–442.

The Calculation of Heat Flow in Melting Solids, by M. Lotkin, *Quarterly Appl. Math.*, vol. 18, no. 1, April 1960, pp. 79–85.

On Lagrangian Characteristics of Turbulence, by A. S. Monin, *Soviet Phys: Doklady*, vol. 5, no. 5, March–April 1961, pp. 952–956.

The Piston Problem in Magnetohydrodynamics, by A. A. Barmin and V. V. Gogosov, *Soviet Phys: Doklady*, vol. 5, no. 5, March–April 1961, pp. 961–963.

Application of Radioactive Isotopes to the Investigation of the Space Distribution of Atoms in a Direct-Current Arc Plasma in Various Atmospheres, by E. E. Vainshtein and Yu. I. Belyaev, *Soviet Phys: Doklady*, vol. 5, no. 5, March–April 1961, pp. 1057–1060.

The Motion of Shock Waves Along a Magnetic Field, by R. V. Polovin, *Soviet Phys: JETP*, vol. 12, no. 4, April 1961, pp. 699–700.

Shock Waves in Relavistic Magnetohydrodynamics, by L. M. Kovrizhnykh, *Soviet Phys: JETP*, vol. 12, no. 4, April 1961, pp. 725–727.

Friction and Heat Transfer in a Compressible Turbulent Boundary Layer in the Presence of Chemical Reactions Caused by the Introduction of Foreign Material, by Yu. V. Lapin, *Soviet Phys. Tech. Phys.* vol. 5, no. 10, April 1961, pp. 1162–1172.

Experimental Investigation of Axially Symmetric Turbulent Jets, by E. I. Polyakov, *Soviet Phys., Tech. Phys.*, vol. 5, no. 10, April 1961, pp. 1173–1179.

Wissenschaftliche Gesellschaft für Luftfahrt e.v. (WGL), Jahrbuch, 1959, Herausgegeben von Hermann Blenk, Braunschweig, Friedr, Wieweg & Sohn, 1960, 442 pp.

Contribution to the Calculation of the Compressible Boundary Layer with Heat Transfer, by A. Walz, pp. 111–119, 18 refs. (In German)

Inlet Diffuers in Supersonic Flow, by W. Trommsdorff and B Crispin, pp. 138–145. (In German)

Flight Mechanics

Investigation of the Aerodynamic Characteristics of Two Preliminary Designs of Scout Research Vehicle at Mach Numbers from 1.77 to 4.65, by Robert J. Keynton and Ann B. Fichter, *NASA Tech. Note*, D-821, April 1961, 60 pp.

On the Virtual Mass of Clustered Boosters, by Holt Ashley and Gifford W. Asher, *Mass. Inst. Tech., Fluid Dynamics Res. Lab. Rep.* 60-7, Dec. 1960, 34 pp.

Investigation of the Static Longitudinal and Lateral Stability Characteristics of a 0.01-Scale Model of a Three-Stage Configuration of the Scout Research Vehicle at Mach Numbers of 2.29, 2.96, 3.96 and 4.65, by Lloyd S. Jernell, *NASA Tech Note* D-711, March 1961, 27 pp.

A Method of Obtaining the Nonlinear Aerodynamic Stability Characteristics of Bodies of Revolution from Free-Flight Tests, by Donn B. Kirk, *NASA Tech Note* D-780, March 1961, 47 pp.

Survey of Characteristic Velocity Requirements for Two-Impulse Transfers Between Circular and Coplanar Exterior Elliptical Orbit with Exposition of Local and Overall Optimum Solutions, by Robert Silber, *NASA Tech Note* D-600, March 1961, 124 pp.

Optimum Orbital Transfer by High Thrust Rockets, by Lu Ting, *Brooklyn Polytech Dept. Aerospace Engng. Appl Mech. PIBAL Rep.* 633, Feb. 1961, 29 pp (*AFOSR* 163)

The Minta Martin Aeronatucal Studen Fund, First Award Student Papers, *Inst. Aeron. Sci.*, 1960, 216 pp.

A Study of the Motion of a Space Vehicle with Friction, by Jackie O. Bunting, pp. 20–25.

Space Trajectories, A Symposium (ed. by Radiation, Inc.), Academic Press, N. Y., 1960, 298 pp.

Satellite and Probe Orbit Determination, Past, Present and Future, by J. W. Siry, pp. 9–14.

General Survey of the Field, by Charles A. Whitney, pp. 15–28.

Astrodynamics, by Robert M. L. Baker Jr., pp. 29–68.

Trajectory Constants, by G. B. Westrom, pp. 69–94.

Trajectory Computation and Optimization, by James A. Ward, pp. 95–118.

Trajectory Computation in Systems Design, by R. Leger and C. E. Herrick, pp. 119–140.

Computer Programs for Space Mission, by S. D. Conte, pp. 141–154.

Space-Borne Computer Design, by Claude F. King, pp. 155–162.

Space Maneuvers, by Armand R. Tanguay, pp. 163–200.

Space Maneuvers: Optimization, by Donald C. Hock, pp. 201–212.

Re-entry Trajectories and Problems of Hypersonic Flow, by Rudolf Hermann, pp. 213–250.

Orbit Determination from Single Pass Doppler Observations, by R. B. Patton Jr., pp. 251–268.

Computer Programming Methods:

ABMA Orbit Computation Programs, by C. L. Bradshaw, pp. 277–279.

United Aircraft Corporation, Computing Programs, by T. H. Edelbaum, pp. 280.

Jet Propulsion Laboratory Computing Programs, by W. R. Hoover, pp. 280–281.

Satellite Orbit Programs, by Y. R. Garrett, pp. 282–286.

Polaris Missile Simulation, by J. H. Long, pp. 283–286.

Orbital Programs Available at Project Space Track, by E. W. Wahl, pp. 287–288.

Theorem of Image Trajectories in the Earth-Moon Space, by A. Miele, *Astronautica Acta*, vol. 6, no. 5, 1960, pp. 225–232.

Satellite Librations in the Vicinity of Equilibrium Solutions, by G. M. Schlindler, *Astronautical Acta*, vol. 6, no. 5, 1960, pp. 233–240.

Optimum Orbital Transfer by Several Impulses, by L. Ting, *Astronautica Acta*, vol. 6, no. 5, 1960, pp. 256–265.

Vehicle Design, Testing and Performance

Artificial Earth Satellites and Successful Solar Probes 1957–1960, by Walter H. Stafford and Robert M. Croft, *NASA Tech. Note* D-601, March 1961, 602 pp.

Vanguard I Satellite Structure and Separation Mechanism, by John T. Shea and Robert C. Baumann, *NASA Tech Note* D-495, March 1961, 13 pp.

The Ionosphere Beacon Satellite, S-45, by M. J. Aucremanne, *NASA Tech Note* D-695, Jan. 1961, 28 pp.

Nuclear Flight; the United States Air Force Programs for Atomic Jets, Missiles and Rockets, Kenneth F. Gantz, ed., Duell, Sloan and Pearce, N. Y., 1960, 216 pp.

Ground Support for Nuclear Aircraft, by Hervey S. Hutchins, pp. 182–188

Temperatures in a Cylindrical Satellite, by J. R. Jenness Jr., *Astronautica Acta*, vol. 6, no. 5, 1960, pp. 241–246.

Requirements of Interstellar Flight, by T. C. Tsu, *Astronautica Acta*, vol. 6, no. 5, 1960, pp. 247–255.

Rendezvous in Space, by Kurt R. Stehling, ASTRONAUTICS, vol. 6, no. 4, April 1961, pp. 20–22, 46.

An Outline of the British Space Research Programme, by M. O. Robins, *J. Brit. Interplanetary Soc.*, vol. 18, no. 1, Jan.–Feb. 1961, pp. 4–10.

Ballistic Research Rockets—With Particular Reference to Black Knight, by D. J. Lyons, *J. Royal Aeron. Soc.*, vol. 65, no. 603, March 1961, pp. 171–187.

Wissenschaftliche Gesellschaft für Luftfahrt e.v. (WGL), Jahrbuch, 1959, Herausgegeben von Hermann Blenk, Braunschweig, Friedr, Wieweg & Sohn,

1960, 442 pp.

The French Research Rocket Vernica Type AgI, and Its First Firing in March 1959 in the Sahara, by W. Pilz, pp. 326–330. (In German)

Guidance and Control

Calculation of Servo Systems with Self-Regulating Parameters, by Iu M. Kozlov, *The Johns Hopkins Univ., Appl. Phys. Lab.* TG 230-T175, Nov. 1960, 11 pp. (*Transl. from Akademii Nauk SSSR, Izvestiia, Otdelenie Tekhnicheskikh Nauk, Energetika i Automatika*, no. 2, 1959, pp. 65–70.)

Optimum Trajectories Between Two Terminals in Space, by Harold M. Stark, ARS JOURNAL, vol. 31, no. 2, Feb. 1961, pp. 261–262.

Statistical Design of Control Systems Containing Digital Devices, by Yasushi Ishii, *Tokyo Univ., Aeron. Res. Inst. Rep.* 360 (vol. 26, no. 11, pp. 215–236), Dec. 1960.

Study of Performance Criteria for Model-Reference Type Adaptive Control System, by Paul U. Osburn, *Mass. Inst. Tech., Dept. Aeron. Astron.*, Thesis, M.S. 1959, 63 pp., (*ASTIA AD* 244, 411.)

An Analysis of the Corridor and Guidance Requirements for Supercircular Entry into Planetary Atmospheres, by Dean R. Chapman, *NASA Tech. Rep.* R-55, 1960, 47 pp.

Dynamic Synthesis of Higher-Order, Optimum Saturating Systems (60-JAC-2), by Fred Kurzweil Jr., *J. Basic Engng.* (*ASME Trans., Series D*), vol. 83, no. 1, March 1961, pp. 45–52.

Solution Space Approach to Optimal Control Problems (60-JAC-11), by Yu-Chi Ho, *J. Basic Engng.* (*ASME Trans., Series D*), vol. 83, no. 1, March 1961, pp. 53–58.

The Optimum Response of Second-Order, Velocity-Controlled Systems with Contractor Control (60-JAC-3), by Irmgard Flugge-Lotz and Mih Yin, *J. Basic Engng.* (*ASME Trans., Series D*), vol. 83, no. 1, March 1961, pp. 59–64.

Pulse-Width Relay Control in Sampling Systems (60-JAC-4) by W. L. Nelson, *J. Basic Engng. ASME Trans., Series D*), vol. 83, no. 1, March 1961, pp. 65–76.

Investigation of Periodic Modes of Sampled-Data Control Systems Containing a Saturating Element (60-JAC-9), by W. E. Meserve and H. C. Torng, *J. Basic Engng.* (*ASME Trans., Series D*), vol. 83, no. 1, March 1961, pp. 77–81.

Reduction of Dimensionality, Dynamic Programming and Control Processes (60-JAC-6), by Richard Bellman and Robert Kalaba, *J. Basic Engng.* (*ASME Trans. Series D*), vol. 83, no. 1, March 1961, pp. 82–84.

Design of Optimum Multivariable Control Systems (60-JAC-5), by E. B. Lee, *J. Basic Engng.* (*ASME Trans., Series D*), vol. 83, no. 1, March 1961, pp. 85–90.

Kinetic Lyapunov Function for Stability Analysis of Nonlinear Control Systems (60-JAC-7), by S. S. L. Chang, *J. Basic Engng.* (*ASME Trans., Series D*), vol. 83, no. 1, March 1961, pp. 91–94.

New Results in Linear Filtering and Prediction Theory (60-JAC-12), by R. E. Kalman and R. S. Bucy, *J. Basic Engng.* (*ASME Trans., Series D*), vol. 83, no. 1, March 1961, pp. 95–108.

Approximate Method for Calculating the Time Response in Linear Time-Varying, and Nonlinear Automatic Control Systems (60-JAC-10), by B. Naumov, *J.*

Basic Engng. (*ASME Trans., Series D*), vol 83, no. 1, March 1961, pp. 109–118.

Improvement of the Power Efficiency of a Hydraulic Control System by the Use of a Gain Compensated Control Valve (60-JAC-8), by S. Y. Lee, *J. Basic Engng.* (*ASME Trans., Series D*), vol. 83, no. 1, March 1961, pp. 119–124.

Satellite Attitude-Detection and Control, by P. H. Savet, *ARMA Engng.*, vol. 3, no. 4, Nov. 1960, pp. 4–9.

Development of a Flight Controller for the Delta Space Research Vehicle, by R. F. Donovan, *Applications and Industry*, no. 51, Nov. 1960, pp. 406–411.

Programmed Error Correction in Project Mercury, by B. Dimsdale and G. M. Weinberg, *Assoc. Computing Machinery, Communications*, vol. 3, no. 12, Dec. 1960, pp. 649–652.

Space Piloting, by P. V. H. Weems, *Navigation*, vol. 7, no. 1, Spring 1960, pp. 63–64.

Communication Satellites: New Problems in Control, by S. Payne, *Control Engng.*, vol. 8, no. 2, Feb. 1961, pp. 35–38.

Conditional-Switching Terminal Guidance (A Terminal Guidance Technique for Satellite Rendezvous), by A. L. Passera, *IRE Trans. Aeron. and Navigational Electronics*, vol. ANE-7, no. 4, Dec. 1960, pp. 110–118.

Man-Machine Concepts, by G. W. Hoover, *Astron. Sci. Rev.*, vol. 1, no. 4, Oct.–Dec 1959, p 30.

Servovalve Control Systems in Spacecraft and Their Energy Supply, *Raketentechnik und Raumfahrtforschung, Germany*, vol. 4, no. 4, Oct.–Dec. 1960, pp. 118–126. (In German.)

Astronavigation Guidance and Control in Space, by R. E. Roberson, *J. Astron. Sci.*, vol. 7, no. 4, Winter 1960, pp. 87–95.

Re-entry Guidance and Flight Path Control, by J. E. Vaeth, *IRE Trans. Space Electronics and Telemetry*, vol. SET-6, no. 3–4, Sept.–Dec. 1960, pp. 99–103.

Calibration Requirements of Aerospace Vehicles, by R. Stolle, *IRE Trans. on Instrumentation*, vol. I-9, no. 2, Sept. 1960, pp. 81–83.

Attitude Control of Space Vehicles (Presented at the National Automatic Control Conference, Dallas, Texas, Nov. 4–6, 1959) by C. R. Gates, *Calif. Inst. Tech., Jet Propulsion Lab.* EP 795, Feb 5, 1960.

Gas-Floated Spinning Spheres, by J H. Laub, and H. D. McGinness, *Calif. Inst. Tech., Jet Propulsion Lab. TR* 32–61, Feb. 28, 1961.

Force and Torque on a Superconducting Ellipsoid in an Axially Symmetric Magnetic Field, by J. T. Harding, *Calif. Inst. Tech., Jet Propulsion Lab. TR* 34–242, Feb. 6, 1961.

Dynamic Analysis and Design Performance for Satellite Vehicle Guidance Systems, *Martin Co., Baltimore, Md., Final Engng. Rep.* 10470–6, Jan. 31, 1959.

Guidance Requirements for a 24-Hour Satellite, *Martin Co., Baltimore, Md., Final Engng. Rep.* 10718–6, Oct. 15, 1959.

An Application of Superconductivity to Inertial Navigation, by W. H. Culver and M. H. Davis, *Rand Corp.*, R-363, Jan. 7, 1957.

An Approach to the Theory of Errors in Space Navigation—USSR (Transl. from: Izvestiya Akademiya Nauk SSSR, Energetika i Avtomatika, no. 2, Moscow, 1960), by V. A. Bodner and V. P. Seleznev, *U. S. Dept. of Commerce, Off. Tech. Services, Washington, D. C. OTS:* 60–31,416, July 20, 1960. (*JPRS:* 3573)

Investigation of a Magnetohydrodynamic Channel for the Control of High Speed Vehicles, by Coleman du P. Donaldson and Evan Gray, *Aeron. Res. Associates of Princeton, Inc., Rep.* 26, June 1960, 37 pp.

On the Application of Lyapunov's Second Method to the Synthesis of Nonlinear Control Systems, by A. Stubberud, C. T. Leondes and M. Margolis, *Univ. of Calif., Los Angeles, Dept. Engng. Rep.* 61-3, Jan. 1961, 11 pp. (*AFOSR* 218)

On the Optimum Synthesis of Discrete Multipole Filters with Random and Nonrandom Inputs, by H. C. Hsieh, *Univ. of Calif., Los Angeles, Dept. Engng. Rep.* 60-106, Dec. 1960, 23 pp. (*AFOSR* 162)

Survey of Adaptive Control Systems, by William H. Surber, General Properties of Control Systems, *Aeron. Res. Associates of Princeton, Inc., ARAP Rep.* 24, part I, May 1960, 74 pp.

Survey of Adaptive Control Systems Part II, by William H. Surber, Principles of Adaptive Control Systems, *Aeron. Res. Associates of Princeton, Inc., ARAP Rep.* 24, part II, July 1960, 112 pp.

Optimum Nonlinear Control of a Second Order Nonlinear System, by Rufus Oldenburger, John C. Nicklas and E. H. Gamble, *NASA Tech. Note* D-825, April 1961, 89 pp.

Study of Systems Using Inertia Wheels for Precise Attitude Control of a Satellite, by John S. White and Q. Marion Hansen, *NASA Tech Note* D-691, April 1961, 71 pp.

Piloted Simulator Tests of a Guidance System which can Continuously Predict Landing Point of a Low L/D Vehicle During Atmosphere Re-entry, by Rodney C. Wingrove and Robert E. Coate, *NASA Tech Note* D-787, March 1961, 36 pp.

Two vs Three-Gyro Guidance Platforms—II: Servo Dynamics, by E. M. Fischel, *Control Engng.*, vol. 8, no. 4, April 1961, pp. 122–126.

What you can Learn from Regulus Control System, by H. S. Hardy, *Control Engng.*, vol. 8, no. 3, March 1961, pp. 143–144.

On Optimum Processes in Pulsed Automatic Systems, by Ya. Z. Tsypkin, *Soviet Phys: Doklady*, vol. 5, no. 5, March–April 1961, pp. 929–931.

Atmospheric and Space Physics

The Duration Distribution of Meteor Radio Echoes II. Reflections from Unstable Trails, by E. I. Fialko, *Soviet Astronomy AJ*, vol. 4, no. 3, Nov.–Dec. 1960, pp. 498–501.

The Fading of Radio Waves Reflected Obliquely from Meteor Trails, by G. S. Kent, *J. Atmospheric and Terrestrial Phys.*, vol. 19, no. 3–4, Dec. 1960, pp. 272–283.

The Mechanism of Formation of a Meteor Trail, by B. A. Mirtov, *Soviet Astronomy AJ*, Nov.–Dec. 1960, pp. 485–488.

Craters of the Moon, by J. M. Macvey, *Spaceflight*, vol. 3, no. 1, Jan. 1961, pp. 13–15.

Dating Lunar Surface Features by Using Crater Frequencies, by T. J. Kreiter, *Astronomical Soc. of the Pacific, Publ.*, vol. 72, no. 428, Oct. 1960, pp. 393–398.

Report of the A.L.P.O. Observations of Crater Times at the March 13, 1960, Lunar Eclipse, by J. Ashbrook, *Strolling Astronomer*, vol. 14, no. 11–12, Nov.–Dec. 1960, pp. 163–167.

Studies in Lunar Topogrqphy, VII: Measurements of the Heights of the Walls of the Crater Archimedes, by G. Turner, *Univ. of Manchester, England, Dept. Astronomy*, Dec. 1959. (*AFCRC TN*-60-271; *ASTIA AD*-243,279)

Relative Intensity of Nitrogen Band Systems in Aurora, by D. M. Hunten, *Univ. of Saskatchewan, Saskatoon, Canada*, BR-22, Dec. 1959. (*AFCRC TN*-60-278; *ASTIA AD*-243,955)

Texaco Incorporated Final Report on Lunar Drill Feasibility Study, *Calif. Inst. Technology, Jet Prop. Lab.*, JPL Contract N-33552, under NASA Contract NASw-6, Jan. 13, 1961.

Hughes Tool Company Final Technical Report on Preliminary Feasibility Study of Drilling a Hole on the Moon, *Calif. Inst. of Tech., Jet Propulsion Lab.*, JPL Contract N-33553, under NASA Contract NASw-6, Sept. 23, 1960.

Armour Research Foundation Final Report on Lunar Drill Study Program, by A. V. Dundzila and J. A. Campbell, *Calif. Inst. Tech., Jet Propulsion Lab.*, JPL Contract N-33554, under NASA Contract NASw-6, July 1961.

Measurements and Standards in Plasma-Physics and Astrophysics at the National Bureau of Standards, by L. N. Branscomb, ed., *National Bur. Standards, Tech. Note* 59, July 1960. (*OTS:PB* 161,560)

Catalogue of Satellite Observations No. C-18, by D. V. Mechau, *Smithsonian Inst., Astrophys. Observatory, Cambridge, Mass. Special Rep.* 54, Dec. 19, 1960.

Catalogue of Satellite Observations No. C-19, by D. V. Mechau, *Smithsonian Inst., Astrophys. Observatory, Cambridge, Mass. Special Rep.* 55, Dec. 19, 1960.

Continuous Spectrum and Color of the Solar Corona.

The Theory of the Linear Spectrograph and a Catalogue of the Color of Stars, B, D, in Areas No. 1-43 of Kapteyn's Systematic Plan.

Catalogue of Colors of Stars in Selected Areas of Kapteyn No. 44-91 Obtained by the Linear Spectrograph Method.

Connection Between the Absolute Value of the Stars of Spectral Classes G4-K1 and their Color According to the Linear Spectrograph.

Determination of the Color of the Stars in Some Additional Fields by the Linear Spectrograph Method.

Concerning the Diffraction of Light Rays in the Field of Gravitation of the Stars, 1938.

Concerning the Diffraction of Light Rays in the Field of Gravitation of the Stars, 1937.

Consequences of Possible Diffraction of Light Rays in the Field of Gravitation of the Stars.

Is the Moon Heated in Part by Solar Corpuscular Radiation, by W. M. Sinton, *Astronomical Soc. of the Pacific, Publ.*, vol. 72, no. 426, Pct. 1960, pp. 362–363.

Introduction to the Motions of the Moon, by J. P. Duda, *Sperry Engng. Rev.* vol. 13, no. 4, Dec. 1960, pp. 19–25.

Radioimage of the Moon at 8 mm, by N. A. Ameniskii, R. I. Noskova and A. E. Salomonovich, *Soviet Astronomy AJ*, vol. 4, no. 1, July–Aug. 1960, pp. 177–178.

Origin and Nature of Lunar Surface Features, by J. J. Gilvarry, *Nature*, London, vol. 188, no. 4754, Dec. 10, 1960, pp. 886–891.

Colorimetric Measurements of Lunar Features, by G. Wegner, *Astron. Soc. of the Pacific, Publ.*, vol. 72, no. 426, Oct. 1960, pp. 364–365.

Photometric Pecularities of the Moon, by V. G. Fesenkov, *Soviet Astronomy AJ*, vol. 4, no. 3, Nov.–Dec. 1960, pp. 468–472.

The 6300 and 5577 Å Oxygen Radiation in Night Sky Luminescence at a Low Latitude Station, by D. Barbier and J. Glaume, *Annales de Géophysique*, vol. 16, no. 3, July–Sept. 1960, pp. 319–334.

Expansion of a Sodium Cloud in Interplanetary Space, by S. A. Koplan and V. G. Kurt, *Soviet Astronomy AJ*, vol. 4, no. 3, Nov.–Dec. 1960, pp. 508–514.

Escape of Planetary Atmospheres I. Escape Layer, by J. J. Gilvarry, *Phys. of Fluids*, vol. 4, no. 1, Jan. 1961, pp. 2–7.

Escape of Planetary Atmospheres II. Lifetimes of Minor Constituents, by J. J. Gilvarry, *Phys. of Fluids*, vol. 4, no. 1, Jan. 1961, pp. 8–12.

Planetary Appulses and Occultations in 1961, by G. E. Taylor, *Strolling Astronomer*, vol. 14, no. 11–12, Nov.–Dec. 1960, pp. 161–162.

The Relation of the Satellite Ionization Phenomenon to the Radiation Belts, by K. D. Kraus and R. C. Higgy, *Proc. IRE*, vol. 48, no. 12, Dec. 1960, pp. 2027–2028.

Recently Observed Rotation Rates on Saturn, by T. A. Cragg, *Strolling Astronomer*, vol. 14, no. 11–12, Nov.–Dec. 1960, pp. 162–163.

The Circulatory Nature of the Eleven-Year Cycle of Solar Activity, by V. F Christyakov, *Soviet Astronomy AJ*, vol. 4 no. 3, Nov.–Dec. 1960, pp. 405–414.

A Comparison of the Curves of Growth for the Center and the Limb of the Solar Disc, by R. B. Teplitshaya, *Soviet Astronomy AJ*, vol. 4, no. 1, July–Aug. 1960, pp. 49–59.

The Solar Supercorona from the Observations of 1951–1958, by V. V. Vitkevich, *Soviet Astronomy AJ*, vol. 4, no. 1, July–Aug. 1960, pp. 31–39.

The Existence of a General Corpuscular Field Due to the Sun, by E. R. Mustel, *Soviet Astronomy AJ*, vol. 4, no. 3, Nov.–Dec. 1960, pp. 380–385.

Corpuscular Velocoties in Streams Responsible for M-Disturbances, by E. R. Mustel, *Soviet Astronomy AJ*, vol. 4, no. 3, Nov.–Dec. 1960, pp. 386–391.

The Solar Eclipse of February 15, 1961, by A. A. Mikhailov, *Soviet Astronomy AJ*, vol. 4, no. 1, July–Aug 1960, pp. 64–73.

The Spectroscopy of Solar Flares with Echelette Gratings, by A. B. Severnyi, N. P. Steshenko, and V. L. Khokhlova, *Soviet Astronomy AJ*, vol. 4, no. 1, July–Aug. 1960, pp. 19–30.

Recent Observations of Dynamical Phenomena Associated with Solar Flares, by G. E. Moreton and H. E. Ramsey, *Astron. Soc. of the Pacific, Publ.*, vol. 72, no. 428, Oct. 1960, pp. 357–358.

10.7 CM Solar Noise Burst of November 20, 1960, by A. E. Covington and G. A. Harvey, *Phys. Rev. Letters*, vol. 6, no. 2 Jan. 1961, pp. 51–52.

Cosmic-Ray Neutron Increase from a Flare on the Far Side of the Sun, by H. Carmichael, J. F. Steljes, D. C. Rose and B. G. Wilson, *Phys. Rev. Letters*, vol. 6, no. 2, Jan. 15, 1961, pp. 49–50.

The Structure of the Sun, by A. G. Masevich and T. G. Volkonskaya, *Soviet Astronomy AJ*, vol. 4, no. 1, July–Aug. 1960, pp. 40–48.

Temperature Variation on Sun with Heliographic Latitude, by J. M. Beckers, *Astronomical Inst. of the Netherlands, Bull.*, vol. 15, no. 497, Dec. 6, 1960, pp. 85–101.

The Effect of Sunspot Magnetic Fields on the Growth Curve, by A. I. Kornilov, *Soviet Astronomy AJ*, vol. 4, no. 1, July–Aug. 1960, pp. 174–176.

Velocity Variation of Leader Sunspots within the Solar Cycle, by R. A. Miller, *Astron. Soc. of the Pacific, Publ.*, vol. 72, no. 428, Oct. 1960, pp. 399–402.

On the Connection Between Solar Noise Storms and Observable Parameters of Sunspots, by P. Maltby and O. Steen, *Astrophysica Norvegica*, Olso, Norway, vol. 7, no. 1, Oct. 1960, pp. 1–11.

Venus From Superior Conjunction, 1957 Through Superior Conjunction, 1958, by J. C. Bartlett Jr., *Strolling, Astronomer*, vol. 14, no. 11–12, Nov.–Dec. 1960, pp. 167–179.

Plasma Physics, by R. M. Kulsrud, *Amer. Scientist*, vol. 48, no. 4, Dec. 1960, pp. 581–598.

Progress in Aeronomy, by T. R. Kaiser, *Nature*, London, vol. 188, no. 4752, Nov. 26, 1960, pp. 712–713.

Propagation of Whistlers to Polar Latitudes, *Nature*, London, vol. 188, no. 4752, Nov. 26, 1960, pp. 732–733.

Simultaneous Observations of the Magnetic Field and the Velocity Field of a Large Group of Sunspots, by M. Semel, *Comptes rendus hebd. Séances de l'Acad. Sci.*, France, vol. 251, no. 14, Oct. 3, 1960, pp. 1346–1348. (In French)

Interpretation of the Polarization of Light from Sunspots, by J. L. Leroy, *Comptes rendus hebd Seances de l'Acad. Sci.*, France, vol. 251, no. 17, Oct. 24, 1960, pp. 1720–1722. (In French)

Recent Re-entry Research and the Cosmic Origin of Tektites, by D. R. Chapman, *Nature*, London, vol. 188, no. 4748, Oct. 29, 1960, pp. 353–355.

Three Velocities of Corpuscular Streams from Chromospheric Flares, by O. M. Barsukov, *Acad. of Sci. USSR, Bull. Geophys. Series*, no. 5, Dec. 1960, pp. 493–495. (In Russian)

The Decisive Space Experiments of August 1960, by N. Vichney, *La Nature*, France, no. 3306, Oct. 1960, pp. 409–413. (In French)

An Engineer Looks at Space Flight, b K. J. Bossart, *Elect. Engng.*, vol. 79, no. 12, Dec. 1960, 960–962.

Fluid Power in Space, by G. R. Keller, *Hydraulics and Pneumatics*, vol. 13, no. 12, Dec. 1960, pp. 69–73.

The Nerv Experiments, *National Acad. Sci., IGY Bull.*, no. 41, Nov. 1960, pp. 10–13.

Propagation of Very Low Frequency Noise in the Exosphere Through the Cerenkov Effect, by R. Gendrin, *Comptes rendus hebd. Seances de de l'Acad. Sci.*, France, vol. 251, no. 10, Sept. 5, 1960, pp. 1122–1123.

Observation of the Planet Mars in 1958, *l'Astronomie*, France, vol. 74, July–Aug. 1960, pp. 336–341. (In French)

A Connexion Between P_e and the F Region, by H. J. Duffus, *Nature*, London, vol. 188, no. 4752, Nov. 26, 1960, pp. 719–721

The Relation of h_{max} F2 to M (3000) F2 and h_t F2, by J. W. Wright and R. E. Duffee, *Radio Res. Labs.*, Japan, vol. 7, no. 32, July 1960, pp. 409–420.

Some Characteristics of Geomagnetic Micropulsations, by J. A. Jacobs and K.

Sinno, *Nature*, London, vol. 8, no. 4747, Oct. 22, 1960, pp. 285–287.

Earth's Magnetic Field as the Sum of Fields of Two Dipoles, by B. M. Lyakhov, *Acad. of Sci., USSR, Bull. Geophys. Series*, no. 4, Nov. 1960, pp. 396–399. (In Russian)

Approximate Empirical Relation Between the Secular Magnetic Variation and the Fluctuations in the Earth's Rotation, by L. Cogniard, *Comptes rendus hebd. des Seances de l'Acad. Sci.*, France, vol. 251, no. 10, Sept. 5, 1960, pp. 1142–1144.

On the Electron and Ion Density Distributions from the Lower up to the Uppermost Part of the F Region, by T. Yonezawa and H. Takahashi, *Radio Res. Labs.*, Japan, vol. 7, no. 32, July 1960, pp. 335–378.

The Belt of Equatorial Spread-F, by A. J. Lyon, N. J. Skinner and R. W. H. Wright, *J. Atmospheric Terrestrial Phys.*, vol. 19, no. 3/4, Dec. 1960, pp. 145–159.

Extensive Air Showers and the Upper Atmosphere, by C. A. Pearson and S. T. Butler, *Nuovo Cimento*, vol. 18, no. 2, Oct. 16, 1960, pp. 251–265.

The Outer Radiation Belt and Aurorae, by H. Liemohn, *Nature*, London, vol. 188, no. 4748, Oct. 29, 1960, pp. 394–395.

Observations of Auroras by Radar in Terre Adelie, November 1957 to January 1958, by K. Bullough, *Comptes rendus hebd. des Seances de l'Acad. Sci.*, France, vol. 25, no. 20, Nov. 14, 1960, pp. 2222–2223.

Some Results of Simultaneous Photographic and Radar Observations of Polar Auroras, by V. I. Pogorelov and F. E. Martvel, *Acad. of Sci. USSR, Bull. Geophys. Series*, no. 5, Dec. 1960, pp. 501–503. (In Russian)

The Escape of Long-Period Comets from the Solar System, by R. A. Lyttleton, *Astron. J.*, vol. 65, no. 9, Nov. 1960, pp. 492–493.

Physical Observations of the Periodic Comet Giacobini-Zinner, 1959b, by P. Mianes, S. Grudzinska and A. Stawikowski, *Annales d'Astrophysique*, vol. 23, no. 5, 1960, pp. 788–796. (In French)

The Abundance of CO^+ Ions in Comet Tails, by S. Grundzinska, *Annales d'Astrophysique*, vol. 23, no. 5, 1960, pp. 797–801. (In French)

The Distribution of C_2 in the Heads of Comets, by F. D. Miller, *Astron. J.*, vol. 65, no. 9, Nov. 1960, p. 494.

On The Structure of the Cometary Nucleus, by F. L. Whipple, *Astron. J.*, vol. 65, no. 9, Nov. 1960, p. 503.

The Coronal Activity on April 5, 1960, *Zeitschrift für Astrophysik*, vol. 51, no. 1, 1960, pp. 1–10. (In German)

Excitation of the Red Coronal Line λ6374, by C. Pecker, *Comptes Rendus Hebd. Seances de l'Acad. Sci.*, France, vol. 251, no. 18, Oct. 31, 1960, pp. 1862–1864. (In French)

Propagation of Solar Cosmic Rays Through Interplanetary Magnetic Field, by T. Obayashi and Y. Hakura, *J. Radio Res. Labs.*, Japan, vol. 7, no. 32, July 1960, pp. 379–388.

On Measuring Corpuscular Radiation in the Upper Atmosphere, by L. A. Antonov and G. S. Ivanov-Kholodny, *Acad. of Sci. USSR, Bull. Geophys. Series*, no. 5, Dec. 1960, pp. 504–505. (In Russian)

A Study of Variations of the Corpuscular Radiation Observed by Satellite 1958 Epsi on Near Japan, by M. Hirono and H. Akima, *Radio Res. Labs. J.*, Japan, vol. 7, nol 32, July 1960, pp. 41–68.

Comet Tails and Solar Corpuscular Radiation (transl. from Zeitschrift für Astrophysik, vol. 29, 1951), by L. Biermann (Germany, Max-Planck Inst.), *Special Libraries Association, Transl. Center, Chicago, Ill., UCRL Transl.* 511(L), 1960.

Solar Activity and its Effect on the Ionosphere (transl. from Solnechnaya Aktivnosti i yeye Vivaniye na Ionosfer, Moscow, 1959), by N. Ya. Bugoslavskaya, *U. S. Dept. Commerce, Off. Tech. Services, Washington, D. C., OTS:* 60-11,955, July 15, 1960. (*JPRS*:5059)

Principal Works in Astronautics 1912–1956—USSR (Transl. from Osnovnyye Trudy, Alma-Ata, vol. 3, 1957), by G. A. Tikhov, *U. S. Dept. Commerce, Off. Tech. Services, Washington, D. C., OTS*:60-31,798, Sept. 30, 1960. (*JPRS*:3990)

Photographs of the Chromosphere and Protuberances, Obtained at Pulkova During the Partial Solar Eclipse, April 17, 1912.

Observations of Total Solar Eclipse, June 29, 1927: Color Temperature of the E ternal Solar Corona (Summary).

Observations of Total Solar Eclipse, June 29, 1927: Temperature of the Equivalent Color of the External Solar Corona.

Color Temperature of the Solar Corona from Observations of the Total Solar Eclipse, June 19, 1936.

Color Temperature of the Solar Corona from Observations of the Total Solar Eclipse, June 19, 1936 (Summary).

Temperature and Color Properties of the Solar Corona of September 21, 1941. One of the Methods which Gives Hope for the Study of the Solar Corona without Eclipse.

Variations of Solar Origin in the Primary Cosmic Radiation, by J. A. Simpson, *Astrophys. J., Suppl.*, vol. 4, no. 44, June 1960, pp. 378–405.

The Origin of the Cosmic Radiation, by G. Cocconi, *Astrophys. J., Suppl.*, vol. 4, no. 44, June 1960, pp. 417–422.

Energy Particle Fluxes in the Solar System and Near the Earth, by T. Gold, *Astrophys. J., Suppl.*, vol. 4, no. 44, June 1960, pp. 406–416.

Cosmic Rays as Received at the Earth, by E. P. Ney, *Astrophys. J., Suppl.*, vol. 4, no. 44, June 1960, pp. 371–377.

Human Factors and Bio-Astronautics

Pyschometric Considerations in Selecting Personnel for Unusual Environments, by A. S. Levine, *Personnel Psychology*, vol. 13, no. 3, Autumn 1960, pp. 233–243.

How to Survive the Trip to Mars, by E. A. Smith and R. W. Connor, *SAE J.*, vol. 68, no. 12, Dec. 1960, pp. 34–38.

Problems of Space Medicine, *Missili*, Rome, vol. 2, no. 1, Feb. 1960, pp. 5–20. (In Italian)

Some Radiation Problems of Space Conquest, by W. H. Langham, *Astron. Sci. Rev.*, vol. 2, no. 4, Oct.–Dec. 1960, pp. 9–18.

Nutrition of Space Travellers, *Aviatik*, Switzerland, no. 2, Feb. 1960, p. 7. (In German)

Maintaining Life on Space Missions, by R. B. Wilson, *SAE J.*, vol. 69, no. 1, Jan. 1961, pp. 55–57.

Agriculture in the Atomic Age, by J. E. Gunckel, *Stanford Research Inst. J.*, vol. 4, no. 3, 1960, pp. 106–112.

Recent Aspects in the Development of a Closed Ecological System, by J. H. Bates, *Aerospace Medicine*, vol. 32, no. 1, Jan. 1961, pp. 12–24.

Primate Bio-Instrumentation for Two Jupiter Ballistic Flights, by W. C. Hixson, C. T. Paludan and S. W. Downs, Jr., *IRE Trans. on Medica Elect.*, vol. ME-7, no. 4, Oct. 1960, pp. 318–325.

Space Cabin Design, by A. M. Mayo, *Astron. Sci. Rev.*, vol. 1, no. 4, Oct.–Dec. 1960, p. 30.

Recent Developments in Aviation Medicine, by J. Horak, *South African Medical J.*, vol. 34, no. 28, July 9, 1960, p. 582.

Lunar Journey, *Lancet*, London, vol. 1, no. 7134, May 21, 1960, pp. 1117–1118.

Limitations on Space Flight Due to Cosmic Radiations, by H. J. Curtis, *Science*, vol. 133, no. 3449, Feb. 3, 1961, pp. 312–316.

Development, Dosimetry, and Use of Micro-Beams of X-Rays for Simulating Micro-Lesions Produced in Animal Tissues by Heavy Cosmic Ray Primaries, by W. E. Straile and H. B. Chase, *School of Aviation Medicine, Brooks, AFB, Texas, Rep.* 60-70, Oct. 1960.

Biological and Artificial Intelligence, by Dorothy I. Sweitzer, *Calif. Inst. of Tech., Jet Propulsion Lab., Lit. Search* 254, Dec. 1960, 185 pp.

Massachusetts Institute of Technology

OPERATIONS EVALUATION GROUP

Venturing Beyond the Confines of Your Discipline

The ultimate argument of the diplomat is still the threat of force; the conduct of war is still the business of the soldier and sailor. But in this era of sensitive political situations and nuclear peril, the immense complexities of armed combat have placed a few scientists in positions of uncommon responsibility.

Imaginative scientists and mathematicians with advanced degrees are invited to share in this uncommon responsibility with the staff of the Operations Evaluation Group of the Massachusetts Institute of Technology. Specifically you will provide the Chief of Naval Operations and Fleet commanders with an analytical basis for decision making on matters of tactics, strategy, composition of forces, employment of weapons and equipment, and research and development needs.

The appointments are permanent and well remunerated, and the peripheral benefits are indeed worth exploring.

Positions available in Cambridge.
Direct your inquiry to:
Dr. Jacinto Steinhardt, Director.

M.I.T.

OPERATIONS EVALUATION GROUP
Washington 25, D. C.
292 Main St., Cambridge 42, Mass.

All applicants will receive consideration for employment without regard to race, creed, color or national origin.

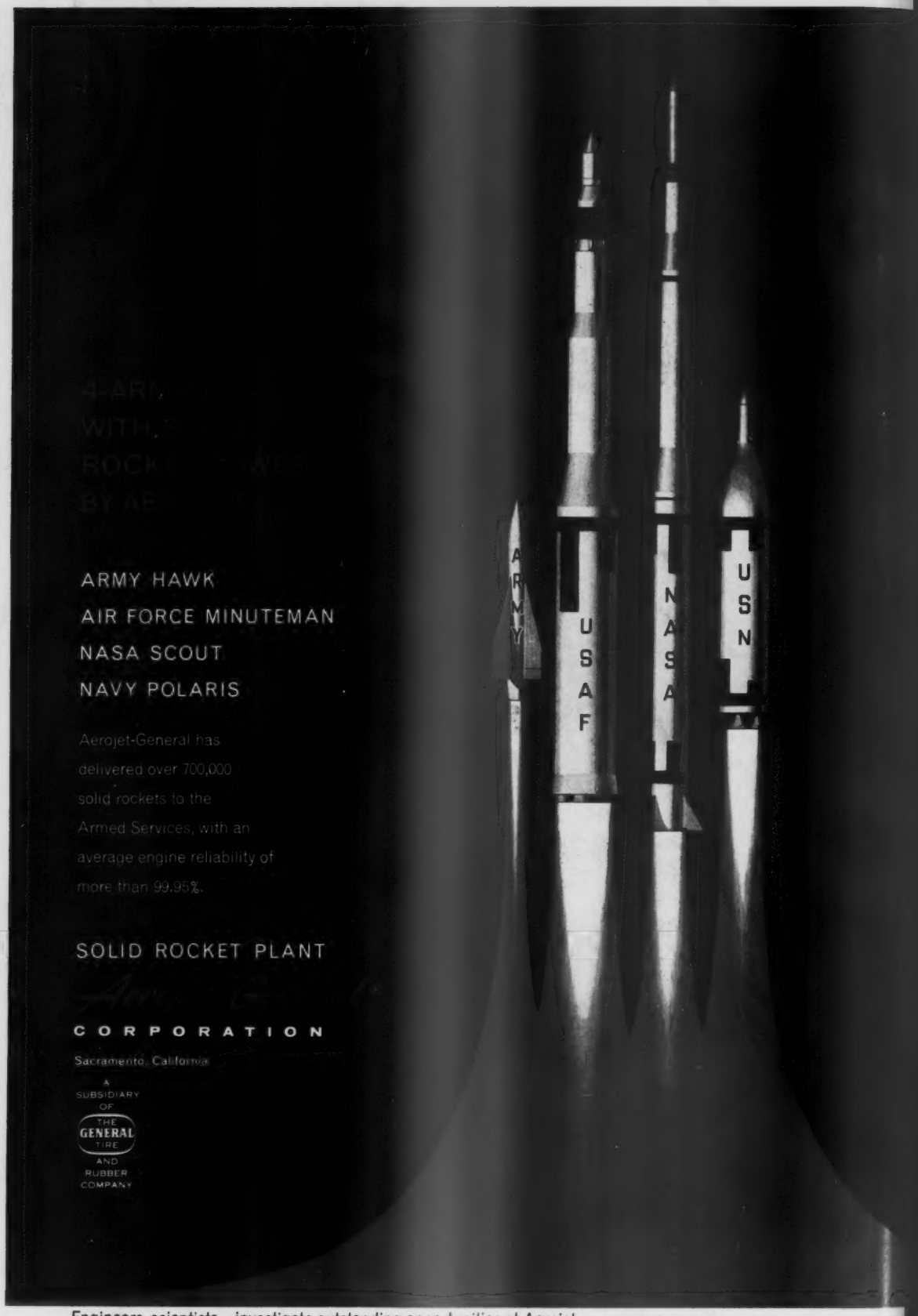

Engineers, scientists—investigate outstanding opportunities at Aerojet